1-1-1989

Radio outbursts in extragalactic sources.

Wayne M. Kinzel
University of Massachusetts Amherst

RADIO OUTBURSTS IN EXTRAGALACTIC SOURCES

A Dissertation Presented

by

WAYNE M. KINZEL

Submitted to the Graduate School of the
University of Massachusetts in partial fulfillment
of the requirements for the degree of

DOCTOR OF PHILOSOPHY

September 1989

Department of Physics and Astronomy

RADIO OUTBURSTS IN EXTRAGALACTIC SOURCES

A Dissertation Presented

by

WAYNE M. KINZEL

Approved as to style and content by:

William A. Dent, Chairperson

Robert L. Dickman, Member

Eugene Tademaru, Member

James F. Walker, Member

Thomas J. Balonek, Member

Robert B. Hallock, Department Head
Department of Physics and Astronomy

ACKNOWLEDGMENTS

First, I thank Bill Dent for supporting me through the years, suggesting the thesis topic to me, and the many long talks. I also thank Bill and Tom Balonek for providing me with many years of unpublished Haystack and Kitt Peak observations.

I want to thank the other members of my committee: Tom for many interesting conversations and encouragement, Bob Dickman for encouragement and helping me through my first publication, Gene Tademaru for many in depth discussions, and Jim Walker for being the outside member and sending many extension requests to the graduate school.

I thank the other members of the department for providing a stimulating atmosphere and particularly David Van Blerkom and Tom Arnyfor many friendly talks. I thank the many graduate students, present and past, for their friendship.

I thank Bill Irvine and Pete Schloerb for providing me with funding for the last four years. The work with the International Halley Watch allowed me to expand my astronomical horizons into cometary astronomy.

Finally, I would like to thank my family: Cheri, Keith, and Paul. I thank Cheri for putting up with me during the rough times in graduate school and being my best friend and companion for the past ten years. I thank Keith and Paul for giving me the joy of being a father. It is to Cheri, Keith, and Paul that I dedicate this work.

ABSTRACT

RADIO OUTBURSTS IN EXTRAGALACTIC SOURCES

SEPTEMBER 1989

WAYNE M. KINZEL, B.S., WESTERN KENTUCKY UNIVERSITY

M.S., UNIVERSITY OF MASSACHUSETTS

Ph.D., UNIVERSITY OF MASSACHUSETTS

Directed by: Professor William A. Dent

Three aspects of the flux density variability of extragalactic radio sources were examined: millimeter wavelength short timescale variability, the spectral evolution of outbursts, and whether the outbursts are periodically spaced.

Observations of extragalactic radio sources were conducted using the Five College Radio Astronomy Observatory between January and June 1985 at 88.2 GHz and during June and July 1985 at 40.0 GHz. Many of the sources exhibited significant flux density variations during the observing span. In addition, the most rapid variations observed (30% flux density change over a few days), were comparable with those reported in previous works. Two sources, 0355+50 and OJ287, both exhibited outbursts whose rise and fall timescales were

less than a month. An anomalous flux density dropout was observed in 3C446 and was interpreted as an occultation event.

Data at five frequencies between 2.7 and 89.6 GHz from the Dent-Balonek monitoring program were used to investigate the spectral evolution of eight outbursts. Outburst profile fitting was used to deconvolve the individual outbursts from one another at each frequency. The fit profiles were used to generate multiple epoch spectra to investigate the evolution of the outbursts. The following results were found: All the outburst spectra are consistent with emission from a simple homogeneous synchrotron source. The initial high frequency spectral slope of the outburst spectra is $\alpha = -0.2$. The high frequency spectral slope of the spectra steepen with time with a change in the slope of at least $\Delta\alpha \approx -0.5$. The spectral evolution of the outbursts is qualitatively in agreement with the model proposed by Marscher and Gear.

Finally, numerical simulations of radio variability curves indicate that a commonly used periodicity search method, the periodogram, will not find the correct period of periodic outbursts if the outbursts have random amplitudes and partial blending. A phase residual minimization method was used to examine four sources for periodic behavior. Two sources, NGC5128 and 3C454.3 each had a small number of sequential outbursts (5 and 6 respectively) whose spacings are consistent with periodicity.

TABLE OF CONTENTS

LIST OF TABLES

LIST OF FIGURES

CHAPTER 1

INTRODUCTION

1.1 Preview

Soon after the discovery of the flux variability of compact extragalactic radio sources (Dent 1965), it was realized that their variability and spectral evolution could be used to investigate the size, physical conditions, as well as the energy gain and loss mechanisms of the radiating particles. The earliest interpretation of the outbursts was the simple expanding source (SES) model (Shklovsky, 1965; van der Laan, 1966; Pauliny-Toth and Kellerman, 1966), which assumed only adiabatic loses and conservation of magnetic flux as the source expanded.

Since then, Very Long Baseline Interferometry (VLBI) has allowed the structural evolution of the inner tens of parsecs of some radio sources to be observed. VLBI has revealed that outbursts are associated with knots of emission that have been ejected from a stationary core structure, sometimes at apparent speeds greater than the speed of light. However, much of the outburst evolution can occur before the outburst component is resolved from the VLBI core (Marscher and Gear, 1985). In addition, the intensive instrument and personnel requirements of VLBI have limited multi-epoch observations to a few strong sources with the best coverage of particular sources being obtained roughly three times a year. Thus,

multifrequency continuum monitoring of extragalactic radio sources remains an important method of investigation into the evolution of outbursts.

Studied in this work is the radio emission from quasars, BL Lac objects, a Seyfert galaxy, and a radio galaxy. However, the evidence of underlining similarities between the different type objects is growing. Therefore, throughout this dissertation the terms compact extragalactic radio sources and active galactic nuclei (AGN) will be used interchangeably and as generic labels for both quasars and active galaxies (See Wiita 1984 and Gaskell 1987 for a broad overview of the characteristics of the different type objects and their similarities.).

It will also be assumed throughout this dissertation that the observed radio emission from compact extragalactic radio sources is incoherent synchrotron radiation (Ginzburg and Syrovatskii, 1965). Many radio sources have spectra which can be described by a power law

$$S \propto \nu^{\alpha} \tag{1.1}$$

over limited frequency ranges; here S is the flux density, ν is the frequency, and α is the spectral index. Given a power law energy distribution of relativistic electrons:

$$N(E) \propto E^{-s} \tag{1.2}$$

it can be shown (Pacholczyk, 1970) that a homogeneous plane parallel synchrotron radiation source will have a dual power law spectrum:

$$S \propto x^{5/2} (1 - e^{-x^p}), \qquad (1.3)$$

where $x=\nu/\nu_1$ and ν_1 is the frequency at which the opacity is unity. At low frequencies the source is self absorbed and has a spectral index of $\alpha=5/2$. At high frequencies the source is transparent with $\alpha = 5/2+p = (1-s)/2$. For large, extended, transparent sources such as the lobes of radio galaxies, a power law spectrum is observed with $\alpha\approx-0.7$. In addition, synchrotron emission is polarized and polarized emission is seen in extragalactic radio sources with the observed degree of polarization always consistent with that predicted by theory. Therefore, the synchrotron process is generally accepted as the emission mechanism.

In general, the radio emission of compact extragalactic sources can be characterized as follows:

1. Over centimeter to millimeter wavelengths, the integrated spectrum is nearly flat ($\alpha\approx0$).

2. Outbursts are seen either simultaneously at millimeter to centimeter wavelengths, or the outbursts peak first at the shorter wavelengths and then later at the longer wavelengths.

3. The outburst spectral maximum decays more slowly as a function of frequency than predicted by the SES model.

1.2 Previous Observations

Altschuler and Wardle (1976) observed 82 variable radio sources at 3.7 and 11.1 cm over a four year period. Their results indicate that the sources do not follow predictions of the SES model. The

model outbursts rise too quickly, fall too slowly, and peak at longer wavelengths too late and with too small an amplitude.

Andrew et al. (1978) observed about 100 sources for a period of 10 years. Their best coverage is of 17 sources at monthly intervals for 10 years at 2.8 cm and at 4.5 cm for a six year period. They simulated 2.8 cm variation curves with random outbursts evolving according to the SES model. This modeling reveled that the number of peaks in the variation curve was about 2/3 the actual number of outbursts because of blending. The simulations also indicated that during a given time span, the difference of the largest and smallest simulated flux values represented the amplitude of the largest outburst during the time span. Using their data and the 3.7 cm and 11.1 cm data of Altschuler and Wardle (1976) they found the maximum (S_{max}) and minimum (S_{min}) flux values at different wavelengths during identical time spans, and formed the ratios:

$$\frac{S_{max}(\lambda_1)-S_{min}(\lambda_1)}{S_{max}(\lambda_2)-S_{min}(\lambda_2)} = \left(\frac{\lambda_1}{\lambda_2}\right)^k . \qquad (1.4)$$

Their simulations imply a relationship between the amplitude of a burst and wavelength ($S_{max} \propto \lambda^{-0.4}$) to hold for wavelengths between one and ten centimeters.

Epstein et al. (1982) presented nine years of observations at 3.3 mm for five sources. By comparing individual outbursts in their data to published centimeter wavelength data, they extended the $S_{max} \propto \lambda^{-0.4}$ relation to 3.3 mm for these five sources.

Valtaoja et al. (1988) combined their data (Salonen et al., 1983; Salonen et al., 1987; Teräsranta et al., 1987) at 12, 22, 77, and 90 GHz with other published millimeter and centimeter wavelength data (Aller et al. 1985) and studied the quiescent and outburst spectra of 27 sources. They found that the outburst spectra were well described by a homogeneous synchrotron source model, with a high frequency spectral index of -0.2 (s=1.4) that is identical with the quiescent spectral index. In addition, they found that the outbursts evolved in a manner consistent with the Marscher and Gear (MG, 1985) model; the outburst spectral maximum has a three stage evolution: sharply increasing amplitude, leveling off, and then decaying amplitude as the outburst spectral maximum evolves to lower frequency.

1.3 Models of Extragalactic Radio Sources

This section will review models of the radio properties of AGN presented in the literature. Most models will be briefly described, while the SES and the MG models will be presented in more detail, so that their predictions can be compared to observations in chapter 3.

Most model development has proceeded with the authors comparing the model with only one or two sources. This has been due in part to the lack of long term multifrequency coverage of many sources. The review will be broken into two sections: models explaining the flat radio spectrum often seen in compact sources and models explaining the behavior of the radio outbursts.

1.3.1 Flat Spectrum Models

In examining the radio spectra of many sources, Owen et al. (1978) and Owen, Spangler, and Cotton (1980) found that many were flat with $\alpha \approx 0$. There have been several proposed models yielding a flat radio spectrum:

1. A transparent source having a power law electron energy distribution with s=1 will produce a flat spectrum.

2. A relativistic Maxwellian particle distribution will also produce a relatively flat spectrum (Jones and Hardee, 1979). The Maxwellian particle distribution can be motivated by the prediction that strong relativistic shocks should produce this particle distribution after passage (Jones and Hardee, 1979).

3. Another way to produce a flat spectrum is by making the source nonuniform. In the spherically symmetric case, the electron distribution and magnetic field strength can be a function of radius in the source (Marscher, 1977), while Blandford and Königl (1979) assume a conical jet and a tapered field geometry to produce a flat spectrum.

4. Cook and Spangler (1980) assumed a source is composed of several overlapping spectral components and found for a source composed of homogeneous synchrotron components that the frequency spacing of the peak frequency for each component would have to be regular to produce a flat integrated spectrum. In fact, they found the spacing would need to be so regular as to be unbelievable. In addition, unpublished simulations mentioned in Jones et al. (1981) indicate that an integrated spectrum of independent homogeneous

components is usually dominated by one component, and thus is not usually flat. However, Cotton et al. (1980) made multifrequency interferometric observations of 0735+178 and concluded that it was most likely composed of four components. They called the physical constraints required to make the four components have a very flat integrated spectrum a "cosmic conspiracy"! In support of this interpretation, VLBI has now shown many sources to be composed of multiple, spatially separate components (spaced along a jet), and for the integrated spectrum to be flat, the individual components must have their spectral peaks spaced regularly in frequency.

1.3.2 Simple Expanding Source Models

The simple expanding source (SES) model despite its unrealistically simple assumptions, is still used as a comparison model. This is due to its simple analytic nature and its prediction of the *qualitative* features observed in outbursts. It predicts the observed time delay of the peak of an outburst at progressively lower frequencies. It also predicts the decrease of the peak amplitude of the outburst as a function of increasing time and wavelength.

In this model, a power law distribution of relativistic electrons is instantaneously generated in a small spherical volume containing a magnetic field uniform in magnitude, and random in direction. The cloud expands radially at constant speed, conserving magnetic flux with the electrons suffering only adiabatic losses. At a fixed frequency the cloud is initially opaque and only the surface of the

cloud is seen. As the source expands, the magnetic field strength and electron particle density decrease and the source becomes partially transparent until maximum flux, when the source is totally transparent. Continued expansion with adiabatic loses in the relativistic electrons and reduction of the magnetic field strength then causes the decrease in the outburst flux.

This model then predicts the flux of an outburst to peak first at a high frequency, then later, with reduced amplitude, at a lower frequency. The spectrum of the burst is that of a homogeneous synchrotron source. As the burst evolves, the spectrum will shift to the left and down in a log flux density - log frequency plot.

The maximum spectral flux density (S_m) and the frequency of the maximum (ν_m) are given by:

$$\nu_m \propto (t-t_0)^{-(4s+6)/(s+4)}, \tag{1.5a}$$

$$S_m \propto (t-t_0)^{-(7s+3)/(s+4)}, \tag{1.5b}$$

$$S_m \propto \nu_m^{-(7s+3)/(4s+6)}, \tag{1.5c}$$

where t_0 is the start time of the burst. A constant expansion velocity has been assumed.

Peterson and Dent (1973) expanded the SES model by providing an extended injection of relativistic electrons and a finite initial size for the emitting region. They were then able to fit the rising part of the 1966 - 1967 outburst in 3C273. However, the decay time

of the model outburst was longer than that observed. In addition, the predicted fall off of S_m versus ν_m was steeper than observed.

Vitello and Pacini (1978 a, b) performed detailed numerical calculations using hydrodynamical expansion of a synchrotron source in the relativistic and nonrelativistic cases for spherical and linear expansion. Both spherical cases gave results very similar to the simple SES model. However, only in the linear expansion case could superluminal motion be explained and in addition, the decay times of the outbursts were longer compared to spherical expansion. They did not try to model observations.

Marscher and Gear (1985) combined most of the features of the previous expanding source models to produce a generalized expanding source model in spherical or linear dimensions with a variable injection rate. They applied this model to the 1983 outburst of 3C273 and found the injection rate had to vary in an ad hoc fashion to fit the data.

1.3.3 Shock in a Jet Model

Inside of a jet flow, instabilities in the jet can cause the formation of a shock. Marscher and Gear (MG, 1985) present a model of a shock in a jet. The jet has an opaque spectrum with spectral index:

$$\alpha_{thick} = [3(2s+3)a+4s-19]/[3(s+2)a+2(2s+1)] \qquad (1.6)$$

where the magnetic field decreases as R^{-a} along the jet. If the perpendicular magnetic field is dominant, then a=1 (Blandford and

Rees, 1974). There are three stages in the burst evolution with three variations of the maximum flux versus frequency relation: inverse Compton losses dominate

$$S_m \propto \nu_m^{-(11-a)/[2(a+1)]}; \qquad (1.7)$$

radiation losses dominate

$$S_m \propto \nu_m^{[(2s-5)(2+3a)]/[4(s+2)+3a(s-1)]}; \qquad (1.8)$$

adiabatic losses dominate

$$S_m \propto \nu_m^{10(s-1)/(7s+8)}. \qquad (1.9)$$

MG compared these results to the observed variations of 3C273 published by Robson et al. (1983) and found agreement between the two epoch spectra and the model. This model was also compared to 17 outbursts by Valtaoja et al. (1988) as discussed earlier (see also chapter 3 of this work).

1.3.4 Model Independent

Jones et al.(1981) developed a method of classifying flux variations that is largely model independent. The variations are caused by *scale* or *structure* changes in the source or changes in the electron energy index (*slope*). Scaling the global parameters of a source, such as the size or magnetic field strength, would cause the source spectrum to translate in a log flux density - log frequency plot without changing shape. Structure changes in a partially

opaque source or the appearance of a new component will, however, change the shape of the spectrum. Finally, the slope of the electron energy index can change via energy loses or reacceleration of the electrons causing the transparent, high frequency, spectral slope to respectively steepen or flatten.

Pacholczyk (1981) found that most spherically evolving source models predict a strong dependence of outburst amplitude with wavelength, while linearly evolving source models predict a weaker dependence. This latter dependence is more in line with what is observed. Pacholczyk also found, for a multiple component source to retain an integrated flat spectrum, the individual outburst components must migrate nearly horizontally on a log flux density - log frequency plot.

1.4 The Data Base

The data used in this thesis is from five main sources:

1. Flux and polarization measurements at 2.7 GHz were made using the 91 meter telescope at Green Bank, West Virginia. The program was initiated in 1972 by Kapitzky and Dent (Kapitzky, 1975) and ended in 1988 with the sudden collapse of the telescope. The program consisted of four week-long runs per year during which about 200 sources (calibrators and program sources) were observed. A description of the observational techniques and the method of data reduction can be found in Kapitzky (1975).

2. Observations at 7.9 and 15.5 GHz were obtained from Dent and Balonek (private communication). These measurements started in 1969

and are made at roughly monthly intervals using the 37m Haystack antenna.

3. Observations at 31.4 and 89.6 GHz were also obtained from Dent, Balonek, and Hobbs (private communication). These measurements started in 1970 and are obtained at about three month intervals using the 12m NRAO Kitt Peak antenna. In 1982 the 31.4 GHz receiver was taken out of service by NRAO. Additional observations from the 14m FCRAO telescope are also included from Balonek (1982) and Barvainis (1984) at λ3mm and from this work at λ3mm and λ7mm.

Other measurements have been culled from the literature mostly by Balonek and added to the data base. These will be identified when used.

1.5 Chapter Summary

This dissertation is broken into three related studies of the flux variability of extragalactic radio sources. Chapter 2 will present 3mm and 7mm observations of extragalactic radio sources performed at the Five Collage Radio Astronomy Observatory in order to look for short time scale variability. Chapter 3 will present the profile fitting and the spectral evolution of 8 outbursts and will compare the evolution of the bursts with two models. Chapter 4 examines the question of periodicity in the flux variations of 4 sources and will present the method of periodicity analysis, the results, and a review of periodic models. Chapter 5 will summarize the results of this dissertation.

CHAPTER 2

FCRAO OBSERVATIONS AND RESULTS

2.1 Introduction

Because of opacity effects, millimeter observations of active galactic nuclei (AGN) probe the deepest into the emission region, where the most rapid variability occurs. The shortest timescale variations can be used to place constraints on the size of the emitting region. Although there have been several studies of the variability of AGN at millimeter wavelengths reported in the literature prior to this work's observations, only three of the studies have examined variability time scales of greater than a day and less than a month (Balonek 1982, Epstein et al. 1982, and Barvainis 1984). These studies have shown that important variability can occur on time scales as short as a day. However, even with these studies, the variability picture at millimeter wavelengths is incomplete.

Balonek (1982) sporadically observed about 20 sources over a 33 month period at λ3mm GHz and recorded a 40% outburst decay in about 7 days in 1749+09. However, most of his observations were spaced by a month or more. Epstein, et al. (1982) observed five sources over a period of up to nine years with roughly 3 to 4 measurements a month. They found one occurrence in OJ 287, and two occurrences in 3C273 of "quenching", that is, a decline in the flux density (≥ 30%)

over a period of one to a few days that is much more rapid than other more typical variations in the source. However, they did not observe any outbursts comparable to the dropouts in magnitude and time scale. On the other hand, the observations by Barvainis (1984) revealed two outbursts in OJ 287 with a rise and fall ≥50% in a few days, but he did not observe any instances of quenching. In addition, BL Lac, one of the most active and variable sources at centimeter thru optical wavelengths, was in a state of low activity during his observing span.

It is therefore clear that additional short-term monitoring will only help define short-time scale variability better.

2.2 FCRAO Observations

In order to investigate short time scale millimeter radio variations in AGN, observations at λ3mm (88.2 GHz) and λ7mm (40.0 GHz) were performed using the Five College Radio Astronomy Observatory 13.7 meter telescope. Observations at λ3mm were made between December 19, 1984, and June 22, 1985. Observations at λ7mm were conducted between June 5, 1985, and July 29, 1985. To maximize the probability of detecting rapid variability, as many sources as possible were monitored. The sources were selected primarily by their flux density and past record of variability. Observing runs were scheduled about once a week, in 12 hour blocks, alternate runs being scheduled in opposite 12 hour LST periods. Because of weather washouts, this schedule allowed the best monitored sources to be observed about twice a month. Other weaker sources monitored by the

Dent Balonek (DB) group were occasionally observed, as time permitted, in order to increase the probability of detecting a change in the flux density level.

Observations were made in double sideband (DSB) mode at λ3mm and λ7mm using cooled receivers. The continuum backend was a square law detector with an effective bandwidth of about 250 MHz. To achieve maximum stability, all sources were observed by beam chopping at 15 Hz against blank sky displaced 6 arcminutes in azimuth from the source position, alternating the main and reference beams on source every eight seconds. Each scan consisted of 10, 20, or 30 cycles, giving a total integration time of 160, 320, or 480 seconds. The system temperature, which ranged between 200K and 300K DSB during clear weather, was measured before each scan using an ambient-temperature absorbing vane (Penzias and Burrus, 1973; Schloerb and Snell, 1980).

At λ3mm, a quarter wavelength mirror was installed which converted linear polarization to circular polarization. This enabled the total flux density to be measured in one measurement with the λ3mm linear polarized feed horn. At λ7mm, only a linearly polarized feed horn was used. However, at these wavelengths, observed polarization is usually less than about 2% for most sources, and its contribution to the error of measurement of total flux density will be ignored.

At λ3mm, the planets and DR21 were used as flux density calibrators, with brightness temperatures determined by Ulich (1981) assumed. At λ7mm, just the planets were used as calibrators, with the assumed brightness temperatures determined by linear

interpolation between the values Ulich (1981) presented for 31.4 and 89.6 GHz. The antenna temperatures for the planets and DR21 were corrected for partial resolution by the telescope beam. The beam size at λ3mm was 60" and at λ7mm it was 129". The double beam switched calibration constant at λ3mm was about 20 Jy/K, and at λ7mm it was about 23 Jy/K. The planets, as well as DR21, 3C84, and 3C273 were also used for focus and pointing checks, which were performed every couple of hours depending upon the temperature stability of the telescope. All observations were made between an elevation of 20 to 60 degrees. Within this elevation range, no gain versus elevation dependence was detected. Additional discussion of similar observations can be found in Balonek (1982) and Barvainis (1984).

2.2.1 Possible Problems: The Radome Effect

During the period from April 7 to June 5, 1985, the beam chopper went slightly out of synchronization with the computer data collection. This had no effect on the calibration of the data, but effectively decreased the integration times and increased the measurement noise.

In fall 1986 a new continuum receiver was installed at FCRAO. The new receiver had a wider bandwidth (700 MHz) and was accompanied by a new voltage to frequency (V to F) converter. The system temperature with the new receiver was still 200K to 300K DSB during clear cold weather, but the wider bandwidth and much lower noise in the V to F converter resulted in rms noise levels 1/3 of previous values for integrations of the same duration. This improvement in

the receiver system allowed the discovery of a possible problem in the telescope system.

Observations at λ3mm made on January 28, 1987, clearly indicated there was occasionally an unexpected modulation of source intensity. The top panels of Figure 2.1 show worse than average examples of the effect. It was found that the effect can be duplicated when the telescope retraces the exact same sky path. This implied that the telescope is probably picking up ground emission scattered off the spars of the radome structure.

For lack of a better name, this will be called the radome effect. It is usually not easily recognizable in scans of sources stronger than about 5 Jy, nor does it appear to be constantly present for all paths on the radome. The effect was occasionally noticeable in past observations; see Figure 9 in Balonek (1982) for example. However, it was then attributed to gain changes in the telescope system or to transient atmospheric effects (See Altenhoff et al., 1987, for documentation of anomalous atmospheric effects at millimeter wavelengths.). It must therefore be assumed that the effect has always been present. But it was only with the marked improvement of the continuum receiver system that the effect became readily apparent.

In January 1987, Mike Brewer developed software that would allow an exact retrace of the sky path for an observation. This capability would allow the retrace scan to be subtracted from the source scan, thus removing the radome effect. Retraces of the observations shown in the top panels of Figure 2.1 are shown in the middle panels; the raw observations minus the retraces are shown in

the bottom panels. For 1510-08 the raw measurement is 3.44 ± 0.29 Jy and the corrected measurement is 2.58 ± 0.26 Jy. For 4C39.25 the raw measurement is 1.99 ± 0.11 Jy and the corrected measurement is 2.03 ± 0.09 Jy. These two examples show that even when the radome effect is clearly visible in the data, it may or may not induce a major error in a source measurement. However, to be conservative we should assume that the radome effect will always affect a raw source measurement.

Continuum observations were made at FCRAO using the retrace mode by Balonek, Dent, and myself in February 1987 and also in March 1988. This data set will allow a determination of the radome effect on measurements made at FCRAO prior to the availability of the retrace mode (February 1987). It should also be noted that a new radome with a different spar structure and surface material was installed at FCRAO in the fall of 1987. Although the radome effect is still present at about the same amplitude the results using the March 1988 data may not perfectly apply to the old radome.

Figure 2.3a shows a plot of the difference of raw and corrected flux density versus corrected flux density for a number of sources observed at FCRAO. Three conclusions can be drawn from the plot. First, Figure 2.3a suggests that the radome effect appears to be an additive error, that is, it does not depend upon source intensity. Second, only rarely is a measurement wildly affected. But in these extreme cases, examination of the raw scan obviously indicated something was amiss. Finally, the formal errors of the raw, unretraced measurements underestimate the true error. While any egregious modulation is obvious, lower level, unnoticeable

modulation is certainly always present and must be accounted for in the quoted error of a measurement.

The distribution of the differences in Figure 2.3b is roughly gaussian. The differences have a mean of 0.08 Jy and rms of 0.49 Jy. However, 68% of the points are found to lie within ±0.39 Jy of this mean. Therefore, the true width of the distribution is probably between 0.39 and 0.49 Jy. If uncorrelated errors are assumed then the scatter in the differences is given by

$$\sigma^2_{diff} = \sigma^2_{radome} + \sigma^2_{raw} + \sigma^2_{corr}. \qquad (2.1)$$

The average error for the corrected measurements is 0.27 Jy and we can assume that $\sigma_{raw} \cong \sigma_{corr}$. Thus, in unbiased measurements, uncorrected FCRAO data should have about σ_{radome} = 0.07 to 0.30 Jy added in quadrature to the formal raw errors, depending upon which σ_{diff} (0.39 or 0.49) is used for the distribution of the differences. Finally, a few of the λ7mm source measurements from 1985 show a hint of what could be the radome effect. However, raw and corrected data was not available for λ7mm, so a separate error analysis for λ7mm was not possible. Therefore to be conservative, for my data at λ3mm and λ7mm, I added 0.20 Jy in quadrature to the error.

Does the radome effect affect the flux density calibration at FCRAO? In May 1985 and November 1986 measurements were made at the NRAO 12m telescope at Kitt Peak, Arizona. This data can be compared to the FCRAO data taken in March-April 1985 and January 1987. The January FCRAO data are uncorrected for the radome effect. Since my

rms uncertainties at FCRAO were usually greater than the NRAO-KP values, I have averaged FCRAO data that lies within about ± two weeks of the May 1985 NRAO-KP measurements. Figure 2.4 shows plots of FCRAO flux density measurements versus NRAO-KP measurements of the same sources during the two date ranges. The bottom plot shows the sources whose flux density is less than 10 Jy. There are four points that deviate from the 45° line by more than 3 sigma whose flux density is greater than 4 Jy. The sources and flux densities (KP, FCRAO) are: 3C120 (2.2, 5.0), OJ287 (7.0, 9.4), 3C279 (7.7, 9.3), and 3C345 (7.9, 6.5). In each case, inspection of the variability curve indicates the discrepancies are due to variation of the source between the two sets of measurements. These points were not used in the following fit. A linear fit to the data using the NRAO-KP data set as the independent axis (because of the smaller errors) produced a=-0.06±0.03 Jy and b=1.01±0.01, where a is the intercept and b is the slope. This result implies the calibration between the two telescopes is identical.

It can therefore be stated that overall, the radome effect does not change the calibration of the FCRAO data. However, even with careful editing of the data, the radome effect is present at some level in all measurements made prior to 1987. The effect is still there, even with the new radome, but the effect can now be removed from the data. However, errors on unretraced measurements should be increased by about 0.2 Jy added in quadrature and any one discrepant point in a source data set should, as always, be viewed with caution.

2.2.2 Results

The FCRAO data are presented in tabular format in Appendix A. Plots of four day averages of the data plus additional points from the NRAO 12m telescope (Dent and Balonek, private communication) are presented in Figure 2.4.

Most of the sources show variability at some level. The continuity between the Kitt Peak and FCRAO data is very good. However, it also emphasizes the need for frequent observations. For example, the steady decline of 3C84 from fall 1984 to spring 1985 would have matched a linear interpolation between the two Kitt peak measurements, but the concurrent Kitt Peak measurements of 3C273, though indicating a similar decline, missed a rapid decay of the flux density. Twelve sources exhibited significant variations and will be discussed individually.

3C84 (Seyfert, z=0.018). This source was in the declining phase of a large outburst that peaked in early 1980 (O'Dea, Dent, and Balonek, 1984). During the early half of 1984, the decline had slightly leveled off. Between mid 1984 to mid 1985 the flux density declined in a linear manner from about 48 Jy to 28 Jy.

0355+50 (empty field, z=?). In 1985, this source was in the declining phase of an outburst that peaked about 1984.5. The NRAO-KP point at 1985.38 is an average of two measurements obtained during an extremely stable observing run. The λ3mm FCRAO point at 1985.43 also consists of two measurements separated by about eight hours and made by two different observers. Thus, the decline of about 0.8 Jy (25%) appears to be real. The next λ3mm point is

consistent with a recovery to the previous level or an outburst. Seven millimeter observations started on the day of the λ3mm decline (June 5), indicate an outburst with at least a 1.2 Jy amplitude and a rise and fall time of about 44 days.

0420-01 (QSO, z=0.915). This source has a broad outburst peaking about 1984.6, followed by a rapid 1.4 Jy (25%) decline in 25 days. All points between 12/26/84 and 5/9/85 are composed of at least two independent measurements.

0440-00 (QSO, z=0.850). During 1984 to early 1985 this source followed an unusual pattern of jumping between two flux density levels with an amplitude of about a 1 Jy and a period of about half a year.

0607-15 (QSO, z=0.324). The data indicates an under sampled outburst in 1985 with a rise time shorter than 128 days and an amplitude peaking near 2.5 Jy.

OJ 287 (BL Lac, z=0.306). This source is well known for its rapid variability at all observed wavelengths and its high polarization. Between January and June 1985, OJ 287 exhibited a 2 Jy outburst followed by a precipitous decline. In addition, the λ7mm observations indicated the possibility of a very short total rise and decay (30 days) 6 Jy amplitude outburst peaking around the end of June 1985.

1156+29 (QSO, z=0.729). This source peaked during the middle of my observations with an outburst that had started about two years earlier.

3C279 (QSO, z=0.538). This source exhibits a constant flux density level during the last half of 1984 that is truncated with a

small half Jansky burst (documented by two measurements), followed by a ~1.5 Jy decline to a new flux density level for about 1/4 year, followed by another ~1.25 Jy decline in as short as 5 days. The source then undergoes a 0.6 year recovery.

1335-12 (galaxy, z=?). This source is at a minimum (~3.5 Jy) at 1985.35 and then under goes a ~2 Jy rise in about 5 days.

3C345 (QSO, z=0.595). The data for this source are consistent with a rapid 25 day 1.5 Jy drop off in the middle of a year-long 4 Jy decline.

1730-13 (QSO, z=0.901). This source exhibits an ~1.2 Jy outburst that lasted about 140 days.

3C446 (QSO, z=1.404). This source was peaking in a relatively flat topped 6 Jy outburst between January and October 1984. Then there is a rapid decay until March 1984 where the flux density stabilized at about 4 Jy. During this later period, the source has a flat spectrum between λ7mm and λ3mm and its flux density is seen to rapidly drop from about 4 Jy to 3 Jy at both λ3mm and λ7mm. At λ3mm the sampling limits the drop time to under 40 days, while at λ7mm the drop time occurred in under 10 days with a recovery to the previous level in 7 days. Unfortunately, the λ3mm point indicating the dropout was the last observation made for the season. In addition, the λ7mm point indicating the dropout is only bracketed by one leading point. 3C446 and 2230+11 were always observed together (back to back). On this particular day, both sources at λ3mm show a roughly 25% drop in flux density. However, the sources just before and after the pair of measurements did not show this discrepancy. Since the sources are about 10° apart in the sky, it is unlikely

that a radome problem could have affected both measurements in the same manner. In addition, pointing could not have caused the reduced flux density at both frequencies. The beam at λ7mm is over twice the size as at λ3mm. Therefore for the same pointing offset, measurements at the two frequencies would give different reduced flux densities. Lastly, the flux density reduction at λ3mm for 2230+11 is only about one sigma below the previous level and 2230+11 did not show the flux density reduction at λ7mm. Therefore, I will assume the the apparent 25% flux density reduction at λ3mm in 2230+11 is a statistical fluctuation and the variation for 3C446 is real.

2.3 Discussion

Inverse compton scattering, limits the observed brightness temperature of a synchrotron source to roughly 10^{12}K, unless bulk relativistic motion doppler enhances the emission (Pauliny-Toth and Kellermann 1966). None of the observed outbursts or dropouts, with the possible exceptions of the λ7mm outburst in OJ287 and the dropout in 3C446, require a relativistic enhancement to explain a large brightness temperature (Table 2.1). The changes in flux density over short time periods are about the same as what was seen by other authors, that is, at most about a 30% to 40% change in the flux density over a period of a few days (Balonek 1982, Epstein, et al. 1982, Barvainis 1984, and Teräsranta, et al. 1987).

Table 2.1. The observed most rapid change in flux density and the corresponding lower limit to the source brightness temperatures. The brightness temperatures were calculated assuming H_0 = 75 Km/s/Mpc and q_0 = 0.5. The observation wavelengths (λ) are λ3mm and λ7mm. The dates are all 1985.

† This date is 1984.

‡ This source had three high-low cycles starting at the beginning of 1984. The rise and fall times were about half a year. The change in flux density given is for the largest observed change.

Table 2.1

Source	λ	Dates (1985)		S_ν [Jy]		T_B[K]
		start	stop	start	stop	
0355+50	7	6/15	6/22	3.6±0.3	4.5±0.3	
0355+50	7	7/23	7/29	5.0±0.3	3.6±0.2	
0420-01	3	12/26†	1/20	5.7±0.2	4.3±0.3	4.5×10^{11}
0440-00	3	‡		2.2±0.1	0.4±0.2	1.4×10^{11}
0607-15	3	2/21	5/21	4.7±0.3	7.3±0.2	7.2×10^{10}
OJ287	3	2/21	4/29	6.1±0.4	9.2±0.5	1.4×10^{11}
OJ287	3	5/ 4	6/14	9.4±0.5	5.3±0.5	8.9×10^{11}
OJ287	7	6/21	7/ 3	5.3±0.3	11.2±0.5	1.1×10^{14}
OJ287	7	7/ 7	7/23	11.2±0.5	6.2±0.3	3.5×10^{13}
1156+29	3	2/21	4/29	3.2±0.3	5.2±0.3	3.8×10^{11}
1156+29	3	5/ 9	6/22	5.3±0.3	3.8±0.4	2.1×10^{11}
3C273	3	1/29	2/21	26.3±0.6	20.2±0.9	3.6×10^{11}
3C279	3	1/29	2/21	8.1±0.3	6.4±0.4	3.4×10^{12}
3C279	3	4/29.1	5/ 4.0	6.8±0.4	5.5±0.5	4.4×10^{12}
1335-12	3	4/29	5/ 4	3.7±0.0	5.5±0.0	
3C345	3	5/21	6/ 5	7.9±0.2	6.5±0.4	5.6×10^{11}
1730-13	3	1/12	3/22	5.5±0.4	6.8±0.3	3.0×10^{10}
1730-13	3	5/ 9	6/ 5	6.6±0.4	5.6±0.5	9.4×10^{10}
3C446	3	5/ 4	6/15	3.9±0.4	2.9±0.3	1.3×10^{11}
3C446	7	6/ 5	6/15	4.3±0.3	3.1±0.5	1.6×10^{13}
3C446	7	6/15	6/22	3.1±0.5	4.0±0.4	2.4×10^{13}

Most of the observed flux density declines were more rapid than the increases in flux density. However, this may be due to irregularities of the sampling. Epstein, et al. (1982) defined their "quenching" in terms of the rate and magnitude of the change (≥ 30% in a few days) as being more rapid when compared to other variations in the same source. However, the definition of rapid variability is subjective. In this work's data, all of the observed rapid declines (except one) occurred just after an outburst and probably should be interpreted as the normal (although rapid) decay of an outburst.

However, the dropout in 3C446 occurred when the flux density had leveled off after a rapid decline. Since the percentage and total flux density drop at λ3mm and λ7mm were about the same, this would argue against the dropout being caused by a synchrotron opacity effect. Also, the flux density at λ7mm returns quickly to the pre-dropout flux density value. If the synchrotron electrons were being quenched, that is, removed by some mechanism such as collisions, why should the source recover to the same level? The frequency independence and the recovery combine to suggest that the source was partially occulted by some object.

Fiedler et al. (1987) monitored daily 36 extragalactic radio sources using the Green Bank interferometer at 2.7 and 8.1 GHz over a seven year period. They found several anomalous minima in the variation curves. They attributed these to occultations of the sources by ionized clouds in our galaxy. If the dropout in 3C446 was caused by the same mechanism, then the number density of the

electrons in the ionized cloud is about 4×10^6 cm^{-3}. This is so high as to suggest a transient structure.

2.4 Conclusions

Flux measurements of extragalactic radio sources at millimeter wavelengths made at FCRAO were presented. The effect of the FCRAO radome on the flux density measurements errors was documented and the calibration between FCRAO and NRAO-KP was shown to be identical. Rapid variability was observed in 12 sources. The most rapid variability observed was comparable to that previously observed by other authors. A flux density dropout in 3C446 was interpreted as an occultion event and briefly discussed. However, further analysis must await the availability of unreduced centimeter wavelength data.

As has been pointed out before (Balonek 1982, Epstein, et al. 1982, Barvainis 1984, and Teräsranta, et al. 1987), significant information is lost at millimeter wavelengths without near daily observations. At this time, the short timescale variability characteristics of AGN at millimeter wavelengths are still relatively unknown. The observations in this work detected one outburst each in 0355+50 and OJ 287 that had a timescale of about one month. Do these short timescale outbursts have the same evolution pattern as the much longer timescale outbursts observed? This question remains unanswered.

Figure 2.1. Double beam switched continuum observations of two sources made at FCRAO demonstrating the radome effect. For each observation the top panel presents the time series of on-on source integrations (the source alternating between the reference and main beams) as the telescope tracked the source. Note the baseline ripple and the modulation of the on-on sequence. The middle panel shows the resulting scan when the telescope retraced the same path across the radome with no source present. Note the duplication of the baseline ripple. The bottom panel shows the difference of the top minus the middle panels.

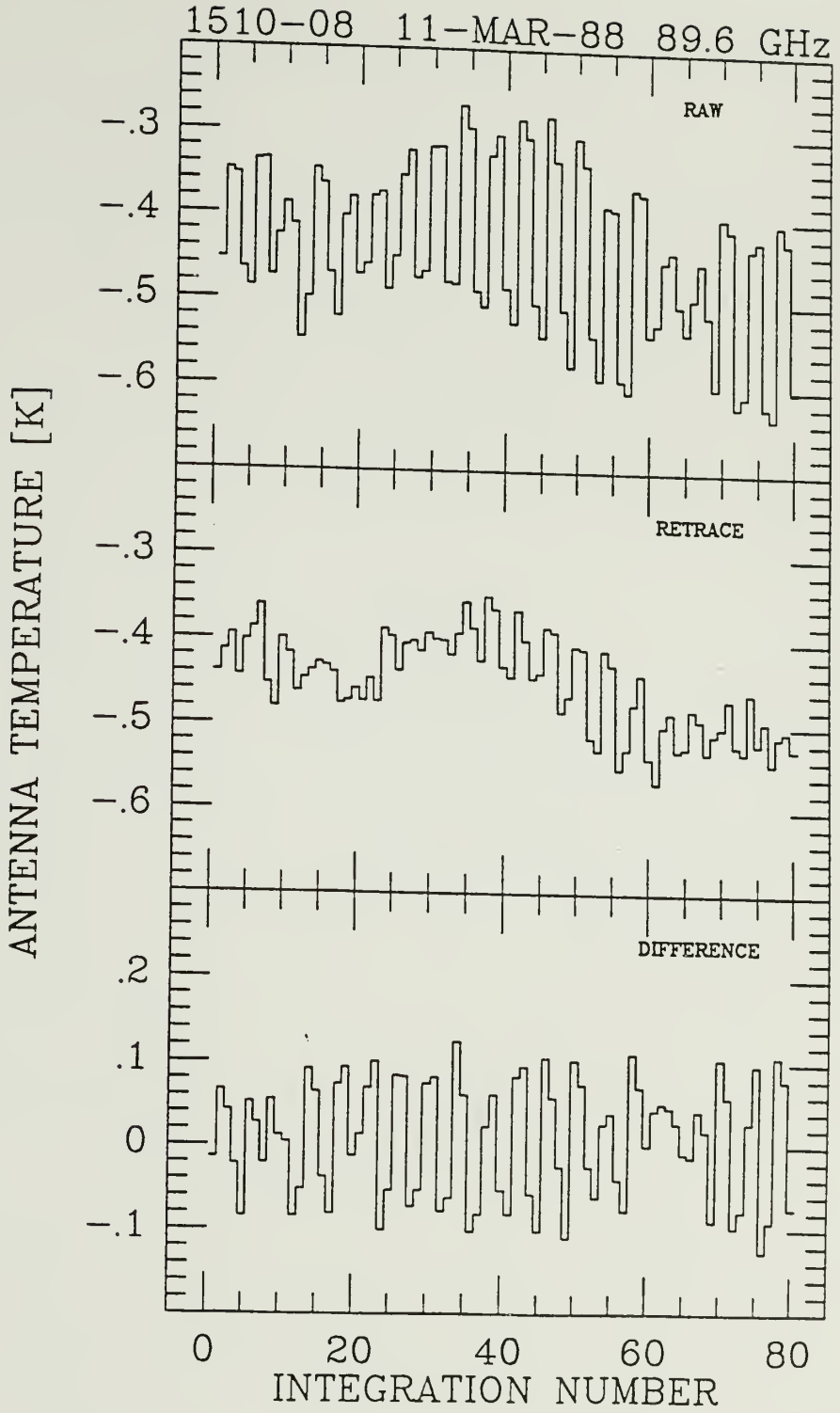

(continued next page)

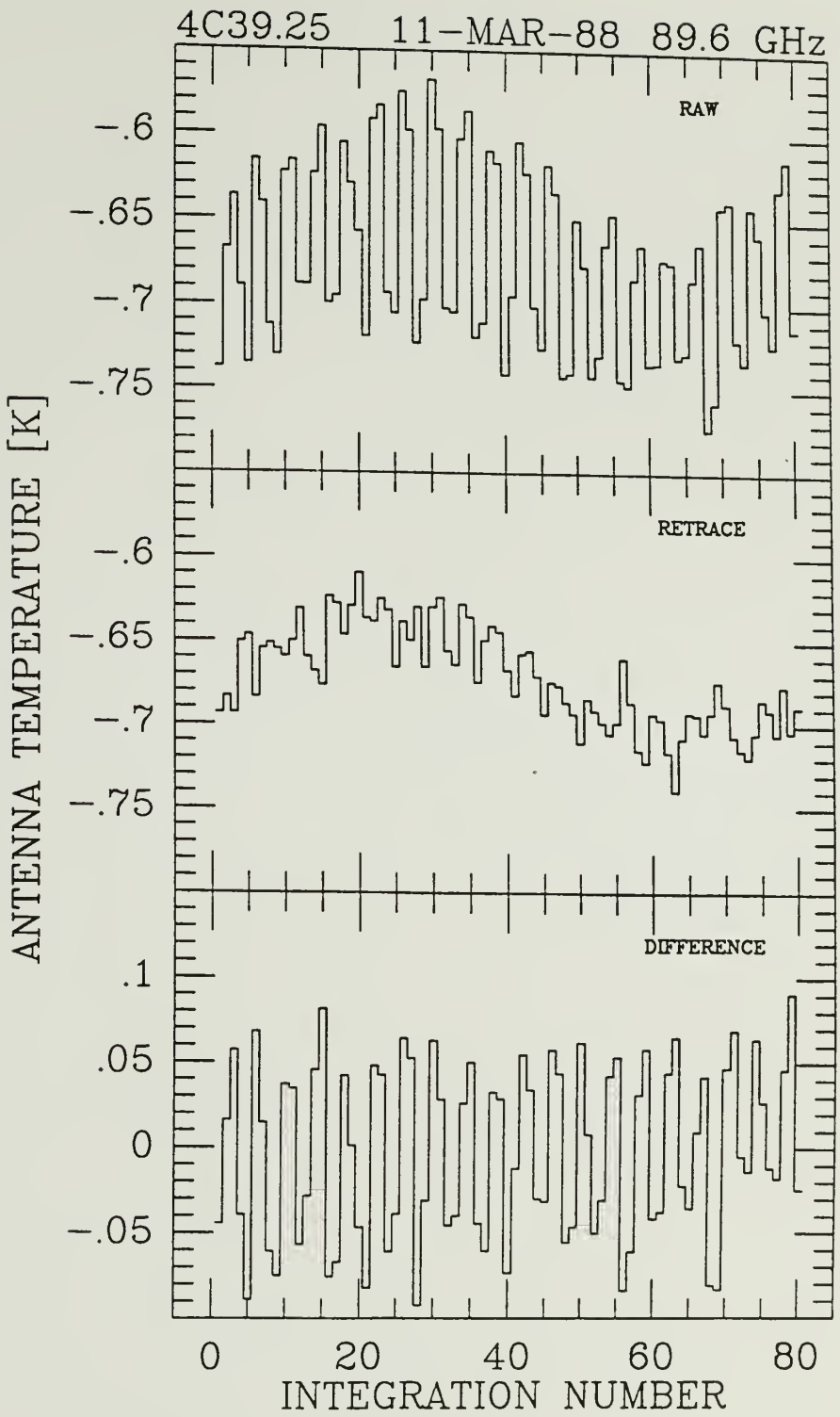

Figure 2.1 continued

Figure 2.2. The difference of raw and corrected flux density measurements in two representations. **a.** The filled circles are from the February 1987 observing run. The open circles are from the March 1988 observing run. **b.** Histogram of the differences of raw and corrected flux density measurements. Note the near gaussian shape.

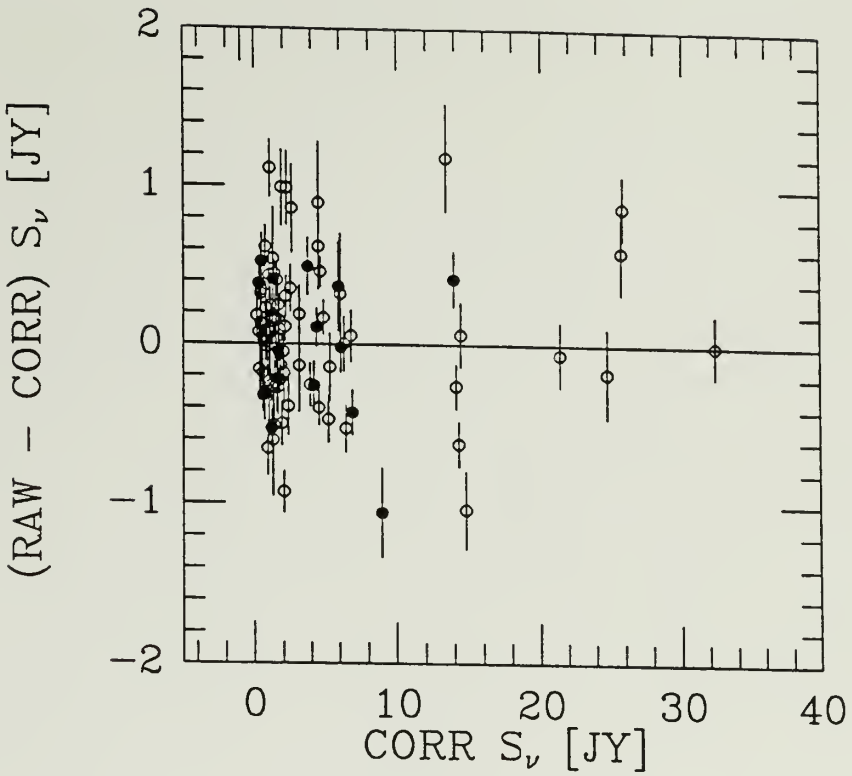
(RAW − CORR) S_ν [JY]
2
1
0
−1
−2
0
10
20
30
40
CORR S_ν [JY]

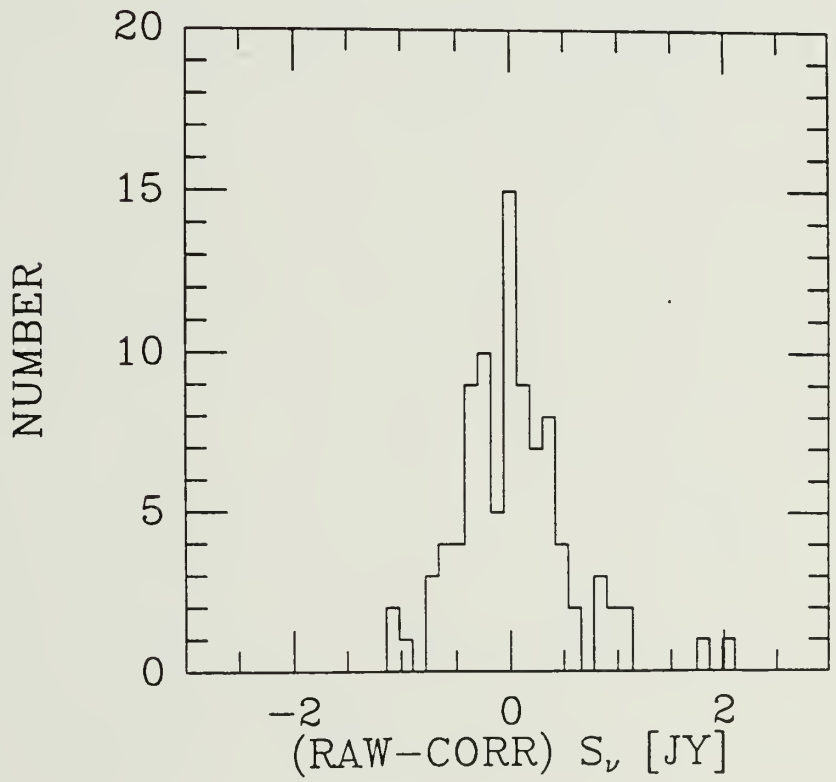
NUMBER
20
15
10
5
0
−2
0
2
(RAW−CORR) S_ν [JY]

Figure 2.3. Plots of flux density measurements for identical sources made at FCRAO versus measurements made at NRAO-KP. The filled circles are measurements made at FCRAO during May-June 1985 and measurements made at NRAO-KP on May 21-22, 1985. The open circles are measurements made at FCRAO during January 28, 1987 and measurements made at NRAO-KP on November 16-17, 1986. Both plots show the same data, but at different scales. The solid line has a slope of one. This is expected if the calibration between the two telescopes is identical.

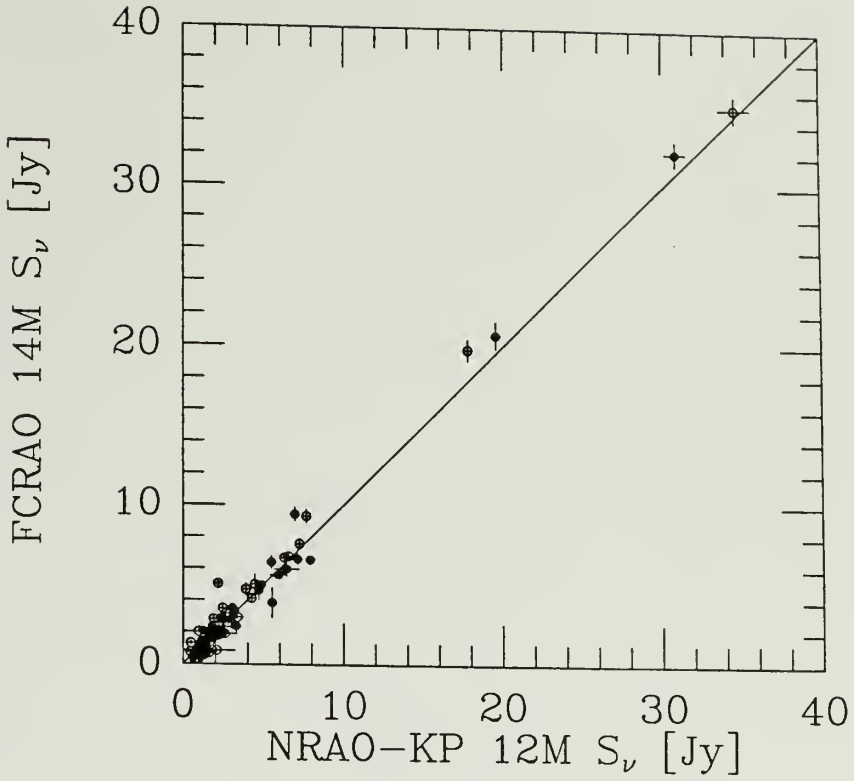
FCRAO 14M S_ν [Jy]
NRAO−KP 12M S_ν [Jy]
0
10
20
30
40

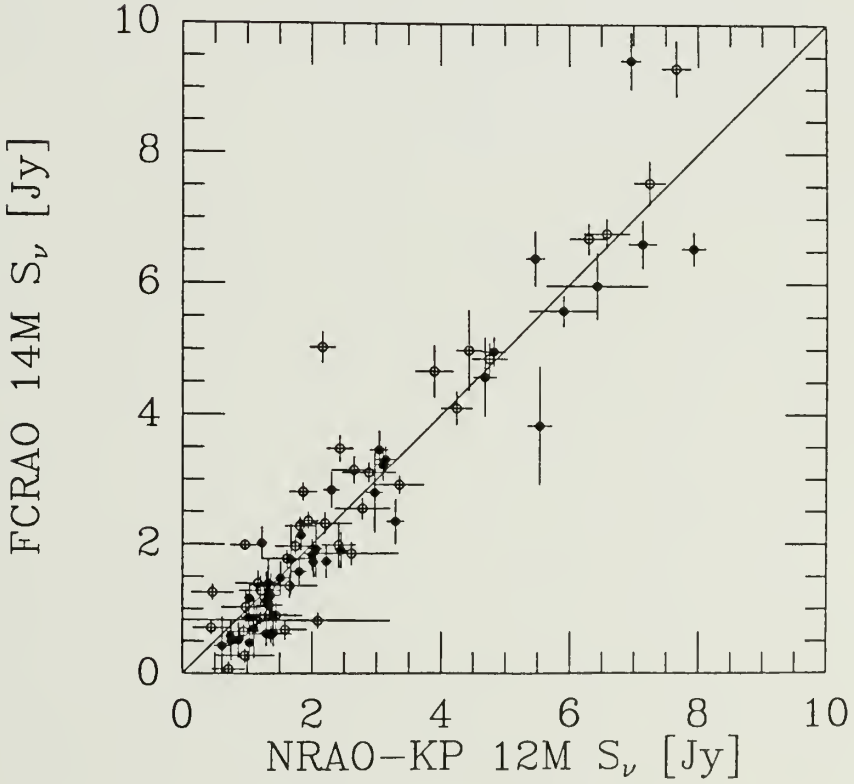
FCRAO 14M S_ν [Jy]
NRAO−KP 12M S_ν [Jy]
0
2
4
6
8
10

Figure 2.4. Plots of the λ3mm and λ7mm flux density versus time of 46 sources. Filled circles represent FCRAO measurements. Open circles are from The NRAO Kitt Peak 12 meter. Most measurements were made at 88.2 (FCRAO) or 89.6 GHz (NRAO-KP). Filled squares are FCRAO measurements made at 40.0 GHz. Crosses shown in the OJ 287 plot were made at 77 GHz and are from Teräsranta et al. 1987.

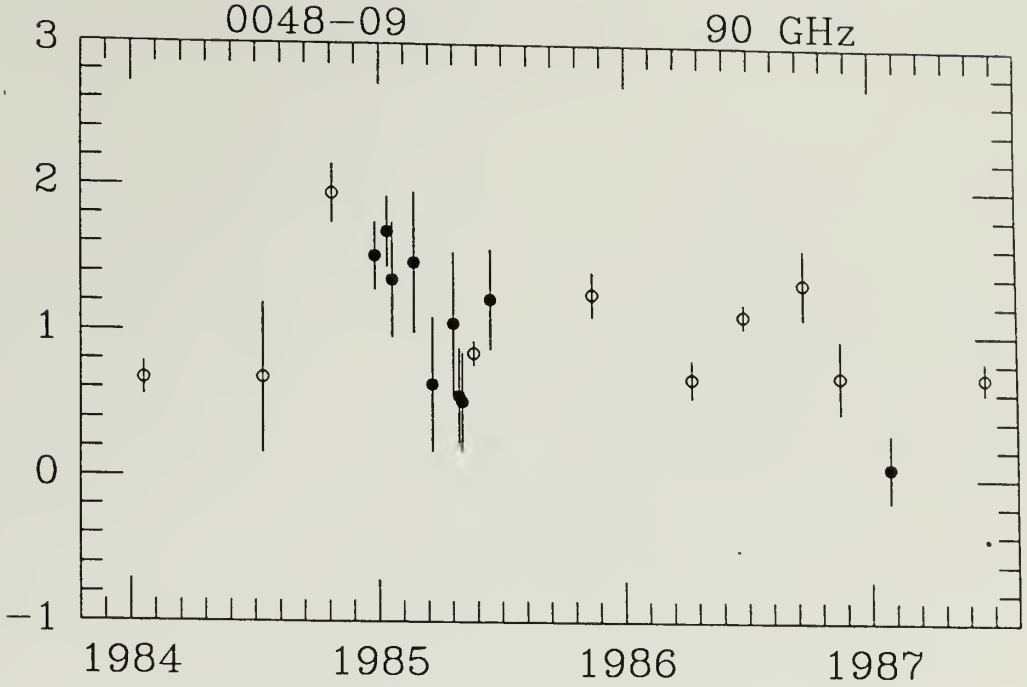

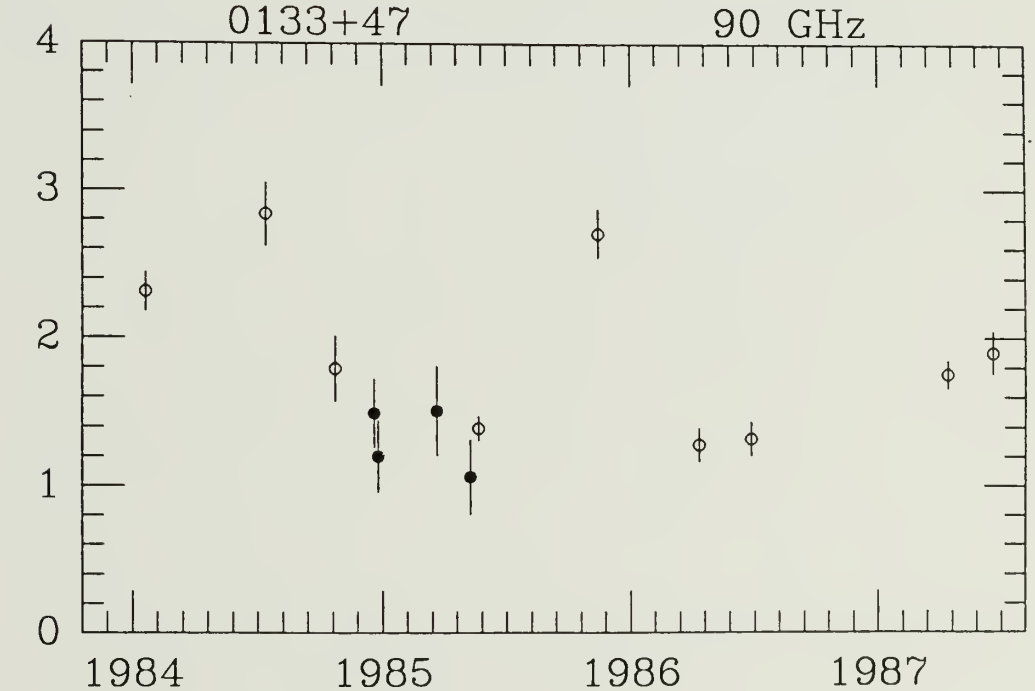

(continued next page)

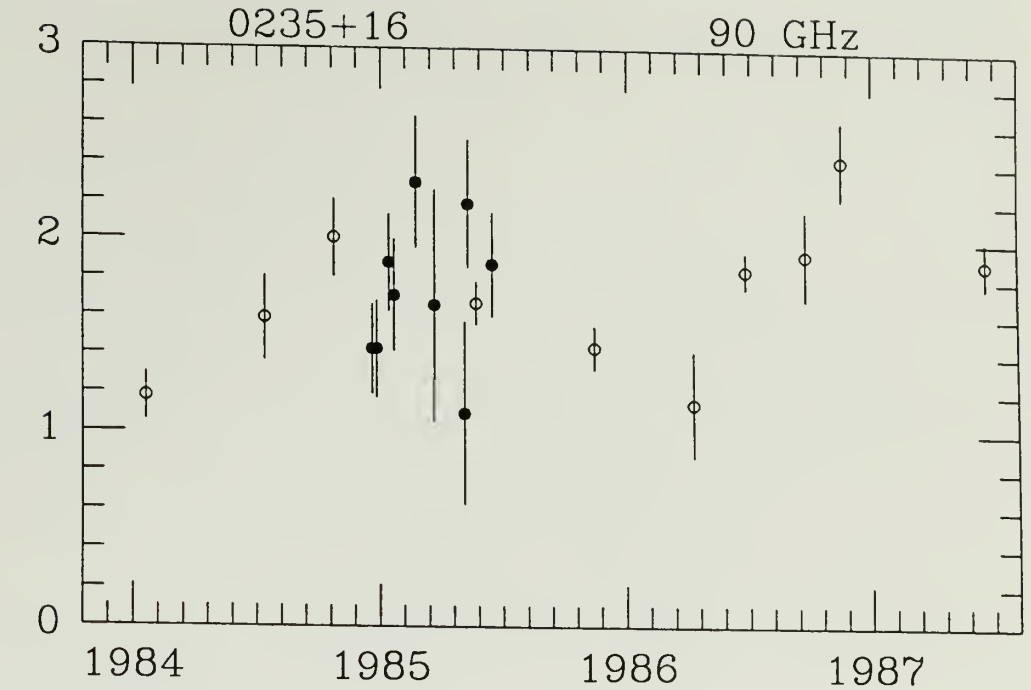

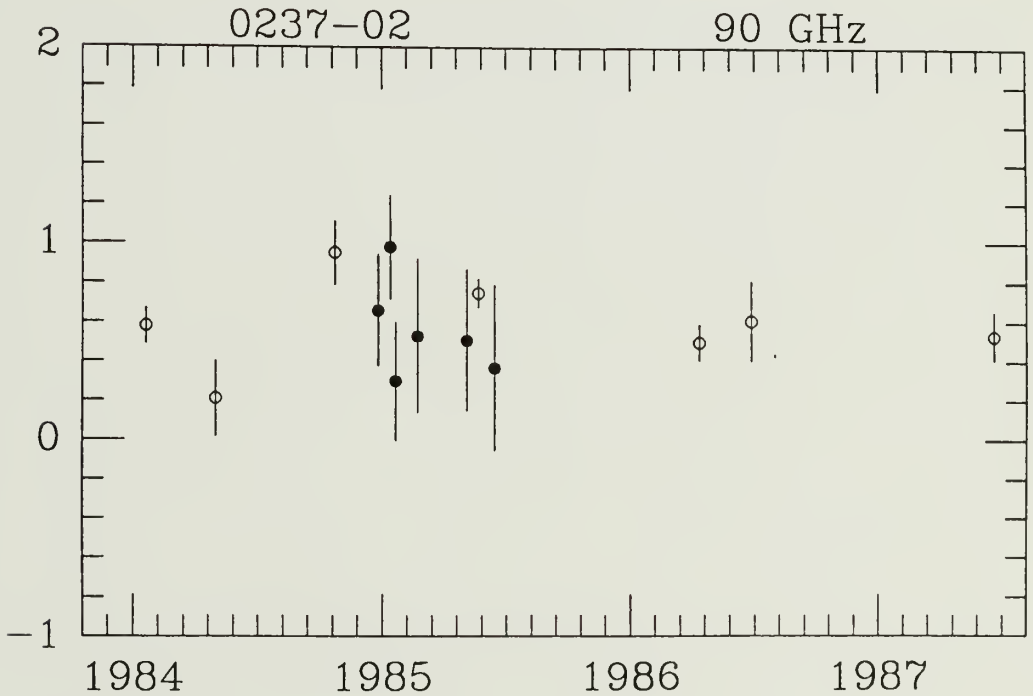

Figure 2.4 continued

(continued next page)

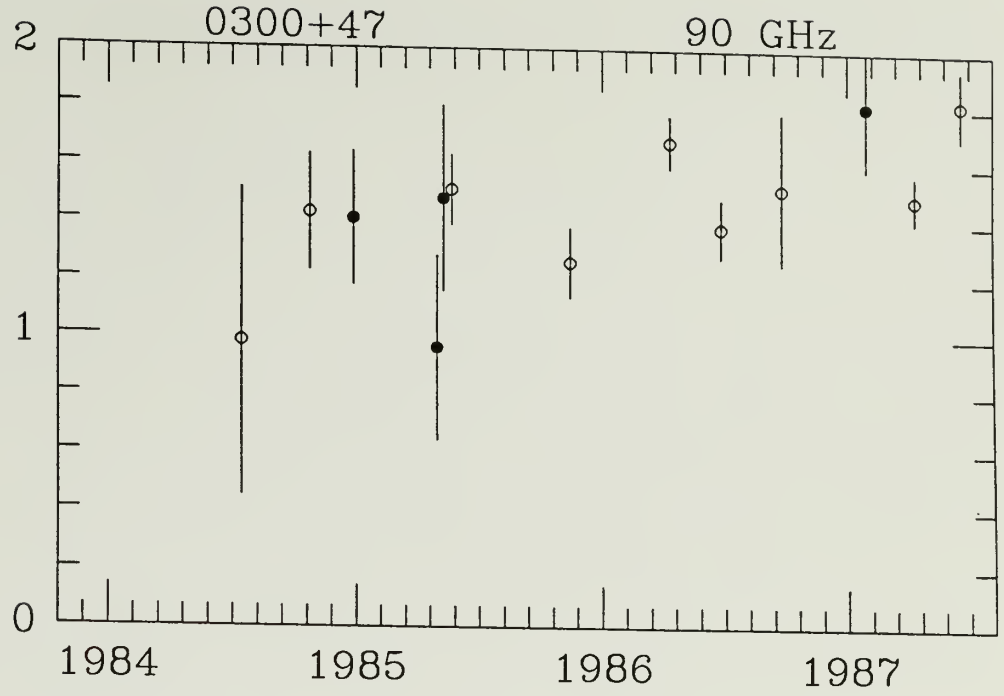

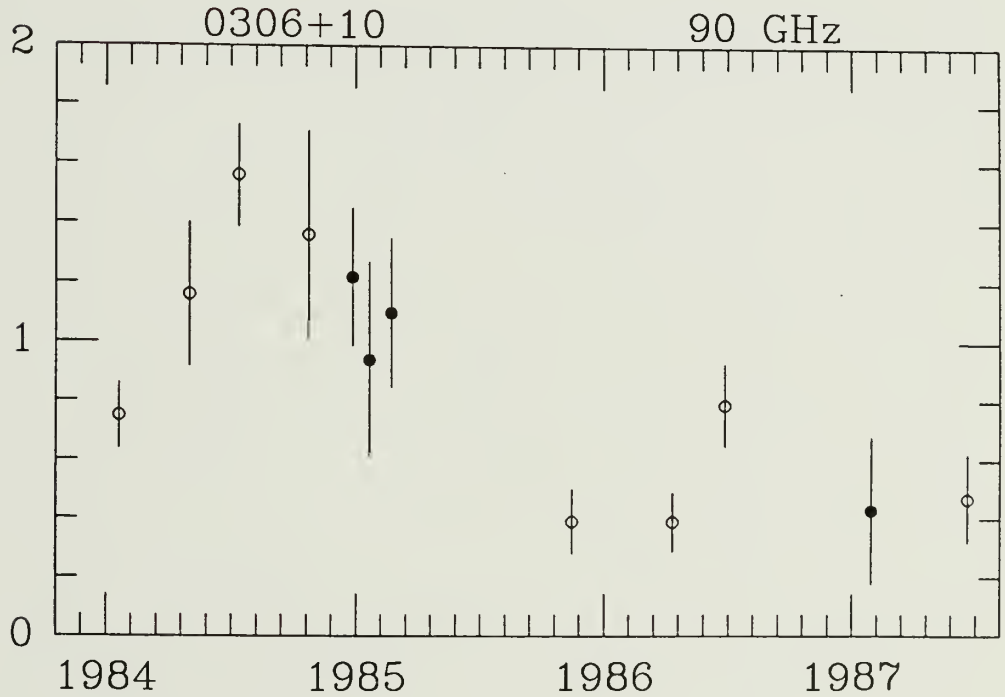

Figure 2.4 continued

(continued next page)

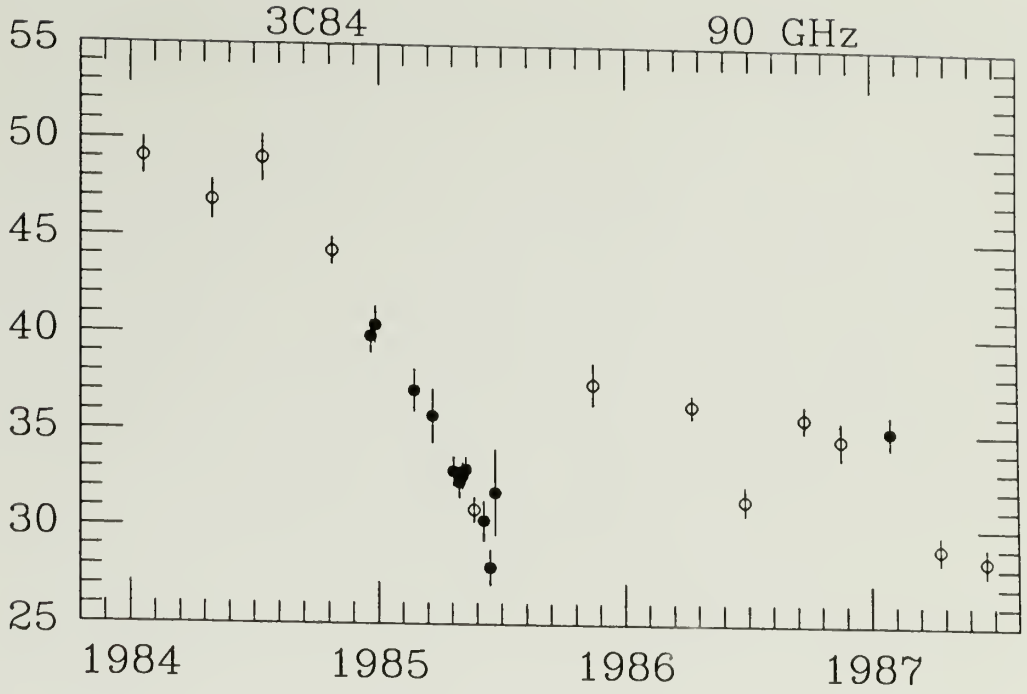

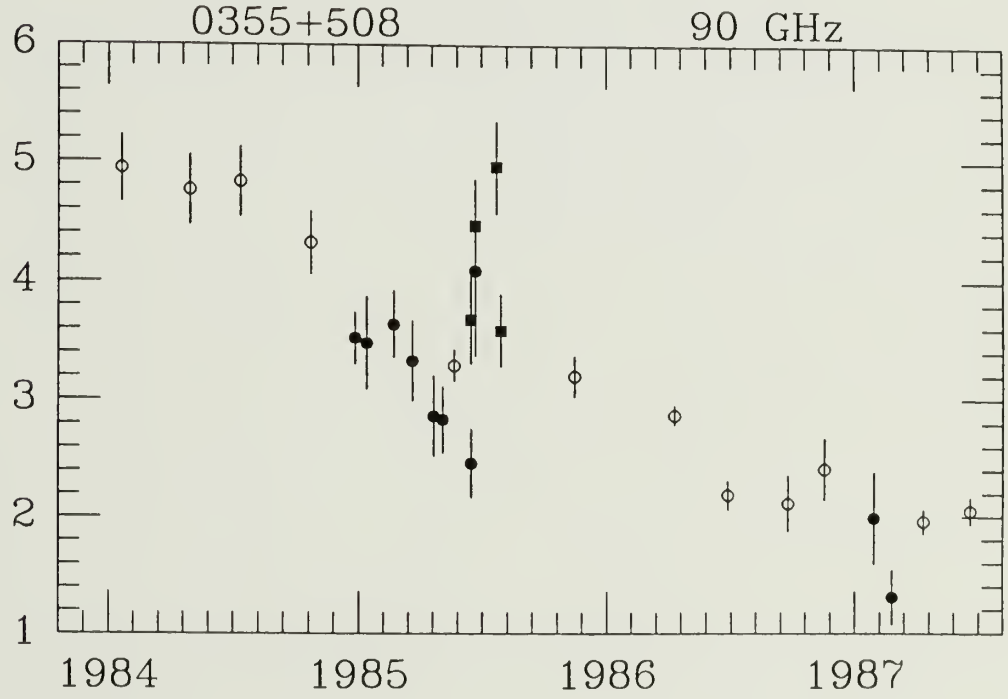

Figure 2.4 continued

(continued next page)

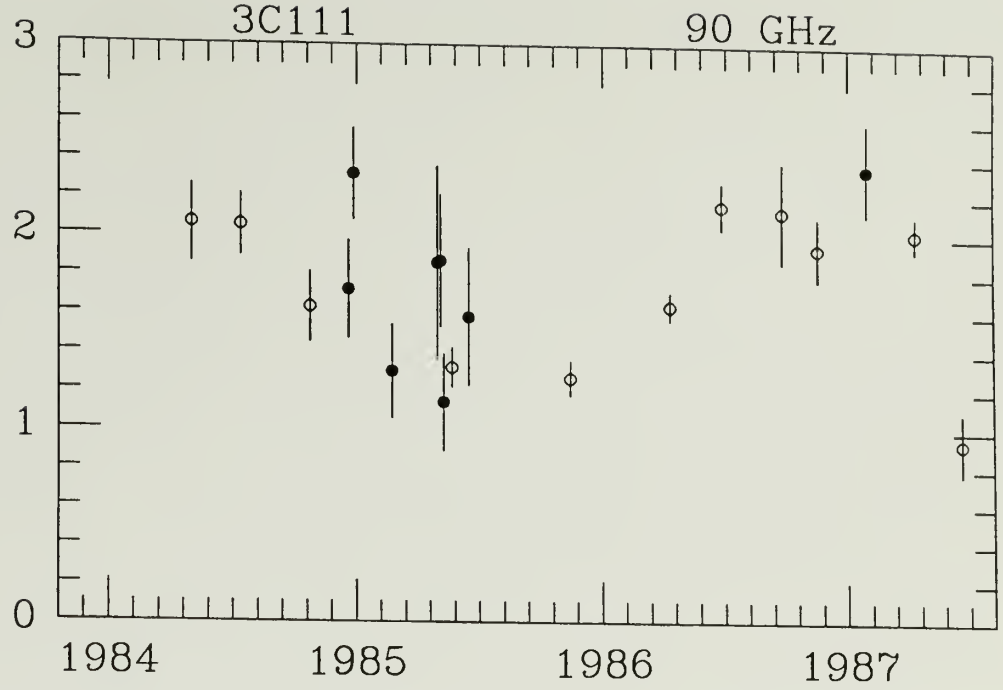

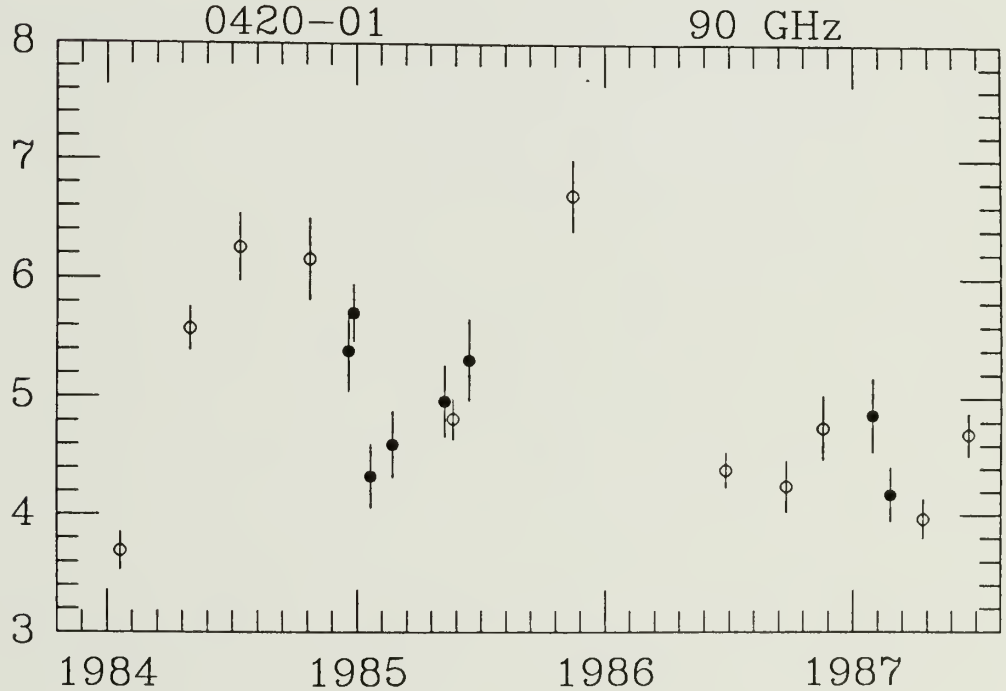

Figure 2.4 continued

(continued next page)

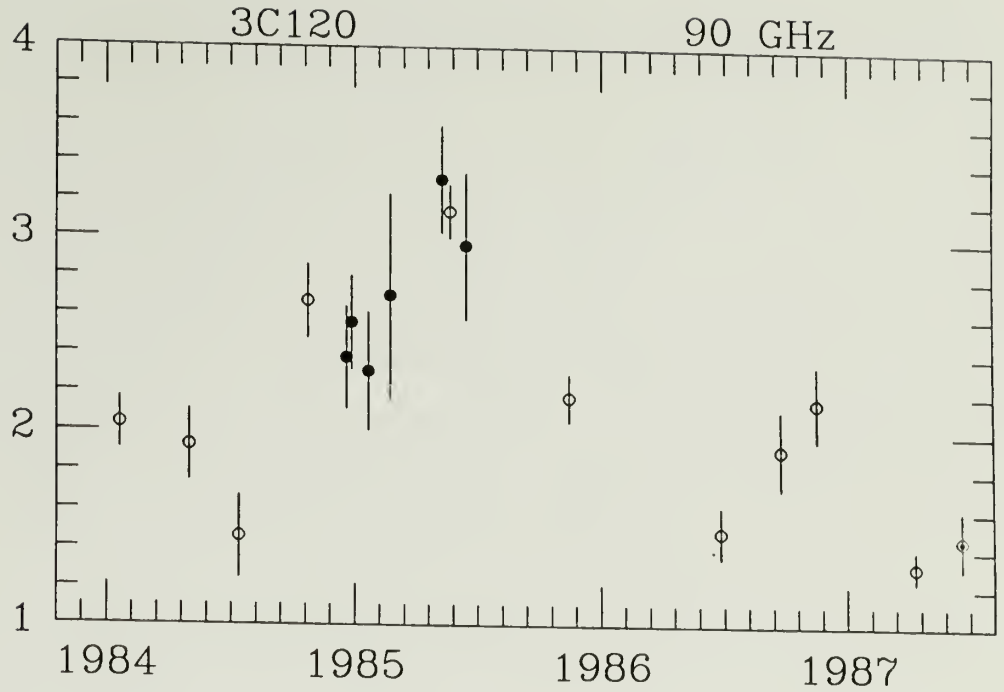

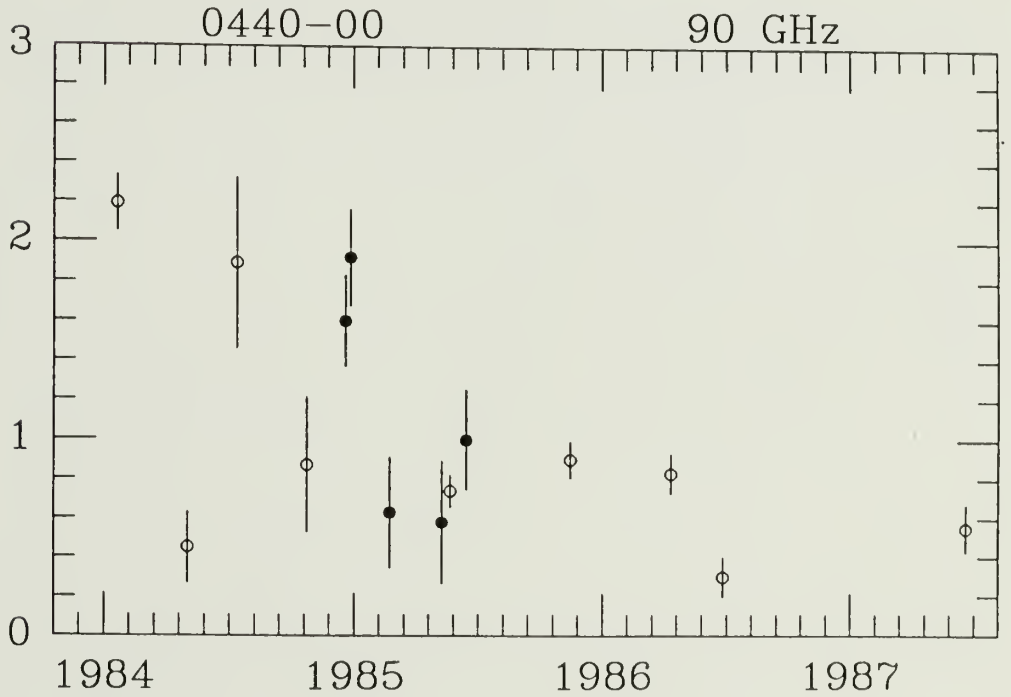

Figure 2.4 continued

(continued next page)

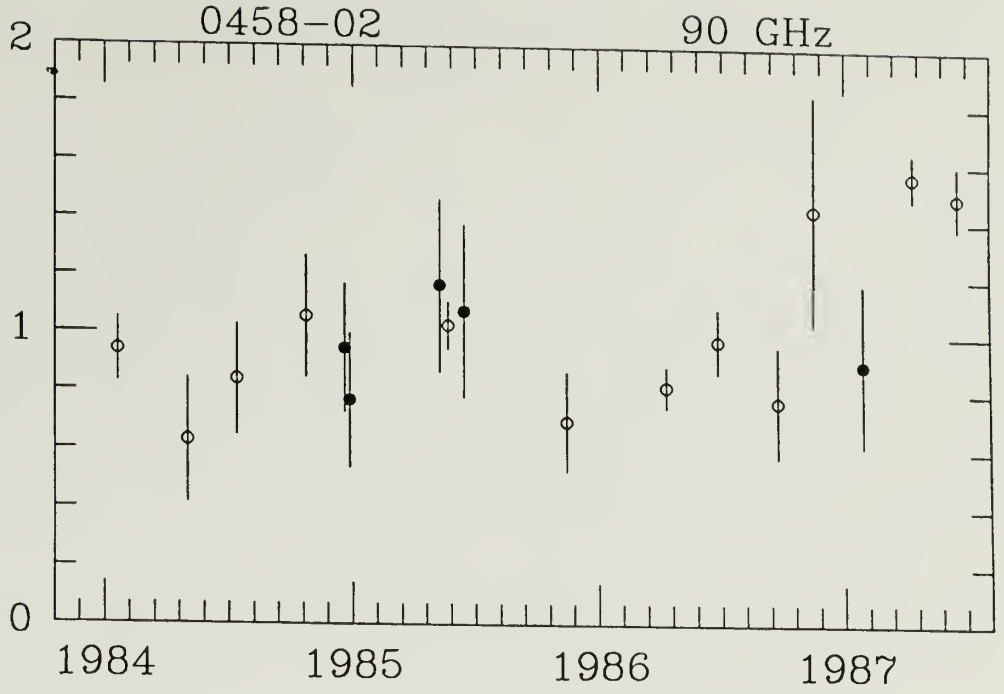

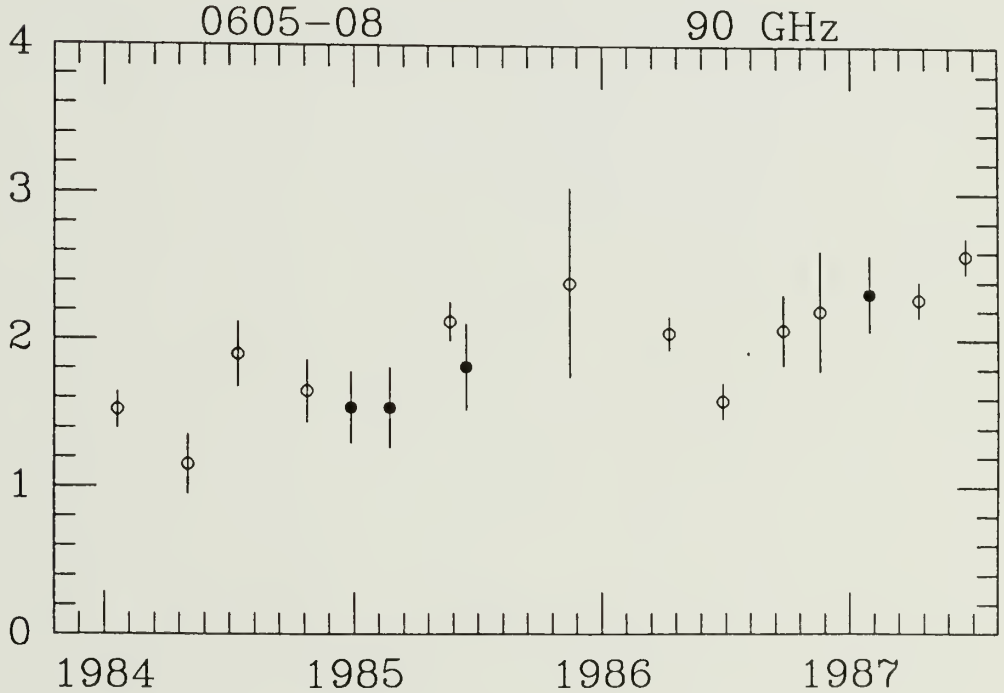

Figure 2.4 continued

(continued next page)

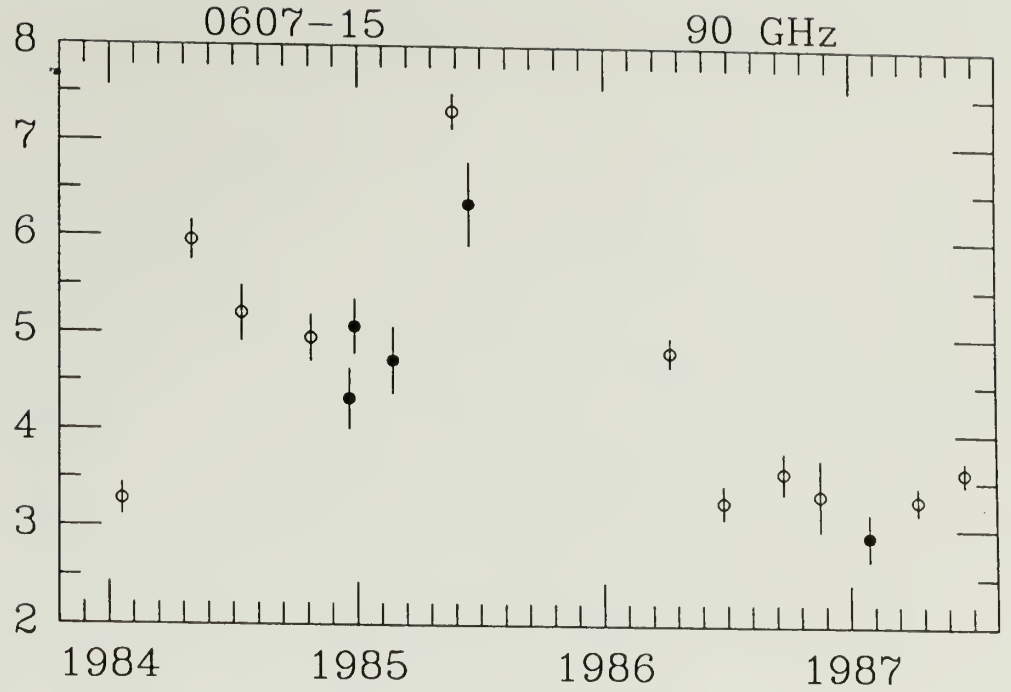

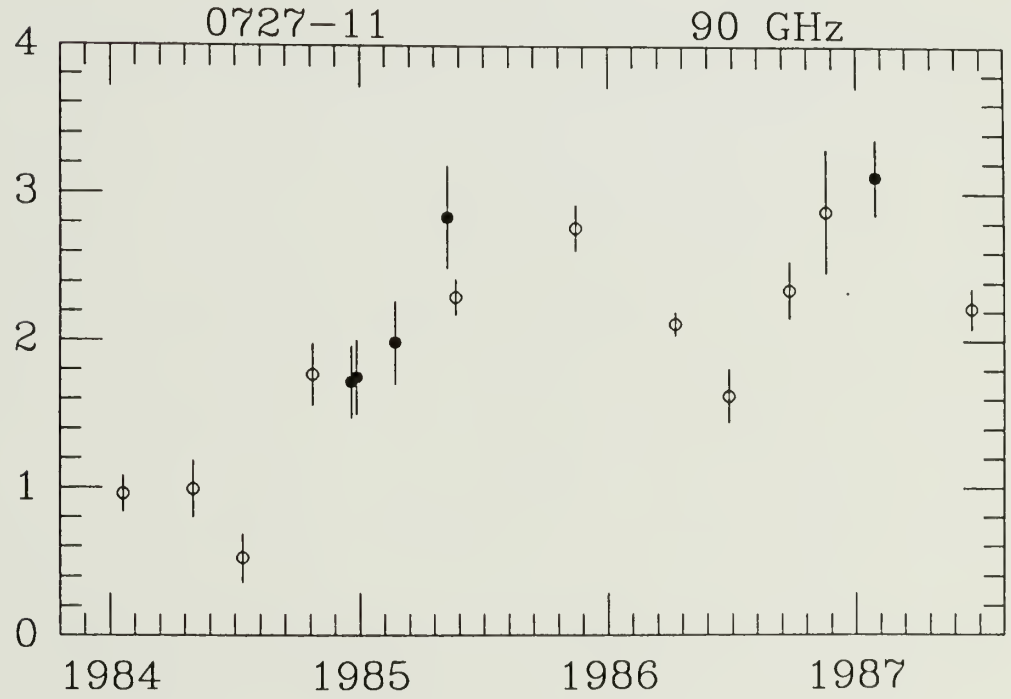

Figure 2.4 continued

(continued next page)

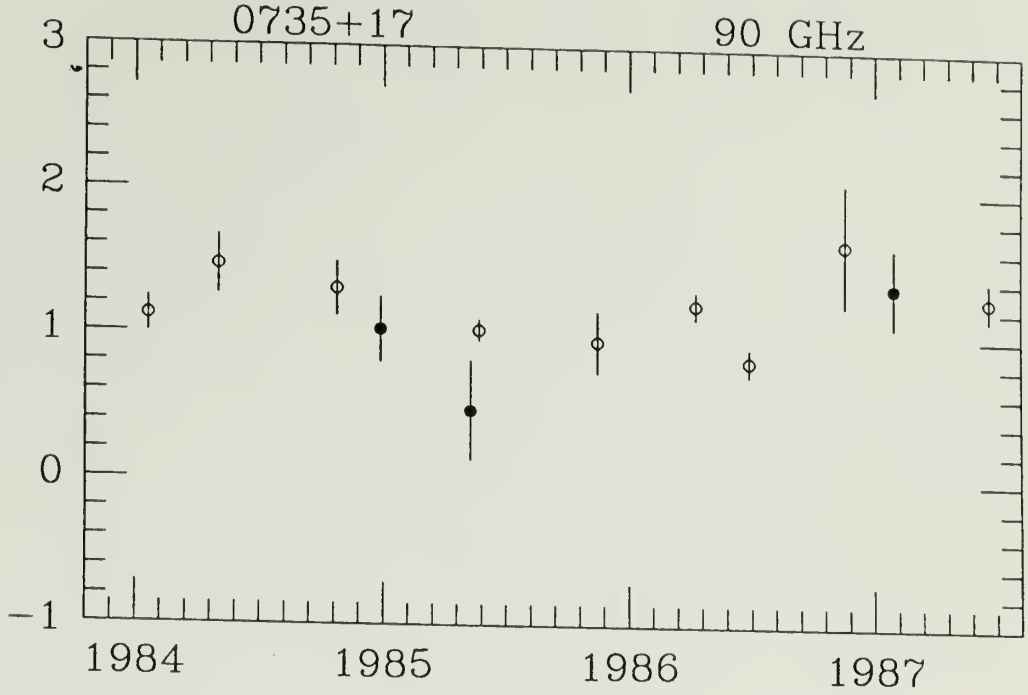

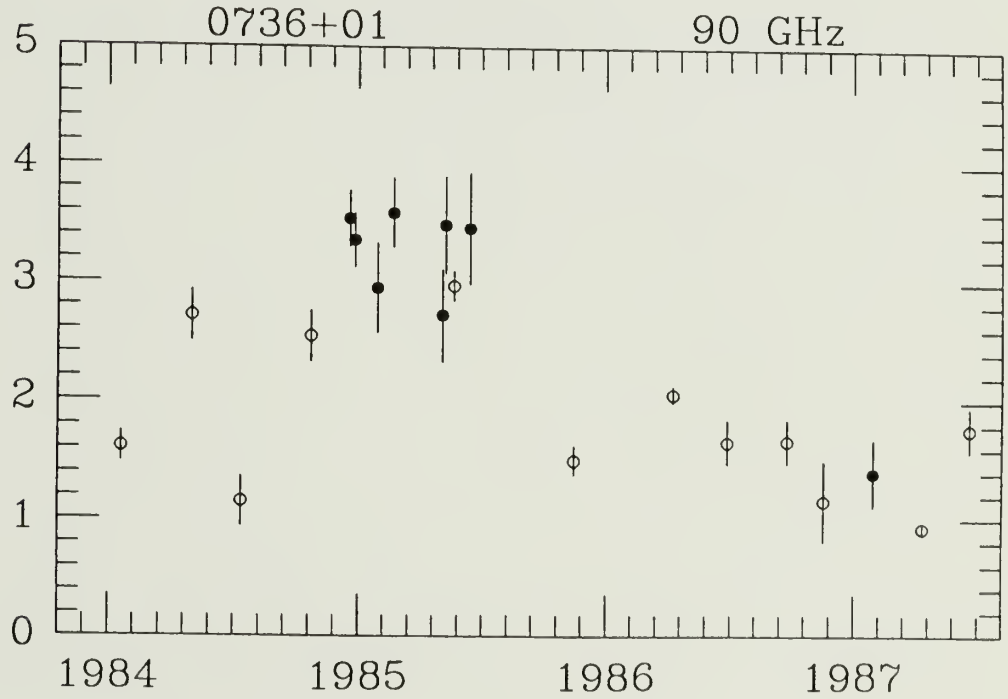

Figure 2.4 continued

(continued next page)

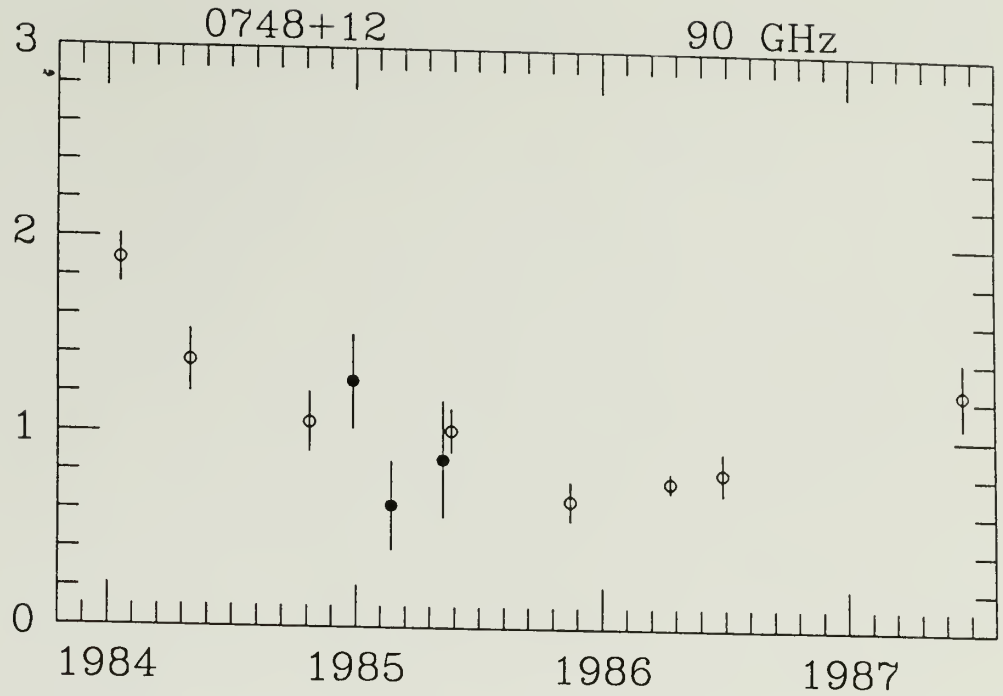

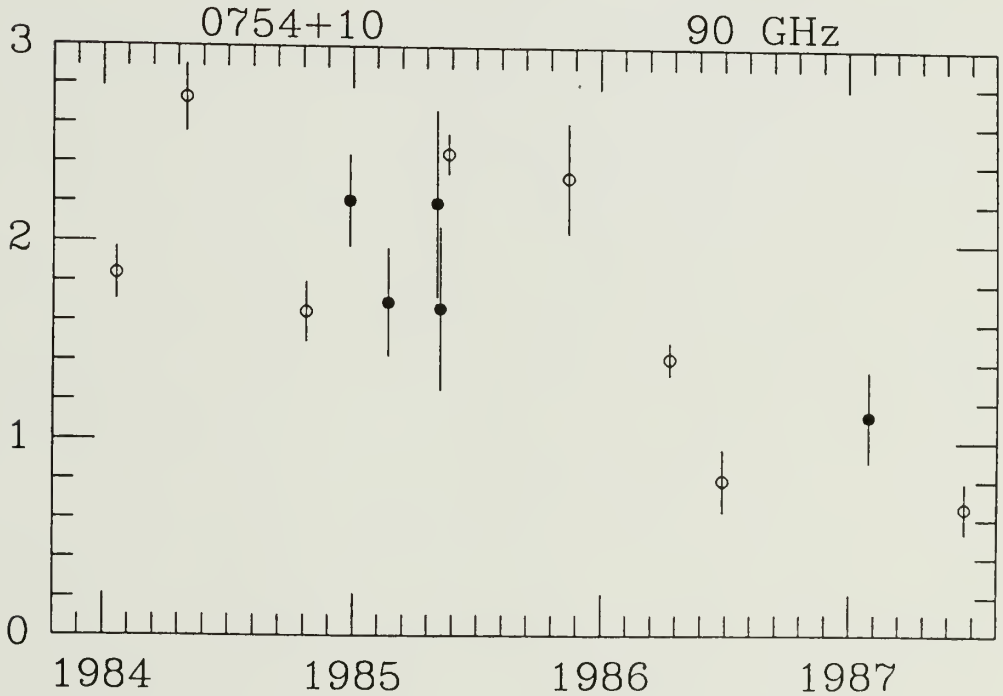

Figure 2.4 continued

(continued next page)

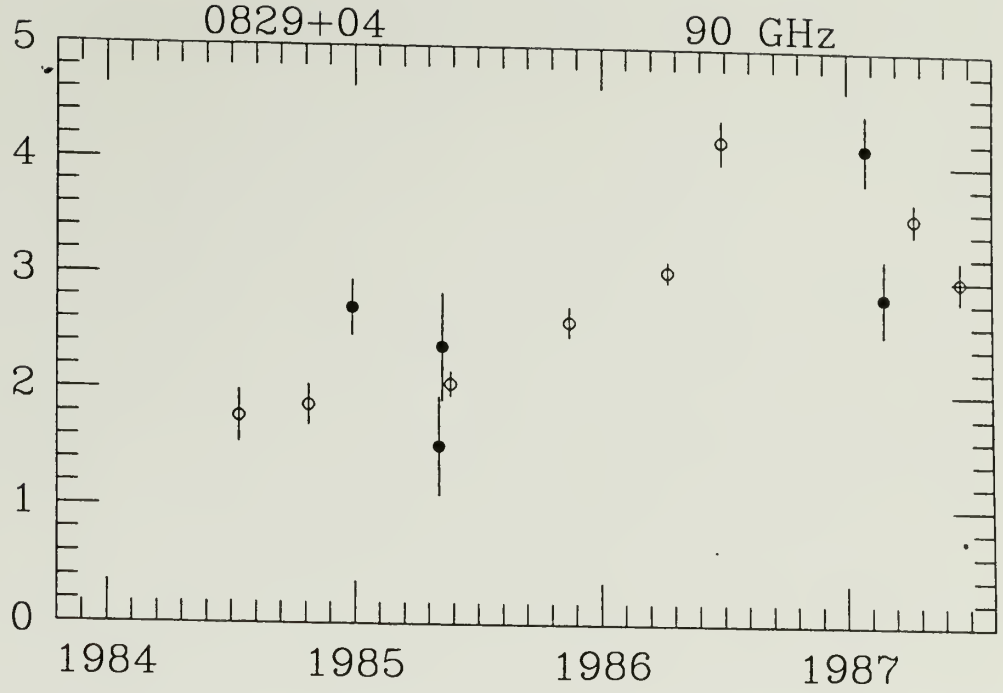

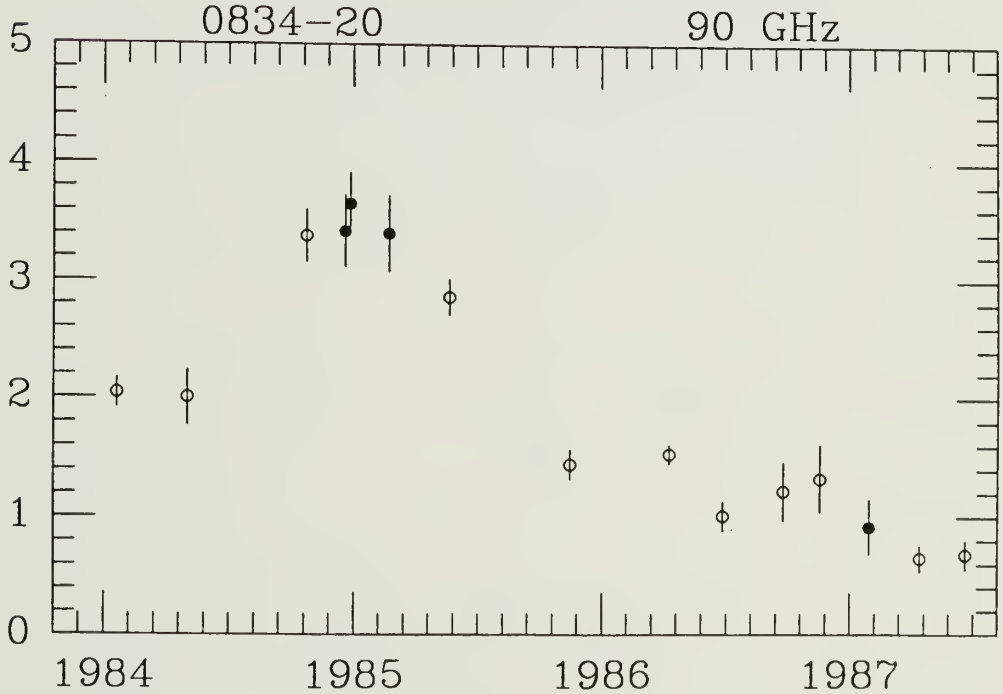

Figure 2.4 continued

(continued next page)

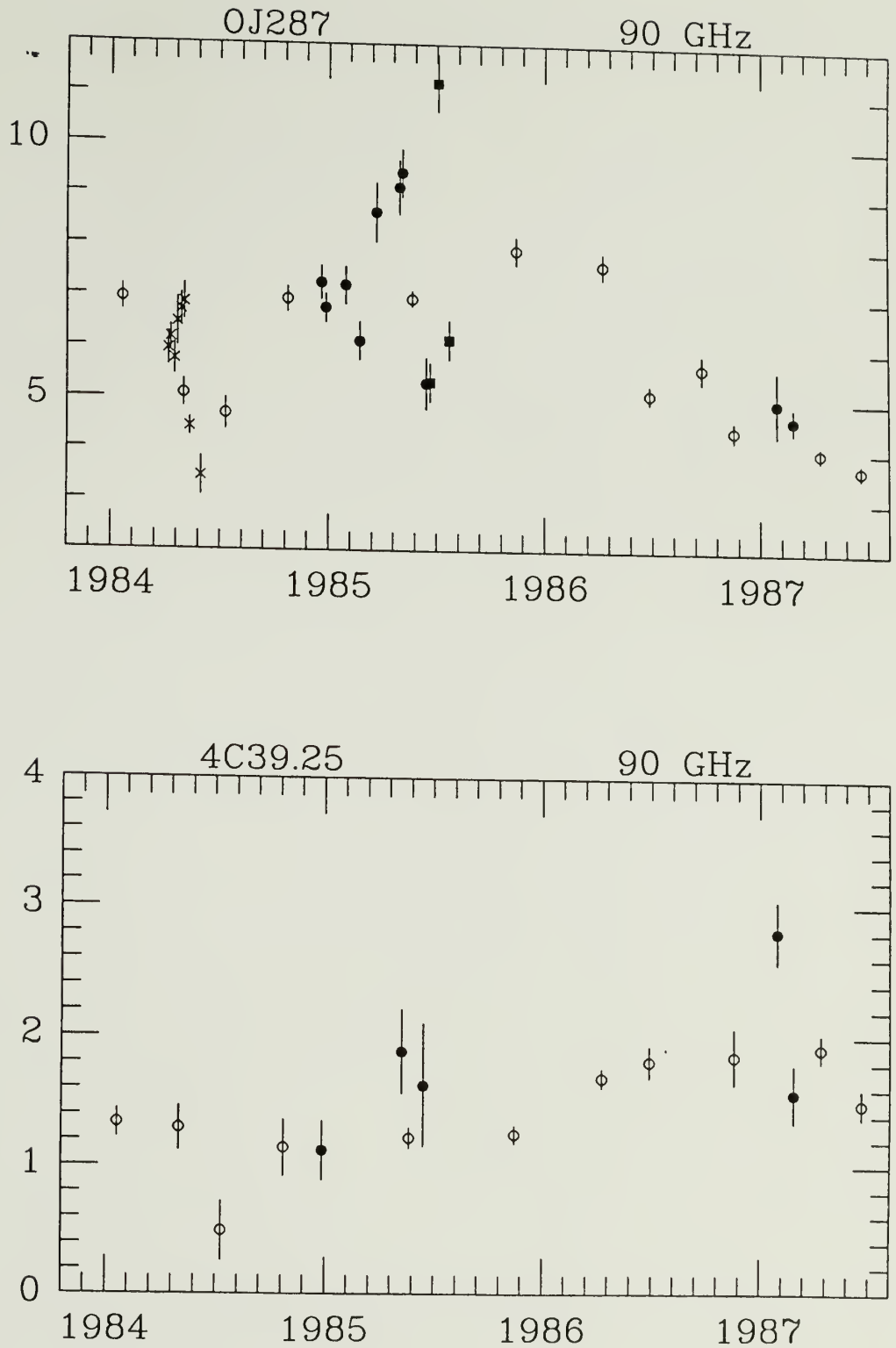

Figure 2.4 continued

(continued next page)

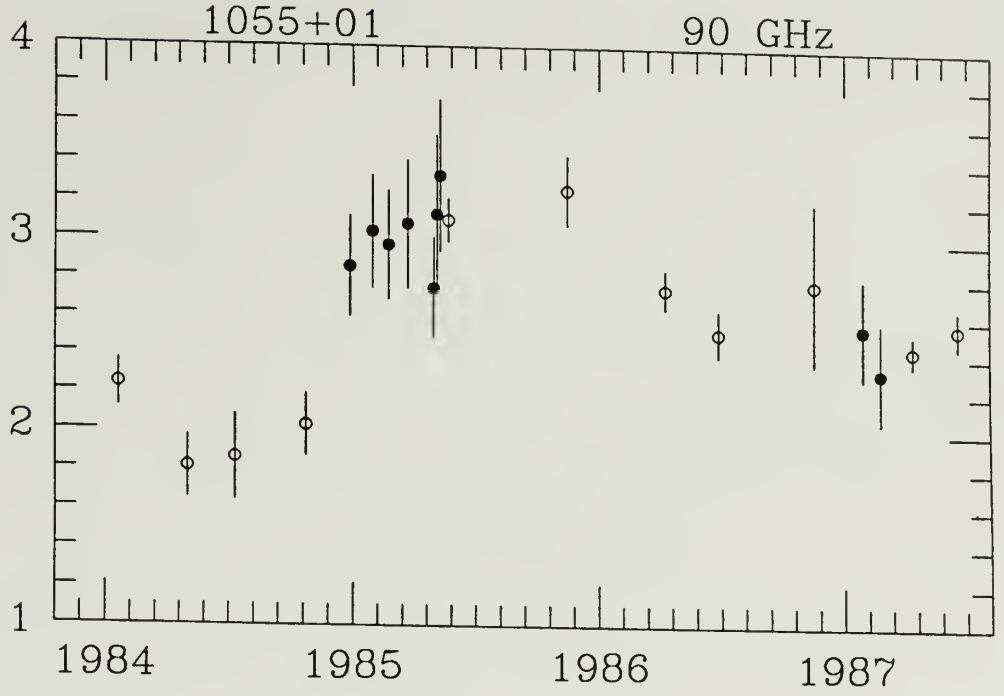

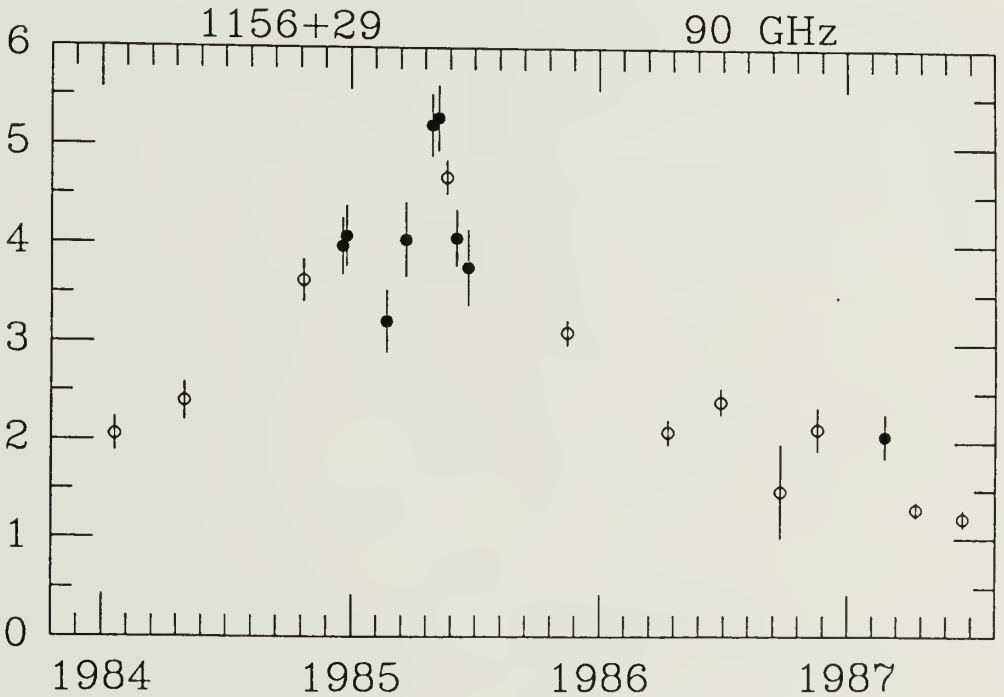

Figure 2.4 continued

(continued next page)

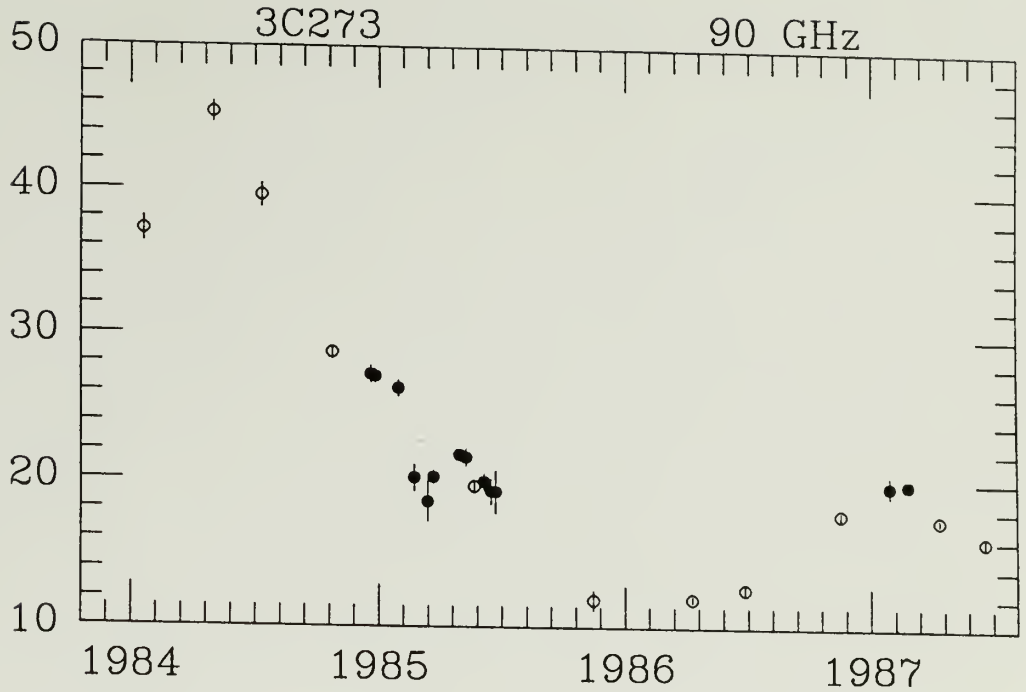

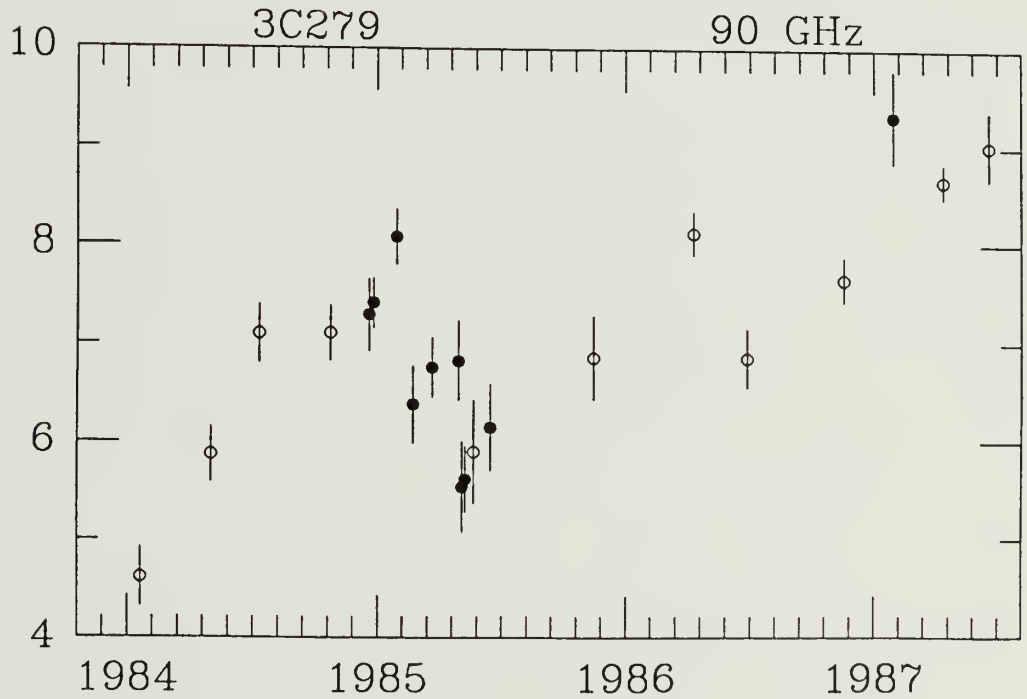

Figure 2.4 continued

(continued next page)

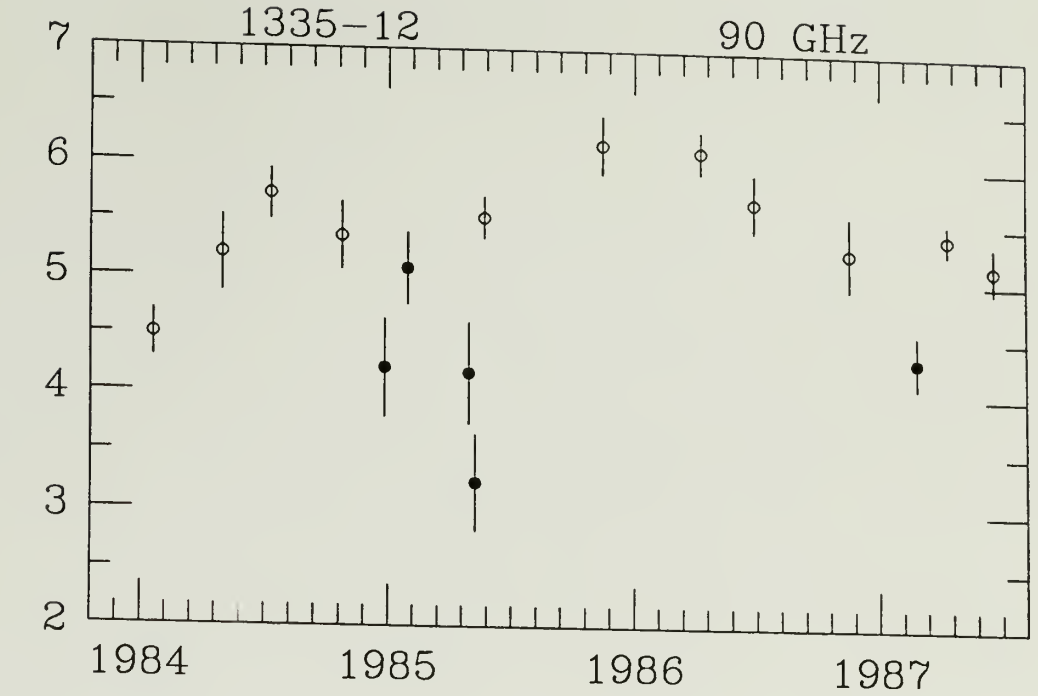

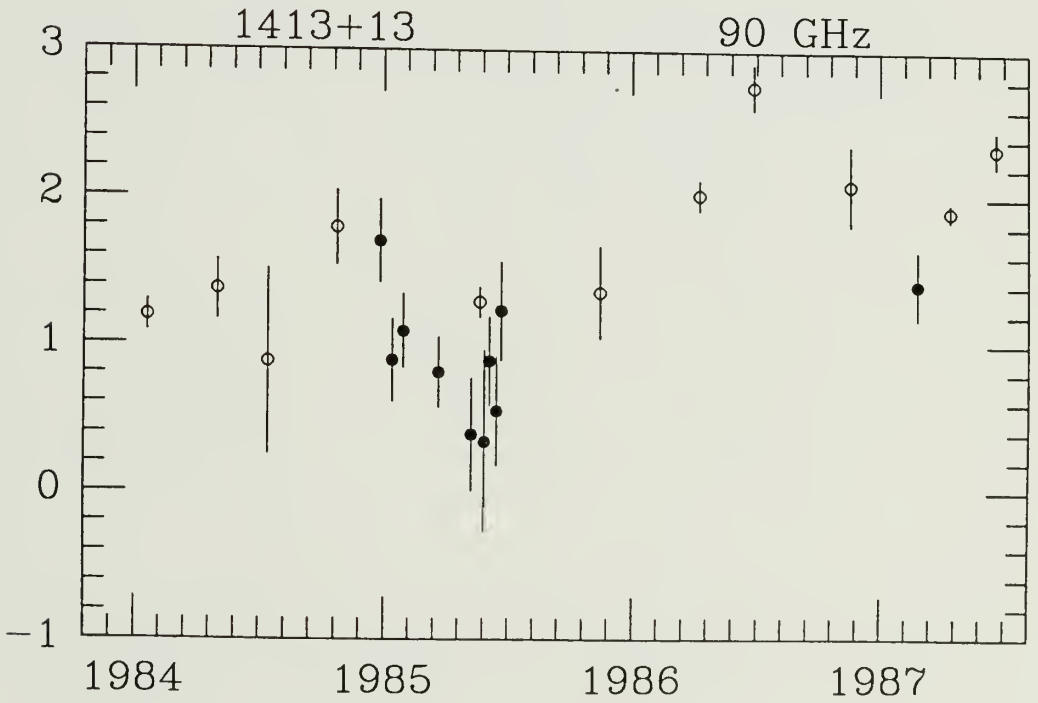

Figure 2.4 continued

(continued next page)

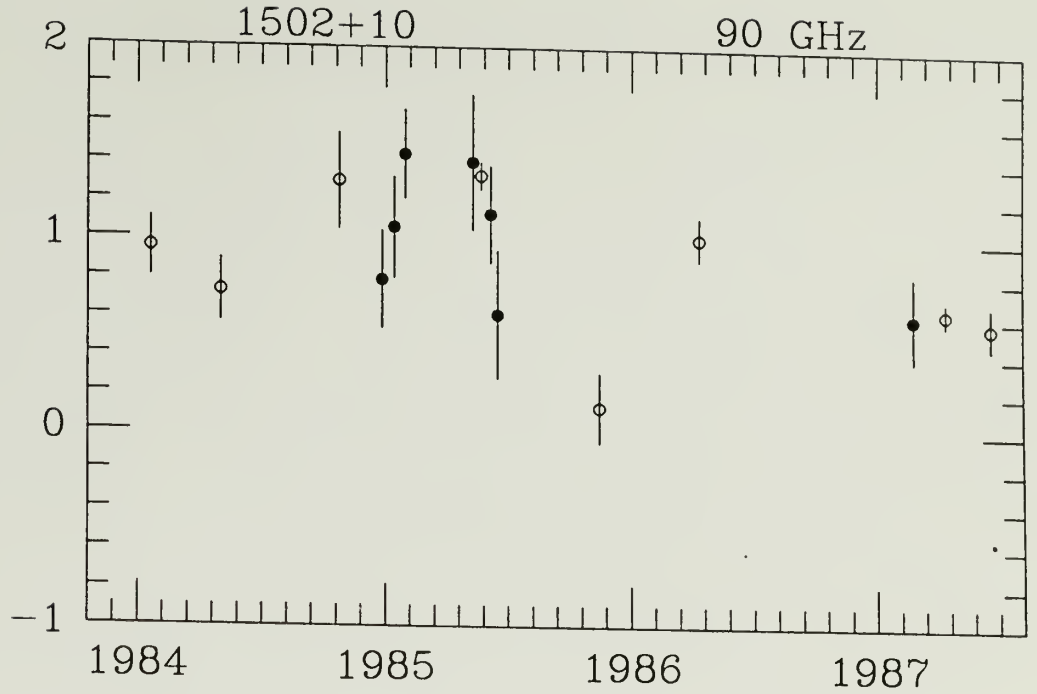

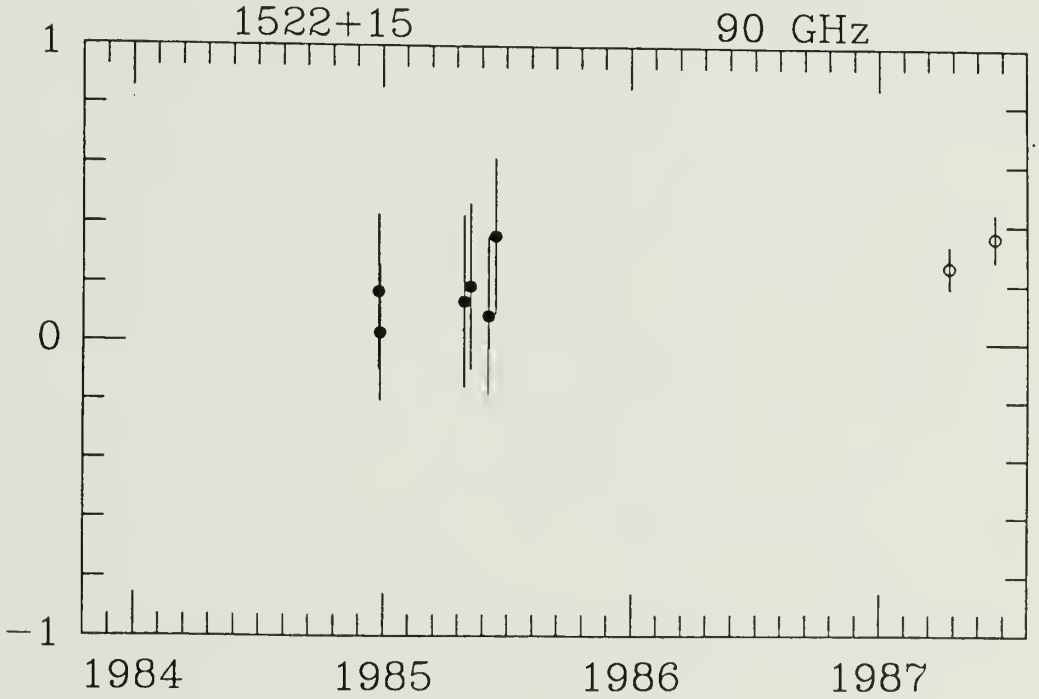

Figure 2.4 continued

(continued next page)

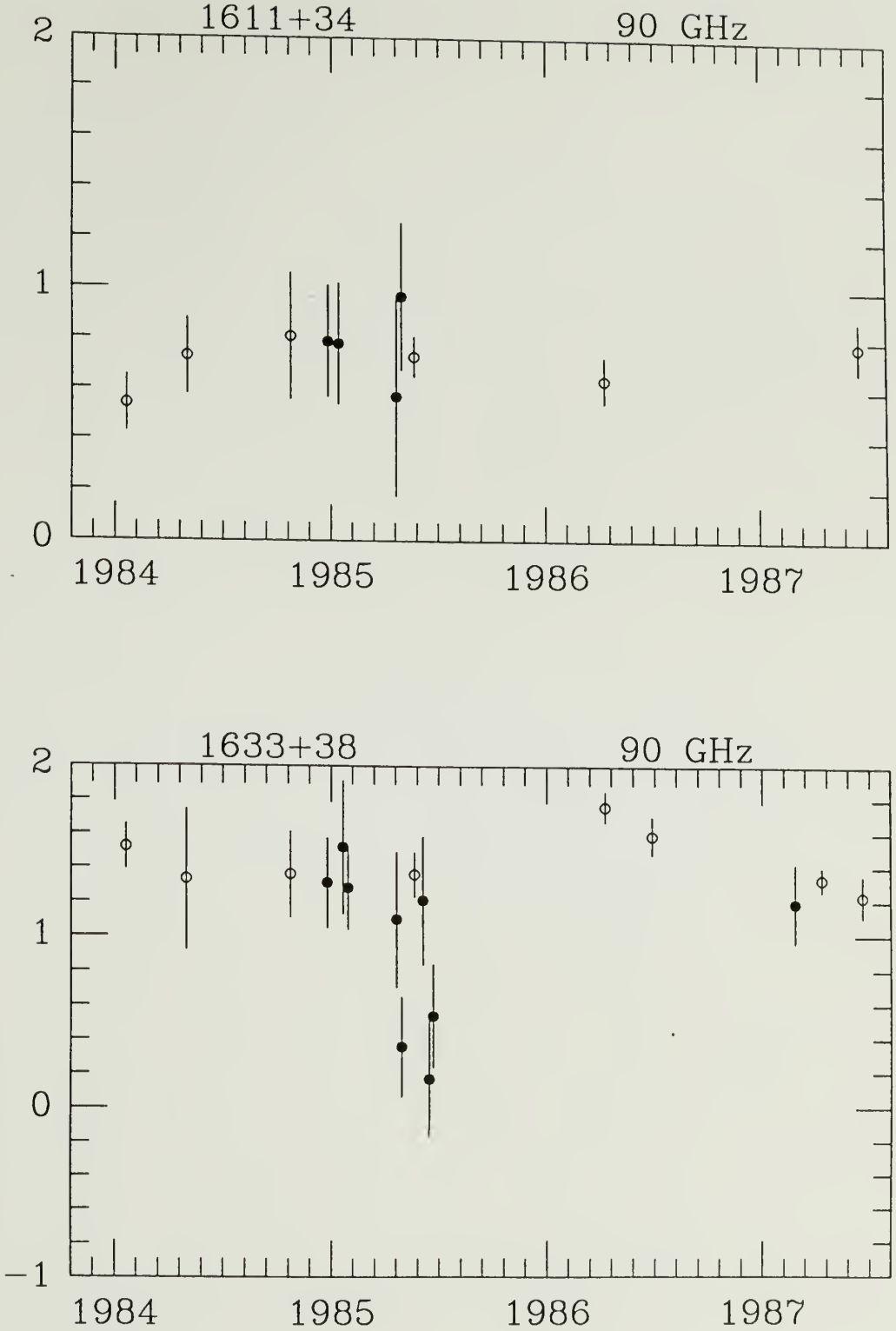

Figure 2.4 continued

(continued next page)

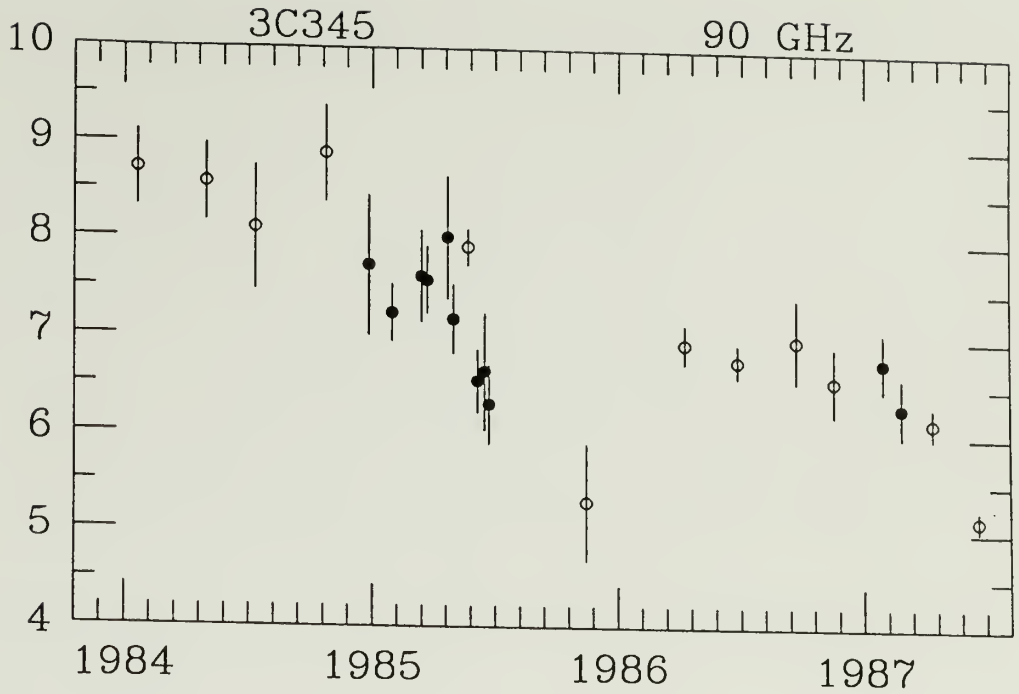

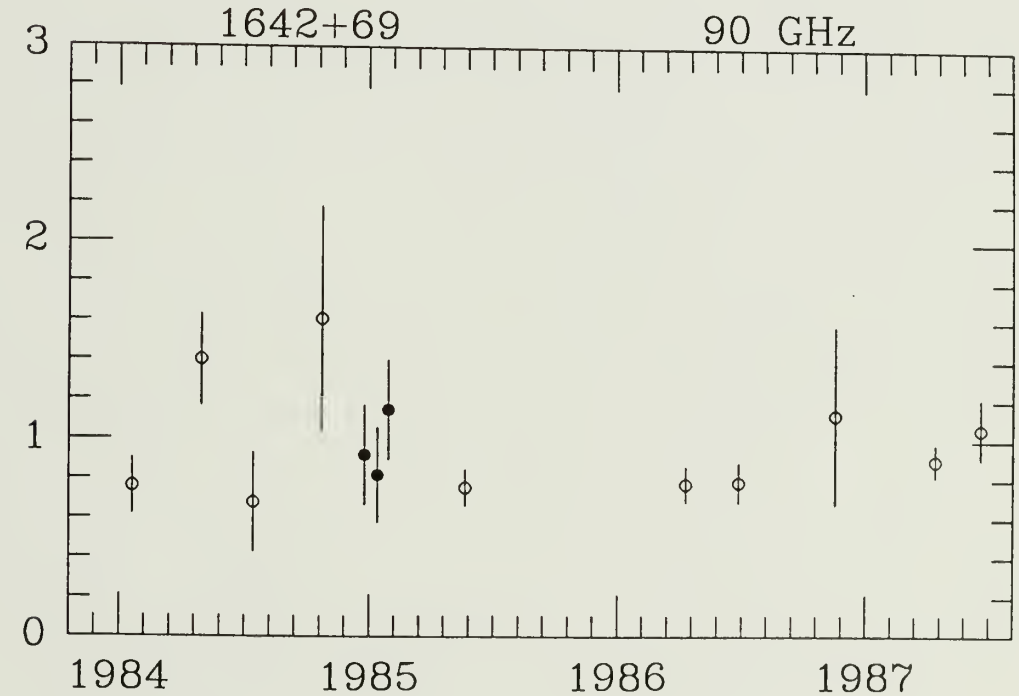

Figure 2.4 continued

(continued next page)

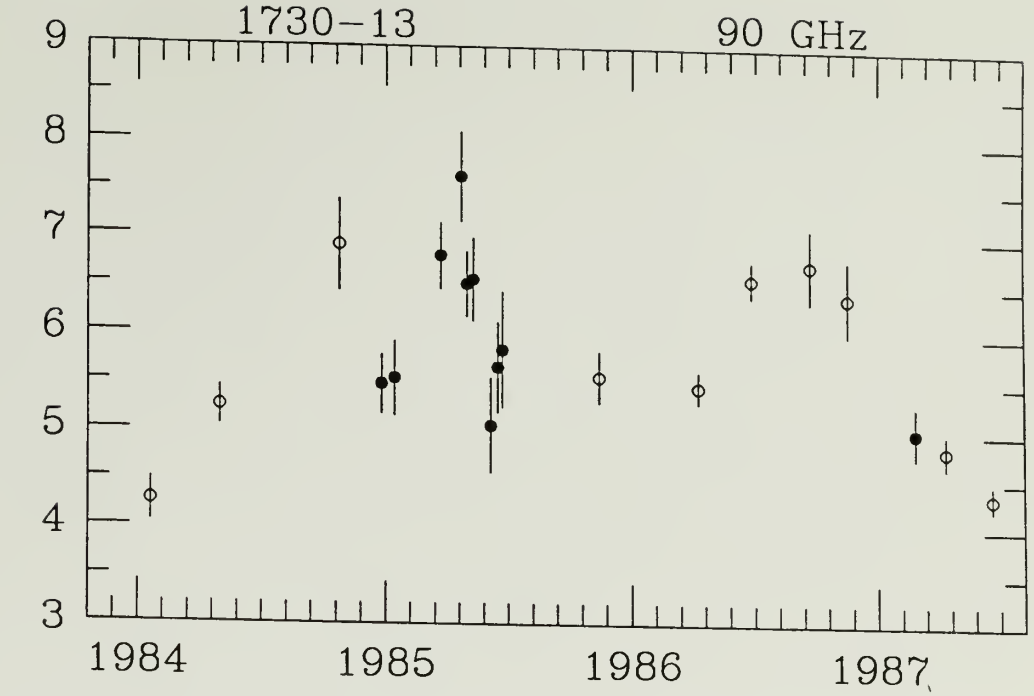

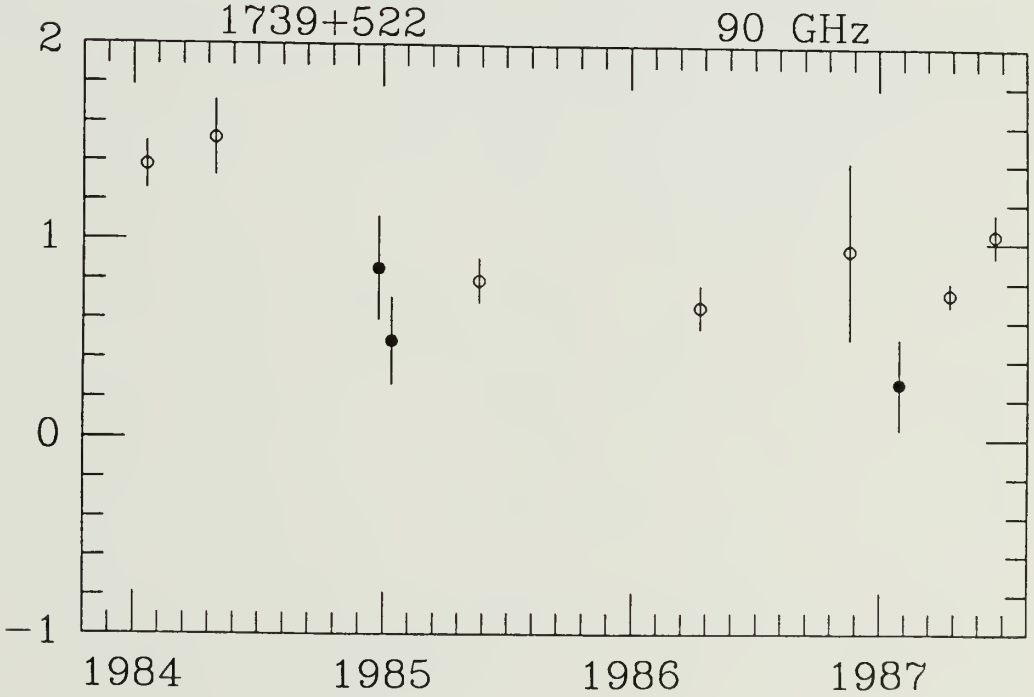

Figure 2.4 continued

(continued next page)

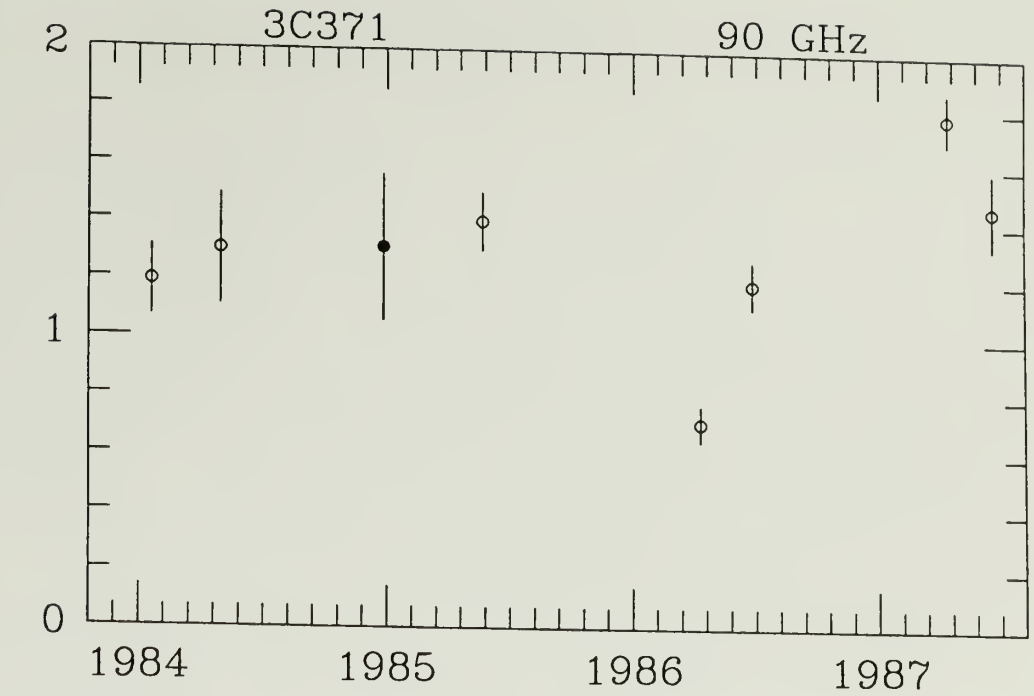

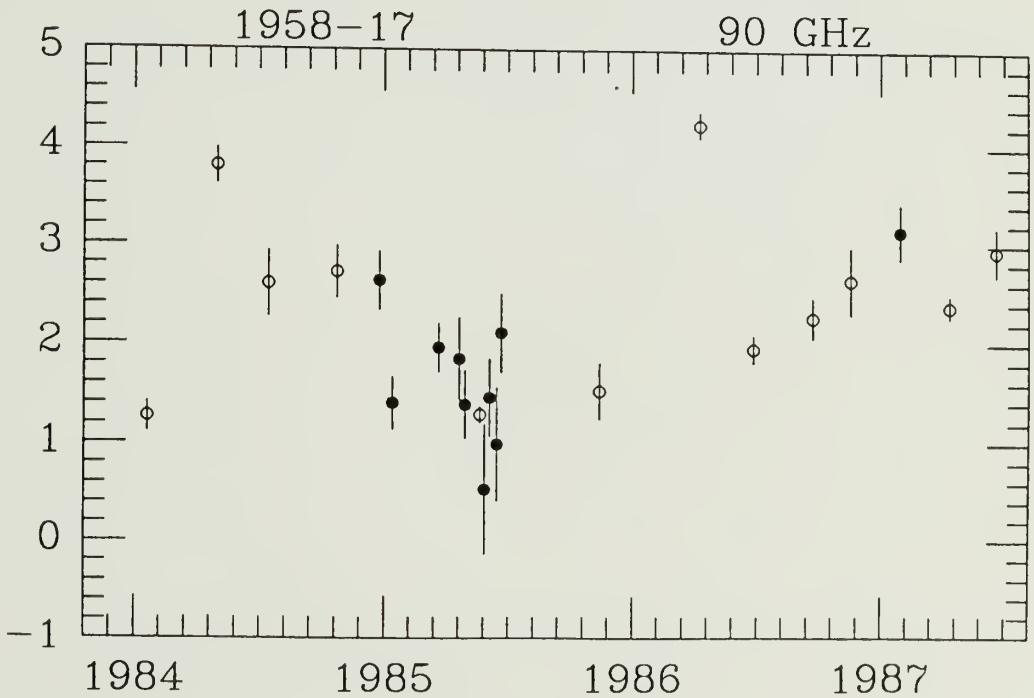

Figure 2.4 continued

(continued next page)

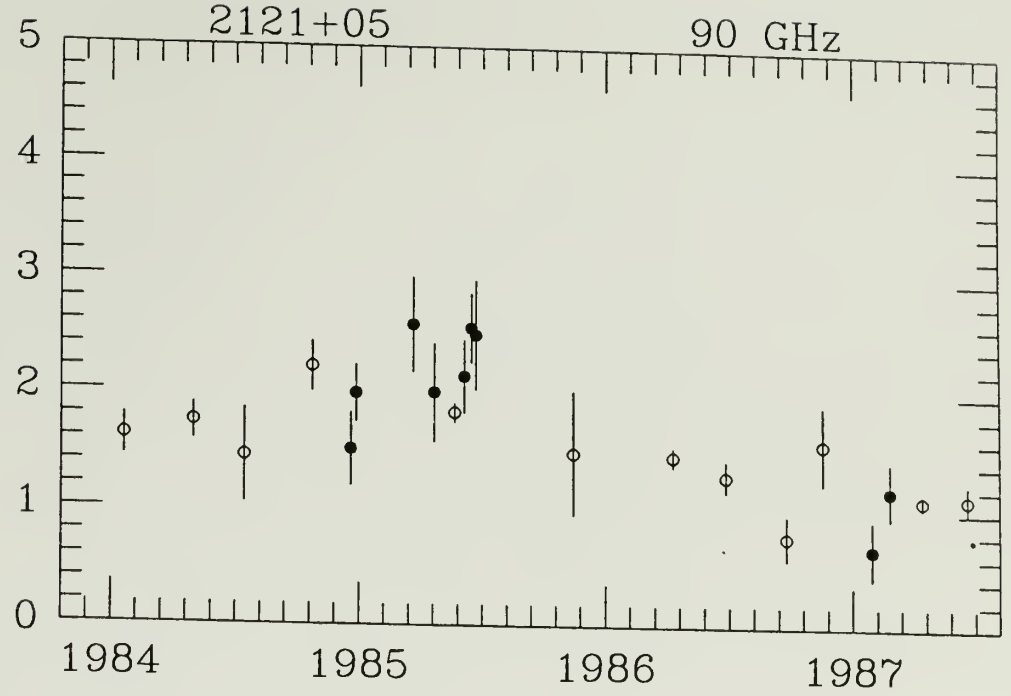

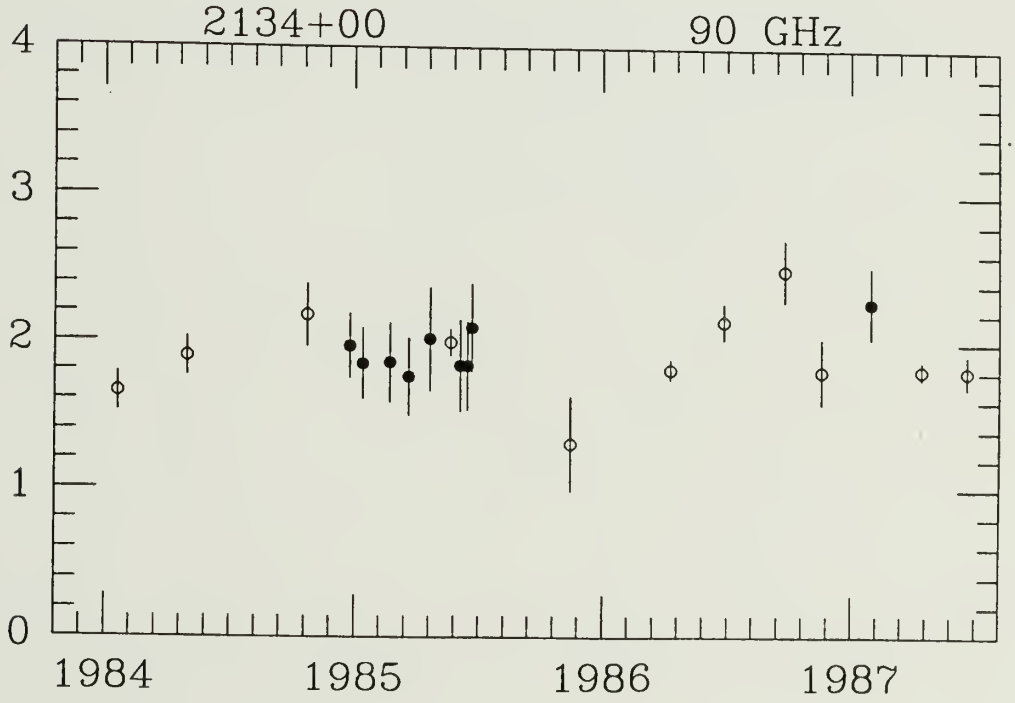

Figure 2.4 continued

(continued next page)

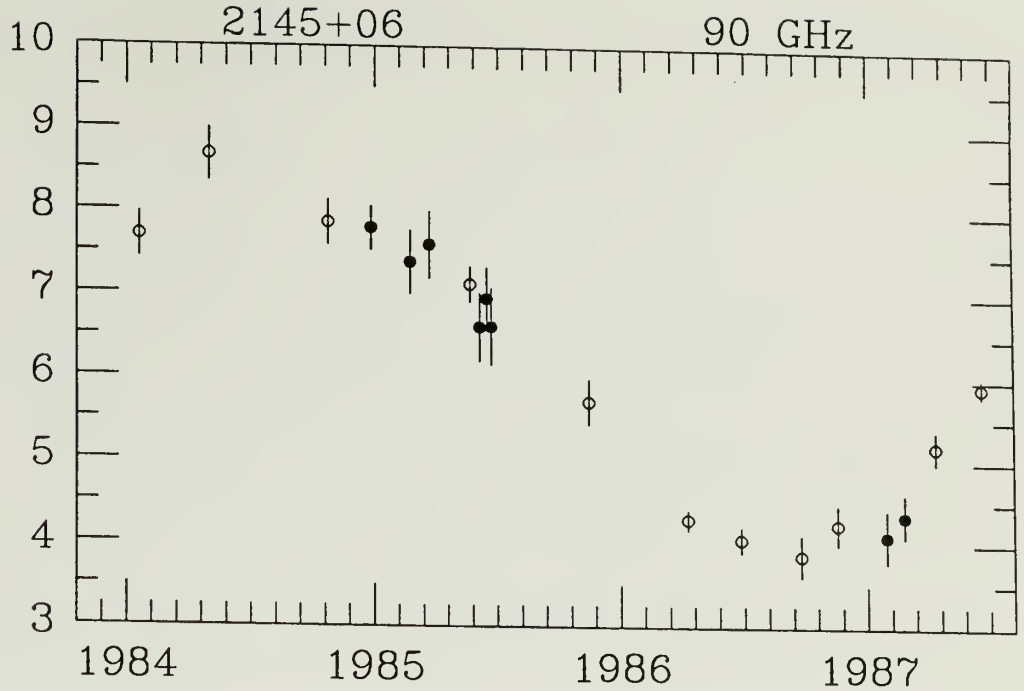

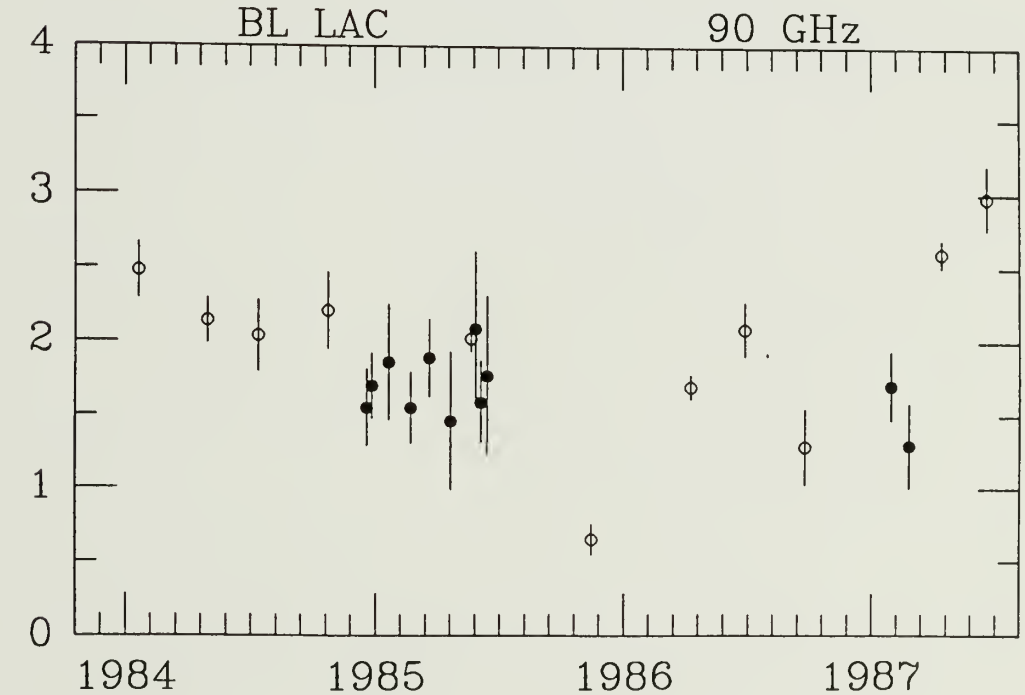

Figure 2.4 continued

(continued next page)

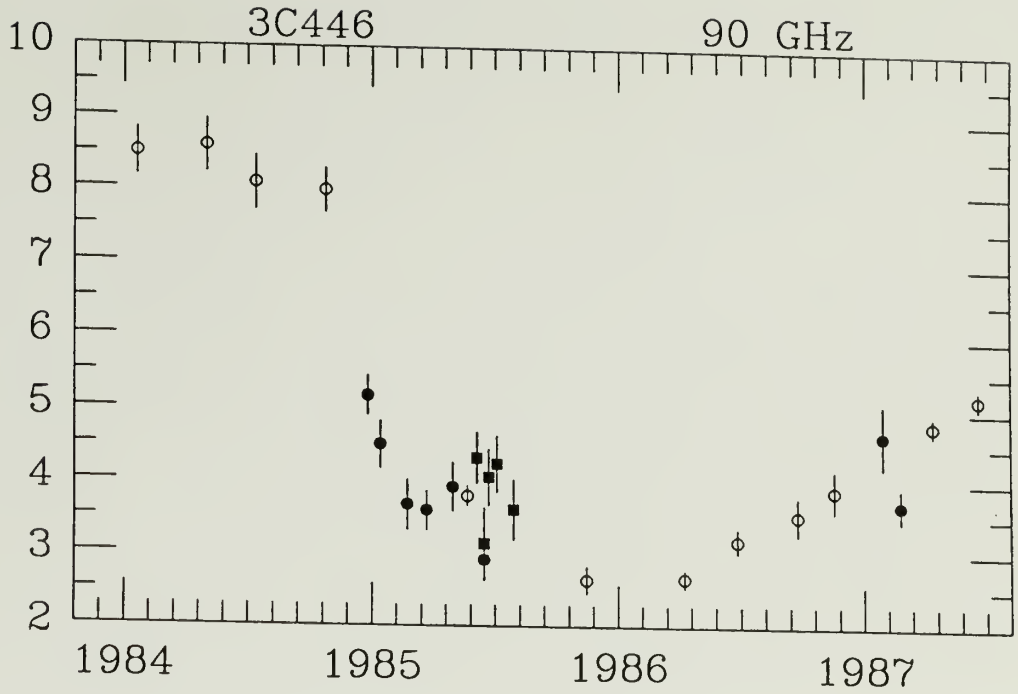

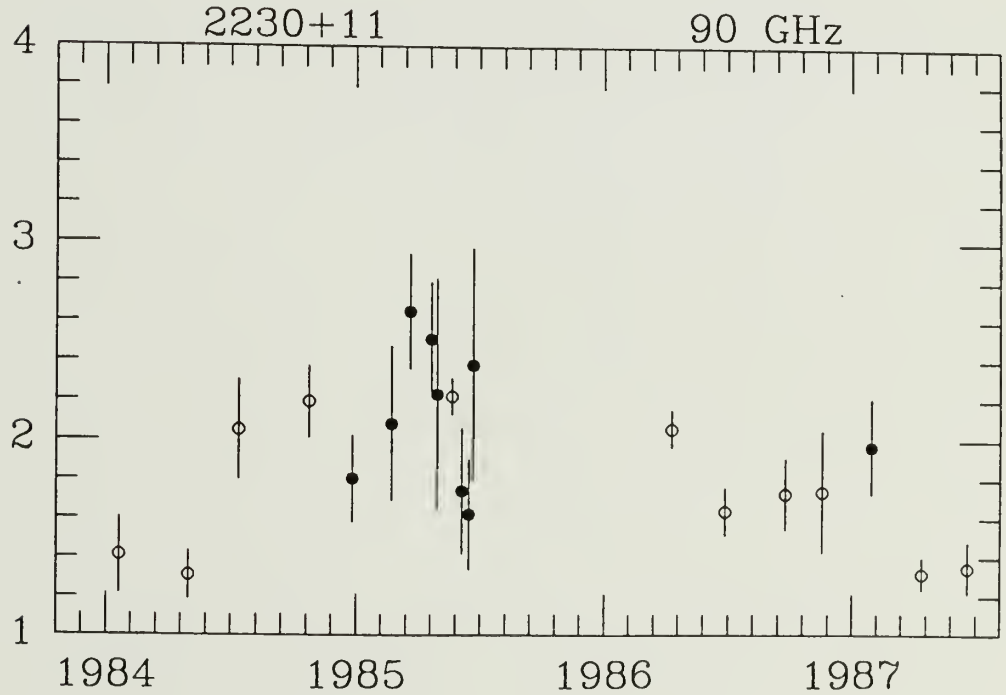

Figure 2.4 continued

CHAPTER 3

OUTBURST EVOLUTION

3.1 Introduction

The study of outburst evolution of compact extragalactic sources at radio wavelengths is complicated by two factors. First, many outbursts are blended because the variation time scale of the bursts is longer than the time of separation between the bursts. Second, the long time scale for the decay of an outburst compared to the time between outbursts makes difficult the determination of the base flux density level. To study burst evolution we therefore need first, to remove the base flux density contribution, second to remove the blending effects of other bursts, and finally, to examine how the spectra evolve with time.

3.2 Base Level Flux Removal

The simplest approach to separate outburst flux density from quiescent flux density is to assume that the outburst flux density is superimposed upon a constant base flux density which is well represented by the minimum flux density recorded during the time span of the observations (if the span is long enough). Thus, a simple subtraction will separate the quiescent and outburst flux densities.

Very Long Baseline Interferometry (VLBI) observational evidence supports this assumption. VLBI studies indicate that compact extragalactic radio sources are usually composed of several spatially separated components. One of the components is the stationary core and the other components move away from this stationary source. In current models the core is identified as the base of a jet, and the moving components are viewed as knots (presumably ejected from the core) propagating along the jet. As a knot moves away from the core, its emitted flux generally decreases. Since the many components are not resolved by single dish measurements, the total observed flux density is that from the core and one or more other propagating components in the jet. The quiescent spectrum at high frequencies, $\nu > 30$ GHz, is dominated by contributions from the flat spectrum core component. At centimeter wavelengths, the quiescent spectrum is dominated by the slowly decaying steep spectrum knots (See papers referenced in Valtaoja et al. (1988).).

Various observations suggest that the quiescent emission varies on a timescale of about a decade. Marscher and Gear (1985) review observations that indicate the quiescent spectrum (radio to IR) of 3C273 remained roughly constant for about 7 years. In addition, Valtaoja et al. (1988) found agreement between two epoch quiescent radio spectra obtained during the 1970s and the 1980s of about two dozen sources. Finally, the sources analyzed in this work were selected from the Dent-Balonek (DB) data base in part because their flux density levels return to nearly the same value during quiescent

periods between outbursts. This suggests that the sources under study here have nearly constant quiescent spectra.

3.3 Outburst Deconvolution: Profile Fitting

One method of deconvolving outbursts from each other is to fit the time variability curve with a model consisting of several outburst profiles. However, since there is so much data and so many possible outburst profiles, it would be impractical to fit every possible profile to every outburst in every source at each frequency in our data base. I have therefore fit only one profile to all the outbursts. This strategy can be motivated by the results of Legg (1984), which I now discuss.

In reanalyzing the data from Andrew et al. (1978), Legg (1984) discovered that six isolated outbursts, each in different sources, had similar profiles. He did this by overlaying the outburst data and scaling the individual time and flux density axes for each burst; the differences in the time scales were explained as a time compression effect due to relativistic beaming along the line of sight. The profiles were reasonably fit by a function of the form:

$$f(t) \propto (t-t_0)^n \, e^{-(t-t_0)/\tau} \qquad (3.1)$$

with n about three or greater. Legg was also able to fit the variability curve of 3C120 with multiple profiles all of the same shape and leaving the base flux density level as a free parameter.

To model the outbursts in this work, I use a rewritten form of the Legg function:

$$S(t) = S_p \left[\frac{t - t_0}{t_p - t_0}\right]^{(t_p - t_0)/\tau} e^{-((t-t_p)/\tau)}, \qquad (3.1)$$

where $S(t<t_0) = 0$ and $t_p - t_0 = n\,\tau$.

The fit at a particular frequency allows a burst to be reduced to four parameters: the amplitude of the burst (S_p), the initiation time of the burst (t_0), the time of peak amplitude (t_P), and the decay constant of the burst (τ). The use of this function is entirely empirical with no physical basis (as yet); nonetheless the function fits the outburst profiles well.

Since we are assuming that the burst profiles are well represented by the Legg function, we can now test the fit procedure by simulating a burst using the Legg function, and fitting the simulated data with noise added.

Two simulated bursts and their fits are shown in Figure 3.1. All fits were done using Marquardt's method (Press, et al. 1986) for χ^2 minimization. Each simulated burst was fit four different ways. In the first fit, t_0 was fixed at the value used to generate the simulated burst and the other parameters were free. In the next two fits, t_0 was fixed at different arbitrary times. In the last fit, all parameters were free. Table 3.1 shows the results of the fits to the simulated bursts.

Table 3.1. Table presenting the coefficients of the Legg function fits to the simulated bursts presented in Figure 3.1. Burst 0 gives the parameter values used to simulate the bursts. Observational noise was simulated using a gaussian distributed variate with σ = 0.19 Jy. An error of 0.00 indicates the parameter was fixed. χ^2_ν is the reduced chi square with 16 degrees of freedom.

Table 3.1

Burst	t_0 [Yr]	t_p [Yr]	S_p [Jy]	τ [Yr]	χ^2_ν
0	75.00	76.00	4.00	0.250	
1	75.00±0.00	76.10±0.03	3.83±0.19	0.282±0.041	0.15
1	74.50 0.00	76.14 0.03	3.86 0.19	0.182 0.025	0.18
1	74.00 0.00	76.16 0.03	3.87 0.19	0.135 0.018	0.24
1	74.91 1.57	76.11 0.05	3.84 0.19	0.255 0.112	0.15
2	75.00±0.00	76.10±0.03	3.94±0.19	0.266±0.037	0.24
2	74.50 0.00	76.13 0.03	3.98 0.19	0.169 0.022	0.33
2	74.00 0.00	76.15 0.03	4.00 0.19	0.125 0.016	0.42
2	75.05 1.00	76.09 0.05	3.94 0.19	0.284 0.107	0.25

In all eight cases the profile fits the data well by eye and, as indicated, by a small χ^2_ν. Also, the fit amplitudes are almost identical. The fact that the fit amplitudes are smaller than the value used to generate the profiles is due to the particular manifestations of the simulated gaussian noise in each profile and the concave down curve of the profile. The fits indicate that the rise and fall parameters are closely coupled. They also show that t_0 is not a well determined parameter and that reasonable assumed values for t_0 still produce good fits to the data.

A another way of parameterizing the bursts is by measuring the rise time (t_r) and the decay time (t_d) between the 50% level and the peak. These quantities are shown in Table 3.2 for the models in Table 3.1. The results in the table indicate that as t_0 is changed for the different fits, that the fit width of the burst stays constant (to within ~ 1%). Also, as t_0 is fixed earlier in time, the burst becomes more symmetric as indicated by the ratio of t_r/t_d. It can be shown (E. Tademaru, private communication) that the ratio is given by $t_r/t_d = (1 + n^{-1/2})^{-1}$. This formula is accurate to within 3% for $1 \leq n \leq 20$.

Because of the coupling between t_0 and τ, and since t_0 was arbitrarily chosen to be about year before t_p (when fitting the real data), no meaningful results can come of examining τ or the ratio t_r/t_d (remember, $n\tau = t_p - t_0$). In addition, the outburst fits give only two meaningful physical parameters, the amplitude, and the time of peak. However, the fits are still useful for defining the profiles of the individual bursts with the contributions from adjacent bursts subtracted.

The van der Laan function , $S = A(t-t_0)^m(1-e^{-a(t-t_0)^b})$, was also fit to a few bursts. By eye, the fits agreed as well as the Legg function, although in a few cases the van der Laan function tried to fit inflections in the burst that subjectively appeared to be noise. In most cases, the χ^2_ν of the van der Laan fit was smaller than the χ^2_ν of the Legg fits. However, since the values of the χ^2_ν for the profile fits are about one or less, it is impossible to tell which function fits the data better.

The similarities between the van der Laan and the Legg profile shapes are shown in Figure 3.2. In this plot a simulated outburst was generated using the van der Laan function and random gaussian distributed noise. The simulated outburst was then fit with a Legg function profile. This shows that if the outburst profiles are correctly described by a van der Laan function, the Legg function can still provide a reasonable representation of the burst.

Table 3.2. Table presenting rise and decay times of the bursts listed in Table 3.1. All the dates and times are in years. t_1 is the date that the increasing flux density reached 50% of maximum amplitude. t_p is the time of peak. t_2 is the date that the flux density decayed to 50% of the maximum value. $t_r = t_p - t_1$. $t_d = t_2 - t_p$. $t_r + t_d$ gives the full width at half maximum . r is the ratio of t_r/t_d. n is the rise exponent from the Legg function.

Table 3.2

Burst	t_1	t_p	t_2	t_r	t_d	t_r+t_d	r	n
1	75.57	76.10	76.89	0.53	0.79	1.33	0.67	3.91
1	75.58	76.14	76.87	0.56	0.73	1.29	0.77	9.02
1	75.58	76.16	76.85	0.57	0.70	1.27	0.82	15.98
1	75.57	76.11	76.89	0.54	0.77	1.31	0.70	4.73
2	75.58	76.10	76.86	0.52	0.76	1.28	0.68	4.12
2	75.59	76.13	76.83	0.54	0.70	1.24	0.78	9.66
2	75.60	76.15	76.82	0.55	0.67	1.23	0.83	17.16
2	75.57	76.09	76.87	0.52	0.78	1.29	0.66	3.67

To fit each real outburst, initial starting conditions were chosen for the burst parameters in addition to a date range for the fit. The date range usually started and stopped at the local minima in the variability curve preceding and following the burst peak. An iterative procedure was used to fit one burst at a time, using the Legg function, keeping the parameters of the other bursts fixed. The process was continued and repeated until convergence was obtained. Then at higher and lower frequencies the process was repeated. Bursts to be analyzed were chosen based on their amplitude and separation from other bursts. Usually, the bursts just before and after the burst of interest were also fit to remove their contribution from the burst of interest. Since the 15.5 GHz data has the best sampling, it was usually used to determine the total number of outbursts that occurred during the time span of observations. In some sources, as many bursts as possible were fit at the higher frequencies in the data set to obtain the times of peak for periodicity analysis in Chapter 4.

Because of the large error in the determination of t_0 and because the fit is insensitive to the precise value of t_0, t_0 was fixed in most of the bursts at about a year before the time of peak. If the burst was too blended, it was also occasionally necessary to fix t_p or τ to obtain a fit. This will be indicated in the individual fit descriptions.

3.4 Spectral fits

When possible, the profile fits at each of the five frequencies for a particular burst were used to generate interpolated flux density values at equally spaced epochs centered about the outburst's time of peak at 15.5 GHz. The error in the interpolated flux densities was initially determined using the errors in the parameters from the fits and standard propagation of error theory. But in most cases this gave abnormally large errors. For most bursts the error in the interpolation is probably smaller than, or the same magnitude as, the mean error of measurement at each frequency for a single point. Therefore the mean error was used for the error of the interpolated point. However, when interpolating values below about 30% of the amplitude of the burst the error will be larger because the uncertainties associated with the burst subtraction procedure.

The spectrum at each epoch was fit using Marquardt's method (Press, et al. 1986), to a dual power law function of the form

$$S_\nu(x) \propto x^q \, (1 - e^{-x^p}), \qquad (3.2)$$

where $x = \nu/\nu_1$, ν_1 is the frequency at which the optical depth is one. This functional form was chosen because both homogeneous and nonhomogeneous source models predict such a dual power law spectrum (see chapter 1). Once the function is fit, the flux density maximum (S_m) and the corresponding frequency of maximum (ν_m) of the spectrum are found numerically. The low frequency spectral index q was originally treated as a free parameter for greater flexibility in

the fit and to see if it matches the slope of 2.5 for a homogeneous synchrotron source. However, most of the outbursts are lacking reliable 2.7 GHz fit profiles. In addition, the two bursts fit that have 2.7 GHz profiles had low frequency slopes consistent with a 2.5 slope. Therefore the low frequency slope was kept fixed at 2.5 for all the fits.

Function 3.2 usually fit the spectra very well. In cases where it did not, closer examination usually indicated the presence of blended outbursts, or a change in the slope at the high frequency end of the spectrum.

3.5 Results

Originally ten sources were selected from the data base for outburst analyses, based upon the flat base level requirement. They were 3C279, 0420-01, 1510-08, 0235+16, CTA26, 3C454.4, 0106+01, 2121+05, 0133+47, 2131-02. However, because of outburst blending the last four sources were dropped. In addition, because of rapid variability, the variation curves of 0235+16 were too under sampled to allow spectra to be reliably generated.

The fit profile parameters are presented in Appendix B. The profile fits with the time variability data are shown in Appendix C. The reference burst numbers are also shown in the plots. An example of the profile fits with the time variability data using 3C454.3 at 15.5 GHz is shown in Figure 3.3. The raw spectral fit parameters are presented in Appendix D, while spectral parameters derived from them are presented in Table 3.3. The outburst profiles and spectra

Table 3.3. The derived parameters from the burst spectral fits. The low frequency spectral slope was always fixed at 2.5 for the fits.

* The epoch of the burst peak at 15 GHz.

Table 3.3

3C454.3

#	Date	ν_m[GHz]	S_m[Jy]	α_{lo}	α_{hi}	χ^2_ν
5	1971.91	0.00± 0.00	0.00±0.00	2.50±0.00	+0.02±0.13	0.77
* 5	1972.31	11.05 1.07	5.75 0.61	2.50 0.00	-0.15 0.09	1.83
5	1972.71	7.71 0.67	5.05 0.60	2.50 0.00	-0.30 0.11	1.48
5	1973.11	5.64 0.58	3.87 0.66	2.50 0.00	-0.54 0.19	0.68
5	1973.51	4.52 0.71	2.96 0.84	2.50 0.00	-0.86 0.40	0.21
6	1973.84	47.91±10.16	3.83±0.96	2.50±0.00	-0.14±0.23	0.86
6	1974.14	27.38 3.41	5.97 0.74	2.50 0.00	-0.29 0.13	2.01
* 6	1974.44	17.42 1.29	6.48 0.53	2.50 0.00	-0.48 0.10	0.47
6	1974.74	12.08 1.14	5.78 0.56	2.50 0.00	-0.66 0.15	0.31
6	1975.04	8.48 1.40	4.69 0.44	2.50 0.00	-0.82 0.20	0.43
6	1975.34	6.10 0.63	4.07 0.55	2.50 0.00	-1.13 0.28	0.48
6	1975.64	4.87 0.56	3.71 0.96	2.50 0.00	-1.59 0.64	0.28
12	1981.25	21.89± 3.16	4.00±0.61	2.50±0.00	-0.24±0.14	0.41
12	1981.55	18.79 1.04	9.29 0.55	2.50 0.00	-0.36 0.06	0.08
*12	1981.85	15.71 0.73	10.87 0.55	2.50 0.00	-0.43 0.06	1.41
12	1982.15	12.23 0.68	10.01 0.56	2.50 0.00	-0.64 0.09	0.01
12	1982.45	10.29 0.69	9.13 0.63	2.50 0.00	-1.13 0.18	1.24

0420-01

#	Date	ν_m[GHz]	S_m[Jy]	α_{lo}	α_{hi}	χ^2_ν
2	1978.15	30.56± 7.73	3.01±0.81	2.50±0.00	-0.30±0.30	2.00
2	1978.45	17.78 2.43	3.91 0.58	2.50 0.00	-0.34 0.16	3.07
* 2	1978.75	15.50 1.62	4.40 0.54	2.50 0.00	-0.54 0.17	2.26
2	1979.05	14.48 1.64	3.90 0.54	2.50 0.00	-0.63 0.22	1.71
2	1979.35	13.48 2.21	2.94 0.54	2.50 0.00	-0.64 0.30	1.32

(continued next page)

Table 3.3 (continued)

3C279

#	Date	ν_m[GHz]	S_m[Jy]	α_{lo}	α_{hi}	χ^2_ν
7	1976.27	12.56± 2.07	3.94±1.23	2.50±0.00	-0.28±0.13	0.58
* 7	1976.57	11.13 1.33	6.04 0.44	2.50 0.00	-0.44 0.09	3.43
7	1976.87	8.40 0.89	5.66 0.34	2.50 0.00	-0.55 0.09	2.17
7	1977.17	4.48 0.26	5.92 0.84	2.50 0.00	-0.72 0.15	3.09

CTA26

#	Date	ν_m[GHz]	S_m[Jy]	α_{lo}	α_{hi}	χ^2_ν
9	1978.15	26.73±13.52	1.90±0.53	2.50±0.00	-0.21±0.28	0.02
* 9	1978.45	27.30 8.47	2.67 0.42	2.50 0.00	-0.30 0.23	0.37
9	1978.75	26.64 10.07	2.12 0.33	2.50 0.00	-0.34 0.29	0.31
9	1979.05	24.84 19.84	1.17 0.02	2.50 0.00	-0.33 0.50	0.08

1510M08

#	Date	ν_m[GHz]	S_m[Jy]	α_{lo}	α_{hi}	χ^2_ν
13	1978.95	27.17± 3.59	5.57±0.76	2.50±0.00	-0.35±0.15	2.52
*13	1979.05	37.21 4.17	7.52 0.87	2.50 0.00	-0.15 0.10	0.31
13	1979.15	29.06 3.03	6.65 0.70	2.50 0.00	-0.18 0.09	9.87
13	1979.25	18.07 2.05	5.01 0.58	2.50 0.00	-0.29 0.11	13.43
15	1980.69	28.58± 6.62	2.99±0.70	2.50 0.00	-0.18±0.20	0.99
*15	1980.79	17.30 3.29	3.15 0.58	2.50 0.00	-0.29 0.18	0.06
15	1980.89	11.52 5.17	2.46 0.61	2.50 0.00	-0.35 0.26	0.26

fits will be discussed in a source by source manner and the overall results and discussion will be presented in the next two sections.

3C454.3 (QSO, z=0.859). This source has the best fit profiles and spectra in the group. The burst variability time scale is about a year and the outbursts do not become severely blended until the frequency is less than 8 GHz. The regular spacing of the outbursts in 3C454.3 will be discussed in chapter 4. The higher frequency burst data were fit easily. Three bursts were analyzed: 5, 6, and 12 (Figures 3.4 to 3.9). Because of their blending at 2.7 GHz, bursts 5, 6, and 7 were fit simultaneously. Bursts 11, 12, and 13 are too blended at 2.7 GHz to deconvolve them even after fixing t_p and forcing τ to be same in all the bursts. The time of peak of burst 6 exhibits a progressive delay of ~ 0.2 years between 31 GHz and 8 GHz (Figure 3.6). While bursts 5 and 12 each peak simultaneously at the higher frequencies (Figures 3.6 and 3.8). The typical delay time between the 8 GHz and 2.7 GHz variability curves is 1.2 years. The spectra of burst 5 (Figure 3.5) were fit only to the lower four frequencies because 90 GHz data were not available. Since the extrapolated flux density at 2.7 GHZ for burst 6 at the first two epochs was very small (< 0.1 Jy) and unreliable, it was not used in the spectra fits. Burst 12 was fit without interpolated flux density values for 2.7 GHz, since the profile fit was unreliable.

The spectra of the three analyzed bursts in this 3C454.3 have a similar evolution. Before the time of peak at 15 GHz the flux density increases at all observed frequencies with the burst spectra keeping the same shape. After the time of peak, the spectra all

exhibit a marked steepening ($\Delta\alpha>-0.6$) of the high frequency spectral index.

0420-01 (QSO, z=0.915). This source exhibits about six years of very low level activity before starting a series of outbursts (Appendix C). Blending required that the times of peak for bursts 2 and 3 at 8 GHz to be fixed at the 15 GHz peak times. Burst 3 was not analyzed because examination of the 7.9 GHz data indicated it could be composed of up to three bursts. Burst 2 exhibits progressive delays in the time of peak from 90 to 15 GHz (Figure 3.10). All bursts in this source become very blended at 2.7 GHz, so the profiles were not used in the generation of spectra. The high frequency spectral index exhibits a steepening ($\Delta\alpha\approx-0.3$) as the burst evolves (Figure 3.11). The steepening is consistent with a break in the spectrum evolving from 90 GHz to lower frequencies.

3C279 (QSO, z=0.536). The outburst profiles for this source were fit easily. Burst 7 exhibits progressive delays in the time of peak from 90 to 7.9 GHz (Figure 3.12). The mean delay between 7.9 and 2.7 GHz is about one year.

The spectrum of the outburst under went the typical rise and fall pattern seen in the other sources. It appears that the high frequency spectral index was steepening from -0.3 before the burst peaked at 15 GHz to -0.7 afterward (Figure 3.13). The steepening is consistent with a break in the spectrum evolving from 90 GHz to lower frequencies.

CTA26 (QSO, z=0.852). Only one burst (9) could be analyzed from this source. The fit outburst profiles peak at nearly the same time for the burst between 8 and 90 GHz (Figure 3.14). The outburst

spectra retained the same shape during the entire observed evolution (Figure 3.15). That is, there is no observed spectral steepening. However, there is structure in the burst data at 8 GHz that indicates that burst 9 might be two blended bursts. This could explain the lack of high frequency spectral steepening.

1510-08 (QSO, z=0.361). This source exhibits very rapid variability. This source also show that different bursts can have different delay times at lower frequencies. For example, burst 13 is delayed at 2.7 GHz while bursts 14 and 15 are not. Two bursts were selected for analysis, bursts 13 and 15. One burst (13) is not fit well by the Legg function. The profile peak (S_p) had to be constrained to fit the outburst's peak amplitude. This causes the decay part of the curve to systematically deviate from the data. The two points near the peak in burst 13 at 15 GHz are at nearly the same value. This indicates that the burst was probably peaking at that time, even though the burst is under sampled. However, the profile fits (because of the under sampling) has the outburst peaking at 15 GHz before the peak at 31 GHz (Figure 3.16). Because of the under sampled rapid rise and the failure of the Legg function to fit the burst after the peak well, the spectra were only generated at the peak and +0.1 and +0.2 years after the peak at 15.5 GHz (Figure 3.17). Burst 13 is consistent with a slight or no steepening of the high frequency spectral index.

The profile fits for burst 15 show the the time of peak of the burst is progressively delayed at lower frequencies (Figure 3.18). Because of the rapid variability, then spectra for burst 15 were only fit at the epoch of the outburst peak at 15 GHz and ±0.1 years

(Figure 3.19). This burst is also consistent with little or no high frequency spectral steepening. However, in both bursts 13 and 15 the time span examined was very small so spectral steepening should not necessarily be expected.

0235+16 (BL Lac, z=0.851). The under sampled rapid variability of this source prevented enough profiles to be fit so the spectral evolution could not be obtained. However, the times of outburst peaks could be obtained and will be used in the periodicity analysis of chapter 4. Notice that the Legg function has difficulty fitting the peak amplitude in some of the bursts (numbers 1, 8, and 9 at 8 GHz). The profiles were not forced to fit the peak amplitudes as in 1510-08.

3.6 Summary of Outburst Evolution

The profile fits at 2.7 GHz were of limited use. The blending of the bursts increases with lower frequencies, thus making fits at 2.7 GHz the most unreliable of all. The long decay times of the bursts also make it difficult to determine an accurate base level at 2.7 GHz, because for the flux density to decay to its lowest level, a wide temporal gap is required between outbursts.

The burst peaks at 2.7 GHz are delayed by about a year or greater relative to burst peaks at 7.9 GHz. At 7.9 and 15.5 GHz, all the burst peaks are simultaneous or slightly (< 0.2 yr) delayed when compared to the 31 and 89.6 data. At all frequencies, the minima are delayed by about the same amount as the peaks. Thus, useful

variability data requires wide frequency coverage and frequent samplings over decades of time.

From the variability curves, it is apparent that the outbursts' maximum flux density occurs at different frequencies. For example, burst 1 in 0235+16 peaks about 15 GHz. While bursts 9 and 10 in 0235+16 are present at 15 GHz, they are more clearly defined and of larger amplitude at 7.9 GHz.

Most of the bursts exhibit an initial flat spectrum of $\alpha \approx -0.2$, implying a electron energy index of s=1.4. All the bursts presented except one, in CTA26, exhibit evidence for high frequency spectral steepening during the decay phase of the outburst. Two bursts possibly show evidence of sudden steepening in the high frequency spectrum. All the outbursts are consistent with the spectral maximum amplitude peaking in the range of 10 to 50 GHz and then decaying as is progresses to lower frequencies. All the bursts are consistent with a low frequency spectral slope of 2.5.

3.7 Discussion

All the outbursts appear to keep the same spectral shape during the rising portion of the outburst. Following the method of Jones et al. (1981), this translation of the spectrum in log s log ν space implies a change in the scale of the global parameters of the outburst. For example, the source is getting bigger, the number of synchrotron electrons is increasing, or possibly the inverse Compton opacity is decreasing. The steepening of the the high frequency spectral index implies the slope of the electron energy index is

also steepening. This is most easily explained as being caused by inverse Compton or synchrotron loses.

We can also compare the observations of the outburst evolution with the simple expanding source (SES) model and the Marscher and Gear (MG) model. The MG model predicts three different sets of relations between S_m, ν_m, and t for the three different regimes in the burst evolution. For comparison with the MG model, I will use the value for the electron energy index obtained from the observations, s=1.4. By contrast, Valtaoja et al. (1988) used s=2, the smallest value allowed in the MG model if the shock is to survive for very long, unless it was initially very strong.

Figure 3.20 presents the evolution of log S_m versus log ν_m for the analyzed bursts. The predicted evolutionary slopes for the different phases in the MG model and the SES model are also shown for comparison. The relations are $S_m \propto \nu_m^{-2.5}$ for the inverse Compton regime, $S_m \propto \nu_m^{-0.74}$ for the synchrotron regime, and $S_m \propto \nu_m^{+0.45}$ for the regime where adiabatic losses dominate. The SES model predicts $S_m \propto \nu_m^{+1.1}$ for s=1.4. Bursts 5 and 12 in 3C454.3 appear to go through all three phases of the MG model. In addition, all of the outburst evolutions are consistent with the MG predictions, except that the last phases of some of the bursts have steeper evolution than that predicted by the MG model and are more consistent with the SES model. As pointed out by Valtaoja et al. (1988) this steepening might be explained as the old shock is decaying and now expanding in three dimensions, as in the SES model. Lastly, when the log S_m - log ν_m plot indicates the the burst should be in the MG adiabatic phase, there is a delay in the time of peak of the burst at lower

frequencies relative to the higher frequencies, as would be expected with an expanding opaque synchrotron source (for example, burst 6 in 3C454.3).

Both the MG and SES model predict the evolution of ν_m with time: $\nu_m \propto t^b$ where t is the observed time with the burst start time subtracted ($t=t_{obs}-t_0$). The MG model predicts $b_{ic}= -0.50$, $b_s=-0.90$, and $b_{ad}=-1.10$ for the three phases of inverse Compton, synchrotron, and adiabatic loss domination. The SES model predicts $b_{ses}=-2.15$ for s=1.4.

The value obtained for b is very dependent upon the the value used for t_0 when doing the fit. Unfortunately, as shown before, the t_0s obtained from the Legg function have a large uncertainty. To better estimate t_0 for each burst, an improved t_0 was determined at 8, 15, and 31 GHz by fitting a line between the 10% and 50% level on the rise portion of the fit profile and then finding the crossing point on the time axis. The t_0s for each of the frequencies were then averaged.

Using the improved t_0s, the log ν_m - log t relations are shown in Figure 3.21. Some plots exhibit linear trends. Linear fits produce slopes clustered in two groups at $b\approx-0.5$ and $b\approx-0.9$. However, an error as small as 0.1 year in determination of t_0 can produce a change in the slope as large as 40%. Valtaoja et al. (1988) in performing the same type of fits, varied t_0 and found a slightly better fit was obtained when $b\approx-2$ and t_0 was earlier (but less than a year) than that originally assumed (the zero point on the 15 GHz rise curve).

However, a linear fit to the data may not be appropriate. The MG model predicts three different phases of the burst evolution for both the ν_m and S_m versus time relations. Because of the possibly changing index and the uncertainty in t_0 the S_m and ν_m versus time plots should only be used as a consistency check for the S_m verses ν_m relation.

For $\nu_m \propto t^b$, the MG model predicts that b should decrease from -0.5 to -1.1 and possibly to -2.15 in the SES regime as the bursts evolve. Burst 12 in 3C454.3 exhibits significant changes in b that are consistent with the MG model predicted evolution in the log S_m- log ν_m plot. In the log ν_m- log t plot, this burst exhibits the strongest concave down curvature. All of the other log ν_m- log t plots, except for 0420-01, are consistent with a linear or slight, concave down, curve.

For $S_m \propto t^d$, the MG model predicts the evolution should begin as a steep rise (d_{ic}= 1.25), followed by a leveling (d_s=0.24), and followed by a gradual fall (d_{ad}-0.55) (Figure 3.22).
If the burst evolves to become consistent with the SES model, then the slope becomes steeper (d_{ses}=-2.4). All the bursts follow the described trend.

3.8 Conclusions

Eight bursts in five AGN were analyzed for profile shape and their evolution was compared to the simple expanding source (van der Laan, 1966) and the Marscher and Gear (1988) models. There are many more outbursts visible in the Dent-Balonek data base, however, the

low amplitude and blending of many bursts, has limited this initial study to just the eight.

The profile fits indicate that the burst profiles retain roughly the same shape over a large frequency range and that fitting profiles to the burst data is in fact a reasonable method of deconvolving the outbursts.

The spectra fits are consistent with a homogeneous synchrotron source (although other low frequency slopes cannot be ruled out) that undergoes expansion and inverse Compton or radiation loses. The initial high frequency spectral slope was $\alpha \approx -0.2$ for all the bursts. In addition, the high frequency spectrum normally steepened by at least -0.5, with two clear examples of $\Delta\alpha \approx -0.9$. This implies that during the evolution observed the synchrotron electrons were not being reaccelerated or resupplied.

The outbursts all seem to follow the same evolution. Comparison of the outburst evolutions led to a qualitative agreement with the predicted three phases of the MG model and possibly into a phase more consistent with the simple expanding source model.

While the qualitative agreement between the observed evolution and that predicted by the MG model appears hopeful, there remains one major inconsistency. The spectra of all the bursts indicate an initial high frequency spectral slope of $\alpha \approx -0.2$. This implies that $s \approx 1.4$ for the relativistic electron distribution, a value larger than allowed by the MG model ($s \approx 2$) if the shock is to be nonradiative and survive for any length of time (unless it was initially very strong).

The observed outburst evolution is consistent with the Marscher and Gear model and the suggested transition of this model into the canonical source model forms a consistent evolutionary picture. However, more quantitative analyses of the source properties should await a more refined version of the model. This does not, however, preclude the possibility of further source analysis, with the inclusion of more sources and other frequencies of data to better define the spectra, especially the inclusion of data in the critical frequency range between 3 and 8 GHz to better define the low frequency slope, and the possible use of polarization information to better deconvolve the burst profiles.

Figure 3.1. Two simulated outbursts each fit with the Legg function. The solid line indicates the best fit profile with all parameters free. The dotted lines indicate the fit profiles when the outburst initiation time (t_0) is fixed at different values.

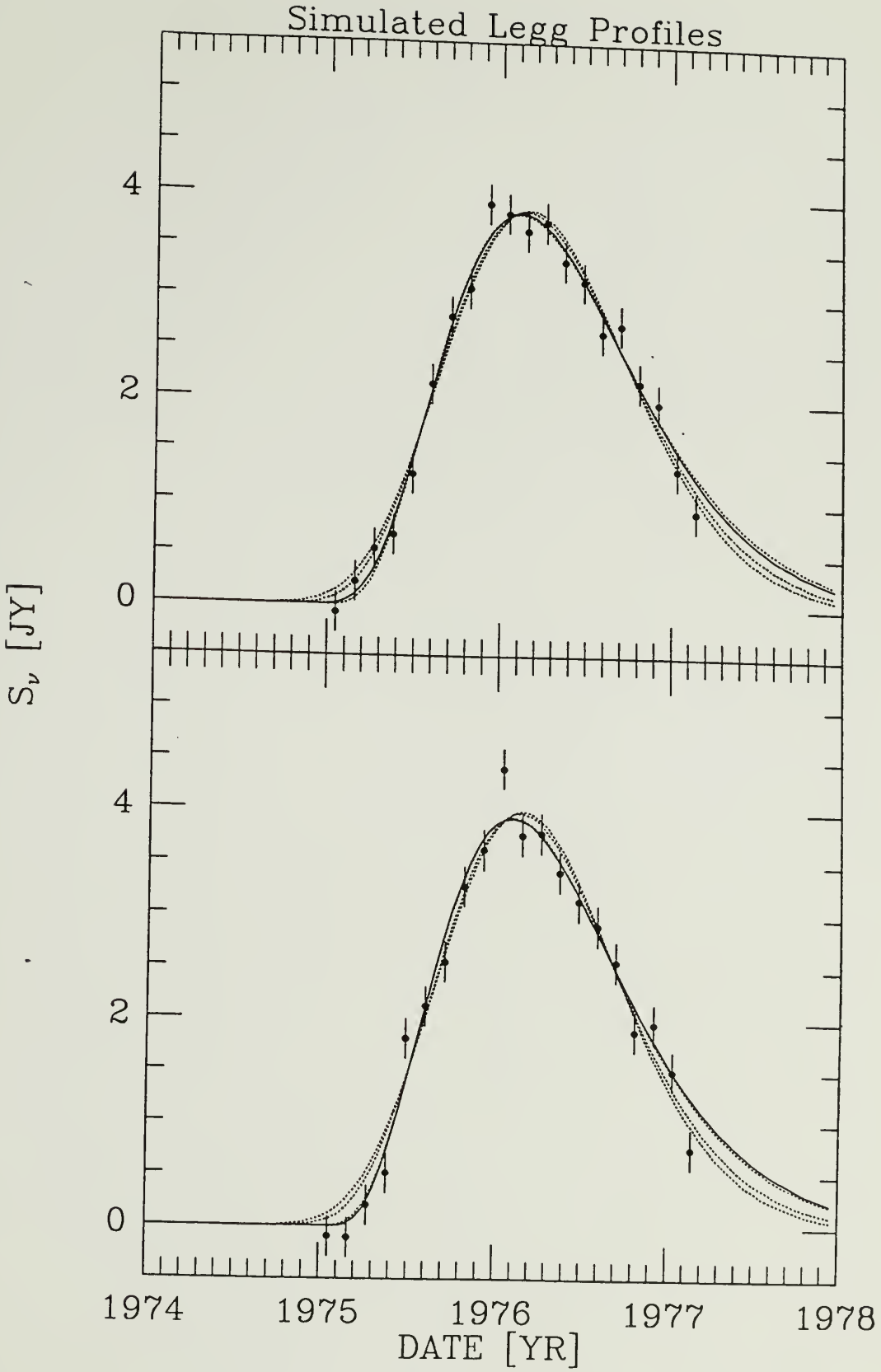
Simulated Legg Profiles
4
2
0
4
2
0
S_ν [JY]
1974
1975
1976
1977
1978
DATE [YR]

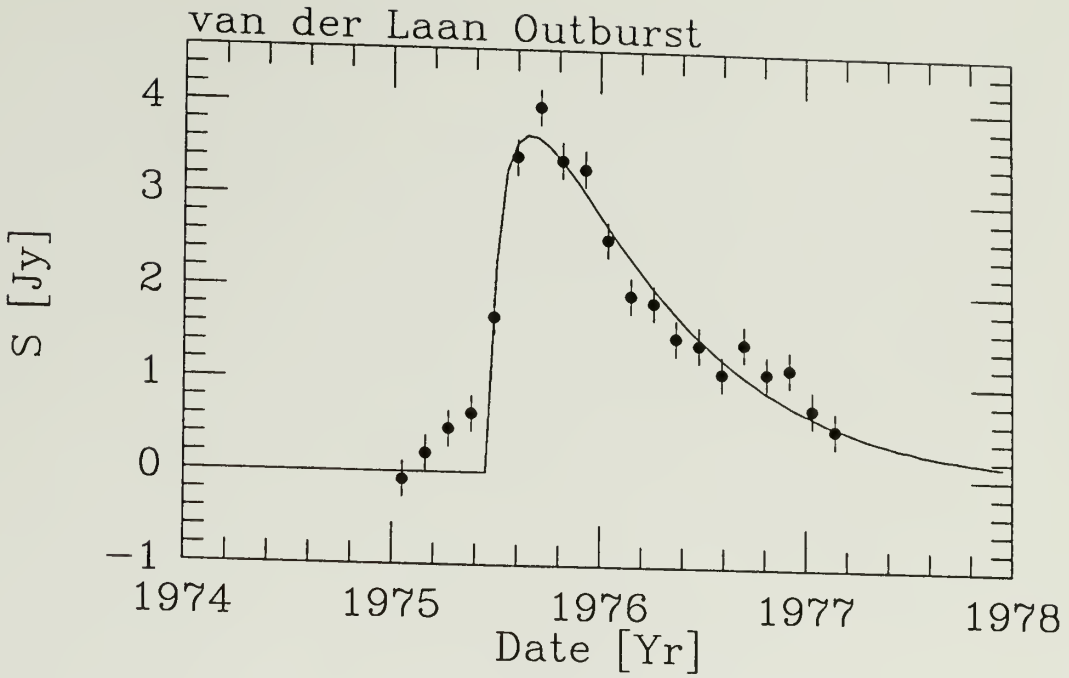

Figure 3.2. Simulated van der Laan outburst fit with the Legg function.

Figure 3.3. Outburst profiles fit to the time variability data for 3C454.3 at 15.5 GHz. The solid circles are measurements made as part of the DB flux density monitoring program. The open circles are measurements from Schwartz (private communication). The dotted lines indicated the individual burst profiles fit to the data. The solid line indicates the combined flux density from all the burst profiles.

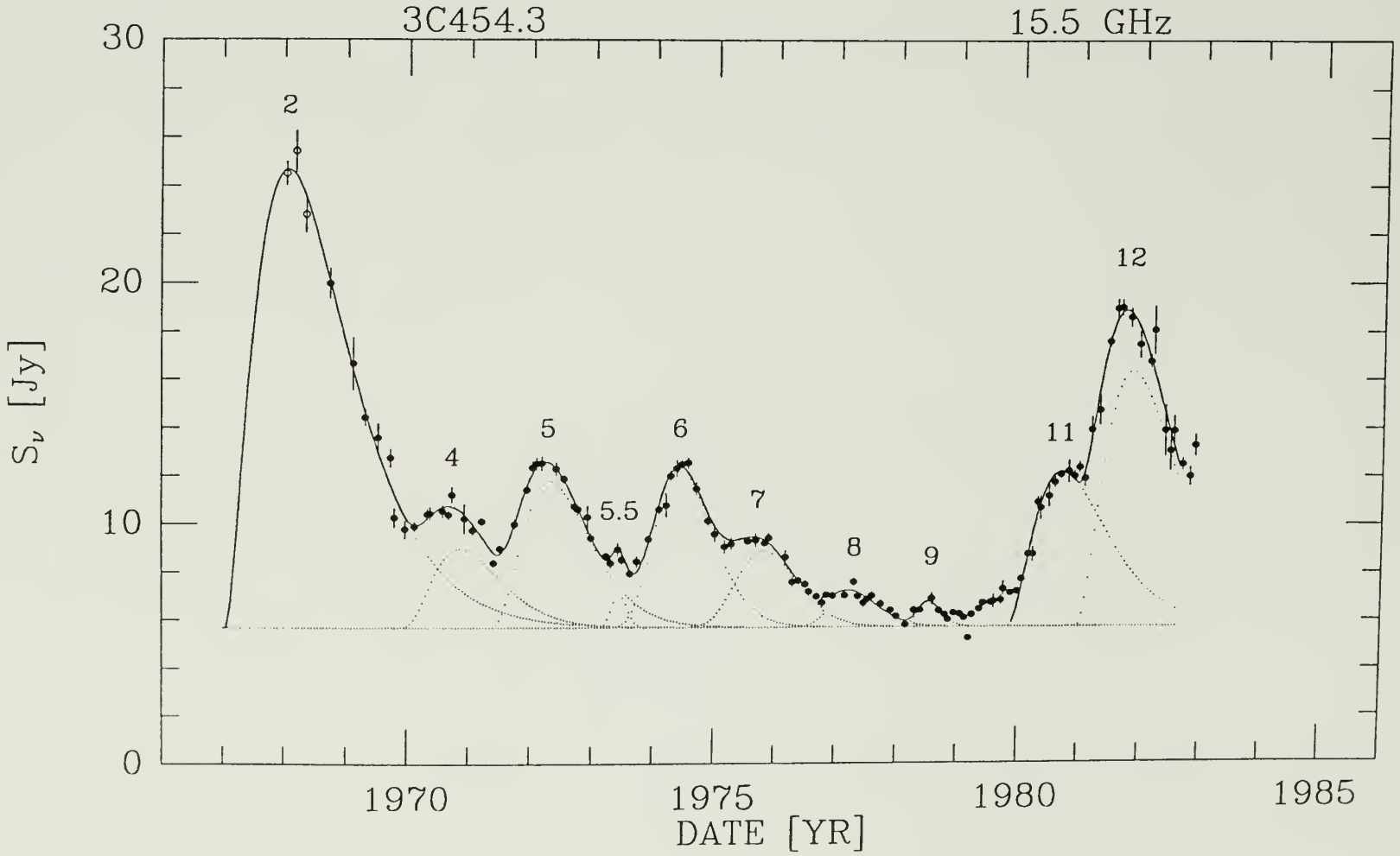
3C454.3
15.5 GHz
30
20
10
0
S_ν [Jy]
2
4
5
5.5
6
7
8
9
11
12
1970
1975
1980
1985
DATE [YR]

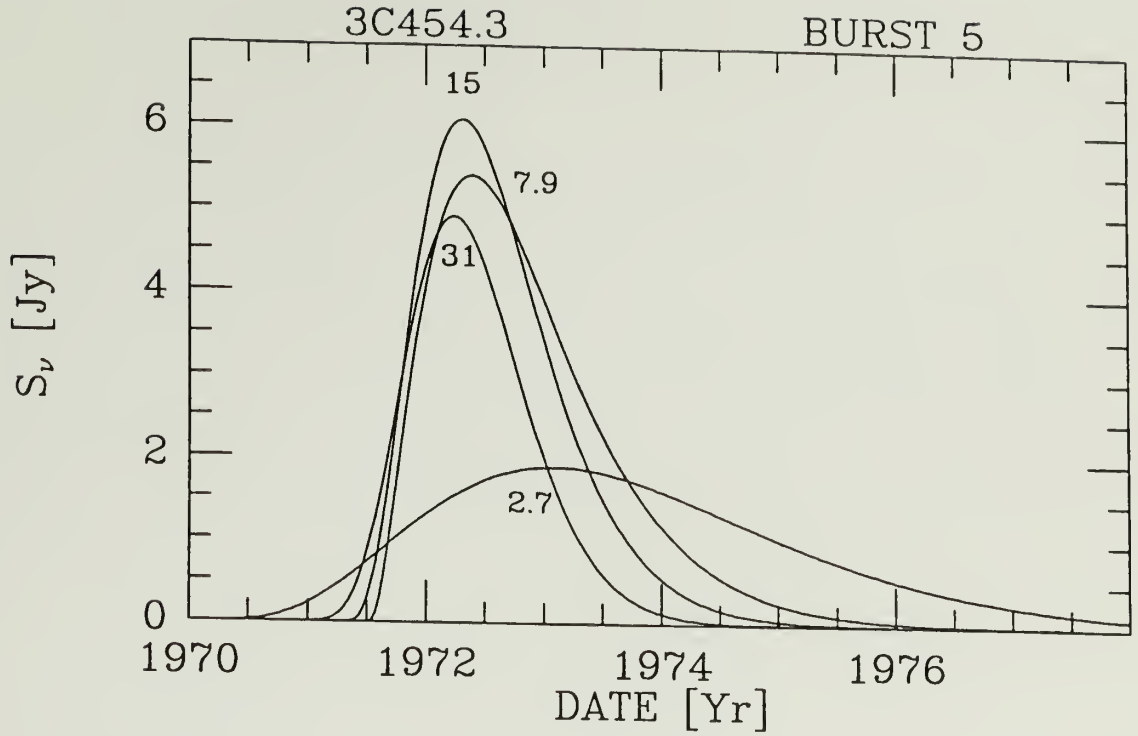

Figure 3.4. The multifrequency outburst profiles for burst 5 in 3C454.3.

Figure 3.5. The spectral evolution of burst 5 in 3C454.3. The solid line indicates the epoch of peak at 15 GHz. The top panel is prepeak and the bottom panel is post peak.

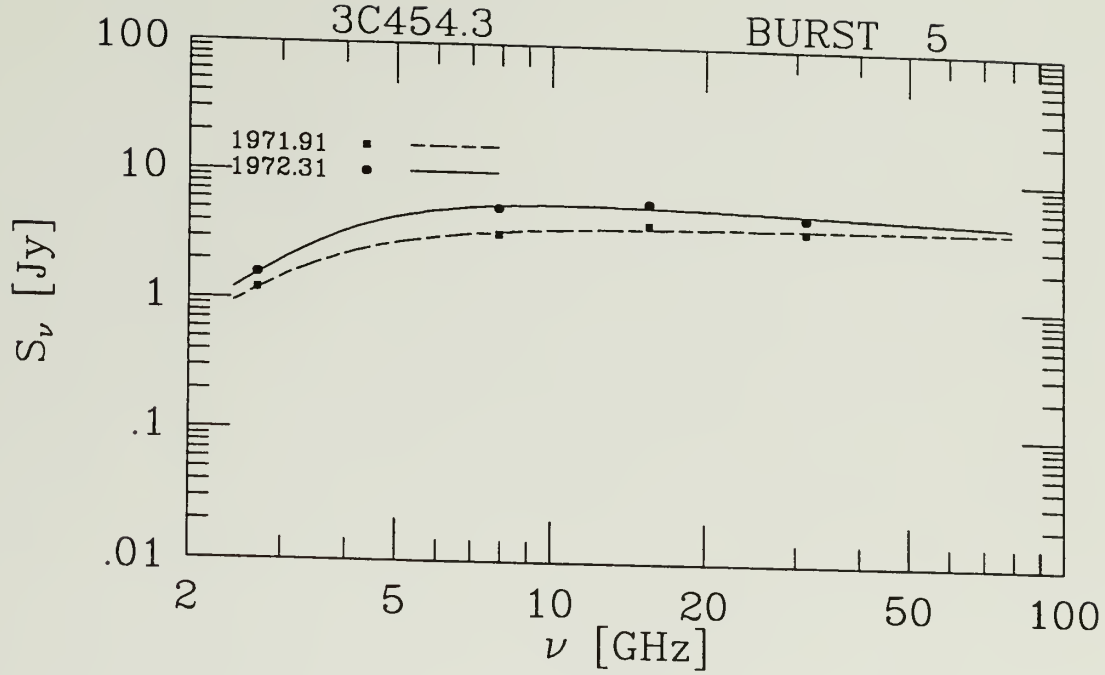
3C454.3
BURST 5
1971.91
1972.31
100
10
1
.1
.01
S_ν [Jy]
2
5
10
20
50
100
ν [GHz]

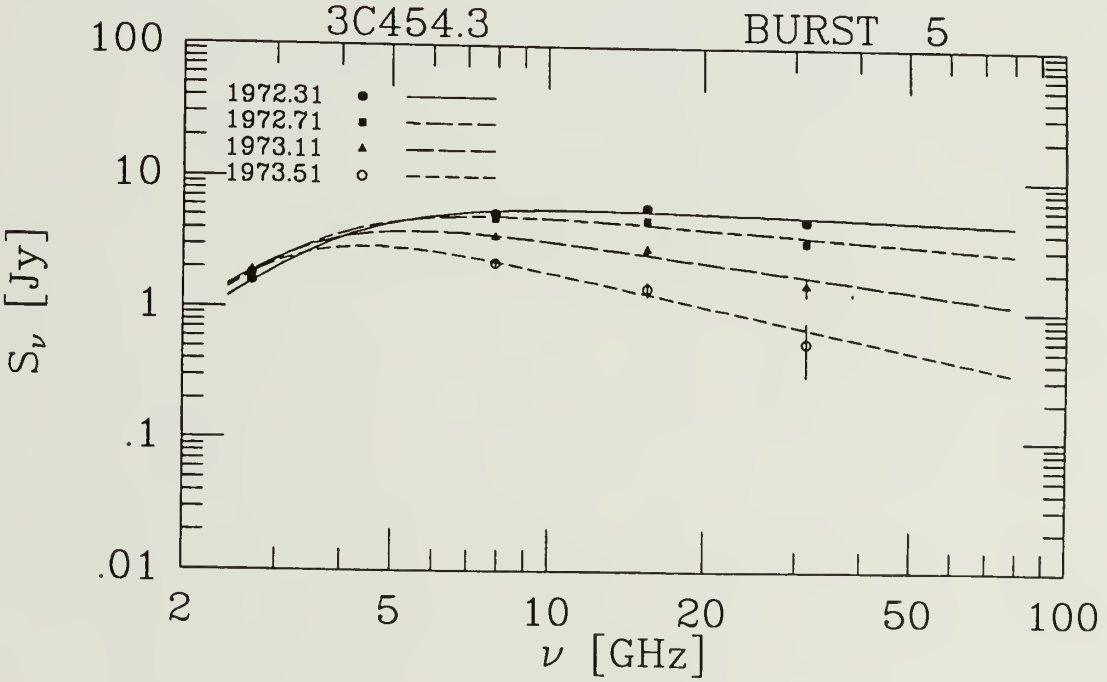
3C454.3
BURST 5
1972.31
1972.71
1973.11
1973.51
100
10
1
.1
.01
S_ν [Jy]
2
5
10
20
50
100
ν [GHz]

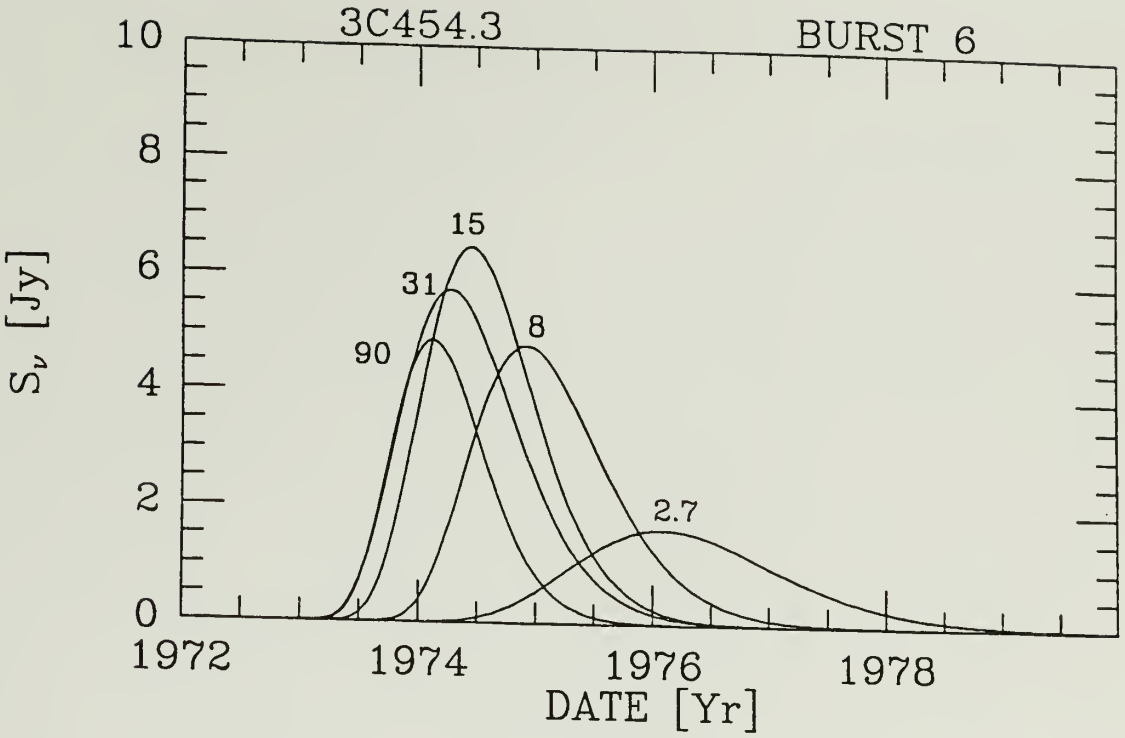

Figure 3.6. The multifrequency outburst profiles for burst 6 in 3C454.3.

Figure 3.7. The spectral evolution of burst 6 in 3C454.3. The solid line indicates the epoch of peak at 15 GHz. The top panel is prepeak and the bottom panel is post peak.

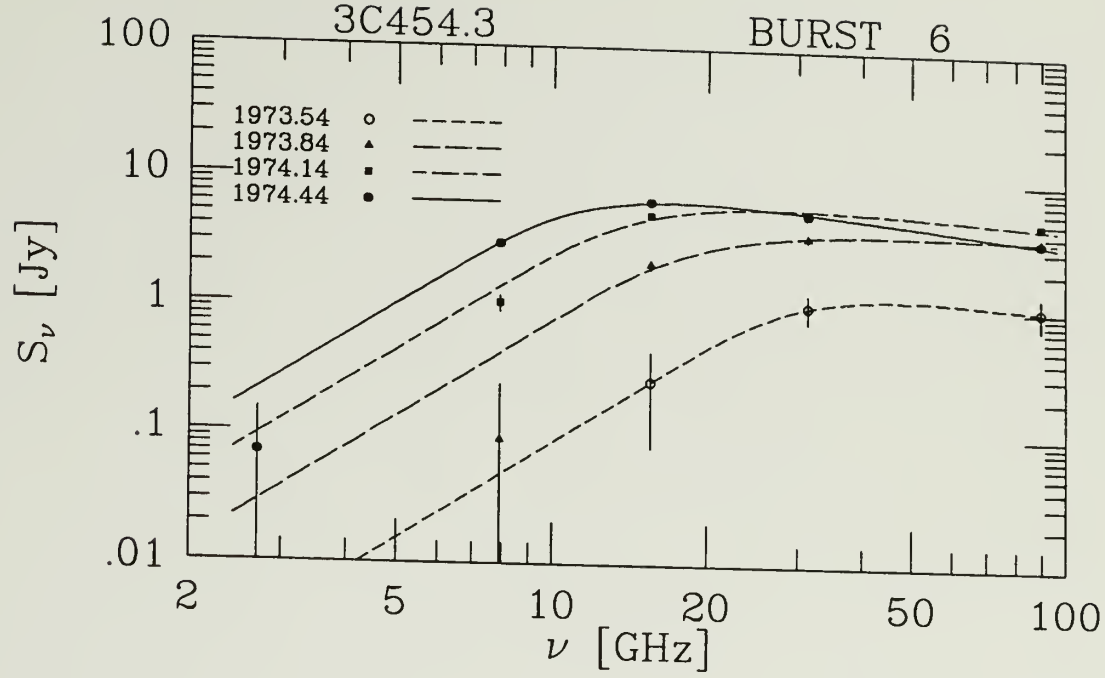
3C454.3
BURST 6
1973.54
1973.84
1974.14
1974.44
100
10
1
.1
.01
2
5
10
20
50
100
S_ν [Jy]
ν [GHz]

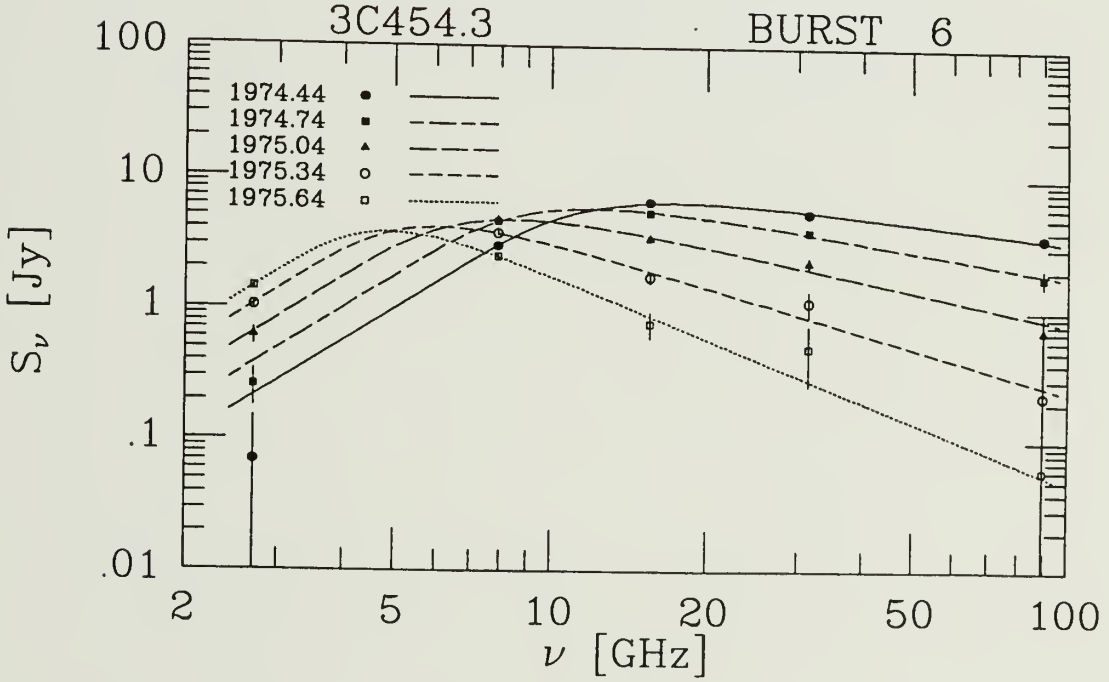
3C454.3
BURST 6
1974.44
1974.74
1975.04
1975.34
1975.64
100
10
1
.1
.01
2
5
10
20
50
100
S_ν [Jy]
ν [GHz]

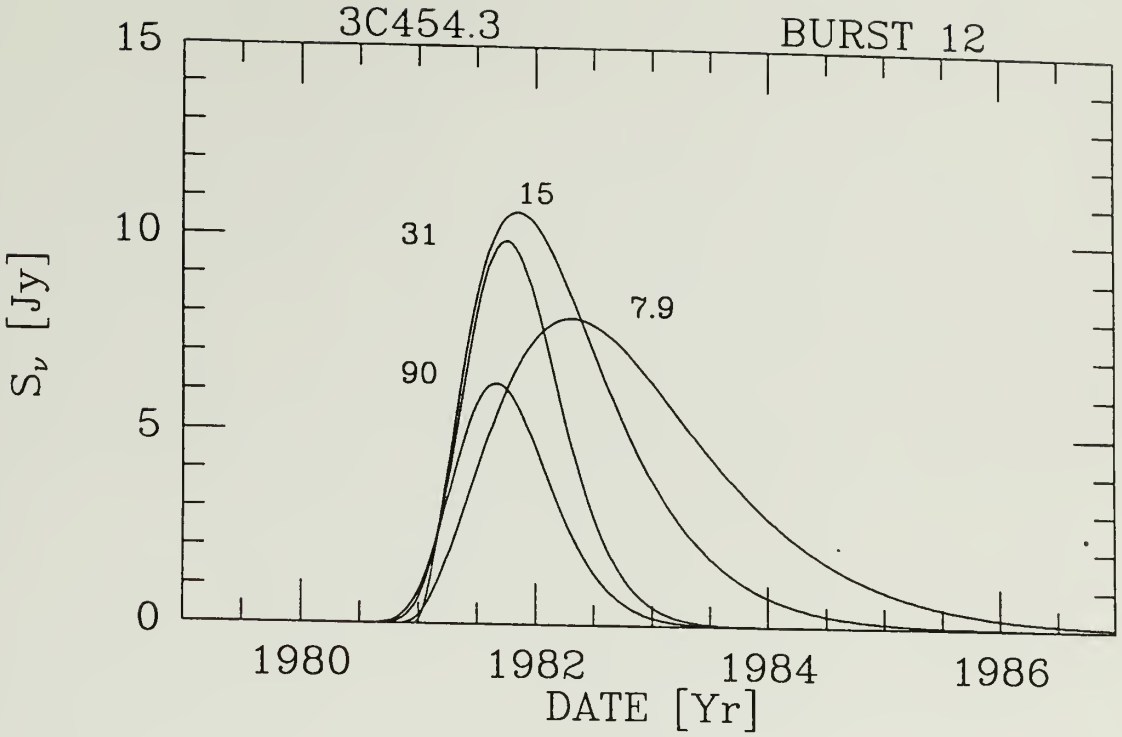

Figure 3.8. The multifrequency outburst profiles for burst 12 in 3C454.3.

Figure 3.9. The spectral evolution of burst 12 in 3C454.3. The solid line indicates the epoch of peak at 15 GHz. The top panel is prepeak and the bottom panel is post peak.

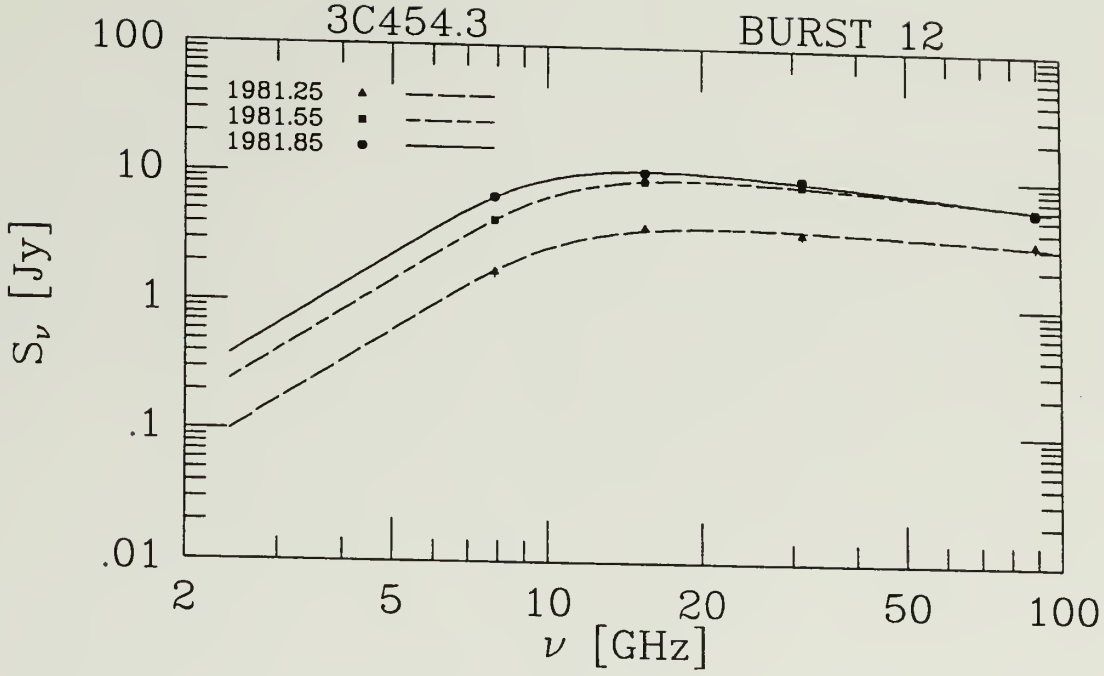
3C454.3
BURST 12
1981.25
1981.55
1981.85
100
10
1
.1
.01
S_ν [Jy]
2
5
10
20
50
100
ν [GHz]

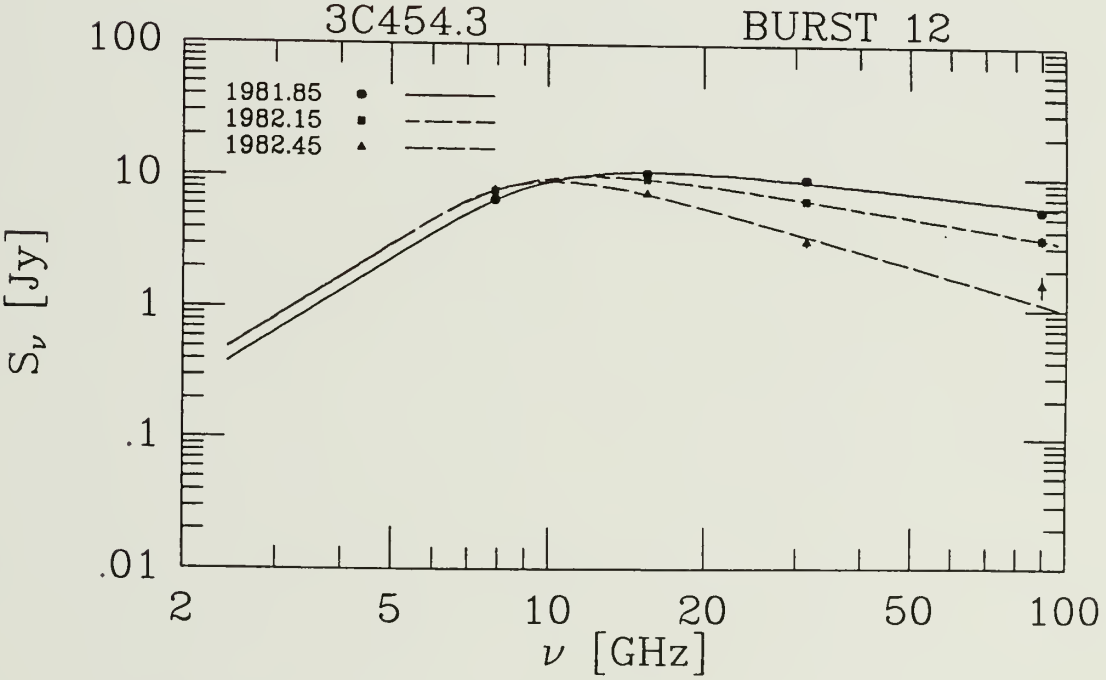
3C454.3
BURST 12
1981.85
1982.15
1982.45
100
10
1
.1
.01
S_ν [Jy]
2
5
10
20
50
100
ν [GHz]

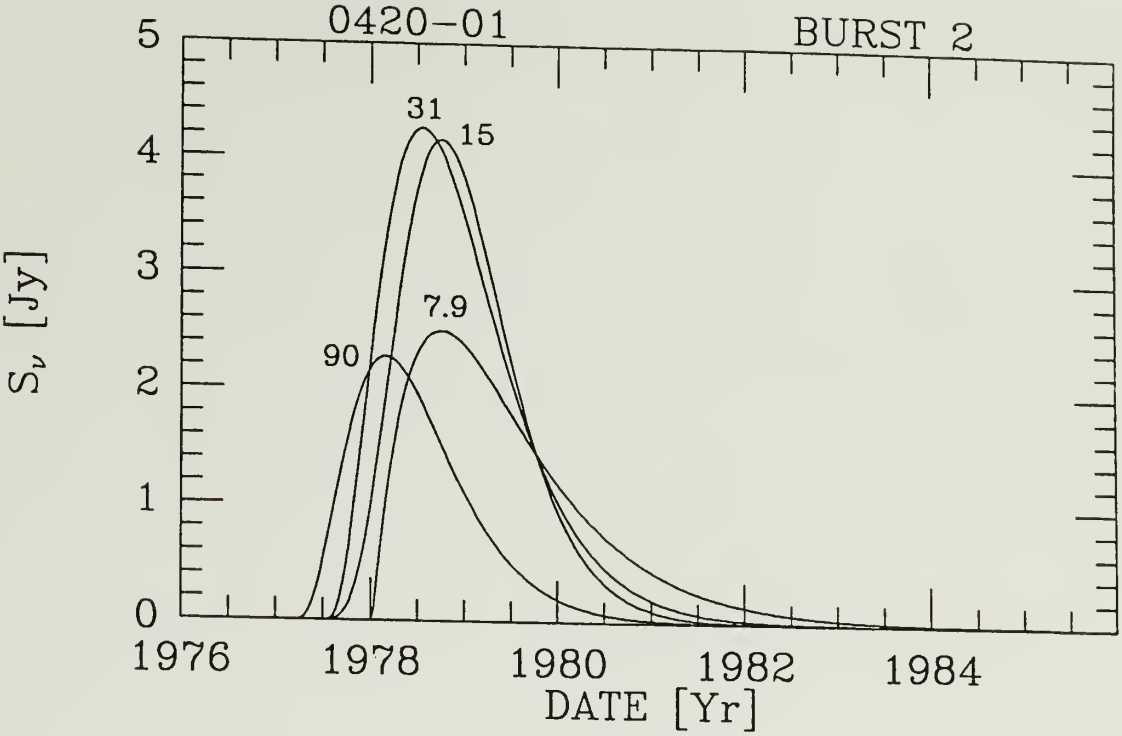

Figure 3.10. The multifrequency outburst profiles for burst 2 in 0420-01.

Figure 3.11. The spectral evolution of burst 2 in 0420-01. The solid line indicates the epoch of peak at 15 GHz. The top panel is prepeak and the bottom panel is post peak.

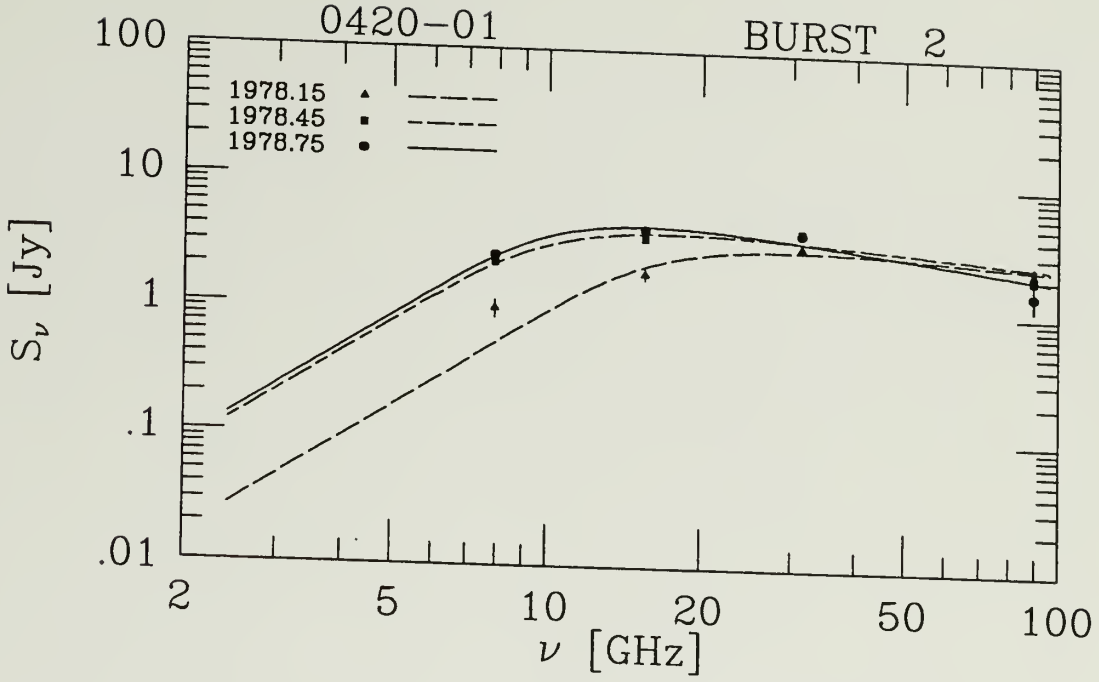
0420−01
BURST 2
1978.15
1978.45
1978.75
100
10
1
.1
.01
S_ν [Jy]
2
5
10
20
50
100
ν [GHz]

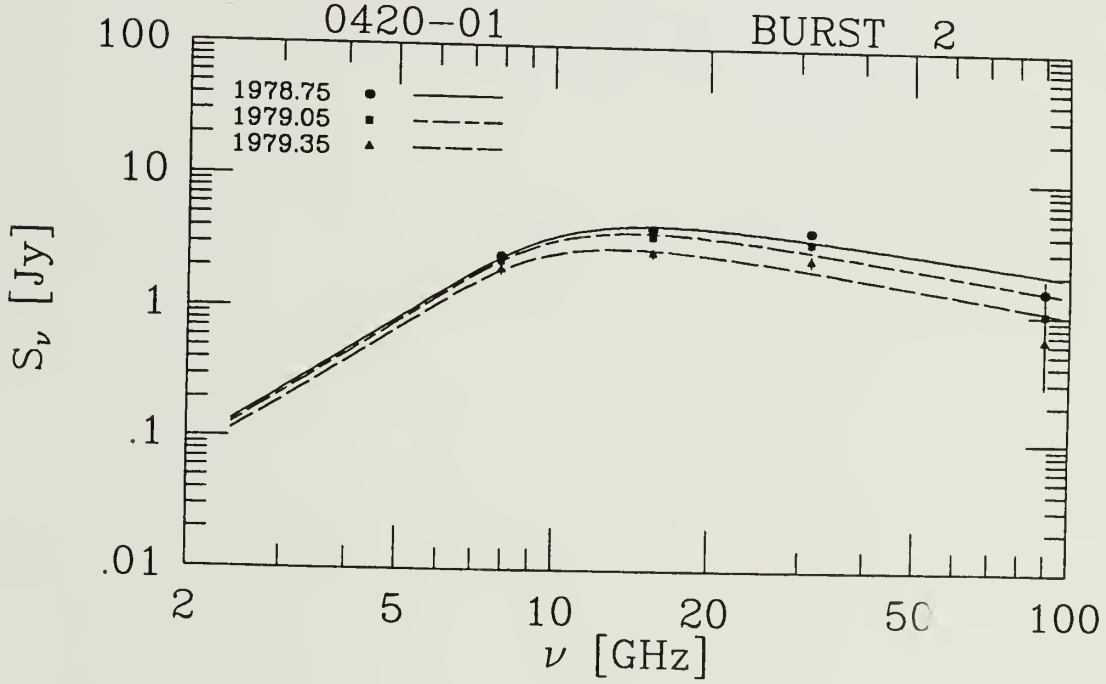
0420−01
BURST 2
1978.75
1979.05
1979.35
100
10
1
.1
.01
S_ν [Jy]
2
5
10
20
50
100
ν [GHz]

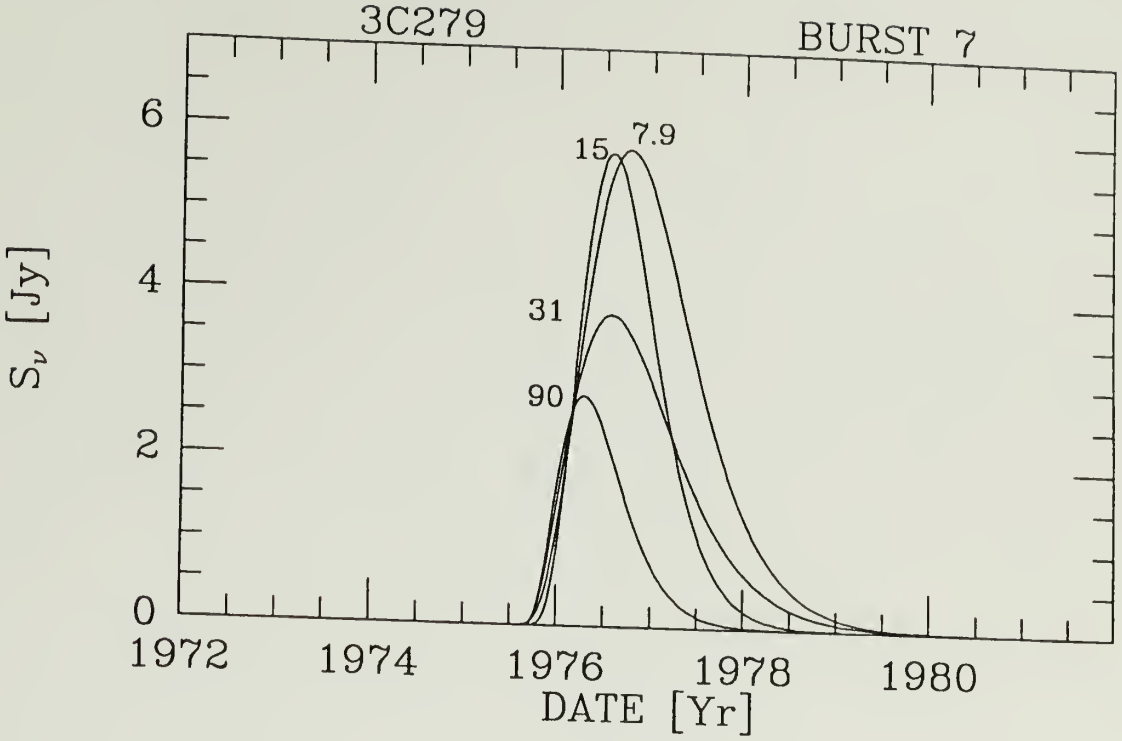

Figure 3.12. The multifrequency outburst profiles for burst 7 in 3C279.

Figure 3.13. The spectral evolution of burst 7 in 3C279. The solid line indicates the epoch of peak at 15 GHz. The top panel is prepeak and the bottom panel is post peak.

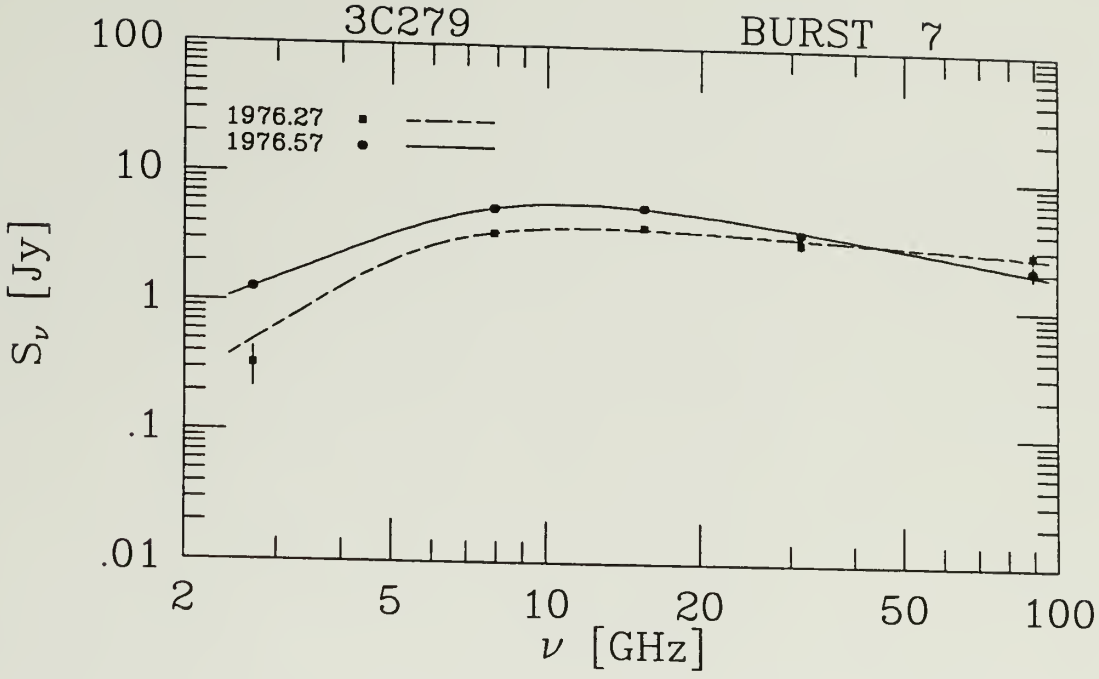
3C279
BURST 7
1976.27
1976.57
100
10
1
.1
.01
S_ν [Jy]
2
5
10
20
50
100
ν [GHz]

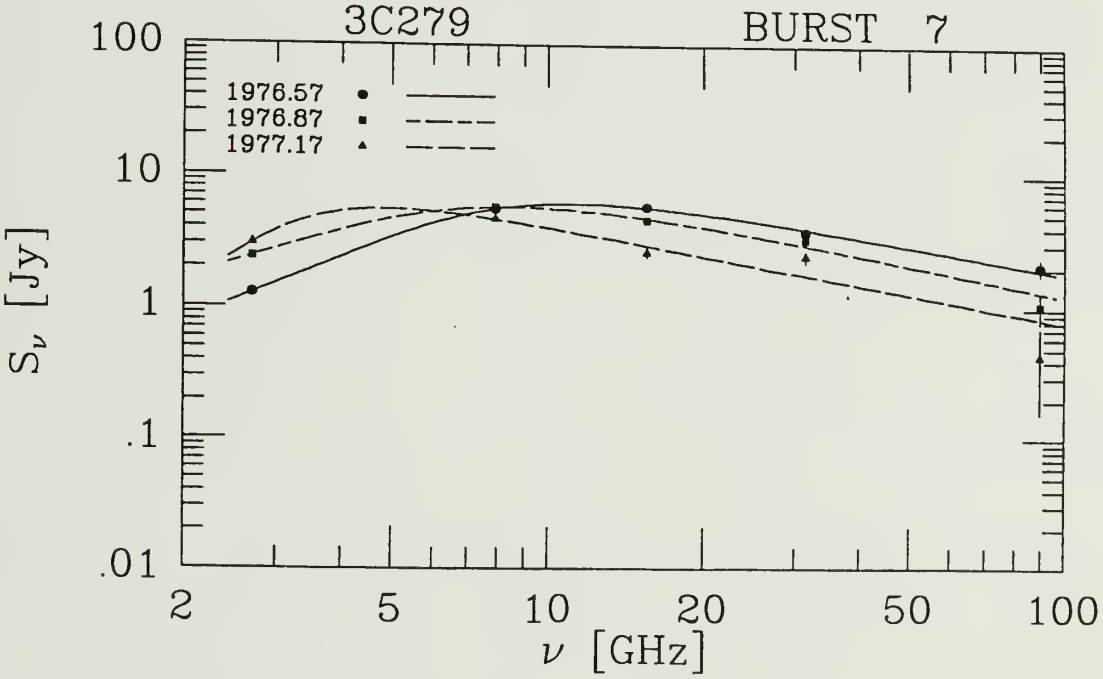
3C279
BURST 7
1976.57
1976.87
1977.17
100
10
1
.1
.01
S_ν [Jy]
2
5
10
20
50
100
ν [GHz]

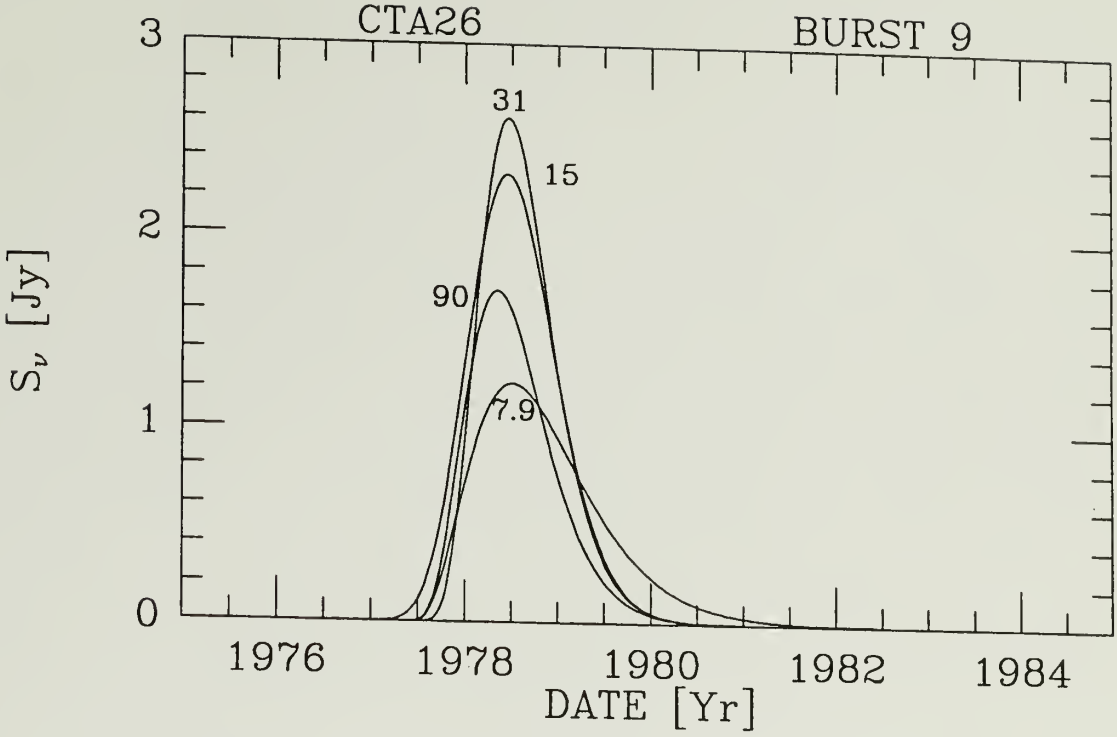

Figure 3.14. The multifrequency outburst profiles for burst 9 in CTA26.

Figure 3.15. The spectral evolution of burst 9 in CTA26. The solid line indicates the epoch of peak at 15 GHz. The top panel is prepeak and the bottom panel is post peak.

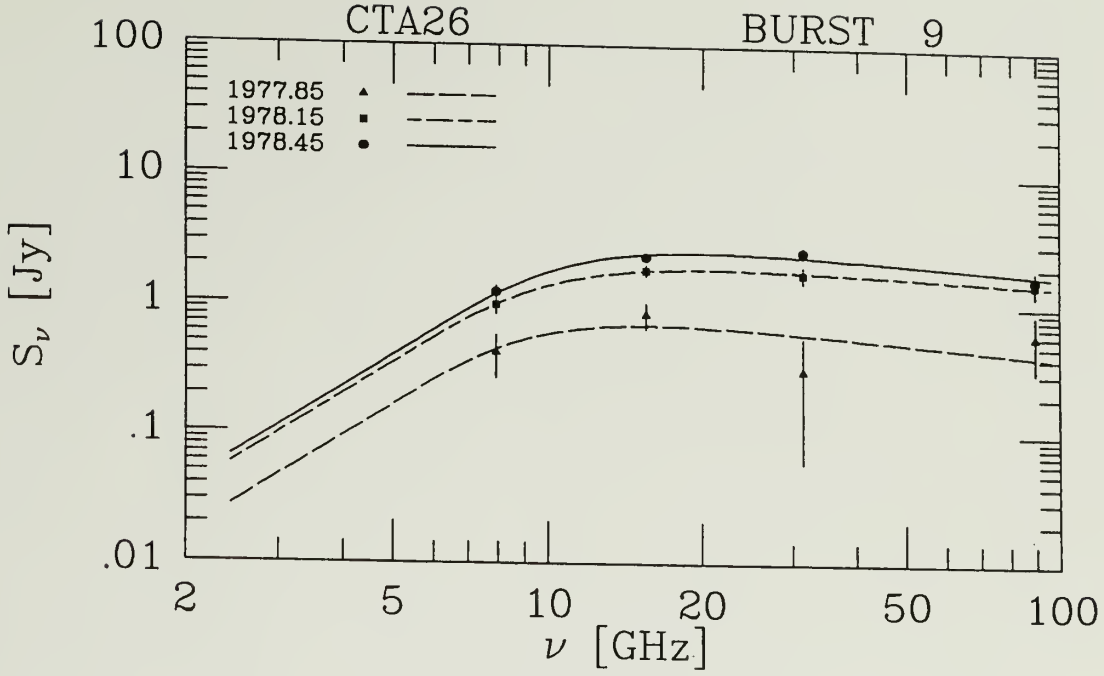
CTA26
BURST 9
1977.85
1978.15
1978.45
100
10
1
.1
.01
S_ν [Jy]
2
5
10
20
50
100
ν [GHz]

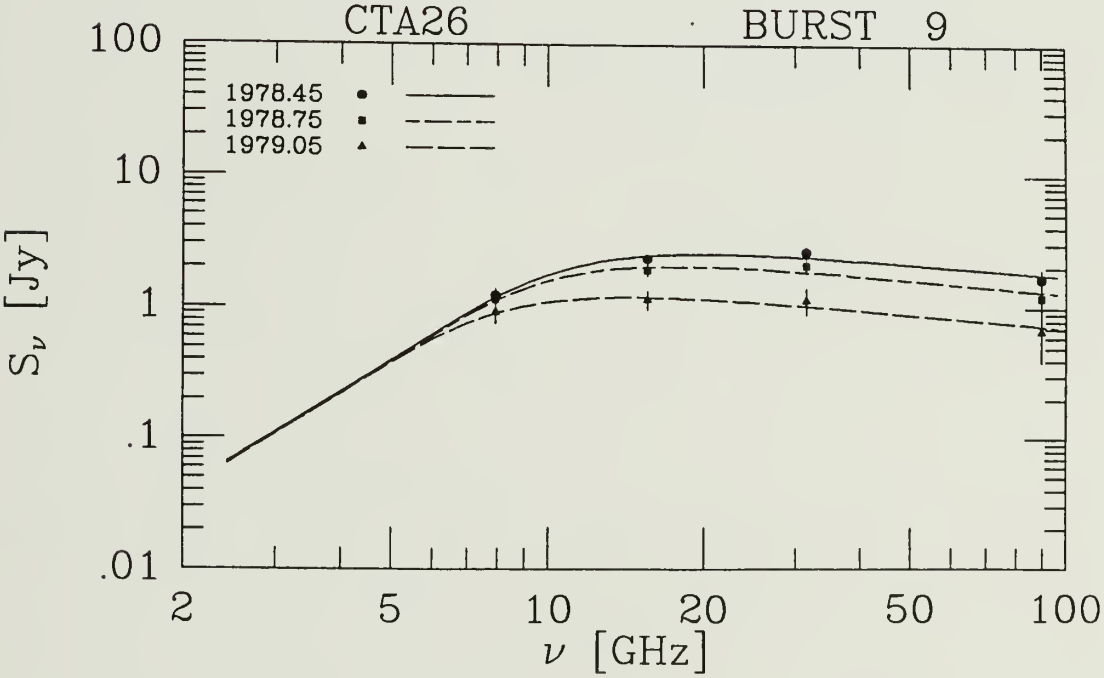
CTA26
BURST 9
1978.45
1978.75
1979.05
100
10
1
.1
.01
S_ν [Jy]
2
5
10
20
50
100
ν [GHz]

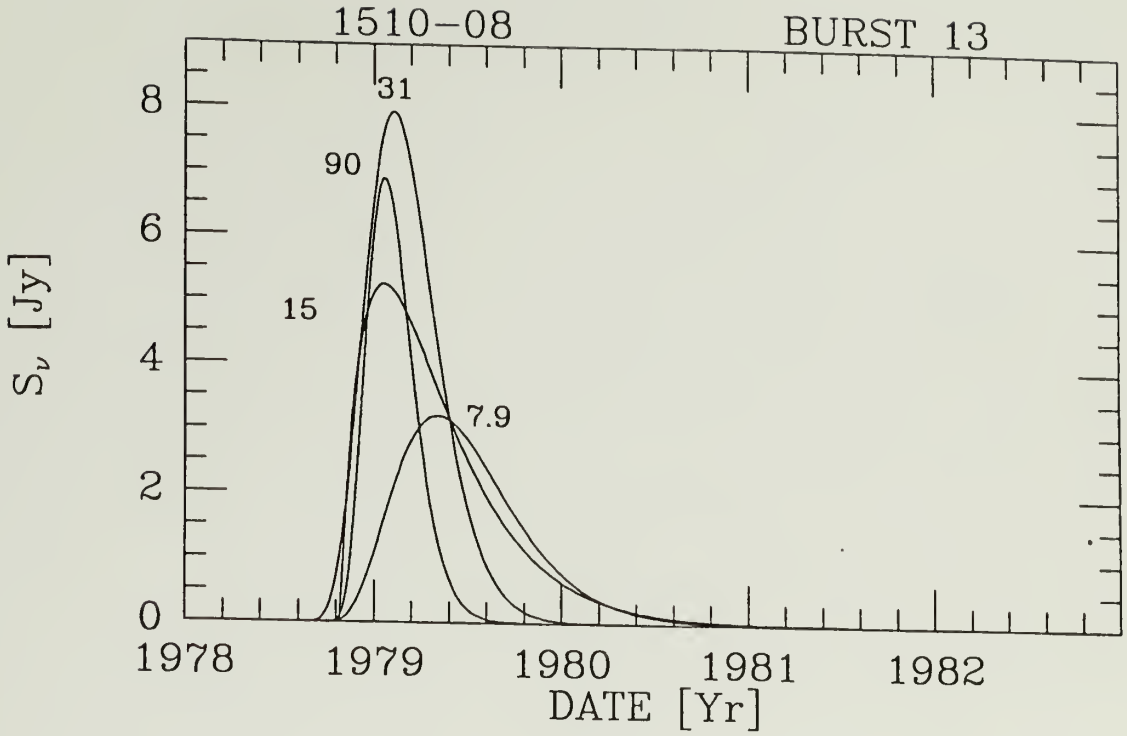

Figure 3.16. The multifrequency outburst profiles for burst 13 in 1510-08.

Figure 3.17. The spectral evolution of burst 13 in 1510-08. The solid line indicates the epoch of peak at 15 GHz. The top panel is prepeak and the bottom panel is post peak.

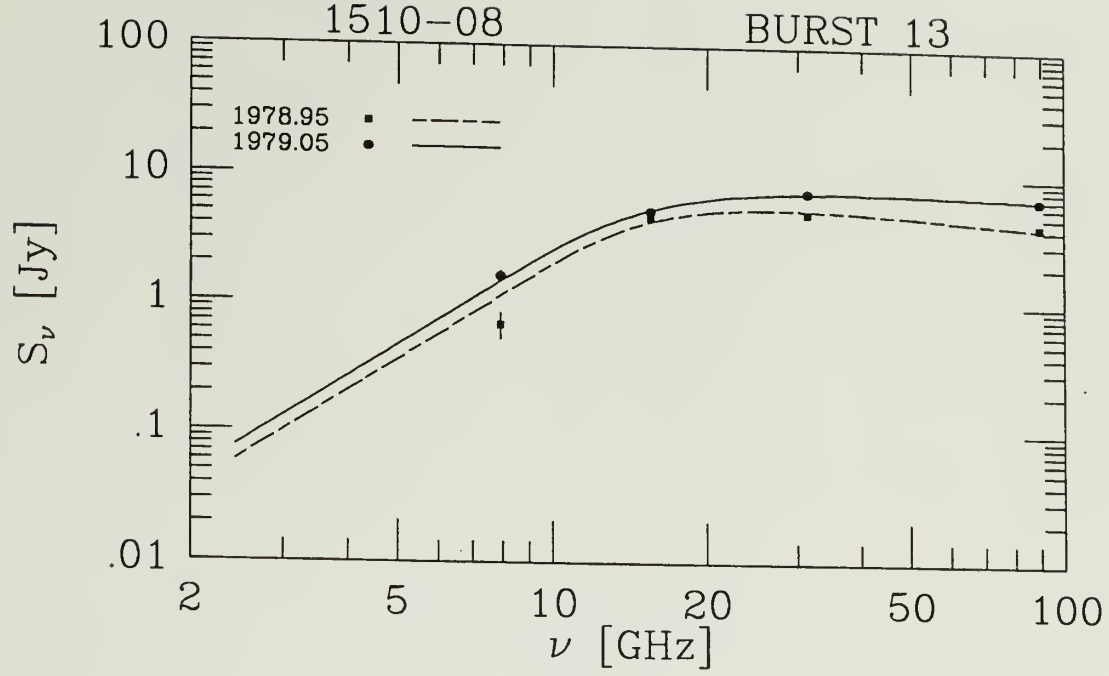
1510−08
BURST 13
1978.95
1979.05
100
10
1
.1
.01
S_ν [Jy]
2
5
10
20
50
100
ν [GHz]

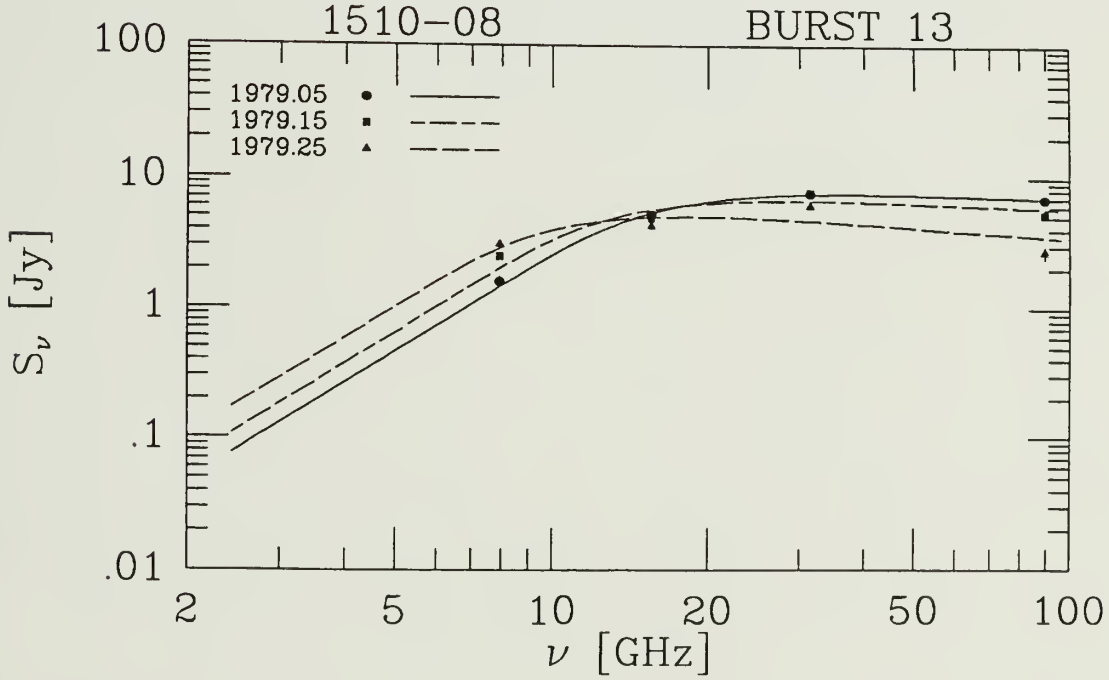
1510−08
BURST 13
1979.05
1979.15
1979.25
100
10
1
.1
.01
S_ν [Jy]
2
5
10
20
50
100
ν [GHz]

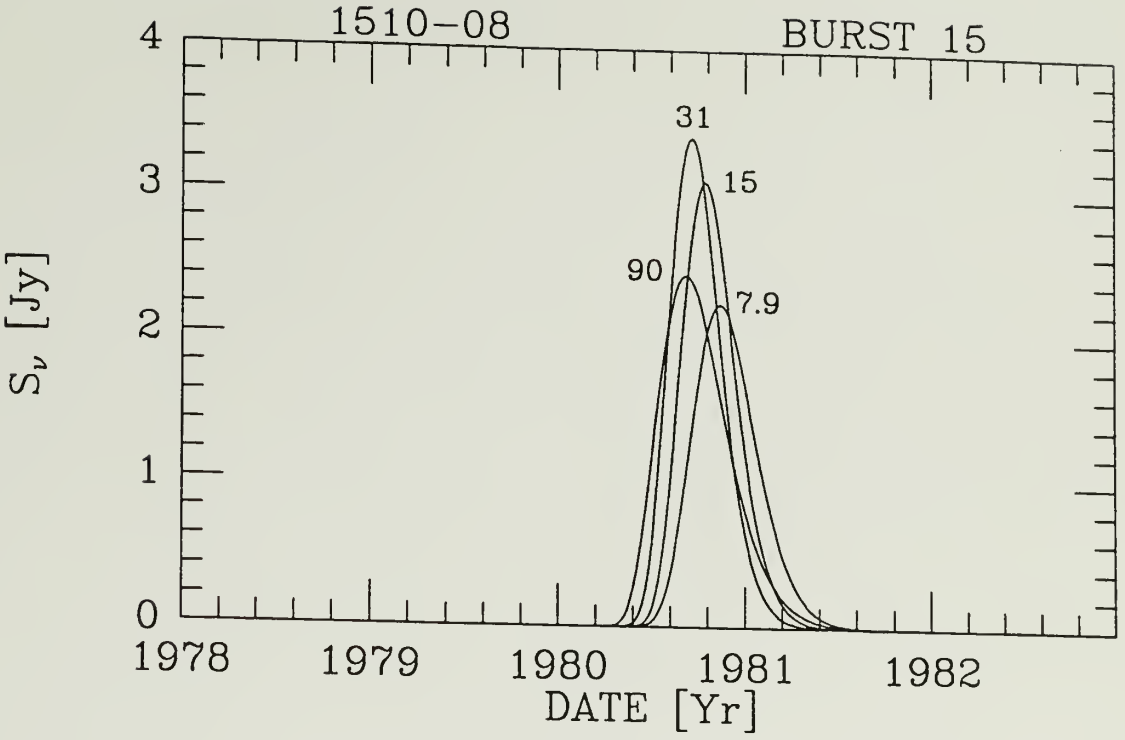

Figure 3.18. The multifrequency outburst profiles for burst 15 in 1510-08.

Figure 3.19. The spectral evolution of burst 15 in 1510-08. The solid line indicates the epoch of peak at 15 GHz. The top panel is prepeak and the bottom panel is post peak.

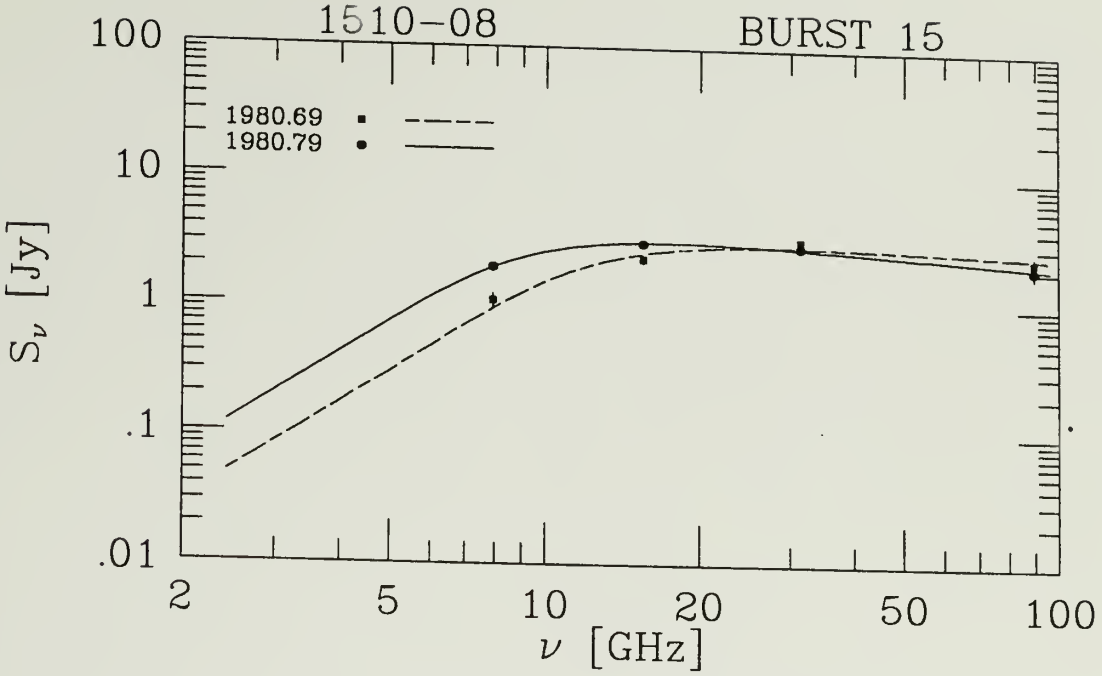
1510−08
BURST 15
1980.69
1980.79
100
10
1
.1
.01
S_ν [Jy]
2
5
10
20
50
100
ν [GHz]

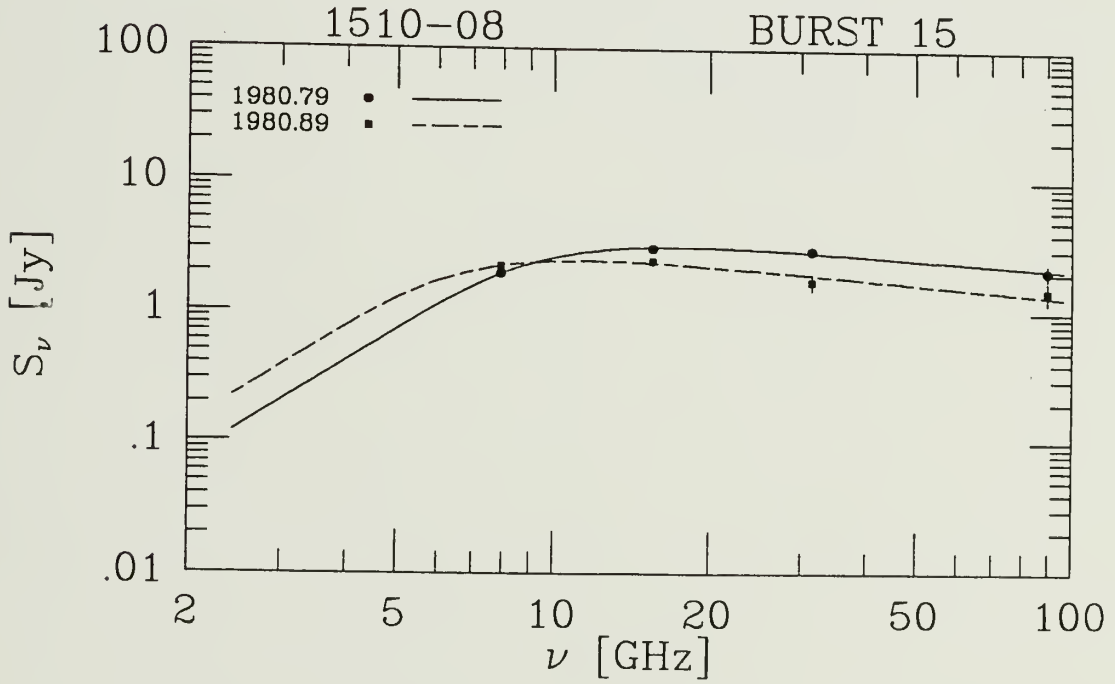
1510−08
BURST 15
1980.79
1980.89
100
10
1
.1
.01
S_ν [Jy]
2
5
10
20
50
100
ν [GHz]

Figure 3.20. The evolution in 8 outbursts of the observed outburst spectral maximum (S_m) as a function of the turn over frequency (ν_m). The dotted lines indicate the predicted migration slopes for the three phases of the MG model (inverse Compton, Synchrotron, and Adiabatic) and the SES model.

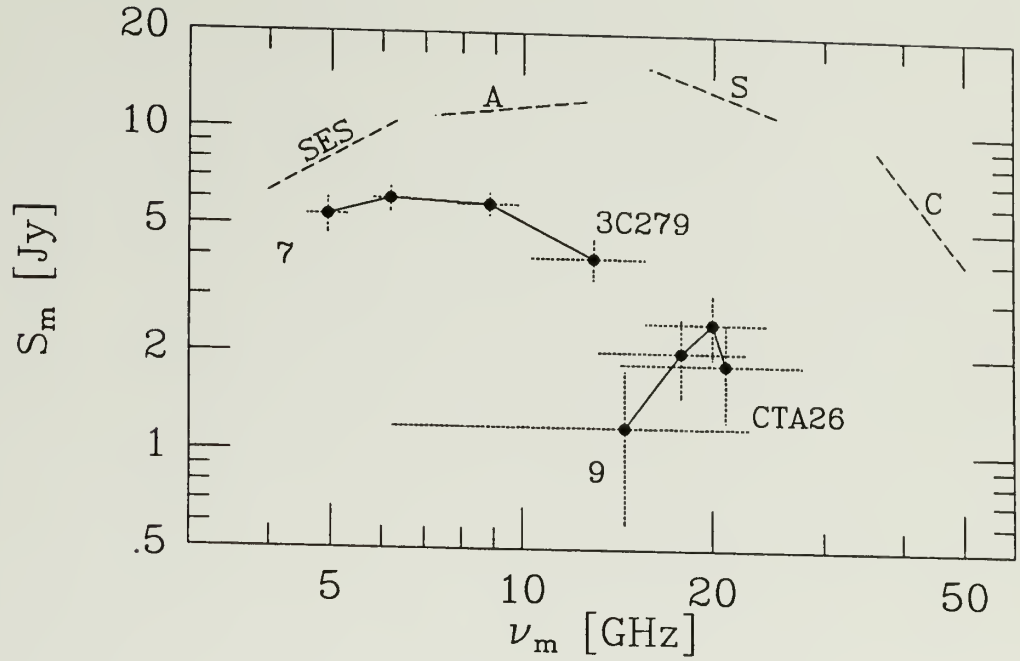

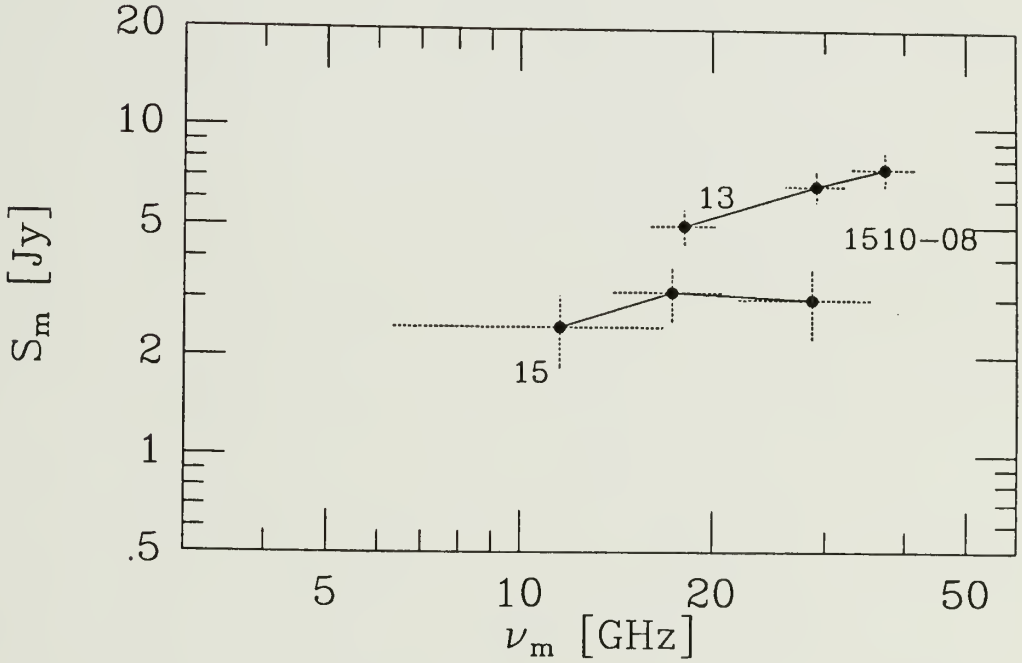

(continued next page)

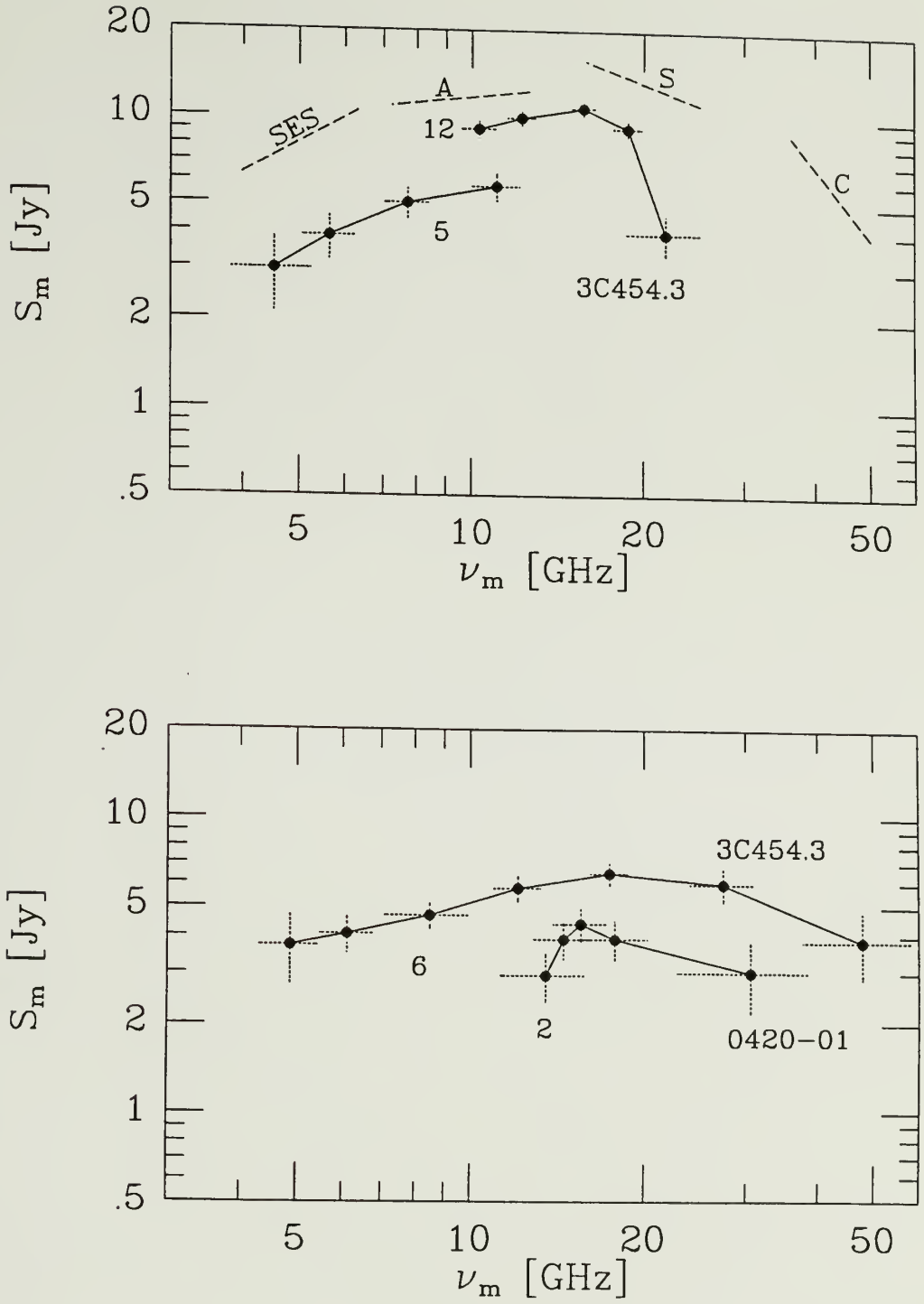

Figure 3.20 continued

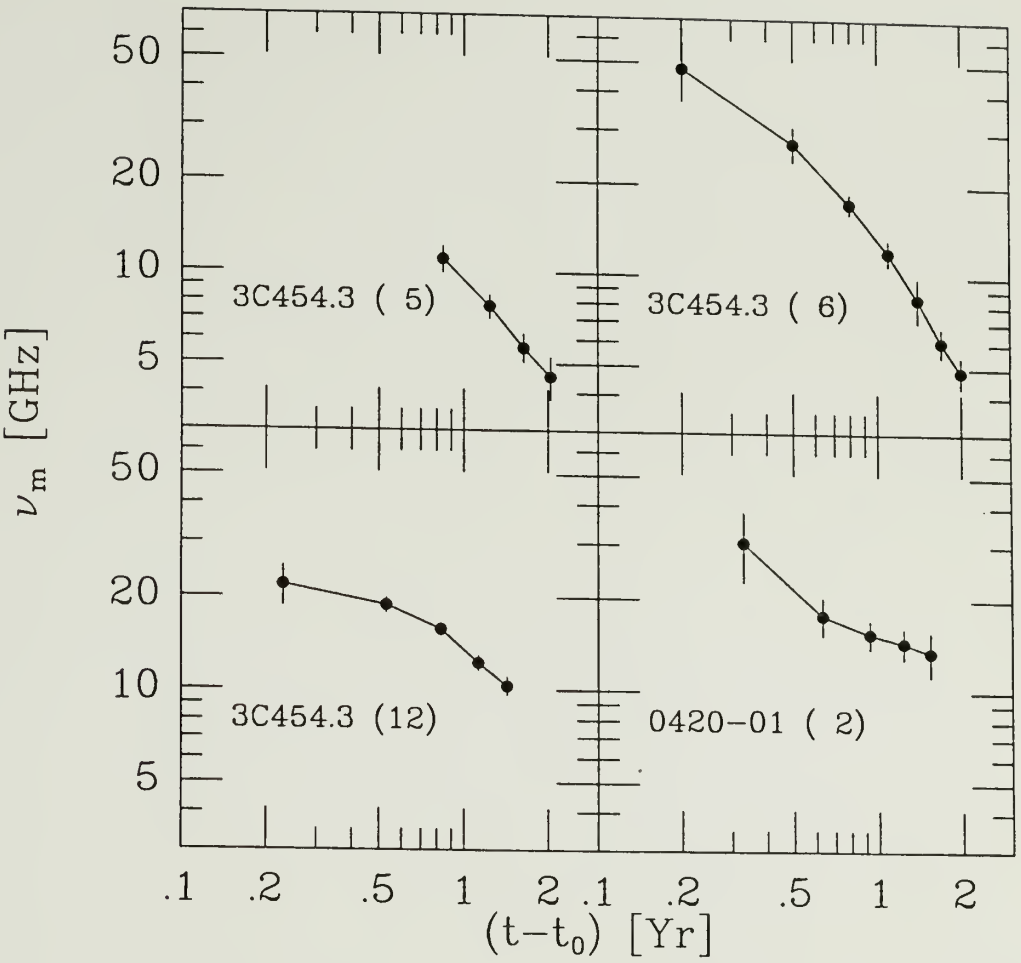

(continued next page)

Figure 3.21. The evolution in 8 outbursts of the turnover frequency as a function of time.

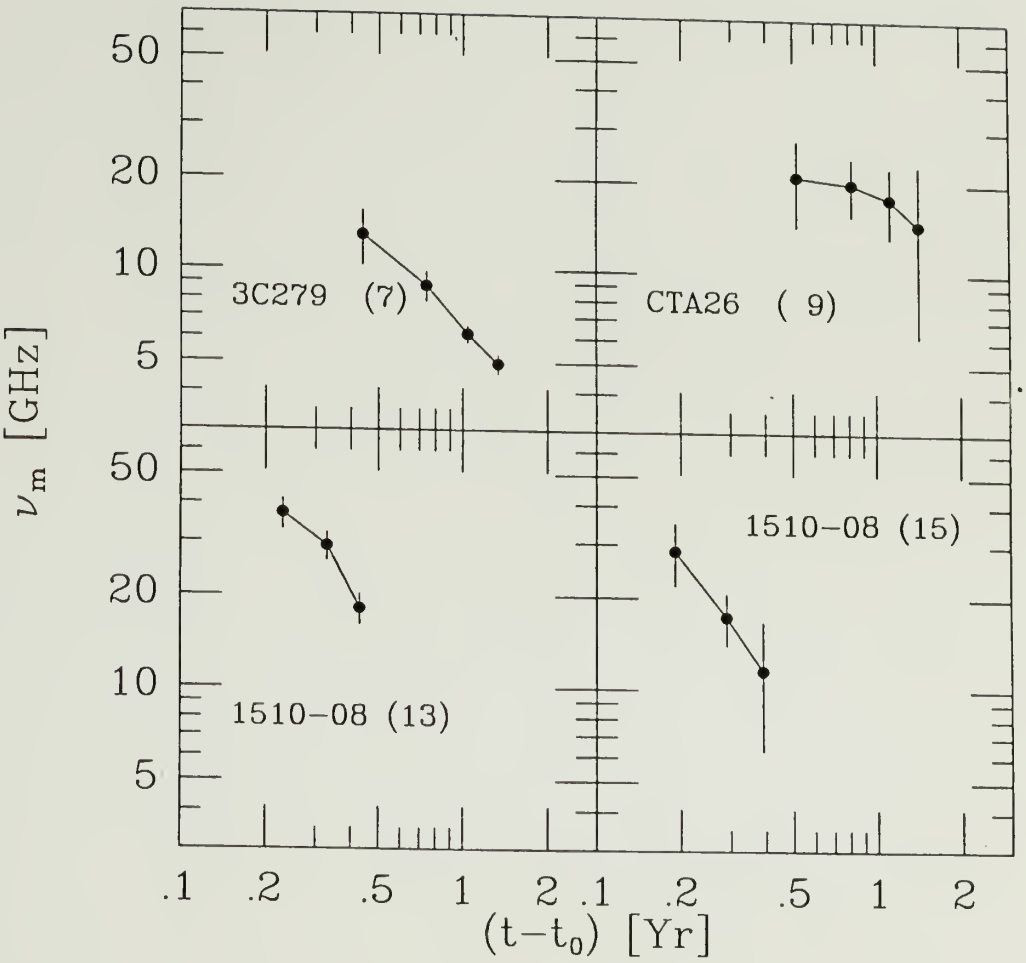

Figure 3.21 continued

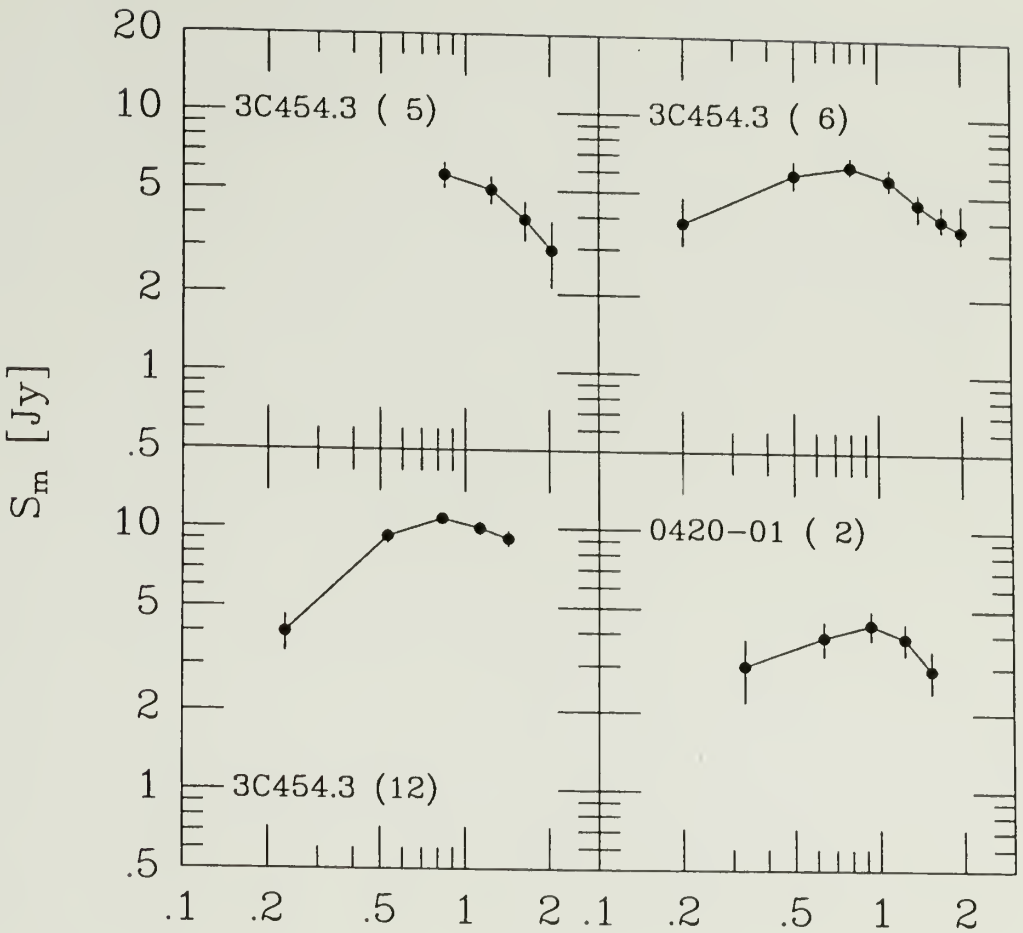

(continued next page)

Figure 3.22. The evolution in 8 outbursts of the spectral flux density maximum as a function of time.

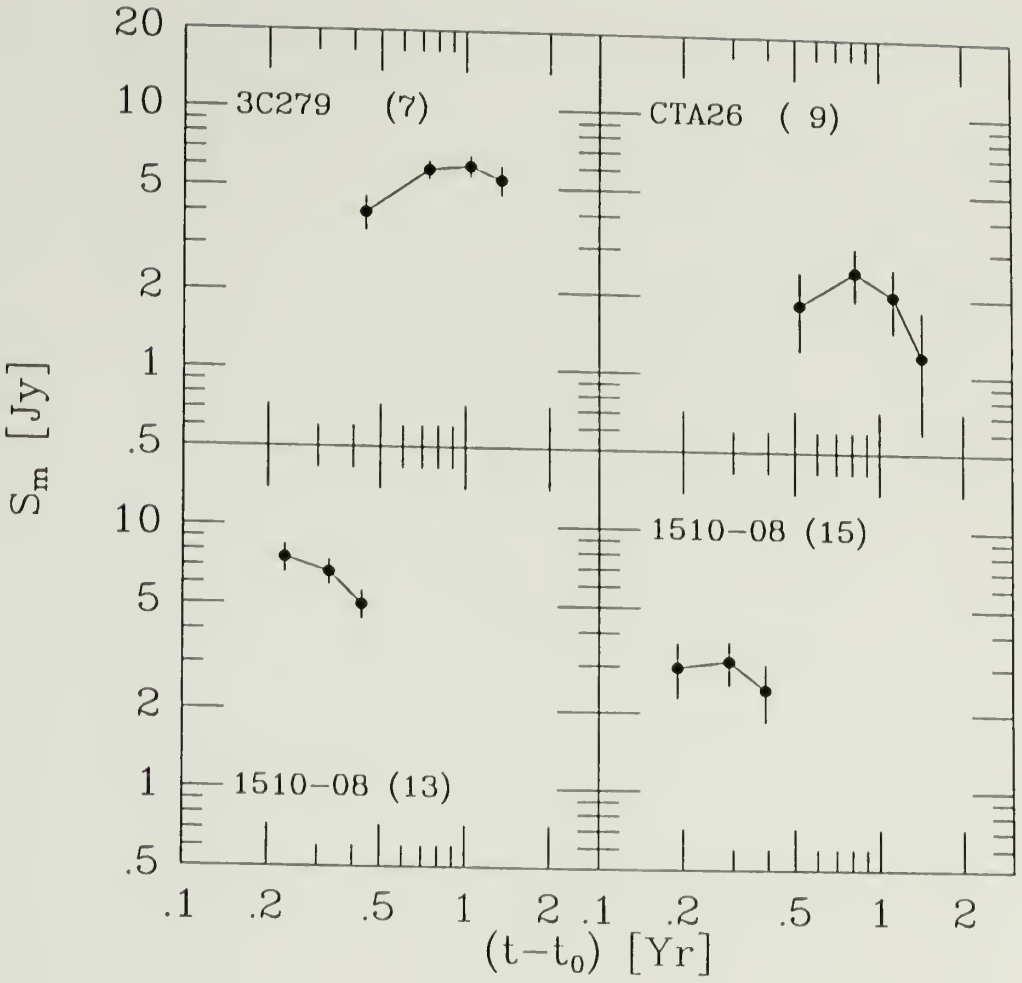

Figure 3.22 continued

CHAPTER 4

PERIODICITIES?

4.1 Introduction

The question of whether or not periodic flux variations exist in Active Galactic Nuclei (AGN) has been debated for almost 25 years. Since the initial report of a quasi-periodic 13 year period in the optical variations of 3C273 by Smith (1965), periodic variations at optical to radio wavelengths have been reported in AGN with periods from minutes to decades (Table 4.1). However, they have also been very elusive to confirm. The confirmation of periodic flux variations would place severe constraints on virtually all AGN models.

Investigating periodic behavior (on timescales greater than about 8 hr) in AGN using radio rather than optical data has the advantage of offering year round source coverage, because the radio data do not suffer from large periodic gaps due to the source's placement in the daytime sky. This is important, because when using discrete Fourier transform based period search algorithms, periodic gaps in the data combined with long time scale variability can cause spurious spikes in the power spectrum at the time scales of interest (Scargle, 1982).

Table 4.1. Representative references of reported periodicity in AGN flux variations.

Table 4.1

Source	Band	Period	Reference
3C273	Opt	~13 yr	Smith (1965)
3C445	Opt	1600 days	Barbieri et al. (1977)
		800 days	
		140 days	
NGC5128	7 & 14mm	8 days	Kaufmann and Raffaelli (1979)
3C446	Opt	1540 days	Barbieri et al. (1985)
		2130 days	
OJ287	7mm	35 min	Kinzel et al. (1988)
OJ287	V band	11.6 yr	Sillanpää et al. (1988)

Visual inspection of the Dent-Balonek (DB) data base suggests possible periodic or quasi-periodic behavior in the flux density variations in several radio sources. Any analytical search for periodicity should be performed primarily on the higher frequency data for three reasons: the amplitudes of the flux variations at the lower frequencies are smaller, the outbursts are broader and thus blend together, and the time from initiation to peak of an outburst may not be constant from burst to burst.

Even at the highest frequency, most of the outbursts in the ~120 sources in the DB observing program are either partially blended or the number of outbursts during the span of measurements is small. Four sources were chosen for investigation: 3C454.3, NGC5128, 0235+16, and 1510-08. NGC5128 and 3C454.3 exhibit nearly equally

spaced outbursts as shown by visual inspection of the variability curves. 0235+16 and 1510-08 were chosen because of the large number (>10) of clearly defined bursts represented in the data set and their inclusion in the outburst analysis of Chapter 3.

4.2 The Scargle Periodogram

Many previous searches for periodicity in source variability have relied upon Fourier transforms methods. A periodogram is an estimate of the power spectrum and is normally defined as the square of the discrete Fourier transform:

$$P_x(\omega) = \frac{1}{N} \left| DFT_x(\omega) \right|^2 = \frac{1}{N} \left| \sum_{j=1}^{N} X(t_j)\exp(-\omega t_j) \right|^2 \qquad (4.1)$$

(Deeming 1975). For equally spaced data the periodogram is normally evaluated at equally spaced frequencies between 2/T and 2N/T, where T is the total time span of the time series. A problem with the classical periodogram is that it is difficult to predict the statistical significance of results.

This problem is alleviated (at least for noisy data) with the Scargle version of the periodogram (Scargle, 1982). The modified periodogram is given by

$$P_x(\omega) = \frac{1}{2}\left\{ \frac{\left[\sum_{j=1}^{N} X(t_j)\cos\,\omega(t_j-\tau)\right]^2}{\sum_{j=1}^{N}\cos^2\,\omega(t_j-\tau)} + \frac{\left[\sum_{j=1}^{N} X(t_j)\sin\,\omega(t_j-\tau)\right]^2}{\sum_{j=1}^{N}\sin^2\,\omega(t_j-\tau)} \right\}, \quad (4.2)$$

where τ is defined by

$$\tan(2\omega\tau) = \left(\sum_{j=1}^{N} \sin\,2\omega t_j \right) \Big/ \left(\sum_{j=1}^{N} \cos\,2\omega t_j \right), \quad (4.3)$$

and where the t_js are the times of observation. The Xs are the observed fluxes and ω is the trial angular frequency ($\omega = 2\pi\nu$). The Scargle periodogram is normalized by the total variance of the data, $P_N = P_x / \sigma^2$.

Scargle's formulation of the periodogram has the following advantages. It allows the largest peak in the periodogram to be assigned a probability that it was caused by gaussian noise. In addition, the factor τ makes the periodogram independent of the choice of origin of the time series. Finally, the method is exactly equivalent to least squares fitting of sine and cosine curves to the data. This implies the Scargle periodogram is giving equal weight to each of the points instead of equal weight to intervals of time, as occurs in the fast Fourier transform (Press and Teukolsky, 1988).

Only Scargle's method of Fourier analysis gives an analytic form for the significance level of a peak in the periodogram. Even then, the significance is for the null hypothesis that the input data are

all noise. This method works well in variable star studies, where the amplitude of any variations is roughly constant, and the problem is detecting a possible periodic variation that is noise limited. In our case, however, the variations are clearly present, but the amplitudes of the outbursts can vary enormously. Thus, our problem is to determine the significance of a spike in the periodogram, given wildly varying amplitudes. An even more basic question is: does this method work at all for this type of data? One way to address the question is with Monte-Carlo simulations.

4.2.1 Monte-Carlo Simulations

Monte-Carlo simulations using randomly spaced outbursts with random amplitudes would allow the construction of an empirical probability distribution of the amplitude of the largest peak in each the periodograms of the simulated data. Thus, a peak in a periodogram of real data could be assigned a probability it was created by just random variations in the source. However, as will be seen, the question of this distribution is moot. Periodograms of simulated *periodic* data quickly indicate the hazards of applying this method to variable radio sources.

The results of Chapter 3 indicate that at short centimeter wavelengths the Legg function models the outburst profiles well. If that is true, what does the periodogram for periodically spaced outbursts look like? For a demonstration, several different cases each with one thousand simulated time series were generated using outbursts spaced with a uniform period of one year. The Legg

function was used to simulate the outburst profiles. The time of initiation to time of peak for each burst was kept constant at one year. The sampling was done at uniform intervals of 0.1 years to simulate the average spacing of the 15 GHz Haystack observations. The outburst amplitudes were held constant or randomized with an exponential probability distribution with a mean of 10. (The choice of probability distribution is motivated solely by the fact that the resulting simulated time series look similar to real variability curves.) Different data set lengths and decay times were also simulated. The simulated variations were allowed to stabilize about some mean level before sampling the time series.

Each time series was analyzed by calculating its Scargle periodogram. Statistics were compiled of the variance of the data set, and the amplitude and frequency of the largest peak in each periodogram. The parameters used to generate the different cases are shown in Table 4.2. The one hundredth generated time series from each of the different cases and their respective periodograms are shown in Appendix E. Plots of the maximum peak amplitude versus the frequency of the peak for each spectrum in each of the different cases are also shown in Appendix E. When the amplitude was constant in all the outbursts, only one time series and transformation was generated as all the time series would be identical. The percentage of times that the largest peak in the periodogram was at the set frequency of 1 yr^{-1} is also shown in Table 4.2.

Table 4.2. Table describing the parameters for the different simulations and the percentage of times the largest peak in the periodogram was at the set frequency of 1 yr^{-1}. NPTS is the number of bursts in the test. Test 0 had uniform burst amplitudes. All the other tests had random burst amplitudes.

Table 4.2

Test	NPTS	τ [yr]	%correct
0	1	0.2	100.0
1	100	0.05	40.4
2	200	0.05	68.6
3	100	0.1	0.7
4	200	0.1	0.1
5	100	0.2	0.0
6	200	0.2	0.0
9	400	0.2	0.0
7	100	0.4	0.0
8	200	0.4	0.0

The figures in Appendix E show several trends. When the amplitudes of all the bursts are equal (Test 0), the Scargle periodogram has no trouble finding the correct frequency (period) for bursts that are partially blended. However, when the amplitudes of individual bursts are different, the periodogram method gets into trouble. As τ is made longer and the bursts become more blended the power contained in the variations is shifted to longer periods (smaller frequencies). Only at the smallest value of the decay constant examined (τ = 0.05 yr), where the duty cycle is small, did the largest spectral peak occur at the set frequency (Tests 1 and 2)

better than about 50% of the time. At this value of τ, a longer data set, as expected, improves the detection rate. However, for the three larger values of the decay constant, the method found the correct burst rate less than one percent of the time. Simulations using the logarithms of the variations produced similar results.

Thus, for reasonable parameter values seen in the outburst profile fits of chapter 3 ($t_p - t_0 \approx 1$ yr and $\tau \approx 0.2$ yr), the range of amplitudes of the different outbursts coupled with the blending of the outbursts causes most of the power in the periodogram to be at lower frequencies than the true outburst rate. Even if the length of our observations were quadrupled, as in test 9, and there were deterministic periodic bursts present, the simulation results indicate that this method would not detect the periodicity. In addition, real variations of the other outburst parameters, plus intrinsic noise in the source and measurement error, would just make the problem worse. Thus it appears that period detections methods based upon the DFT or least squares fittings of sines and cosines to the data will probably not detect a periodic burst rate in AGN radio variability data.

4.2.2 Periodogram Analysis of Real Data

For completeness, before the periodogram method is abandoned, the variability data and the respective periodograms for the four selected sources are shown in Figures 4.1 to 4.4. The 15 GHz data were analyzed for three sources because of the relatively high frequency and frequent sampling of the observations. The 31.4 GHz

data, although under sampled, were used for NGC5128, since this southern source could only be observed from Kitt Peak.

0236+16. The periodogram for this source (Figure 4.1) indicates most of the power is at time scales greater than half a year. Note that there is a small spike that is about twice the local noise at $\nu = 4.12\ yr^{-1}$ (P = 0.24 yr).

NGC5128. This source is one of the two sources in the data base to indicate quasi-periodic behavior by eye. In addition, this source has five nearly equal amplitude bursts and is thus a reasonable candidate for use with the Scargle periodogram. The periodogram (Figure 4.2) indicates a clear peak at a frequency of $0.87\ yr^{-1}$ (P = 1.15 year).

1510-08. The periodogram (Figure 4.3) for this source exhibits a spike at $0.55\ yr^{-1}$ (P = 1.82 yr). This is probably due to the four bursts that are separated by about 2 years each, between 1970 and 1976.

3C454.3. Once again, for this source the periodogram (Figure 4.4) shows most of the power appearing at very low frequencies ($\nu < 0.6$ yr). The largest spike appears at $0.15\ yr^{-1}$ (P = 6.7 yr). This is probably due to the large bursts in 1968, 1975, and 1982. Note that the data suggest that bursts occur about once a year. However, there is no indication of this in the periodogram.

All the periodograms exhibit several peaks at low frequencies. However, only one of the periodograms (NGC5128) has a large isolated peak that does not appear to be 1/f noise and we still lack a statistical significance for this peak. Clearly an alternative analysis scheme should be sought.

4.3 Phase Residual (O-C) Diagram

The profile fits from Chapter 3 provide a time of peak for each burst. Therefore, we should be able to use these times of peak to search for periodicities. In addition, once given the best fit period to the burst peak times and assuming the bursts are strictly periodic, the χ^2 test can be used to give the probability that the differences between the observed burst peak times and the calculated burst peak times are just due to measurement errors.

The O-C diagram (Observed minus Calculated time of maximum) is a phase residual diagram that is used in the study of periodic variable stars (Willson, 1986). Usually it is a plot of the difference of the time of peak and the calculated time of peak versus the burst number:

$$(O\text{-}C)_j = t_p(j) - I(j) - t_0 * P) \qquad (4.4)$$

where $t_p(j)$ is the time of peak, $I(j)$ is the assigned burst number for each burst, P is the period, and t_0 is the calculated epoch of the zero burst. The phase residual diagram verifies the assumed period and reveals changes in the period and phase of periodic variations.

Given periodic data, the phase residual diagram has the following properties: if the assumed period is correct, the data will be scattered about a horizontal line and the y intercept will show the error in the epoch of the zero burst. If the period used in the diagram is incorrect, the data will be scattered about a line with a nonzero slope as shown in examples 1 and 2 (Figure 4.5). Sudden changes in the phase of the variations will show as jumps in the

epoch as in examples 3 and 4 (Figure 4.6). A slowly changing period will produce a curved phase residual diagram.

Although, the period value used to make the phase residual diagram can come from anywhere, the phase residual diagram itself can provide the best fit period for the data. But before the method can be used, the burst numbers must be assigned. By examining the spacings between adjacent bursts it was usually obvious as to what the approximate period should be. Then using equation 4.6 the burst numbers are assigned.

$$I(j)=INT((t_p(j)-t_p(1))/P + 0.5)+1 \qquad (4.5)$$

This equation ensures that a burst is assigned the closest burst number. The peak times have the time of peak of the first burst subtracted thus ensuring that I(1)=1. Note that the equation implies that two (or more) bursts could be assigned to the same burst number. However, this would imply that ether the period used is too long or the bursts are not periodic. If necessary, the period can be made shorter (in fact, it could be cut in half), assuming only half the true number of outbursts are being seen. However, in order to have a believable period, there should be more detected bursts than missing bursts, so some judgment must be used.

Once the burst numbers are assigned, the best fit period can be found. The method is conceptually similar to, and gives identical results as, fitting the data with a linear function of burst time versus burst number. Over a range of periods centered on the first trial period the mean and the χ^2 about the mean of the differences (observed - calculated times of peak) times is calculated. The minimum in χ^2, for the different assumed periods, indicates the best

fit period and the value of χ^2_ν can be used to estimate the statistical significance of the best fit period.

Finally, examination of the phase residual diagram generated with the best fit period will also indicate the viability of the assigned burst numbers. Phase errors that are larger than π, indicate incorrectly assigned burst numbers or lack of periodicity.

4.4 Results

All the times of peak came from the profile fits of chapter 3. Additional profile fits of the bursts in NGC5128 were performed to obtain the times of peak (the fit values and plot are in Appendices B and C). The errors on the time of peak from the profile fits appeared to be too small, in some cases less than 0.05 yr. The errors are the formal errors returned from the fitting program, fitting one burst at a time. That is, there is no allowance for the errors introduced by separating blended outbursts or the assignment of t_0. Thus, in fitting the periods, the errors on t_p were assumed to have a minimum error of 0.05 years.

The forward differences, $\Delta t_p = t_p(j+1) - t_p(j)$, between bursts and the phase residual diagrams for the four sources are shown in Figures 4.7 to 4.11. χ^2 minimization was used to find the best fit period. The χ^2_ν significance test results depend *critically* upon the assignment of the error sizes. If the test is to establish periodicity, then to be conservative, it is better to use too small an error than too large, so that χ^2 is overestimated, thus reducing

the statistical significance of the fit. As explained above, the errors used are probably underestimated.

0235+16. The best fit to this source shows four burst times missing from data. Three of the bursts are visible in the data (Appendix C), but are too blended to get a reliable time of peak. Burst 13 should appear near an observed minimum in the variation curve. Since outburst amplitudes can have a wide range, its apparent absence can be interpreted as being the result of a very small amplitude. The forward differences and phase residuals plots are shown in Figure 4.7 The forward differences indicate a mean spacing between bursts of about 0.45 years. Assuming a constant period and epoch for the bursts, the best fit to the data gives: P=0.46±0.02 yr, E=1975.47±0.07, and χ^2_ν=2.74. The χ^2_ν value implies a goodness of fit at less than 1%. However, this result is still consistent with a periodicity. If the errors are made larger by a factor of 1.5 then the significance jumps to the 50% level. It is interesting to remember that the periodogram for this source exhibits a peak at 4.12 yr^{-1}. This is exactly twice the frequency found with the phase residual method. And is probably a harmonic with the fundamental frequency buried in the larger noise.

NGC5128. This source shows six bursts in its data set. However, due to the low amplitude and blending of burst 2, a time of peak was not reliably determined. The forward differences and phase residuals plots are shown in Figure 4.8 The forward differences indicate a mean spacing between bursts of about 1.2 years. The best fit for a constant period and epoch gives: P=1.15±0.02 yr,

E=1974.67±0.09, χ^2_ν=0.86. The χ^2_ν value implies a goodness of fit at the 45% level.

1510-08. This source shows the least probability of periodic behavior. The forward differences and phase residuals plots are shown in Figure 4.9 The forward differences indicate a mean spacing between bursts of 0.8 years. The best fit assuming a constant period and epoch gives: P=0.73±0.03 yr, E=1969.75±0.11 yr, and χ^2_ν=5.64. The χ^2_ν value implies a goodness of fit at less than 0.1% level. Even if the errors were increased by a factor of two the χ^2 significance would still be only 5%. Thus, this source's behavior is not consistent with periodicity.

3C454.3. This source has 14 sequential bursts recorded in the data. The time of peak for burst 1 was not used in the analysis due to the poor profile fit. The forward differences and phase residuals plots are shown in Figures 4.10 and 4.11. The forward differences indicate a mean spacing between bursts of 1.2 years. The best fit to the data assuming a constant period and epoch gives: P=1.21±0.05 yr, E=1966.12±0.16, and χ^2_ν=8.78. The χ^2_ν value implies a goodness of fit at less than the 0.1% level. However, in the phase residual diagram, note that bursts nine through 14 form a linear trend and that bursts 2 through 5 and 7 through 9 suggest two parallel linear trends. This suggests the possibility of a period change and phase change during the time span of observations.

Figure 4.11 presents the results of testing this hypothesis. The top panel shows the best fit to the burst times assuming that bursts 2 through 9 are at the same period and that a phase shift occurred between burst 5 and burst 7. Burst 6 is just barely visible in the

data at 15 GHz and was not included in the fit. The results are: P=1.42±0.00 yr, E=1965.21±0.00 yr, and χ^2_ν=0.34. The χ^2_ν test gives a probability of 80%. The bottom panel presents the best fit to the data using just the last six bursts and assuming a constant period and epoch. The results are: P=1.09±0.02 yr, E=1967.53±0.14 yr, and χ^2_ν=0.87. This implies a confidence level of 45%. However, the possible phase and period change shown by the first seven bursts is considered speculative, because of the small number of bursts involved. Due to the short number of cycles the burst timing in 3C454.3 can also be modeled as a constant period with a linear increase in the phase.

4.5 Discussion

In the Monte-Carlo simulations, most of the low frequency structure in the periodograms came from the randomness of the outburst amplitudes. The low frequency peaks in the periodograms were almost always larger than any peak near the true burst rate. Thus, low frequency large amplitude peaks in the periodogram of a real source variability curve may signify the presence of a series of bursts with random amplitudes. This is also borne out by the fact that when different time spans of data for the same source are examined, different periods are found (Webb et al., 1988). In addition, the presence of a periodic component that is short-lived does not imply that it was caused by a real periodic physical process (Webb et al., 1988).

In my study, all the sources except 1510-08 exhibit burst spacings that are consistent with periodicity. However, the periodic behavior is not maintained for more than a few cycles. It could be argued that the sources are not periodic. Nevertheless, that the bursts are not totally random can be argued as follows: if the last six bursts in 3C454.3 were random and their spacing followed, say, an exponential probability distribution; then the probability that a pair of bursts would have a spacing between 1.1 and 1.3 years given a mean of 1.2 years is 7.3%. To have six bursts occur sequentially with spacings in that range has a probability of 0.073^5 or 1 in 10^8! This same argument can be applied to the other sources and other probability distributions (like the uniform distribution). This suggests there is some underlying process controlling the timing of the bursts. If it is not a true periodic physical process, then for short periods of time it can emulate one. Thus any models of AGN must be capable of explaining variability ranging from random to periodic variations.

4.6 Models of Periodicity

Recent modeling of periodic behavior in AGN has proceeded along the lines of an accretion disk about a supermassive black hole. One model assumes pulsations in an accretion disk normal to the plane of the disk (Villa, 1979). The disk is self-gravitating and is supported by radiation pressure. The period of pulsation is given by

$$P = 6.8 \times 10^{-3} \left(\frac{R_{15}^3}{M_8} \right)^{0.5} \text{ [YR]} \qquad (4.6)$$

where the radial distance from the central mass, R_{15}, is in units of 10^{15} cm and the mass of the central mass, M_8, is in units of 10^8 $M_\odot$. For expected ranges of the central mass 10^6 - 10^9 $M_\odot$, and typical periods about 1 year, the radial distance would be 1 - 6 x 10^{16}cm (700 - 4000 AU). At these radii the material is too cool to cause optical variations (Sitko 1985). In addition, a brightening of the core of a radio source with out the ejection of a VLBI knot has yet to be observed (Valtaoja et al. 1988). Thus, this model won't work for long time scale radio variations.

Another model assumes a luminous hot spot in an accretion disk in Keplerian orbit about a supermassive black hole (Novikov and Thorne 1973). FLux modulations could be caused by eclipsing or gravitational effects. The period of orbital motion is given by

$$P = 0.055 \left(\frac{R_{15}^3}{M_8} \right)^{0.5} \text{ [YR]} \qquad (4.7)$$

where R_{15} and M_8 have the same units as in equation 4.5. It is possible that the hot spot could produce synchrotron emission and possibly jets of material like a giant solar flare (Pineault, 1980). If such spots randomly form and then decay within a few orbital periods, this could explain the character of our observations.

Another proposed variability model supposes the existence of binary black holes (See Sillanpää et al. (1988) for a discussion of observations supporting binary black holes.). One way to obtain modulation is to have jets that emanate from one of the black holes precess due to gravitational effects. As a jet sweeps across our

line of sight, there is a marked increase and then decrease in the observed flux. However, this model is probably not the appropriate for describing the present observations as the precession has a period on the order of 10^4 years (Abramowicz et al. 1980). However, if there are two black holes, with an accretion disk around the larger, tidal forces from the smaller black hole could perturb the accretion disk around the larger black hole, dumping matter onto the hole and thus producing an outburst. The periodicity would then come from the orbital period of the the pair (Sillanpää et al. 1988).

Finally, it is possible that thermal and viscous instabilities in an accretion disk can cause variations with time scales in the right range (on the order of a year), and these variations may be quasiperiodic (Abramowicz et al. 1986). However, no detailed model has been published.

4.7 Summary

Monte-Carlo simulations of periodically spaced outbursts with constant and random outburst amplitudes and varying degrees of outburst blending were generated. These simulations were examined for periodicity by a well-used technique to search for periodicity, the periodogram (Scargle, 1982). It was found that the periodogram method will not detect the true periodicity in a periodic time series if the outbursts have random amplitudes and partial outburst blending.

Four sources were examined for periodic outburst spacing using phase residual diagrams and the chi square test. One source, 1510-08, was found not to exhibit periodic behavior. Another source, 0235+16 was marginally consistent with periodicity. The last two sources, NGC5128 and 3C454.3 were each found to have a small number of sequential outbursts (5 and 6 respectively) whose spacings are consistent with periodicity.

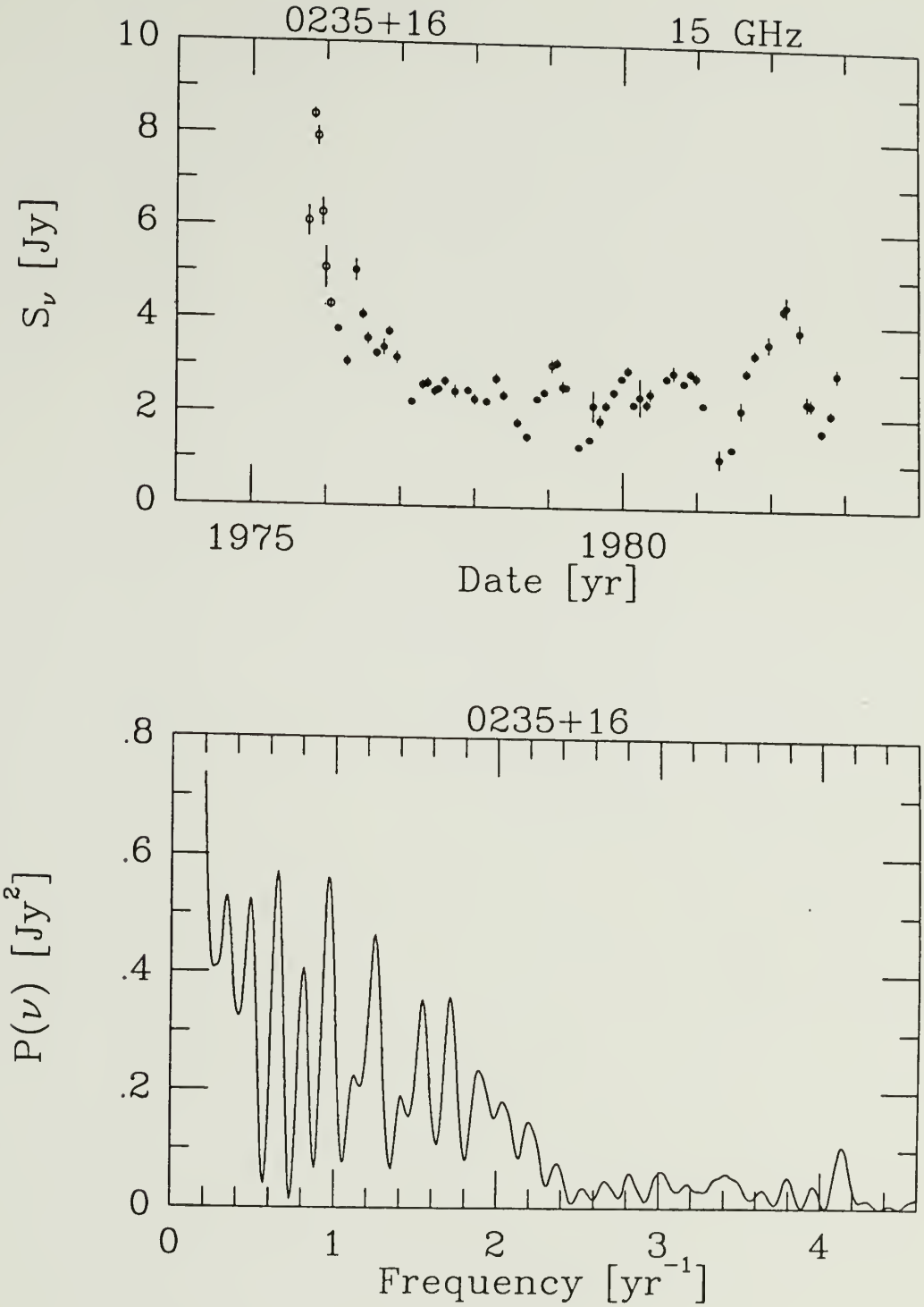

Figure 4.1. The time variability data and periodogram for 0235+16.

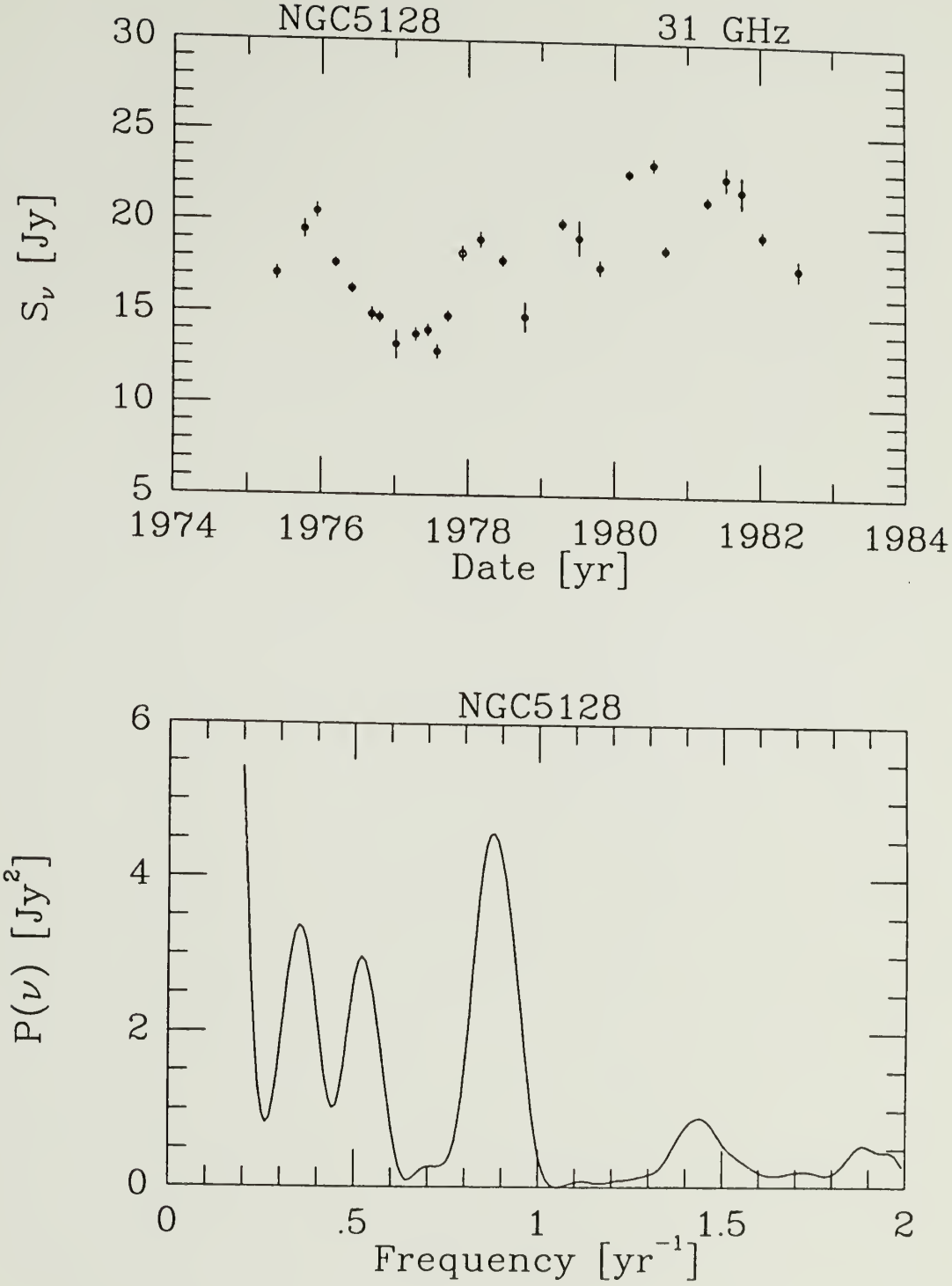

Figure 4.2. The time variability data and periodogram for NGC5128.

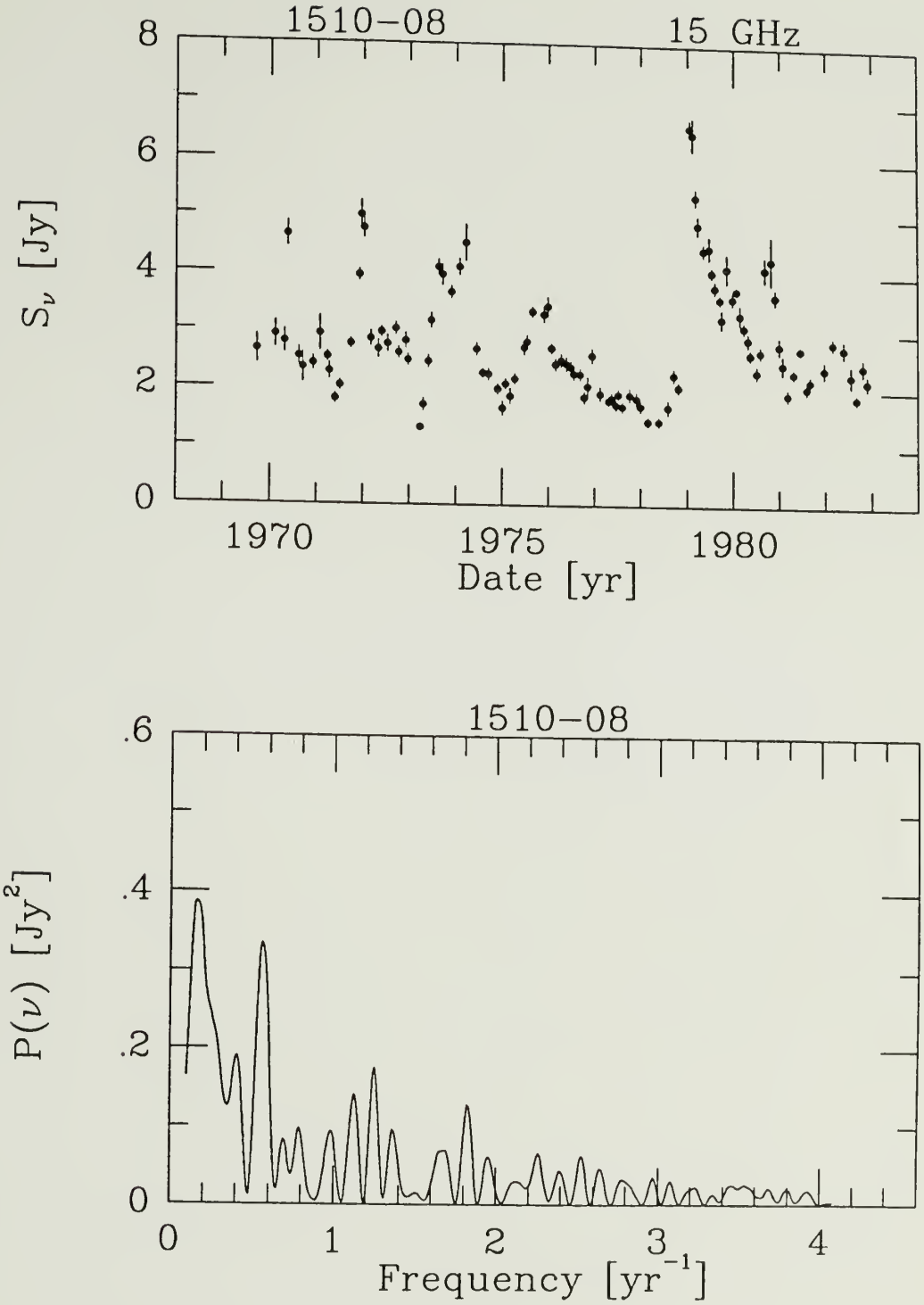

Figure 4.3. The time variability data and periodogram for 1510-08.

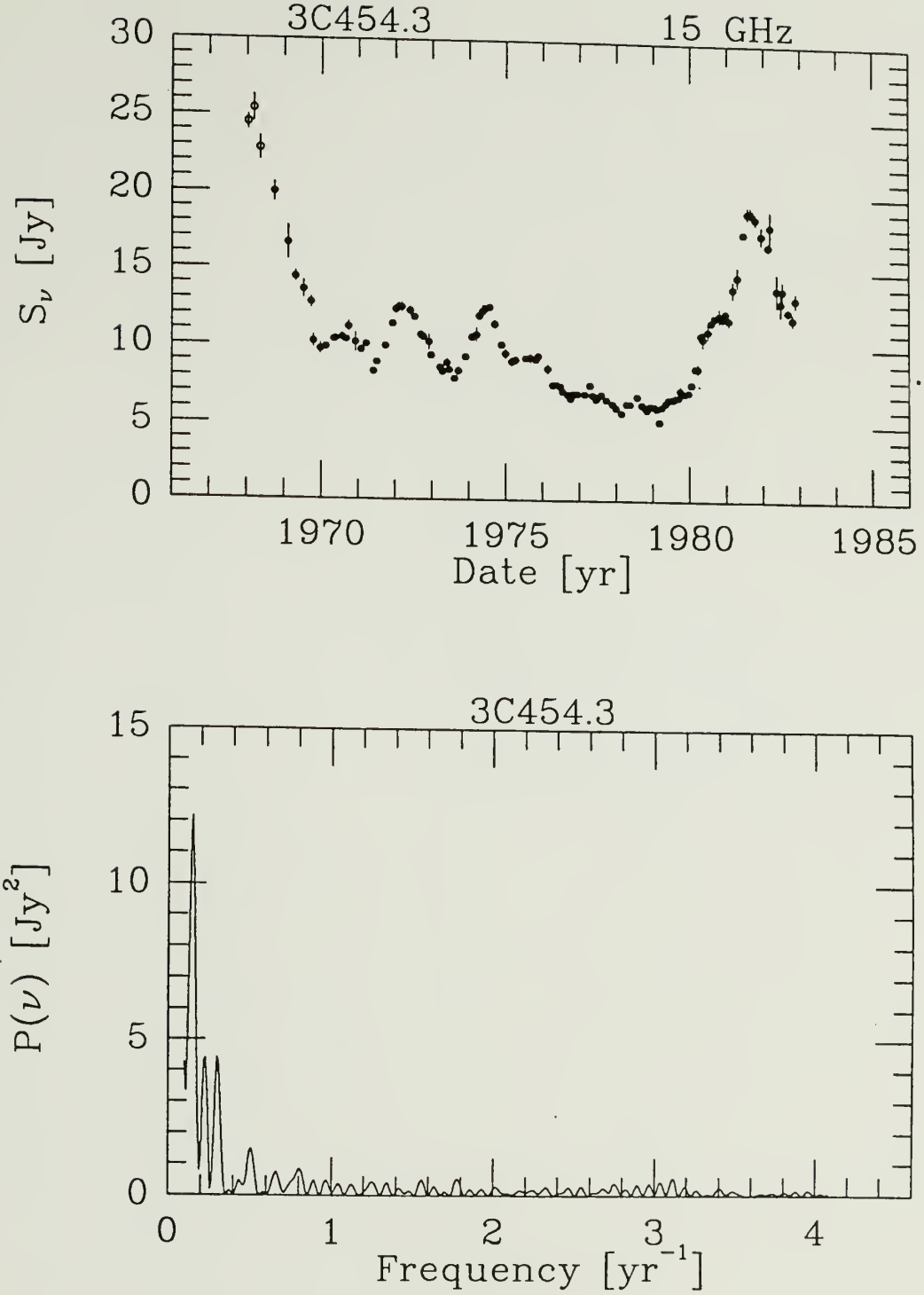

Figure 4.4. The time variability data and periodogram for 3C454.3.

Figure 4.5. Two plots showing the phase residual diagrams for simulated periodic data. The times of peak were generated by a function $t_p = P\ i + E + G_i$, where i is the burst number. The period, P, was one year. The epoch of the zero burst, E, was 1966. Each time was perturbed by a random gaussian distributed phase error, G_i, where $\sigma = 0.11$ yr. The top panel demonstrates how the phase residual diagram appears with periodic data when the period used to make the diagram is incorrect. The period of 1.05 yr was arbitrarily chosen. Note the negative sloped linear trend in the plotted data indicative of an incorrect period being used to make the diagram. The bottom panel shows the same data now fit with the best fit period as described in the text. The fit results are: P=1.00±0.04 yr, E=1966.00±0.03 yr, and χ^2_ν=1.05. Note the data are now scattered about a horizontal line indicative of the correct period being used to make the diagram. The χ^2_ν significance is 40%.

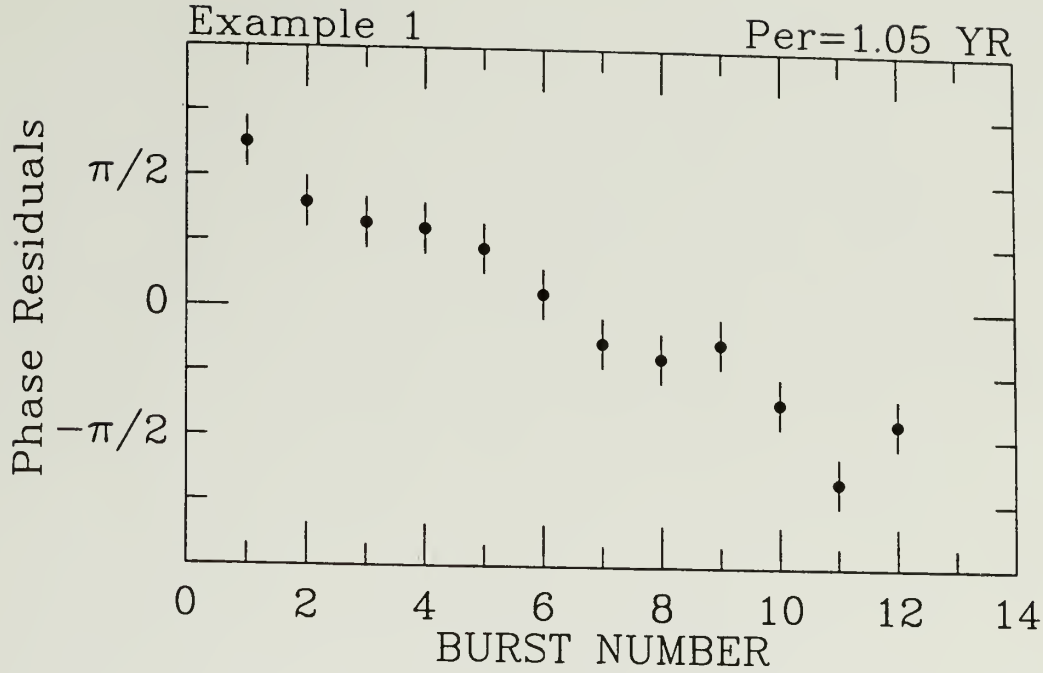
Example 1
Per=1.05 YR
Phase Residuals
π/2
0
−π/2
0
2
4
6
8
10
12
14
BURST NUMBER

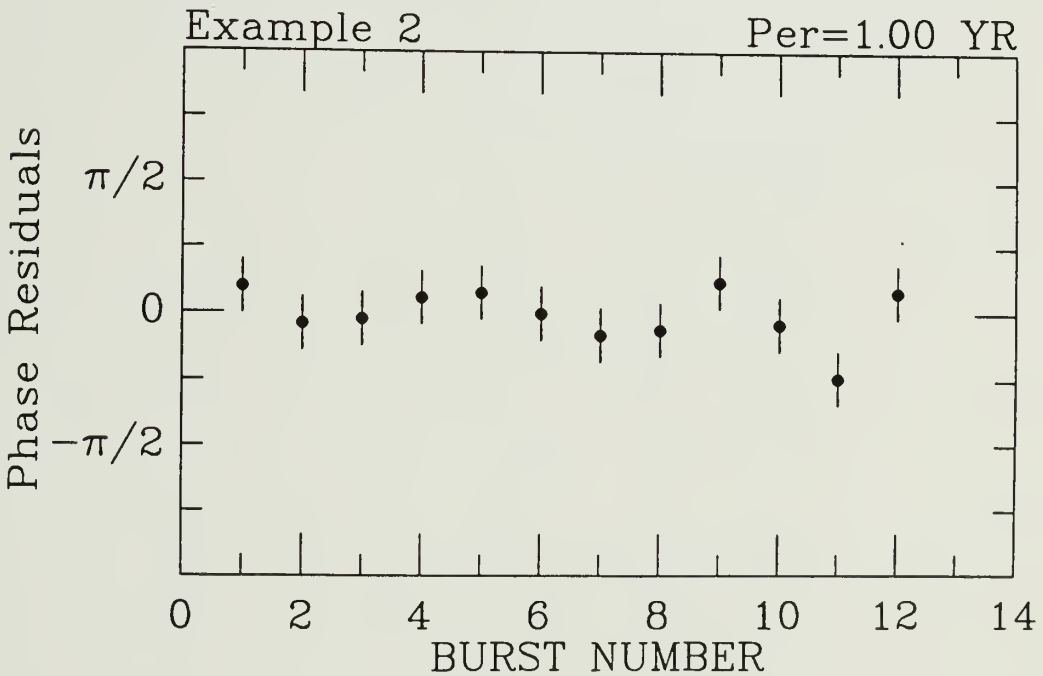
Example 2
Per=1.00 YR
Phase Residuals
π/2
0
−π/2
0
2
4
6
8
10
12
14
BURST NUMBER

Figure 4.6. Two more examples of phase residual diagrams with simulated periodic data. The data is the same as in Figure 4.5 except now the times for burst seven and greater have an additional phase of 0.4 years added. The top plot shows the data using the best fit period and epoch assuming a single period and phase. The fit results are: P=1.05±0.03 yr, E=1965.87±0.09 yr, and χ^2_ν=4.88. Note the two parallel linear trends in the diagram indicative of an incorrect period. The bottom plot presents the same data now fit with the assumption that a phase shift of arbitrary value existed between burst six and seven. The algorithm was able to find the correct period.

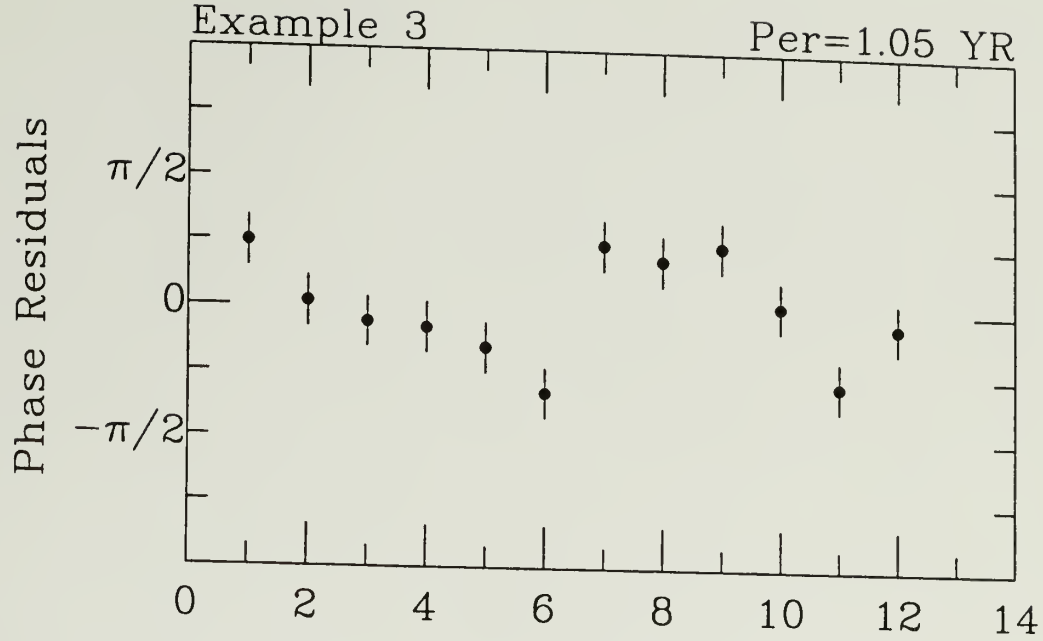
Example 3
Per=1.05 YR
Phase Residuals
π/2
0
−π/2
0
2
4
6
8
10
12
14

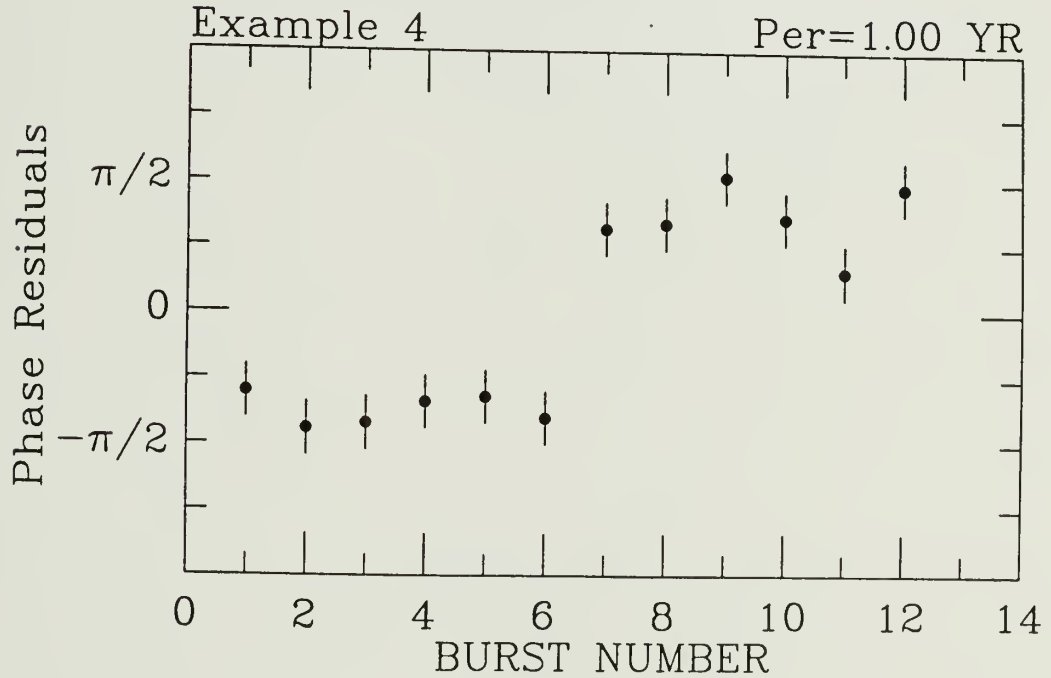
Example 4
Per=1.00 YR
Phase Residuals
π/2
0
−π/2
0
2
4
6
8
10
12
14
BURST NUMBER

Figure 4.7. Presentation of the forward differences and the phase residual diagram for 0235+16. The top plot presents the forward differences for 0235+16. Open symbols indicate where there is assumed to be a missing burst and the difference was divided by two. The circles represent 15 GHz data. The squares represent 8 GHz data. The bottom plot presents the phase residual diagram plot for the best fit period. The burst numbers on the bottom plot are positioned such that they line up with the calculated time of peak in the top plot.

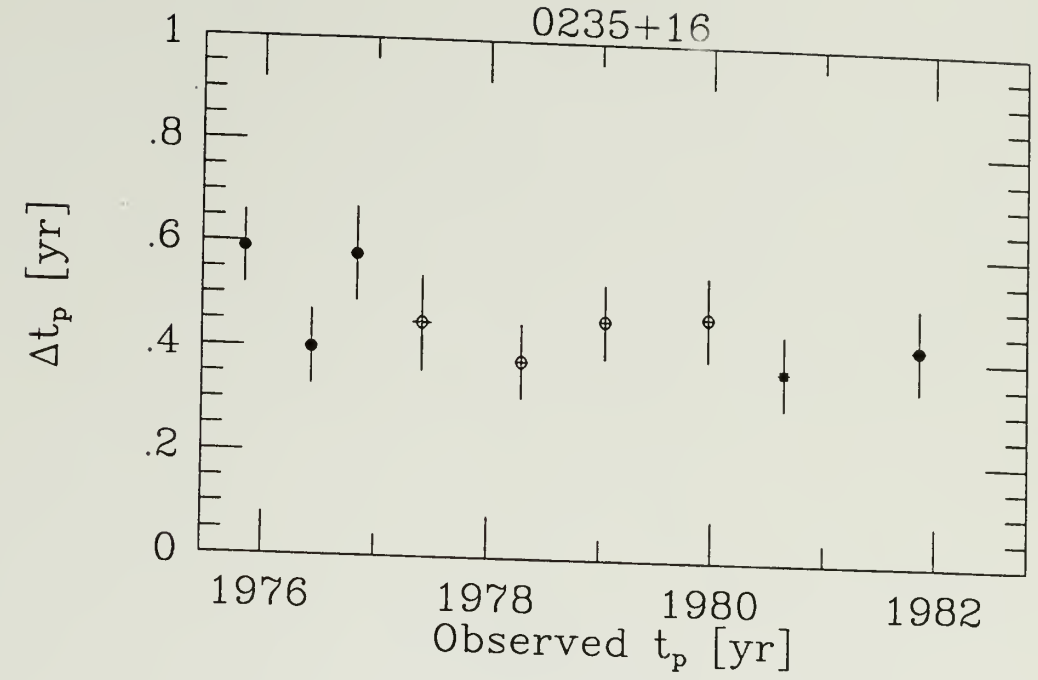
0235+16
1
.8
.6
.4
.2
0
Δt_p [yr]
1976
1978
1980
1982
Observed t_p [yr]

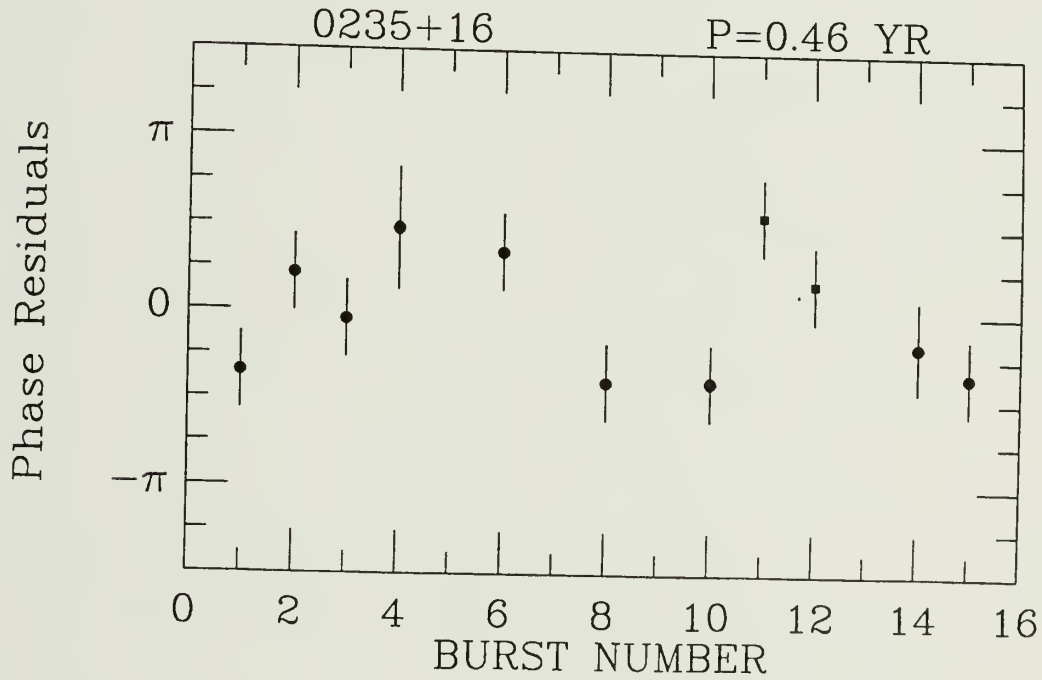
0235+16
P=0.46 YR
π
0
−π
Phase Residuals
0
2
4
6
8
10
12
14
16
BURST NUMBER

Figure 4.8. Presentation of the forward differences and the phase residual diagram for NGC5128. The top plot presents the forward differences for NGC5128. The open symbol indicates there is assumed to be a missing burst and the difference was divided by two. The bottom plot presents the phase residual diagram plot for the best fit period. The burst numbers on the bottom plot are positioned such that they line up as the calculated time of peak in the top plot.

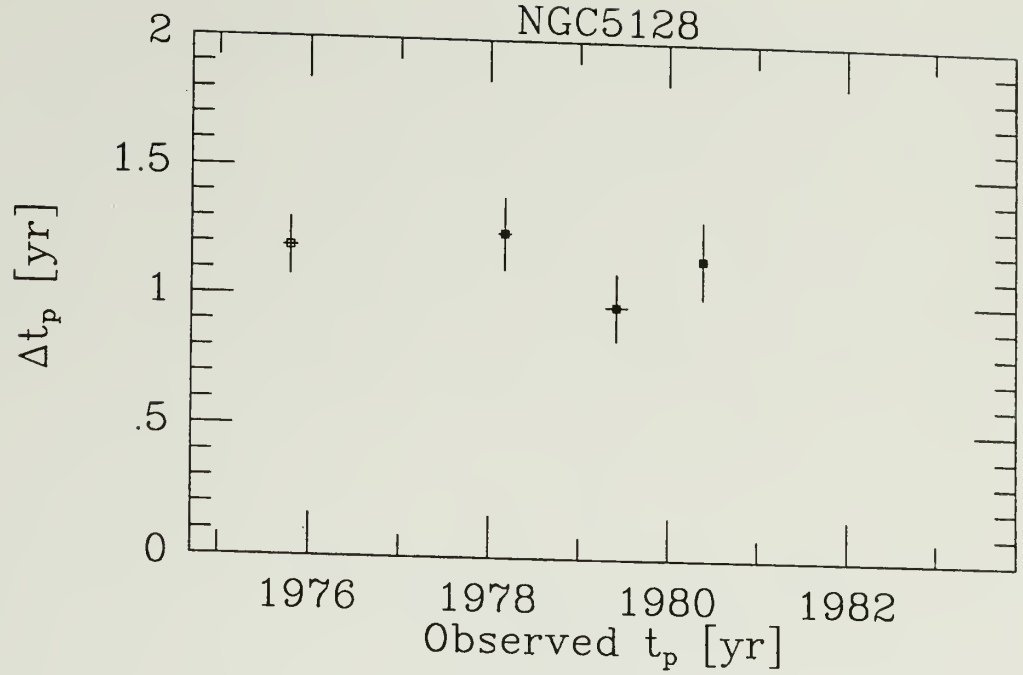
NGC5128
2
1.5
1
.5
0
Δt_p [yr]
1976
1978
1980
1982
Observed t_p [yr]

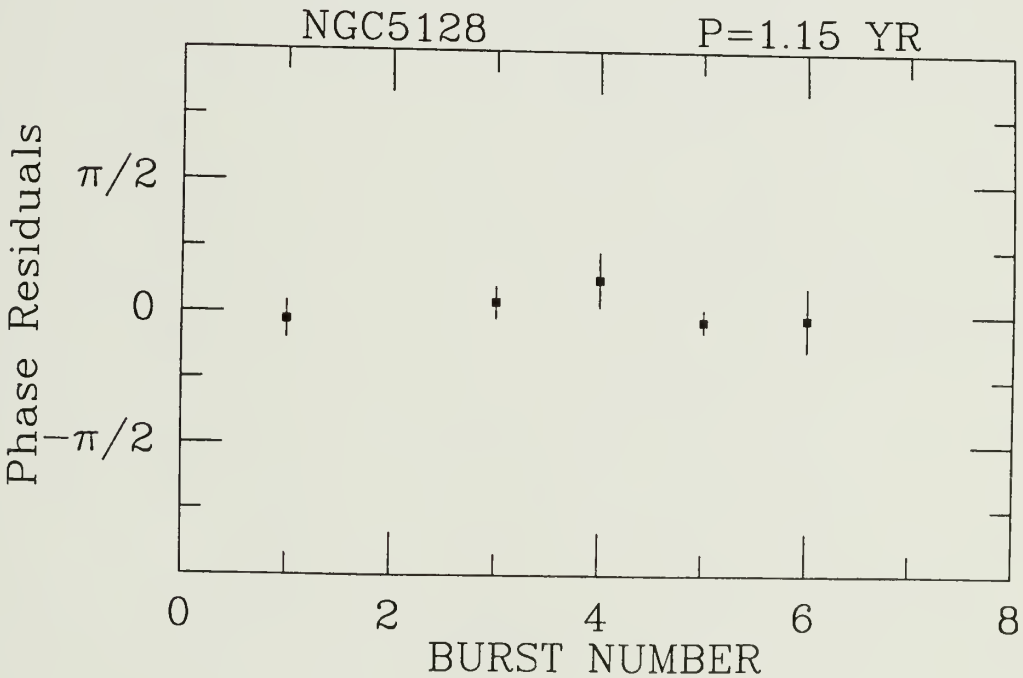
NGC5128
P=1.15 YR
Phase Residuals
$\pi/2$
0
$-\pi/2$
0
2
4
6
8
BURST NUMBER

Figure 4.9. Presentation of the forward differences and the phase residual diagram for 1510-08. The top plot presents the forward differences for 1510-08. Note the large scatter in the plot. The bottom plot presents the phase residual diagram plot for the best fit period. The burst numbers on the bottom plot are positioned such that they line up with the calculated time of peak in the top plot.

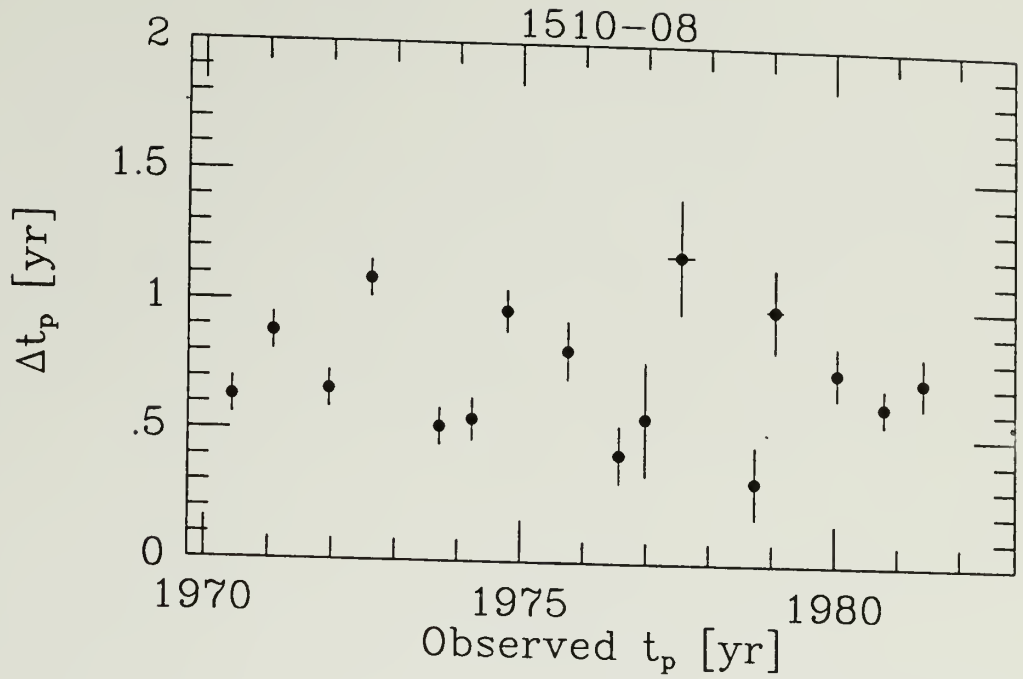
1510−08
2
1.5
1
.5
0
Δt_p [yr]
1970
1975
1980
Observed t_p [yr]

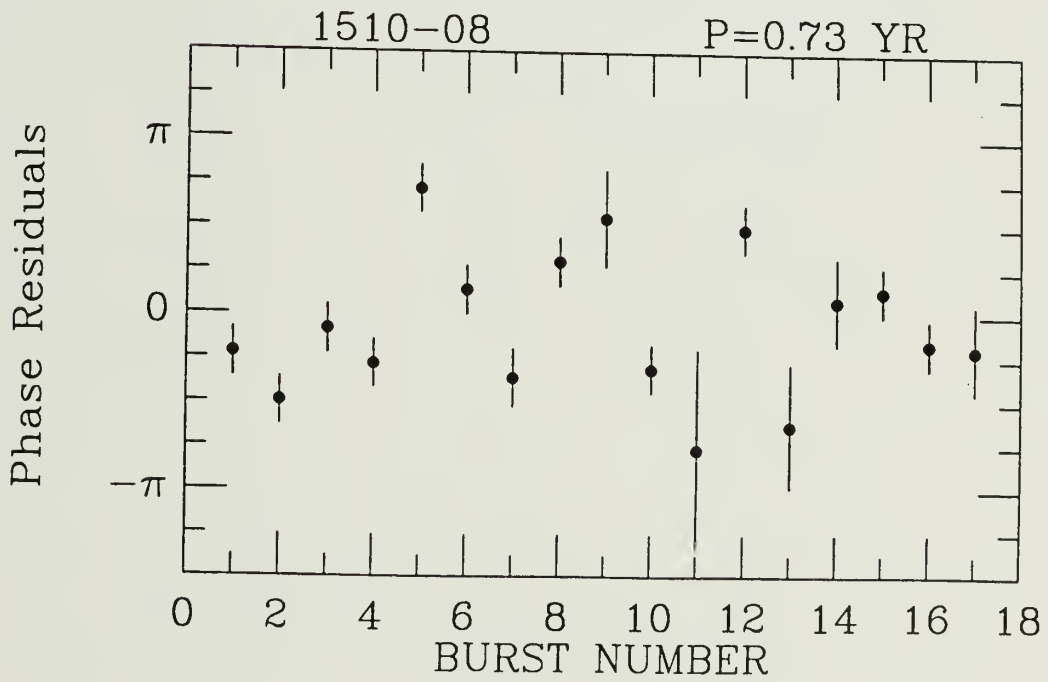
1510−08
P=0.73 YR
π
0
−π
Phase Residuals
0
2
4
6
8
10
12
14
16
18
BURST NUMBER

Figure 4.10. Presentation of the forward differences and the phase residual diagram for 3C454.3. The top plot presents the forward differences for 3C454.3. The open symbol indicates there is assumed to be a missing burst and the difference is divided by two. The bottom plot presents the phase residual diagram plot for the best fit period. The burst numbers on the bottom plot are positioned such that they line up as the calculated time of peak in the top plot. The squares represent 31.4 GHz data. The circles represent 15.5 GHz data. The triangles represent 90 GHz data. The 31 GHz points were shifted up 0.1 burst number and the 90 GHz points were shifted down 0.1 burst number to separate the symbols on the diagram.

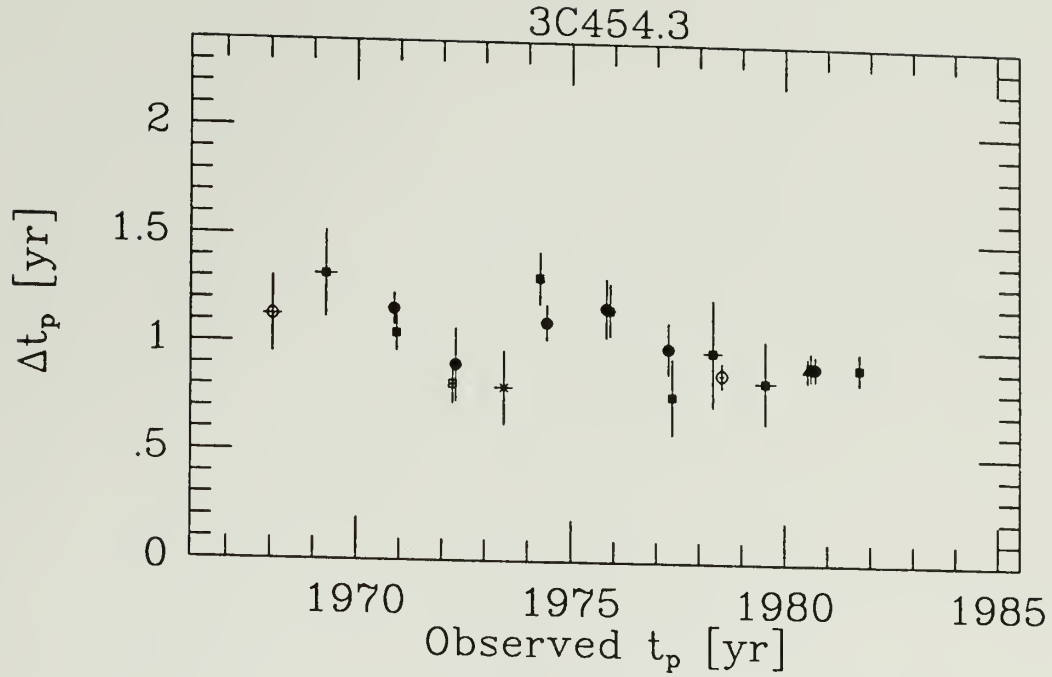
3C454.3
Δt_p [yr]
2
1.5
1
.5
0
1970
1975
1980
1985
Observed t_p [yr]

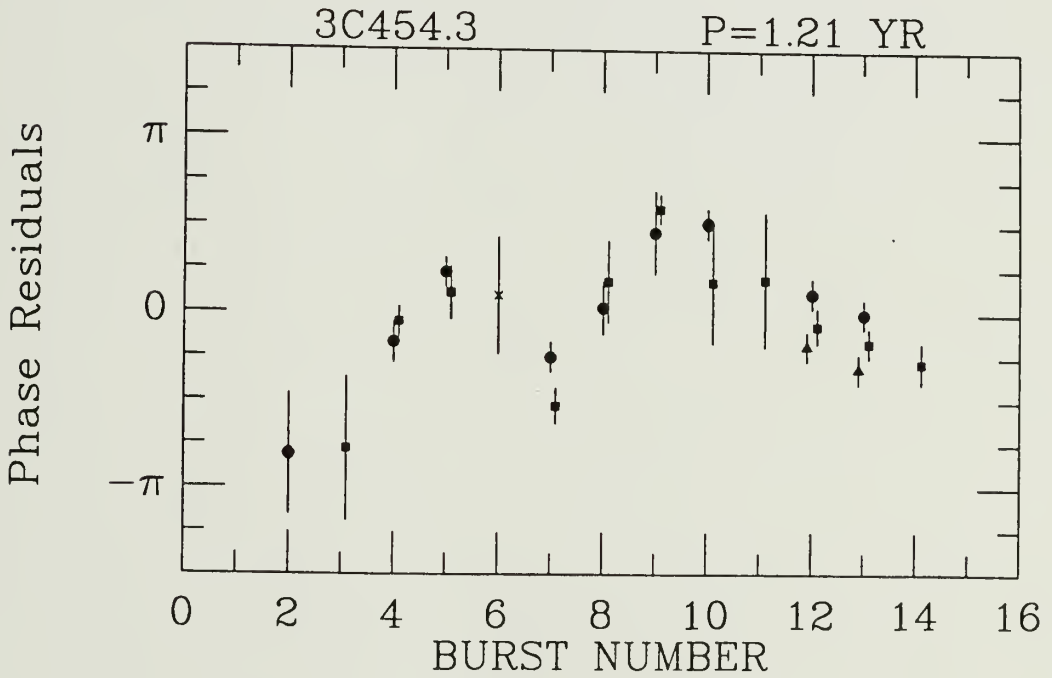
3C454.3
P=1.21 YR
Phase Residuals
π
0
−π
0
2
4
6
8
10
12
14
16
BURST NUMBER

Figure 4.11. Two phase residual diagrams showing additional interpretations of the 3C454.3 data presented in Figure 4.10. The top plot shows the best fit to the burst times assuming that bursts 2 through 9 are at the same period and that a phase shift occurred between burst 5 and burst 7. Burst 6 and bursts 9 to 14 were not included in the fit. The results are: P=1.42±0.13 yr, E=1965.21±0.03 yr, and χ^2_ν=0.34. The χ^2_ν test is at a probability of 80%. The bottom panel presents the best fit to the data using just the last six bursts and assuming a constant period and epoch. The results are: P=1.09±0.02 yr, E=1967.53±0.14 yr, and χ^2_ν=0.87. This implies a confidence level of 45%.

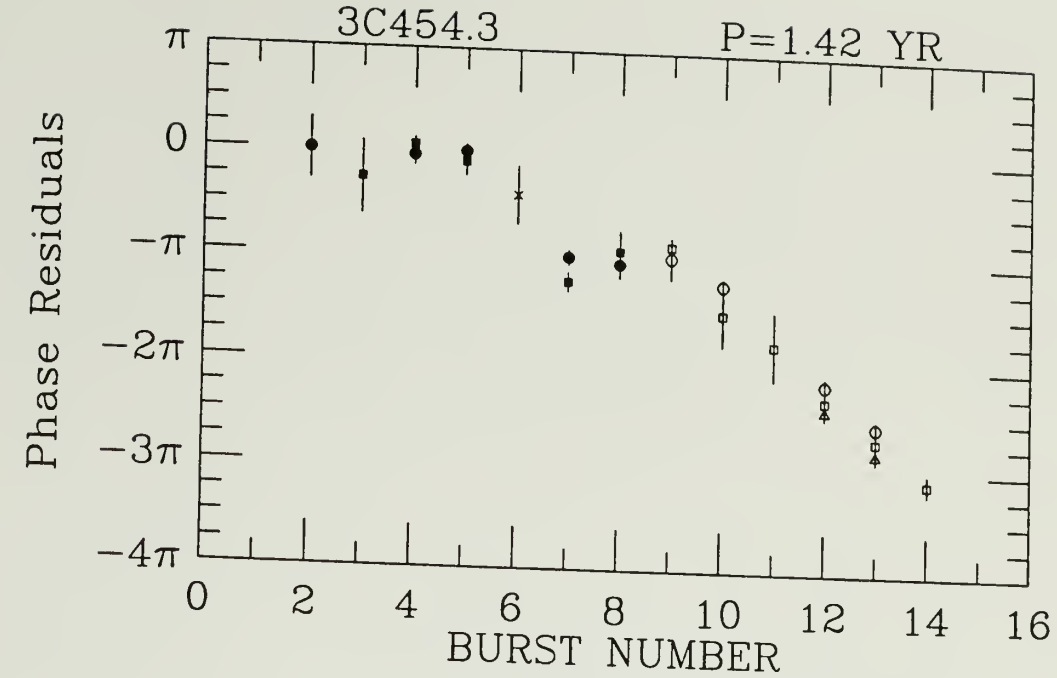
3C454.3
P=1.42 YR
Phase Residuals
π
0
−π
−2π
−3π
−4π
0
2
4
6
8
10
12
14
16
BURST NUMBER

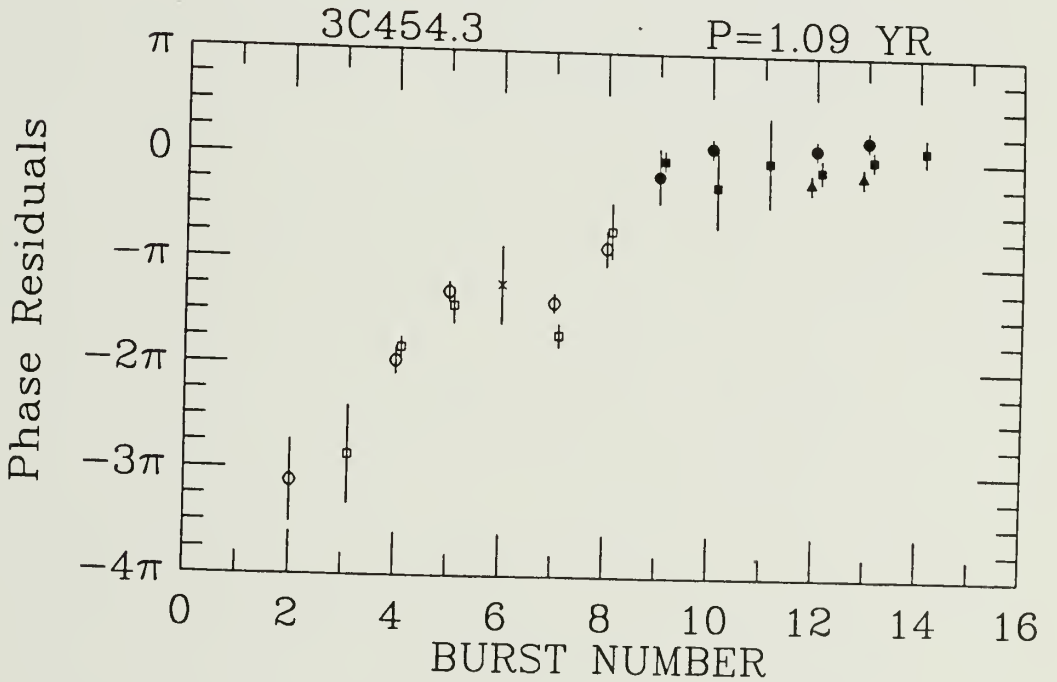
3C454.3
P=1.09 YR
Phase Residuals
π
0
−π
−2π
−3π
−4π
0
2
4
6
8
10
12
14
16
BURST NUMBER

CHAPTER 5

SUMMARY

This dissertation examined three aspects of the flux density variability of extragalactic radio sources: millimeter wavelength short timescale variability, the spectral evolution of outbursts, and periodic spacing of the outbursts. The main results from this dissertation are presented below.

Observations investigating millimeter wavelength short timescale flux density variability of extragalactic sources were conducted using the FCRAO at λ3mm and λ7mm. Most of the sources observed that had good temporal coverage exhibited significant flux density variations over the six month observing span. In addition, the most rapid variations observed (30% flux density change over a few days), were comparable with those seen by previous observers. An anomalous flux density dropout was observed in 3C446 and was interpreted as an occultation event.

The second area of investigation used data from the Dent-Balonek monitoring program to investigate the spectral evolution of eight outbursts. In this thesis, for the first time, outburst profile fitting was systematically used to deconvolve the individual outbursts from one another to enable the evolution of the outbursts to be monitored. The fit profiles were used to generate multiple epoch spectra to investigate the evolution of the outbursts. The

following results were found: The outburst temporal profiles keep roughly the same shape over millimeter to centimeter wavelengths. All the outburst spectra are consistent with emission from a simple homogeneous synchrotron source. The initial high frequency spectral slope of the outburst spectra is $\alpha = -0.2$, implying a initial electron energy index of $s = 1.4$. The high frequency spectral slope of the spectra steepen with time with a change in the slope of at least $\Delta\alpha \approx -0.5$. This is consistent with an initial acceleration or injection of relativistic synchrotron electrons that then suffer inverse Compton or synchrotron losses. The spectral evolution of the outbursts is qualitatively in agreement with the model proposed by Marscher and Gear. However, the initial electron energy index value of $s = 1.4$, is smaller than that allowed in their model ($s = 2.0$) unless the shock is initially very strong.

Finally, numerical simulations of radio variability curves were made. These synthetic time series were analyzed using a periodogram method. The results indicate that if the variations are composed of periodic identically shaped outbursts with random amplitudes and partial blending, the periodogram method will not detect the true burst rate. A phase residual minimization method was used to examine four sources for periodic behavior. The source 1510-08, did not exhibit periodic behavior, while 0235+16 was marginally consistent with periodicity. The last two sources, NGC5128 and 3C454.3 each had a small number of sequential outbursts (5 and 6 respectively) whose spacings are consistent with periodicity.

APPENDIX A

MILLIMETER FLUX DENSITY MEASUREMENTS

Flux density measurements of compact extragalatic radio sources at λ3mm (88.2 GHz) and λ7mm (40.0 GHz) made at FCRAO. N is the number of independent observations.

Source	Date	λ3mm Year	S_ν [Jy]	N
0048-09	12/25/84	1984.984	1.52±0.23	2
	01/12/85	1985.033	1.69 0.24	1
	01/20/85	1985.055	1.36 0.39	2
	02/21/85	1985.142	1.48 0.48	1
	03/21/85	1985.219	0.64 0.46	1
	04/21/85	1985.304	1.06 0.49	1
	04/29/85	1985.326	0.56 0.33	1
	05/04/85	1985.340	0.52 0.34	2
	06/15/85	1985.455	1.23 0.34	1
0133+47	12/19/85	1984.967	1.49±0.23	1
	12/24/84	1984.981	1.20 0.24	1
	03/21/85	1985.219	1.51 0.30	2
	05/09/85	1985.353	1.06 0.25	1
0235+16	12/19/85	1984.967	1.43±0.23	1
	12/25/84	1984.984	1.43 0.25	2
	01/12/85	1985.033	1.88 0.25	1
	01/20/85	1985.055	1.71 0.29	1
	02/21/85	1985.142	2.30 0.34	1
	03/21/85	1985.219	1.66 0.60	1
	05/04/85	1985.340	1.10 0.47	1
	05/09/85	1985.353	2.19 0.33	1
	06/14/85	1985.453	1.87 0.27	1
0237-02	12/25/84	1984.984	0.66±0.28	2
	01/12/85	1985.033	0.98 0.26	1
	01/20/85	1985.055	0.30 0.30	1
	02/21/85	1985.142	0.53 0.39	1
	05/04/85	1985.340	0.51 0.36	1
	06/14/85	1985.452	0.37 0.42	1
0300+47	12/26/84	1984.986	1.41±0.23	1
	04/29/85	1985.326	0.96 0.32	1
	05/09/85	1985.353	1.48 0.32	1
0306+10	12/26/84	1984.986	1.22±0.23	1
	01/20/85	1985.055	0.94 0.33	1
	02/21/85	1985.142	1.10 0.25	1

Source	Date	λ3mm Year	S_ν [Jy]	N
3C84	12/19/85	1984.967	39.91±0.83	2
	12/25/84	1984.984	40.47 0.95	3
	02/21/85	1985.142	37.12 1.10	2
	03/21/85	1985.219	35.78 1.39	2
	04/21/85	1985.304	32.90 0.72	2
	04/29/85	1985.326	32.34 0.81	2
	05/04/85	1985.340	32.68 0.69	2
	05/09/85	1985.353	32.99 0.64	2
	06/05/85	1985.427	30.33 1.01	1
	06014/85	1985.453	27.92 0.90	3
	06/22/85	1985.474	31.81 2.20	1
0333+32	12/26/84	1984.986	0.52±0.23	1
0355+50	12/26/84	1984.986	3.52±0.22	1
	01/12/85	1985.033	3.48 0.39	1
	02/21/85	1985.142	3.64 0.28	1
	03/21/85	1985.219	3.33 0.34	1
	04/21/85	1985.304	2.86 0.34	1
	05/04/85	1985.340	2.83 0.28	1
	06/15/85	1985.455	2.46 0.29	2
	06/22/85	1985.474	4.09 0.71	1
0404+76	12/26/84	1984.986	0.41±0.23	1
3C111	12/19/85	1984.967	1.72±0.25	1
	12/26/84	1984.986	2.32 0.24	1
	02/21/85	1985.142	1.30 0.24	1
	04/29/85	1985.326	1.86 0.50	1
	05/04/85	1985.340	1.87 0.34	1
	05/09/85	1985.353	1.14 0.25	1
	06/15/85	1985.455	1.58 0.35	1
0420-01	12/19/85	1984.967	5.39±0.34	1
	12/26/84	1984.986	5.71 0.24	4
	01/20/85	1985.055	4.33 0.27	2
	02/21/85	1985.142	4.60 0.28	3
	05/09/85	1985.353	4.97 0.30	2
	06/14/85	1985.452	5.32 0.34	1

Source	Date	λ3mm Year	S_ν [Jy]	N
3C120	12/19/85	1984.967	2.38±0.26	1
	12/26/84	1984.986	2.56 0.24	1
	01/20/85	1985.055	2.31 0.30	1
	02/21/85	1985.142	2.70 0.53	1
	05/09/85	1985.353	3.31 0.28	1
	06/14/85	1985.452	2.96 0.38	1
3C123	12/26/84	1984.986	0.66±0.23	1
0440-00	12/19/85	1984.967	1.60±0.23	1
	12/26/84	1984.986	1.92 0.24	1
	02/21/85	1985.142	0.63 0.28	1
	05/09/85	1985.353	0.58 0.31	1
	06/14/85	1985.452	1.00 0.25	1
0454-23	06/14/85	1985.452	0.72±0.41	1
0458-02	12/19/85	1984.967	0.95±0.22	1
	12/26/84	1984.986	0.77 0.23	1
	05/09/85	1985.353	1.17 0.30	1
	06/14/85	1985.452	1.08 0.30	1
0552+39	12/26/84	1984.986	1.67±0.22	1
	05/09/85	1985.353	1.58 0.28	1
0605-08	12/26/84	1984.986	1.54±0.24	1
	02/21/85	1985.142	1.54 0.27	1
	06/14/85	1985.452	1.82 0.29	1
0607-15	12/19/85	1984.967	4.33±0.31	1
	12/26/84	1984.986	5.08 0.28	1
	02/21/85	1985.142	4.73 0.34	1
	06/14/85	1985.452	6.36 0.43	1
0723-00	12/26/84	1984.986	0.86±0.24	1
0727-11	12/19/85	1984.967	1.72±0.24	1
	12/26/84	1984.986	1.75 0.25	1
	02/21/85	1985.142	1.99 0.28	1
	05/09/85	1985.353	2.84 0.34	1

Source	Date	λ3mm Year	S_ν [Jy]	N
0735+17	12/26/84	1984.986	1.03±0.22	1
	05/09/85	1985.353	0.48 0.34	1
0736+01	12/19/85	1984.967	3.54±0.24	2
	12/26/84	1984.986	3.36 0.23	1
	01/29/85	1985.079	2.95 0.38	1
	02/21/85	1985.142	3.59 0.29	1
	05/04/85	1985.340	2.72 0.39	1
	05/09/85	1985.353	3.49 0.41	1
	06/14/85	1985.452	3.46 0.47	1
0748+12	12/26/84	1984.986	1.27±0.24	1
	02/21/85	1985.142	0.63 0.23	1
	05/09/85	1985.353	0.87 0.30	1
0754+10	12/26/84	1984.986	2.21±0.23	1
	02/21/85	1985.142	1.70 0.27	1
	05/04/85	1985.340	2.20 0.47	1
	05/09/85	1985.353	1.67 0.41	1
0829+04	12/26/84	1984.986	2.71±0.24	1
	05/04/85	1985.340	1.52 0.42	1
	05/09/85	1985.353	2.38 0.46	1
0834-20	12/19/85	1984.967	3.42±0.30	1
	12/26/84	1984.986	3.65 0.26	1
	02/21/85	1985.142	3.40 0.32	1
OJ287	12/19/85	1984.967	7.27±0.32	1
	12/26/84	1984.986	6.78 0.28	1
	01/29/85	1985.079	7.22 0.36	1
	02/21/85	1985.142	6.14 0.37	1
	03/22/85	1985.222	8.64 0.58	1
	04/29/85	1985.326	9.15 0.53	1
	05/04/85	1985.340	9.43 0.47	1
	06/14/85	1985.452	5.32 0.50	2
0859-14	12/26/84	1984.986	0.54±0.24	1
0906+01	12/26/84	1984.986	0.70±0.22	1
	05/09/85	1985.353	0.43 0.49	1

Source	Date	λ3mm Year	S_ν [Jy]	N
4C39.25	12/26/84	1984.986	1.12±0.23	1
	05/09/85	1985.353	1.89 0.32	1
	06/14/85	1985.452	1.63 0.47	1
1055+01	12/26/84	1984.986	2.86±0.26	1
	01/29/85	1985.079	3.04 0.29	1
	02/21/85	1985.142	2.97 0.28	1
	03/22/85	1985.222	3.08 0.33	1
	04/29/85	1985.326	2.75 0.26	1
	05/04/85	1985.340	3.13 0.41	1
	05/09/85	1985.353	3.33 0.39	1
1116+12	12/26/84	1984.986	0.81±0.22	1
1127-14	12/26/84	1984.986	1.07±0.24	1
	05/04/85	1985.340	0.70 0.50	1
1156+29	12/19/85	1984.967	3.98±0.28	1
	12/24/84	1984.981	4.08 0.30	1
	02/21/85	1985.142	3.22 0.31	1
	03/22/85	1985.222	4.05 0.37	1
	04/29/85	1985.326	5.21 0.31	1
	05/09/85	1985.353	5.28 0.33	2
	06/05/85	1985.427	4.07 0.28	2
	06/22/85	1985.474	3.77 0.38	1
1219+28	12/24/84	1984.981	0.80±0.22	1
3C273	12/19/85	1984.967	27.26±0.59	2
	12/26/85	1984.985	27.13 0.47	3
	01/29/85	1985.079	26.31 0.57	2
	02/21/85	1985.142	20.18 0.89	1
	03/13/85	1985.197	18.56 1.34	1
	03/22/85	1985.222	20.24 0.45	3
	04/29/85	1985.326	21.75 0.39	4
	05/09/85	1985.353	21.59 0.58	3
	06/05/85	1985.427	19.89 0.56	2
	06/15/85	1985.455	19.27 0.87	1
	06/22/85	1985.474	19.24 1.44	1

Source	Date	λ3mm Year	S_ν [Jy]	N
3C279	12/19/85	1984.967	7.29±0.36	1
	12/26/85	1984.985	7.41 0.25	3
	01/29/85	1985.079	8.08 0.28	2
	02/21/85	1985.142	6.38 0.39	1
	03/22/85	1985.222	6.76 0.30	1
	04/29/85	1985.326	6.83 0.40	1
	05/04/85	1985.340	5.54 0.46	2
	05/09/85	1985.353	5.62 0.33	3
	06/15/85	1985.455	6.15 0.44	1
1308+32	12/19/85	1984.967	2.49±0.26	1
	12/26/84	1984.986	2.61 0.26	1
	01/12/85	1985.033	3.54 0.30	1
	02/21/85	1985.142	3.07 0.27	1
	03/22/85	1985.222	3.04 0.27	1
	04/29/85	1985.326	3.33 0.32	1
	06/05/85	1985.427	3.46 0.34	1
	06/15/85	1985.455	3.21 0.29	1
	06/22/85	1985.474	3.26 0.42	1
1335-12	12/25/84	1984.984	4.22±0.42	2
	01/29/85	1985.079	5.08 0.31	1
	04/29/85	1985.326	4.18 0.43	1
	05/09/85	1985.353	3.24 0.41	1
1354-15	12/25/84	1984.984	0.54±0.23	2
1404+28	12/26/84	1984.986	0.12±0.25	1
1413+13	12/25/84	1984.984	1.70±0.28	2
	01/12/85	1985.033	0.89 0.28	1
	01/29/85	1985.079	1.09 0.25	1
	03/22/85	1985.222	0.81 0.24	1
	05/09/85	1985.353	0.39 0.38	1
	05/28/85	1985.405	0.34 0.62	1
	06/05/85	1985.427	0.89 0.30	1
	06/15/85	1985.455	0.55 0.37	1
	06/22/85	1985.474	1.23 0.33	1
1418+54	12/24/84	1984.981	1.51±0.26	1
	01/12/85	1985.033	0.42 0.26	1

Source	Date	λ3mm Year	S_ν [Jy]	N
1502+10	12/25/84	1984.984	0.79±0.25	2
	01/12/85	1985.033	1.06 0.26	1
	01/29/85	1985.079	1.44 0.23	1
	05/09/85	1985.353	1.40 0.35	1
	06/05/85	1985.427	1.13 0.25	1
	06/15/85	1985.455	0.61 0.33	1
1522+15	12/24/84	1984.981	0.17±0.26	1
	12/26/84	1984.986	0.03 0.23	1
	04/29/85	1985.326	0.14 0.29	1
	05/09/85	1985.353	0.19 0.28	1
	06/05/85	1985.427	0.09 0.27	1
	06/15/85	1985.455	0.36 0.26	1
1555+00	12/26/84	1984.986	0.22±0.24	1
1611+34	12/25/84	1984.984	0.79±0.22	2
	01/12/85	1985.033	0.78 0.24	1
	04/21/85	1985.304	0.57 0.39	1
	04/29/85	1985.326	0.97 0.29	1
1633+38	12/25/84	1984.984	1.31±0.26	2
	01/20/85	1985.055	1.52 0.39	1
	01/29/85	1985.079	1.28 0.24	1
	04/21/85	1985.304	1.10 0.39	1
	04/29/85	1985.326	0.36 0.29	1
	06/05/85	1985.427	1.21 0.37	1
	06/15/85	1985.455	0.17 0.34	1
	06/22/85	1985.474	0.54 0.30	1
3C345	12/25/84	1984.984	7.73±0.72	2
	01/29/85	1985.079	7.24 0.29	1
	03/13/85	1985.197	7.62 0.47	2
	03/22/85	1985.221	7.58 0.34	2
	04/21/85	1985.304	8.02 0.63	1
	04/29/85	1985.326	7.18 0.35	1
	06/05/85	1985.427	6.54 0.32	1
	06/15/85	1985.455	6.64 0.60	1
	06/22/85	1985.474	6.30 0.40	1
1642+69	12/24/84	1984.981	0.92±0.25	1
	01/12/85	1985.033	0.82 0.24	1
	01/29/85	1985.079	1.15 0.25	1

Source	Date	λ3mm Year	S_ν [Jy]	N
1730-13	12/24/84	1984.981	5.48±0.30	1
	01/12/85	1985.033	5.54 0.38	1
	03/21/85	1985.220	6.80 0.34	1
	04/21/85	1985.304	7.63 0.47	1
	04/29/85	1985.326	6.51 0.33	1
	05/09/85	1985.353	6.56 0.42	1
	06/05/85	1985.427	5.06 0.49	1
	06/15/85	1985.455	5.66 0.46	1
	06/22/85	1985.474	5.84 0.59	1
1739+52	12/24/84	1984.981	0.86±0.26	1
	01/12/85	1985.033	0.49 0.22	1
1741-03	12/24/84	1984.981	2.36±0.27	1
	03/22/85	1985.222	2.26 0.29	1
	04/21/85	1985.304	1.94 0.37	1
1749+70	12/25/84	1984.984	0.50±0.21	2
	01/12/85	1985.033	0.48 0.25	1
3C371	12/25/84	1984.984	1.31±0.25	2
1921-29	12/24/84	1984.981	5.61±0.34	1
1958-17	12/24/84	1984.981	2.63±0.29	1
	01/12/85	1985.033	1.40 0.26	1
	03/22/85	1985.221	1.96 0.24	1
	04/21/85	1985.304	1.85 0.41	1
	04/29/85	1985.326	1.39 0.34	1
	05/28/85	1985.405	0.53 0.66	1
	06/05/85	1985.427	1.46 0.39	1
	06/15/85	1985.455	0.99 0.57	1
	06/22/85	1985.474	2.11 0.39	1
3C418	12/26/84	1984.986	0.99±0.26	1
NGC7027	12/24/84	1984.981	3.91±0.36	1
	05/04/85	1985.340	4.72 0.47	1

Source	Date	λ3mm Year	S_ν [Jy]	N
2121+05	12/19/85	1984.967	1.51±0.31	1
	12/26/84	1984.986	1.99 0.24	1
	03/21/85	1985.219	2.59 0.41	1
	04/21/85	1985.304	2.00 0.42	1
	06/05/85	1985.427	2.14 0.31	1
	06/15/85	1985.455	2.56 0.30	1
	06/22/85	1985.474	2.50 0.47	1
2134+00	12/25/84	1984.984	1.97±0.22	2
	01/12/85	1985.033	1.85 0.24	1
	02/21/85	1985.142	1.86 0.27	1
	03/21/85	1985.219	1.76 0.26	1
	04/21/85	1985.304	2.02 0.35	1
	06/05/85	1985.427	1.84 0.31	1
	06/15/85	1985.454	1.84 0.30	1
	06/22/85	1985.474	2.10 0.30	1
2145+06	12/25/84	1984.984	7.80±0.26	2
	02/21/85	1985.142	7.39 0.38	1
	03/22/85	1985.221	7.60 0.40	1
	06/05/85	1985.427	6.61 0.41	1
	06/15/85	1985.455	6.96 0.37	1
	06/22/85	1985.474	6.62 0.46	1
BL LAC	12/19/85	1984.967	1.55±0.26	1
	12/26/84	1984.986	1.70 0.22	1
	01/20/85	1985.055	1.86 0.39	1
	02/21/85	1985.142	1.55 0.24	1
	03/21/85	1985.219	1.89 0.26	1
	04/21/85	1985.304	1.46 0.47	1
	05/28/85	1985.405	2.09 0.52	1
	06/05/85	1985.427	1.59 0.28	1
	06/14/85	1985.452	1.77 0.54	1
3C446	12/25/85	1984.984	5.18±0.27	2
	01/12/85	1985.033	4.50 0.32	1
	02/21/85	1985.142	3.67 0.35	1
	03/22/85	1985.221	3.59 0.27	2
	04/29/85	1985.326	3.92 0.34	1
	06/15/85	1985.455	2.91 0.28	1

Source	Date	λ3mm Year	S_ν [Jy]	N
CTA102	12/25/84	1984.984	1.80±0.22	2
	02/21/85	1985.142	2.08 0.39	1
	03/21/85	1985.219	2.65 0.29	1
	04/21/85	1985.304	2.51 0.29	1
	04/29/85	1985.326	2.23 0.59	1
	06/05/85	1985.427	1.74 0.32	1
	06/15/85	1985.455	1.62 0.28	1
	06/22/85	1985.474	2.38 0.59	1
3C454.3	12/25/84	1984.984	4.78±0.29	2
	04/29/85	1985.326	4.55 0.35	1
	05/04/85	1985.340	6.39 0.46	1

Source	Date	λ7mm Year	S_ν [Jy]	N
0048-09	06/22/85	1985.474	2.03±0.35	1
0106+01	07/29/85	1985.575	2.32±0.34	1
0235+16	06/22/85	1985.474	2.58±0.30	1
	07/04/85	1985.507	2.69 0.35	1
	07/29/85	1985.575	2.63 0.30	1
3C84	06/05/85	1985.427	43.63±1.07	2
	06/15/85	1985.455	40.70 0.91	1
	06/22/85	1985.474	43.64 1.29	2
	07/04/85	1985.507	44.64 1.00	1
	07/23/85	1985.559	43.04 1.85	1
	07/29/85	1985.575	40.55 1.09	1
0355+50	06/15/85	1985.455	3.68±0.37	1
	06/22/85	1985.474	4.47 0.38	1
	07/23/85	1985.559	4.96 0.39	1
	07/29/85	1985.575	3.59 0.30	2
3C111	07/04/85	1985.507	2.57±0.43	1
0735+17	07/23/85	1985.559	1.02±0.28	1
OJ287	06/21/85	1985.471	5.34±0.38	1
	07/03/85	1985.504	11.23 0.57	1
	07/23/85	1985.559	6.17 0.38	1
1055+01	06/15/85	1985.455	4.19±0.35	1
	06/21/85	1985.471	3.84 0.36	1
	07/03/85	1985.504	3.22 0.42	1
	07/23/85	1985.559	4.12 0.34	1
1156+29	06/15/85	1985.455	4.53±0.31	1
	07/26/85	1985.567	4.90 0.47	1
	07/29/85	1985.575	4.86 0.30	1
1219+28	07/29/85	1985.575	1.55±0.31	1

Source	Date	λ7mm Year	S_ν [Jy]	N
3C273	06/15/85	1985.455	25.18±0.66	1
	06/21/85	1985.471	24.51 0.79	3
	07/03/85	1985.504	22.55 0.59	2
	07/23/85	1985.559	23.46 0.99	1
	07/26/85	1985.567	21.89 0.52	1
	07/29/85	1985.575	23.93 0.71	1
3C274	06/15/85	1985.455	12.54±0.43	1
	06/21/85	1985.471	14.60 0.82	2
	07/03/85	1985.504	12.31 0.61	1
	07/23/85	1985.559	14.41 0.68	1
	07/26/85	1985.567	12.37 0.66	1
	07/29/85	1985.575	13.35 0.42	1
3C279	06/15/85	1985.455	8.54±0.46	1
	06/21/85	1985.471	9.31 0.49	2
	07/03/85	1985.504	7.25 0.48	1
	07/23/85	1985.559	8.41 0.44	1
	07/26/85	1985.567	7.05 0.58	1
	07/29/85	1985.575	7.07 0.48	1
1308+32	07/04/85	1985.507	4.39±0.46	1
	07/29/85	1985.575	4.11 0.28	1
1335-12	06/15/85	1985.455	5.40±0.33	1
	06/21/85	1985.471	5.16 0.46	1
	07/23/85	1985.559	6.32 0.36	1
	07/29/85	1985.575	6.51 0.40	1
1413+13	06/15/85	1985.455	0.43±0.34	1
	06/21/85	1985.471	2.41 0.55	1
	07/04/85	1985.507	0.94 0.53	1
	07/29/85	1985.575	1.31 0.26	1
1502+10	07/29/85	1985.575	1.61±0.40	1
1510-08	07/29/85	1985.575	1.93±0.30	1
1514-24	07/29/85	1985.575	1.40±0.54	1
1555+00	07/29/85	1985.575	0.37±0.31	1

Source	Date	λ7mm Year	S_ν [Jy]	N
1622-25	07/29/85	1985.575	2.15±0.31	1
1633+38	06/21/85	1985.471	1.39±0.51	1
	07/04/85	1985.507	2.28 0.32	1
3C345	06/05/85	1985.427	8.83±0.72	1
	06/21/85	1985.471	10.29 0.90	1
	07/04/85	1985.507	10.43 0.47	1
	07/29/85	1985.575	8.92 0.37	1
1656+05	07/29/85	1985.575	0.52±0.31	1
1730-13	06/15/85	1985.455	7.74±0.62	1
	07/04/85	1985.507	6.14 0.42	1
	07/26/85	1985.567	6.24 0.43	1
	07/29/85	1985.575	6.23 0.42	1
1741-03	07/29/85	1985.575	3.57±0.28	1
1749+09	07/19/85	1985.548	10.13±0.39	1
	07/26/85	1985.567	9.99 0.22	3
	07/29/85	1985.575	9.52 0.37	4
1921-29	07/29/85	1985.575	0.83±0.36	1
1958-17	07/04/85	1985.507	1.05±0.36	1
	07/29/85	1985.575	1.40 0.34	1
2121+05	06/15/85	1985.455	2.99±0.38	1
	06/22/85	1985.474	3.57 0.32	1
	07/04/85	1985.507	3.54 0.43	1
	07/29/85	1985.575	3.20 0.30	1
2134+00	06/15/85	1985.455	4.16±0.39	1
	06/22/85	1985.474	3.71 0.47	1
	07/04/85	1985.507	2.25 0.34	1

Source	Date	λ7mm Year	S_ν [Jy]	N
2145+06	06/05/85	1985.427	8.85±0.60	1
	06/15/85	1985.455	8.63 0.47	1
	06/22/85	1985.474	8.54 0.59	1
	07/04/85	1985.507	8.56 0.35	1
	07/29/85	1985.575	9.55 0.36	1
BL LAC	07/29/85	1985.575	1.38±0.30	1
3C446	06/05/85	1985.427	4.33±0.35	1
	06/15/85	1985.455	3.13 0.50	1
	06/22/85	1985.474	4.05 0.39	1
	07/04/85	1985.507	4.25 0.39	1
	07/29/85	1985.575	3.61 0.42	1
CTA102	06/15/85	1985.455	2.03±0.34	1
	06/22/85	1985.474	2.79 0.37	1
	07/04/85	1985.507	1.64 0.39	1
	07/29/85	1985.575	1.93 0.26	1
3C454.3	06/05/85	1985.427	5.94±0.65	1
	07/04/85	1985.507	6.44 0.41	1
	07/29/85	1985.575	6.35 0.42	1

APPENDIX B

OUTBURST PROFILE COEFFICIENTS

Coefficients obtained from fitting the Legg function to individual outbursts in the time variability data. An error of zero for a coefficient indicates the parameter was held fixed during the fit.

† The number of free parameters equals the number of data points, thus a reduced chi square can not be calculated.

2.7 GHz — Base flux density 8.9 Jy

Burst	t_0[Yr]	t_p[Yr]	S_p[Jy]	τ[Yr]	χ^2_ν
5.0	70.10±0.00	73.08±0.52	1.89±0.21	0.706±1.545	0.41
6.0	73.20 0.00	76.08 0.13	1.65 0.22	0.250 0.104	0.36
7.0	77.16 0.00	77.86 0.21	0.72 0.27	0.301 0.293	0.10
12.0	80.30 0.00	83.24 0.04	5.92 0.22	0.329 0.034	0.26

7.9 GHz — Base flux density 7.8 Jy

Burst	t_0[Yr]	t_p[Yr]	S_p[Jy]	τ[Yr]	χ^2_ν
1.0	62.17±6.99	67.77±0.02	19.22±0.18	0.235±0.060	1.56
4.0	70.17 0.00	71.50 0.38	2.27 0.30	0.191 0.752	1.45
5.0	71.52 0.21	72.39 0.05	5.41 0.17	0.457 0.078	0.46
6.0	73.42 0.00	74.92 0.03	4.82 0.25	0.203 0.027	0.15
7.0	74.77 0.00	76.33 0.61	1.74 0.25	0.244 4.601	0.04
8.0	76.19 0.00	77.60 0.22	0.71 0.26	0.063 0.450	0.08
9.0	78.00 0.00	79.18 0.34	0.42 0.26	0.058 0.536	0.23
11.0	79.78 0.00	81.27 0.09	5.43 0.40	0.540 0.000	0.38
12.0	80.83 0.51	82.31 0.06	7.91 0.27	0.540 0.228	0.49

15.5 GHz — Base flux density 5.7 Jy

Burst	t_0[Yr]	t_p[Yr]	S_p[Jy]	τ[Yr]	χ^2_ν
2.0	67.06±3.14	68.05±0.21	19.00±0.58	0.596±0.440	1.61
4.0	69.88 1.59	70.86 0.07	3.26 0.29	0.304 0.260	0.92
5.0	71.32 0.60	72.31 0.03	6.09 0.24	0.291 0.072	0.28
5.5	72.65 0.00	73.44 0.05	1.40 0.37	0.019 0.012	0.20
6.0	72.97 4.43	74.44 0.03	6.50 0.24	0.153 0.089	0.62
7.0	73.89 0.00	75.82 0.09	3.18 0.26	0.125 0.209	0.33
8.0	75.79 0.00	77.29 0.14	1.35 0.20	0.102 0.264	0.72
9.0	77.80 0.00	78.53 0.05	1.02 0.40	0.047 0.036	0.18
11.0	79.82 0.00	80.71 0.03	6.48 0.19	0.400 0.000	0.89
12.0	80.96 0.44	81.85 0.03	10.66 0.34	0.400 0.135	0.98

3C454.3

31.4 GHz — Base flux density 4.8 Jy

Burst	t_0[Yr]	t_p[Yr]	S_p[Jy]	τ[Yr]	χ^2_ν
1.0	65.80±0.00	67.37±0.04	16.68±0.66	0.271±0.069	4.84
3.0	68.20 0.00	69.28 0.25	4.86 1.61	0.052 0.076	†
4.0	69.60 0.00	70.93 0.03	6.87 0.70	0.053 0.013	24.20
5.0	70.78 7.31	72.24 0.09	4.92 0.57	0.166 0.158	0.32
6.0	72.89 4.45	74.27 0.06	5.76 0.39	0.176 0.100	0.14
7.0	74.86 0.00	75.91 0.14	1.93 0.32	0.116 0.178	0.32
8.0	77.10 0.00	77.37 0.04	1.35 0.66	0.044 0.045	1.22
9.0	77.95 0.00	78.33 0.21	1.35 0.92	0.080 0.401	1.24
10.0	79.33 0.00	79.55 0.23	1.00 0.53	0.092 0.470	0.99
11.0	79.39 9.17	80.60 0.06	5.67 0.34	0.117 0.123	3.62
12.0	80.30 0.00	81.75 0.02	9.91 0.41	0.115 0.009	1.42
13.0	81.90 0.00	82.89 0.07	3.37 0.99	0.060 0.032	0.47

89.6 GHz — Base flux density 3.0 Jy

Burst	t_0[Yr]	t_p[Yr]	S_p[Jy]	τ[Yr]	χ^2_ν
6.0	72.85 0.00	74.11 0.12	4.89 0.91	0.121 0.057	1.99
7.0	74.87 0.00	75.71 0.11	1.77 0.44	0.068 0.182	4.18
8.0	76.50 0.00	77.32 0.18	1.00 1.19	0.013 0.055	0.99
9.0	77.73 0.00	78.05 0.41	1.83 0.38	1.013 0.998	0.28
11.0	79.56 0.00	80.53 0.05	4.29 0.48	0.105 0.033	0.49
12.0	80.23 0.00	81.66 0.03	6.23 0.35	0.115 0.017	1.44
13.0	81.50 0.00	82.87 0.04	4.31 0.87	0.049 0.012	†

2.7 GHz — Base flux density 1.1 Jy

Burst	t_0[Yr]	t_p[Yr]	S_p[Jy]	τ[Yr]	χ^2_ν
0.0	76.92±0.24	77.50±2.31	0.18±0.14	1.304±-.999	0.03
1.0	78.10 0.00	79.01 0.13	0.59 0.23	0.065 0.054	0.00
2.0	77.52 0.00	80.57 0.17	1.20 0.12	0.222 0.115	0.06
3.0	79.19 0.00	83.52 0.50	1.85 0.11	0.714 0.442	0.46
4.0	83.70 2.55	84.45 0.42	0.41 0.23	0.350 1.247	0.02

7.9 GHz — Base flux density 1.2 Jy

Burst	t_0[Yr]	t_p[Yr]	S_p[Jy]	τ[Yr]	χ^2_ν
0.0	73.52±-.99	76.23±0.39	0.60±0.22	0.093±2.158	0.04
1.0	76.52 5.36	77.52 0.36	1.12 0.14	0.386 1.815	0.12
2.0	77.43 0.00	78.95 0.11	2.78 0.12	0.319 0.114	0.52
3.0	79.10 0.00	80.19 0.10	2.98 0.11	1.060 0.303	0.44
4.0	80.82 0.00	82.14 0.11	2.19 0.21	0.353 0.133	0.36

15.5 GHz — Base flux density 1.5 Jy

Burst	t_0[Yr]	t_p[Yr]	S_p[Jy]	τ[Yr]	χ^2_ν
1.0	76.34±0.00	77.38±0.00	1.47±0.12	0.276±0.000	0.63
2.0	77.43 2.38	78.75 0.04	4.16 0.22	0.252 0.185	0.29
3.0	79.10 0.12	79.99 0.03	3.47 0.15	0.573 0.128	0.28
4.0	80.82 0.00	81.88 0.09	2.61 0.17	0.617 0.174	0.66

31.4 GHz — Base flux density 1.8 Jy

Burst	t_0[Yr]	t_p[Yr]	S_p[Jy]	τ[Yr]	χ^2_ν
1.0	74.23±-.99	76.86±0.20	1.85±0.32	0.186±0.648	0.95
2.0	77.55 1.00	78.55 0.13	4.26 0.41	0.392 0.457	0.27
3.0	78.95 0.00	80.04 0.09	2.90 0.22	0.488 0.161	1.07
4.0	80.97 0.74	81.29 0.22	2.50 0.32	0.503 0.747	0.48

0420-01

89.6 GHz — Base flux density 2.4 Jy

Burst	t_0[Yr]	t_p[Yr]	S_p[Jy]	τ[Yr]	χ^2_ν
2.0	77.22±0.00	78.16±0.09	2.28±0.41	0.331±0.130	0.34
3.0	78.50 0.00	79.59 0.00	1.71 0.29	0.331 0.000	0.92
4.0	80.08 0.00	81.20 0.14	1.24 0.41	0.137 0.079	0.91

3C279

2.7 GHz — Base flux density 9.4 Jy

Burst	t_0[Yr]	t_p[Yr]	S_p[Jy]	τ[Yr]	χ^2_ν
5.0	74.70±0.00	75.78±0.07	2.12±0.36	0.132±0.083	0.36
7.0	75.64 0.00	77.27 0.07	3.01 0.27	0.244 0.068	0.01
8.0	76.81 0.00	78.55 0.00	1.03 0.24	0.275 0.298	0.02

7.9 GHz — Base flux density 10.8 Jy

Burst	t_0[Yr]	t_p[Yr]	S_p[Jy]	τ[Yr]	χ^2_ν
6.0	75.33±0.00	75.68±0.00	2.48±0.52	0.145±0.061	1.02
7.0	75.54 0.00	76.76 0.03	5.79 0.24	0.266 0.036	0.23
8.0	76.81 0.00	78.00 0.05	2.88 0.39	0.094 0.034	0.53
9.0	77.90 0.00	78.97 0.08	1.71 0.25	0.182 0.061	0.21

15.5 GHz — Base flux density 9.7 Jy

Burst	t_0[Yr]	t_p[Yr]	S_p[Jy]	τ[Yr]	χ^2_ν
6.0	75.33±0.00	75.68±0.02	3.64±0.48	0.105±0.042	0.24
7.0	75.64 0.00	76.57 0.03	5.74 0.29	0.172 0.023	0.33
8.0	77.20 0.00	77.96 0.05	3.16 0.41	0.191 0.071	0.49
9.0	78.00 0.00	79.11 0.08	1.80 0.20	0.204 0.078	0.60

3C279

31.4 GHz — Base flux density 6.6 Jy

Burst	t_0[Yr]	t_p[Yr]	S_p[Jy]	τ[Yr]	χ^2_ν
6.0	74.54±0.00	75.47±0.00	3.55±0.28	0.327±0.000	0.70
7.0	75.64 0.00	76.56 0.06	3.77 0.35	0.327 0.078	0.94
8.0	76.81 0.00	78.11 0.05	3.47 0.39	0.069 0.022	0.73
9.0	78.00 0.00	79.16 0.06	3.17 0.55	0.130 0.041	0.35

89.6 GHz — Base flux density 4.5 Jy

Burst	t_0[Yr]	t_p[Yr]	S_p[Jy]	τ[Yr]	χ^2_ν
6.0	74.80±0.00	75.21±0.09	2.75±0.46	0.241±0.197	2.48
7.0	75.64 0.00	76.28 0.06	2.78 0.35	0.181 0.061	0.27
8.0	77.21 0.00	78.12 0.05	3.18 0.71	0.036 0.021	0.20
9.0	78.00 0.00	79.07 0.13	2.52 0.28	0.222 0.102	0.34

CTA26

2.7 GHz — Base flux density 1.7 Jy

Burst	t_0[Yr]	t_p[Yr]	S_p[Jy]	τ[Yr]	χ^2_ν
5.0	73.90±0.00	74.94±0.22	0.45±0.24	0.135±0.170	0.68
6.0	74.80 0.00	76.05 1.79	0.52 0.00	0.014 0.705	0.01
7.0	75.80 0.00	77.14 0.12	0.64 0.23	0.105 0.073	0.03
9.0	77.40 0.00	79.22 0.26	0.78 0.16	0.734 0.463	0.12
10.0	80.00 0.00	81.42 0.22	0.67 0.18	0.171 0.199	0.07

7.9 GHz — Base flux density 2.2 Jy

Burst	t_0[Yr]	t_p[Yr]	S_p[Jy]	τ[Yr]	χ^2_ν
9.0	77.44 0.00	78.51 0.13	1.23 0.16	0.335 0.191	0.18

15.5 GHz — Base flux density 1.9 Jy

Burst	t_0[Yr]	t_p[Yr]	S_p[Jy]	τ[Yr]	χ^2_ν
8.0	75.11±0.00	77.27±0.41	0.34±0.19	0.100±0.000	0.12
9.0	76.29 0.00	78.45 0.04	2.32 0.20	0.100 0.017	0.08

CTA26

31.4 GHz — Base flux density 1.5 Jy

Burst	t_0[Yr]	t_p[Yr]	S_p[Jy]	τ[Yr]	χ^2_ν
8.0	76.47±0.00	77.48±0.18	1.28±0.28	0.152±0.000	0.32
9.0	77.45 0.00	78.46 0.05	2.61 0.34	0.152 0.037	0.44

89.6 GHz — Base flux density 0.7 Jy

Burst	t_0[Yr]	t_p[Yr]	S_p[Jy]	τ[Yr]	χ^2_ν
8.0	76.26±0.00	77.24±0.20	1.00±0.24	0.185±0.000	0.09
9.0	77.36 0.00	78.35 0.16	1.71 0.67	0.185 0.128	0.19

1510-08

2.7 GHz — Base flux density 1.2 Jy

Burst	t_0[Yr]	t_p[Yr]	S_p[Jy]	τ[Yr]	χ^2_ν
13.0	78.60±0.00	79.75±0.00	1.19±0.20	0.200±0.000	0.15
14.0	79.52 0.00	80.10 0.00	0.95 0.29	0.200 0.000	0.01
15.0	80.30 0.00	80.89 0.06	1.43 0.35	0.079 0.040	†
16.0	80.93 0.00	81.60 0.00	1.47 0.19	0.200 0.000	0.01

7.9 GHz — Base flux density 1.2 Jy

Burst	t_0[Yr]	t_p[Yr]	S_p[Jy]	τ[Yr]	χ^2_ν
13.0	78.74±0.00	79.34±0.02	3.20±0.21	0.150±0.032	0.53
14.0	79.52 0.00	80.07 0.05	1.98 0.15	0.232 0.068	0.15
15.0	80.20 0.00	80.87 0.02	2.23 0.30	0.041 0.009	0.32
16.0	80.93 0.00	81.53 0.10	1.43 0.19	0.149 0.137	0.18

1510-08

15.5 GHz — Base flux density 1.3 Jy

Burst	t_0[Yr]	t_p[Yr]	S_p[Jy]	τ[Yr]	χ^2_ν
1.0	69.60±0.00	70.44±0.02	3.34±0.00	0.019±0.004	5.17
2.0	70.50 0.00	71.07 0.04	1.65 0.42	0.060 0.035	0.01
3.0	71.40 0.00	71.95 0.02	3.51 0.00	0.052 0.010	2.10
4.0	72.10 0.00	72.61 0.04	1.76 0.24	0.135 0.044	1.12
5.0	73.10 0.00	73.70 0.03	2.82 0.28	0.096 0.030	0.73
6.0	73.60 0.00	74.22 0.03	2.50 0.48	0.046 0.015	0.08
7.0	74.10 0.00	74.77 0.06	0.81 0.34	0.045 0.045	0.02
8.0	75.30 0.00	75.74 0.03	2.17 0.26	0.210 0.086	1.76
9.0	75.60 0.00	76.56 0.10	0.63 0.22	0.046 0.053	0.16
10.0	76.30 0.00	76.98 0.04	1.09 0.48	0.011 0.009	0.06
11.0	77.00 0.00	77.54 0.21	0.53 0.16	0.312 0.471	0.17
12.0	78.10 0.00	78.73 0.05	0.94 0.00	0.017 0.014	0.03
13.0	78.82 3.17	79.05 0.13	5.24 0.00	0.270 0.298	1.90
14.0	79.45 6.78	80.04 0.09	1.86 0.19	0.132 0.218	0.31
15.0	80.21 0.00	80.79 0.03	3.08 0.44	0.035 0.038	0.43
16.0	80.80 0.00	81.41 0.03	1.40 0.28	0.033 0.017	0.26
17.0	81.50 0.00	82.13 0.09	1.46 0.24	0.219 0.103	0.40

31.4 GHz — Base flux density 0.9 Jy

Burst	t_0[Yr]	t_p[Yr]	S_p[Jy]	τ[Yr]	χ^2_ν
13.0	78.59±2.69	79.11±0.03	7.94±0.00	0.067±0.030	37.10
14.0	79.52 0.00	80.04 0.00	3.12 0.45	0.100 0.000	3.19
15.0	80.20 0.00	80.71 0.03	3.39 0.30	0.035 0.010	†
16.0	80.83 0.00	81.39 0.13	1.12 0.32	0.212 0.207	0.00

1510-08

89.6 GHz — Base flux density 0.7 Jy

Burst	t_0[Yr]	t_p[Yr]	S_p[Jy]	τ[Yr]	χ^2_ν
13.0	78.74±0.00	79.06±0.01	6.90±0.00	0.047±0.006	0.89
14.0	79.52 0.00	80.07 0.28	3.18 0.00	0.012 0.237	†
15.0	80.20 0.00	80.69 0.05	2.43 0.41	0.065 0.036	†
16.0	80.93 0.00	81.29 0.28	0.55 0.47	0.070 0.196	0.00

0235+16

2.7 GHz — Base flux density 0.7 Jy

Burst	t_0[Yr]	t_p[Yr]	S_p[Jy]	τ[Yr]	χ^2_ν
1.0	75.41±0.00	75.91±0.08	2.99±0.23	0.374±0.110	†
2.0	76.19 0.00	76.68 0.00	1.08 0.18	0.045 0.021	†
3.0	76.61 0.00	77.08 0.00	0.84 0.18	0.209 0.000	0.01
4.0	76.96 0.00	77.66 0.00	1.22 0.16	0.209 0.179	0.07
7.0	78.59 0.00	79.29 0.00	1.48 0.28	0.281 0.144	0.02
8.0	79.34 0.00	80.22 0.00	1.14 1.29	0.021 0.424	†

7.9 GHz — Base flux density 1.4 Jy

Burst	t_0[Yr]	t_p[Yr]	S_p[Jy]	τ[Yr]	χ^2_ν
1.0	75.71±0.00	75.85±0.01	5.24±0.22	0.143±0.018	2.76
2.0	76.19 0.00	76.43 0.01	3.25 0.23	0.073 0.013	0.42
3.0	76.61 0.00	76.84 0.00	1.49 0.26	0.339 0.266	2.24
4.0	76.96 0.00	77.60 0.08	0.91 0.23	0.070 0.082	0.02
7.0	78.59 0.00	79.13 0.02	2.01 0.21	0.034 0.009	1.53
8.0	79.31 0.00	80.05 0.06	1.54 0.16	0.078 0.054	0.50
9.0	79.98 0.00	80.65 0.02	1.92 0.23	0.026 0.008	1.33
10.0	80.30 0.00	81.02 0.03	1.31 0.21	0.020 0.009	0.19

0235+16

15.5 GHz — Base flux density 1.3 Jy

Burst	t_0[Yr]	t_p[Yr]	S_p[Jy]	τ[Yr]	χ^2_ν
1.0	75.72±0.38	75.84±0.02	6.92±0.29	0.125±0.037	1.99
2.0	76.19 2.78	76.43 0.04	3.11 0.35	0.065 0.056	1.32
3.0	76.61 1.76	76.83 0.05	2.15 0.24	0.096 0.085	1.11
4.0	76.96 0.00	77.41 0.08	1.22 0.29	0.099 0.619	0.17
6.0	77.30 0.00	78.30 0.04	1.33 0.24	0.031 0.017	0.13
7.0	78.59 0.00	79.05 0.02	1.76 0.21	0.065 0.020	1.22
8.0	79.34 0.00	79.97 0.04	1.45 0.18	0.080 0.042	1.00
11.0	81.25 8.52	81.86 0.06	2.35 0.36	0.084 0.176	0.73
12.0	81.75 0.00	82.28 0.03	2.49 0.51	0.041 0.067	0.40

0235+16

31.4 GHz — Base flux density 1.5 Jy

Burst	t_0[Yr]	t_p[Yr]	S_p[Jy]	τ[Yr]	χ^2_ν
1.0	75.71±0.00	75.84±0.01	5.68±0.54	0.127±0.033	†
2.0	76.00 0.00	76.42 0.15	2.97 0.44	0.024 0.029	†
3.0	76.51 0.00	76.91 0.15	2.02 0.46	0.220 0.373	†
7.0	78.59 0.00	78.97 0.06	1.73 0.00	0.052 0.024	0.62
8.0	79.34 0.00	79.74 0.00	1.33 0.31	0.101 0.059	1.54
11.0	81.25 0.00	81.86 0.00	2.85 0.48	0.084 0.000	0.04
12.0	81.40 0.00	82.28 0.00	0.37 0.66	0.043 0.000	0.00

89.6 GHz — Base flux density 1.0 Jy

Burst	t_0[Yr]	t_p[Yr]	S_p[Jy]	τ[Yr]	χ^2_ν
1.0	75.61±0.00	75.86±0.03	5.46±0.66	0.107±0.035	†
2.0	76.08 0.00	76.44 0.32	3.00 1.51	0.032 0.100	†
3.0	76.61 0.00	76.83 0.00	1.71 0.47	0.321 0.426	0.03
7.0	78.59 0.00	78.98 0.07	1.70 0.31	0.105 0.060	0.34
8.0	79.34 0.00	79.74 0.07	2.03 0.91	0.048 0.030	0.02

NGC5128

31.4 GHz Base flux density 12.9 Jy

Burst	t_0[Yr]	t_p[Yr]	S_p[Jy]	τ[Yr]	χ^2_ν
1.0	74.70±0.00	75.79±0.03	7.26±0.49	0.171±0.032	1.42
3.0	77.00 0.00	78.17 0.03	6.74 0.53	0.092 0.017	1.17
4.0	78.20 0.00	79.42 0.05	7.23 0.61	0.107 0.043	0.93
5.0	79.24 0.00	80.39 0.01	12.37 0.94	0.046 0.008	0.07
6.0	80.49 0.00	81.55 0.04	9.87 0.59	0.207 0.061	0.02

APPENDIX C

OUTBURST PROFILE AND TIME VARIABILITY PLOTS

Source variability curves are plotted at each observed frequency with the fit profiles superimposed. The dotted lines are the individual fit outburst profiles. The solid line is the summation of the outburst profiles. The solid circles are measurements from the DB flux monitoring program, Balonek (1982), Barvainis (1984), and this work. The open circles are measurements from: Altschuler and Wardle (1976), Epstein, Landau, and Rather (1980), Flett and Henderson (1981), Geldzahler and Witzel (1981), Jones et al. (1981), Ledden, Aller, and Dent (1976), Owen, Spangler, and Cotten (1980), Salonen et al. (1983), and Terasranta et al. (1987).

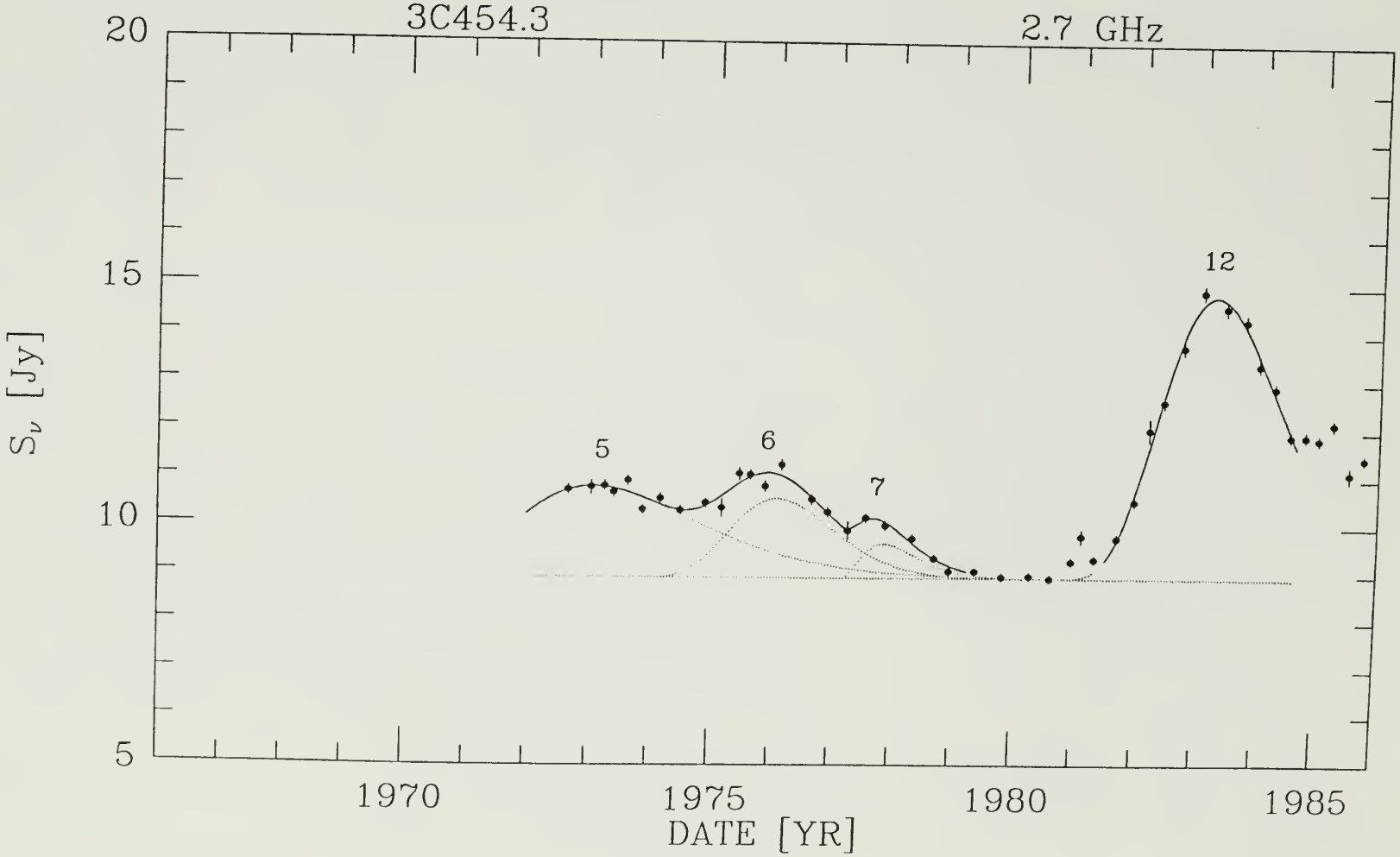
3C454.3
2.7 GHz
20
15
10
5
S_ν [Jy]
5
6
7
12
1970
1975
1980
1985
DATE [YR]

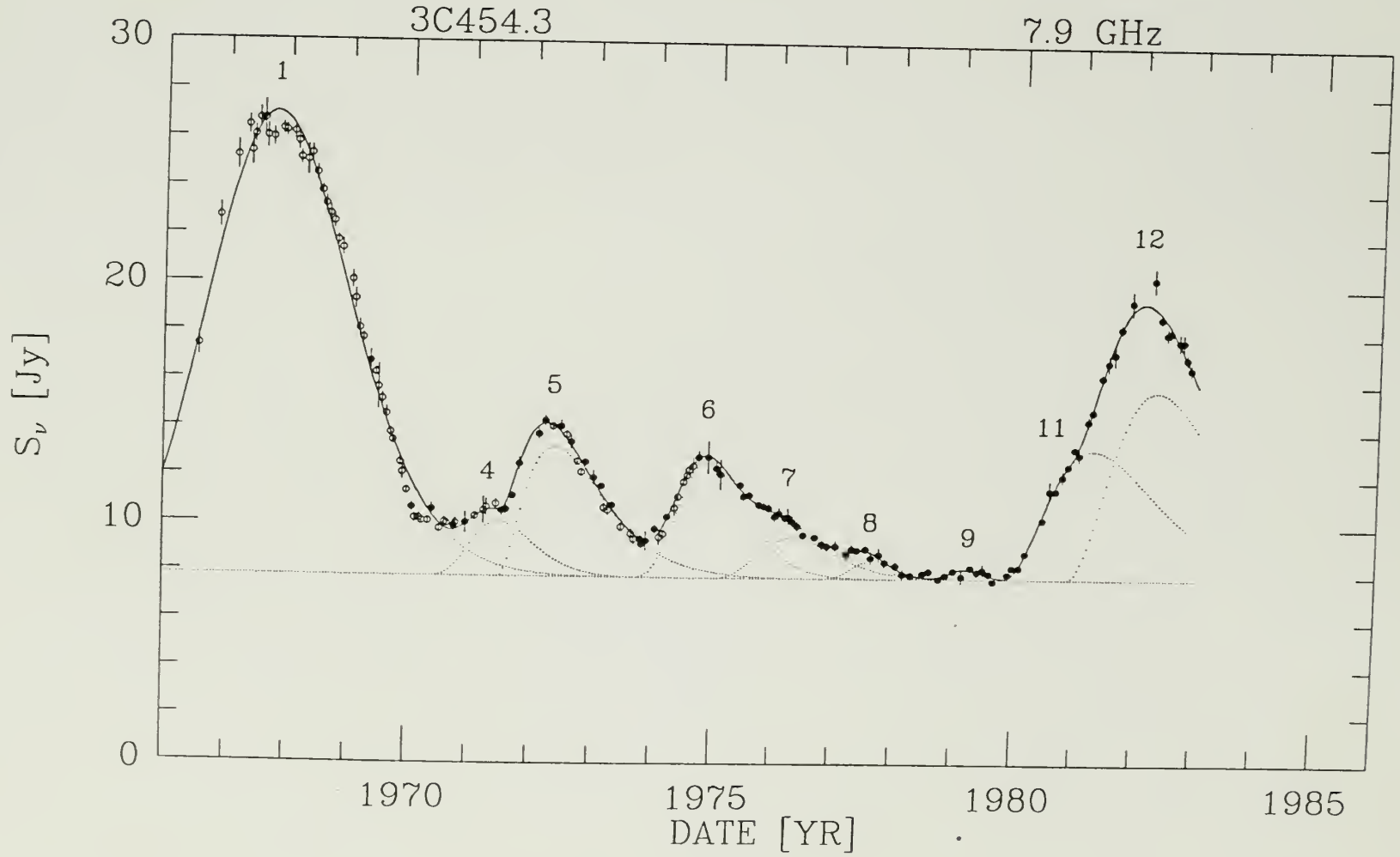
3C454.3
7.9 GHz
30
20
10
0
S_ν [Jy]
1
4
5
6
7
8
9
11
12
1970
1975
1980
1985
DATE [YR]

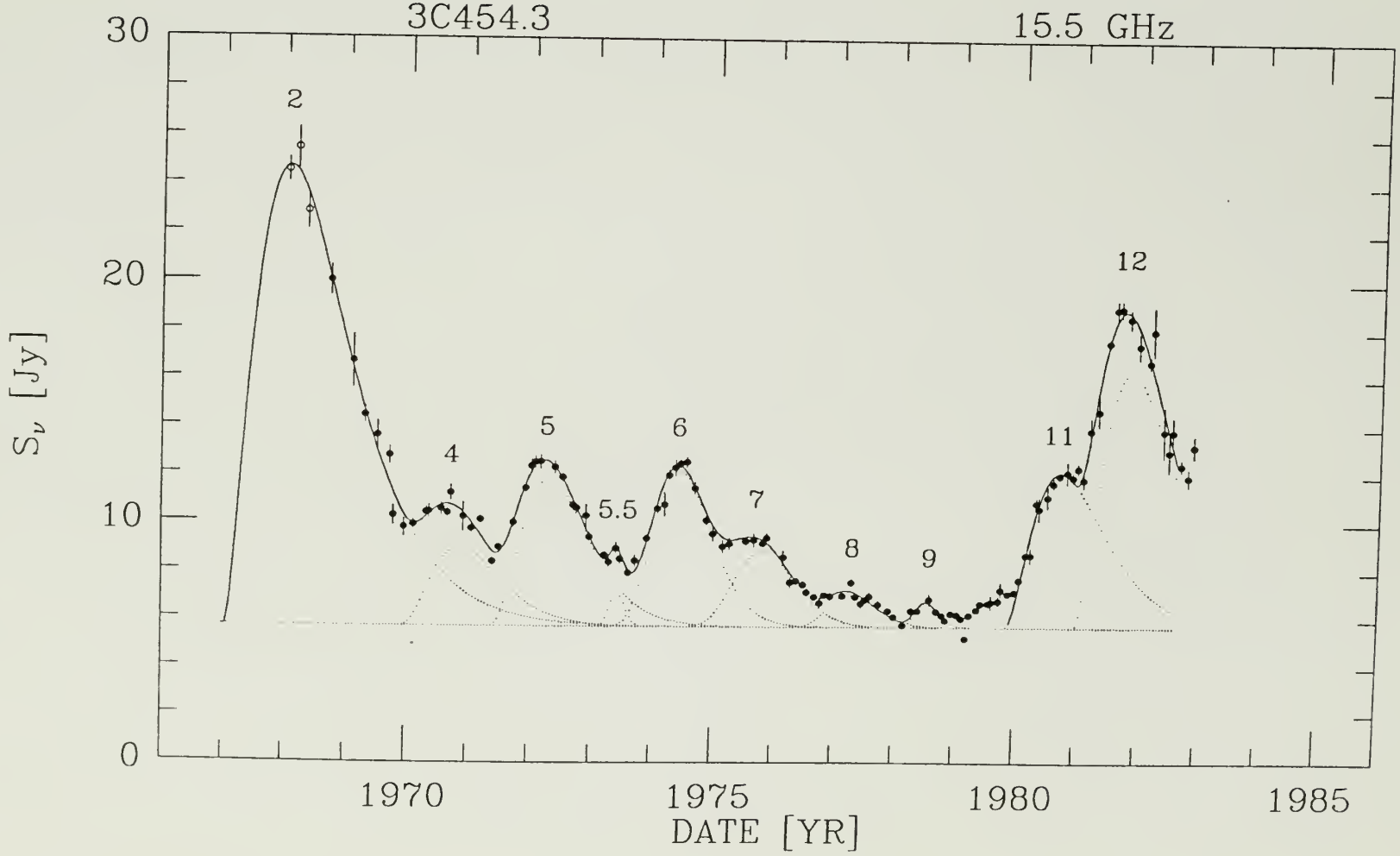
3C454.3
15.5 GHz
30
20
10
0
S_ν [Jy]
1970
1975
1980
1985
DATE [YR]
2
4
5
5.5
6
7
8
9
11
12

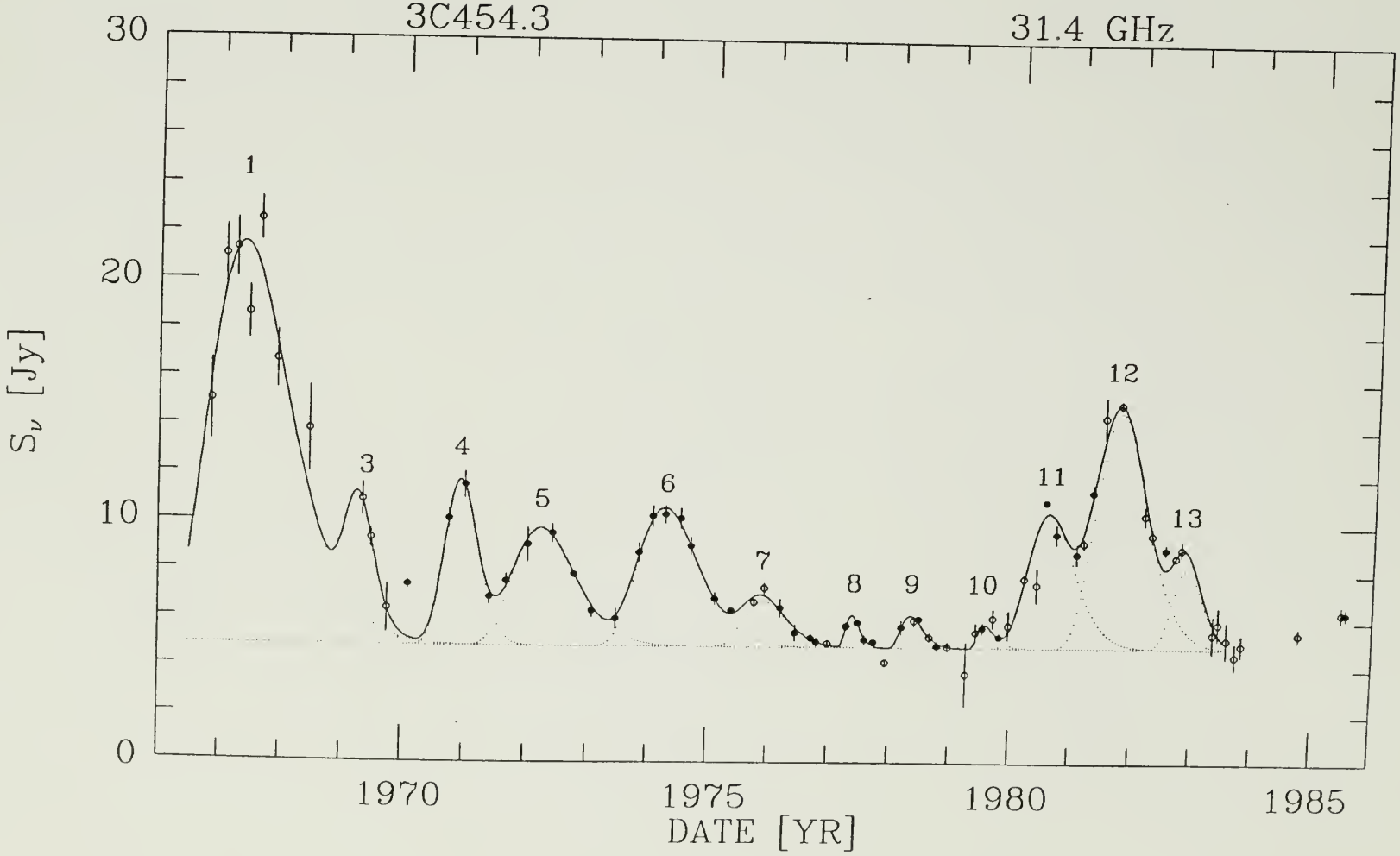
3C454.3
31.4 GHz
30
20
10
0
S_ν [Jy]
1
3
4
5
6
7
8
9
10
11
12
13
1970
1975
1980
1985
DATE [YR]

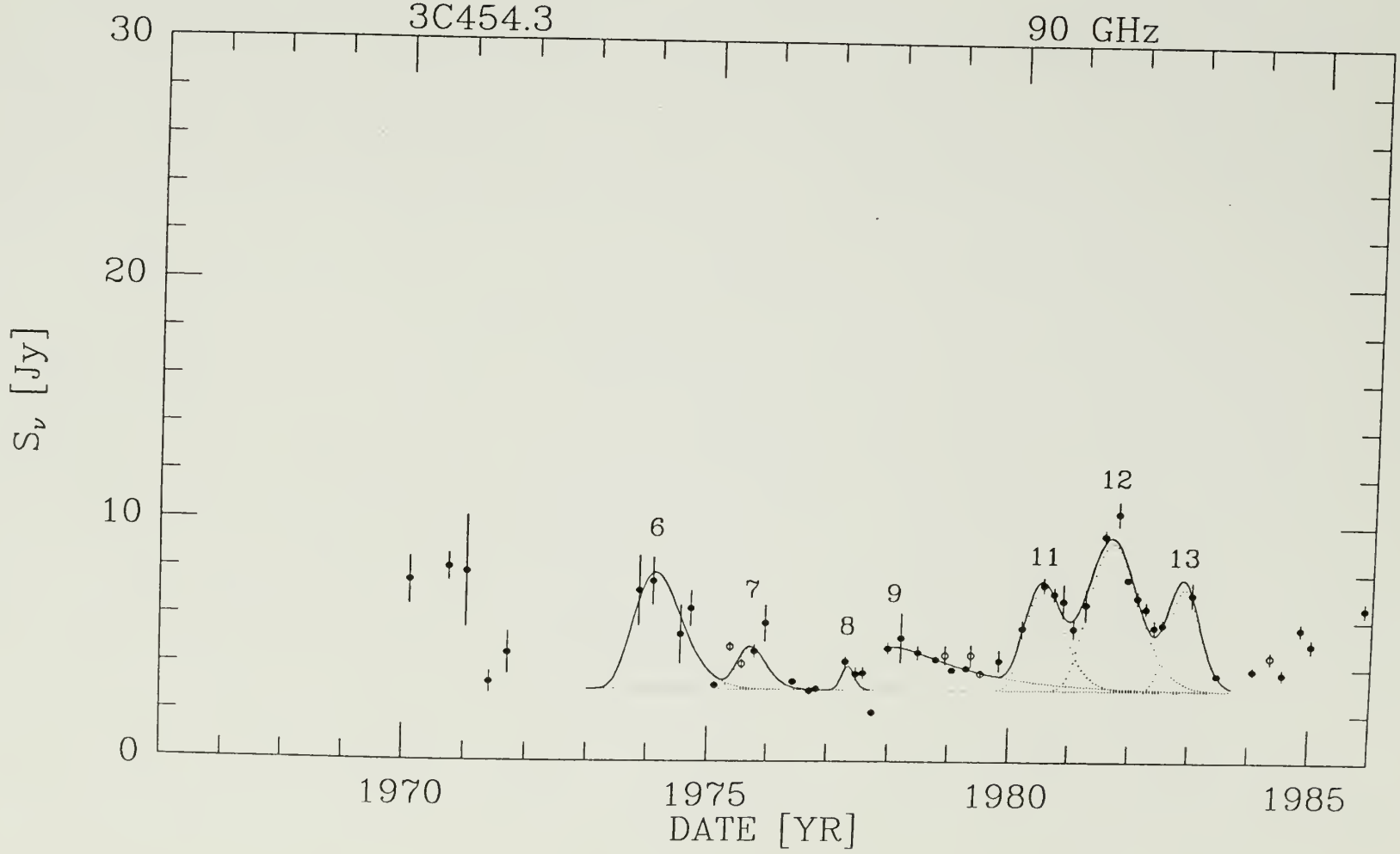
3C454.3
90 GHz
30
20
10
0
S_ν [Jy]
1970
1975
1980
1985
DATE [YR]
6
7
8
9
11
12
13

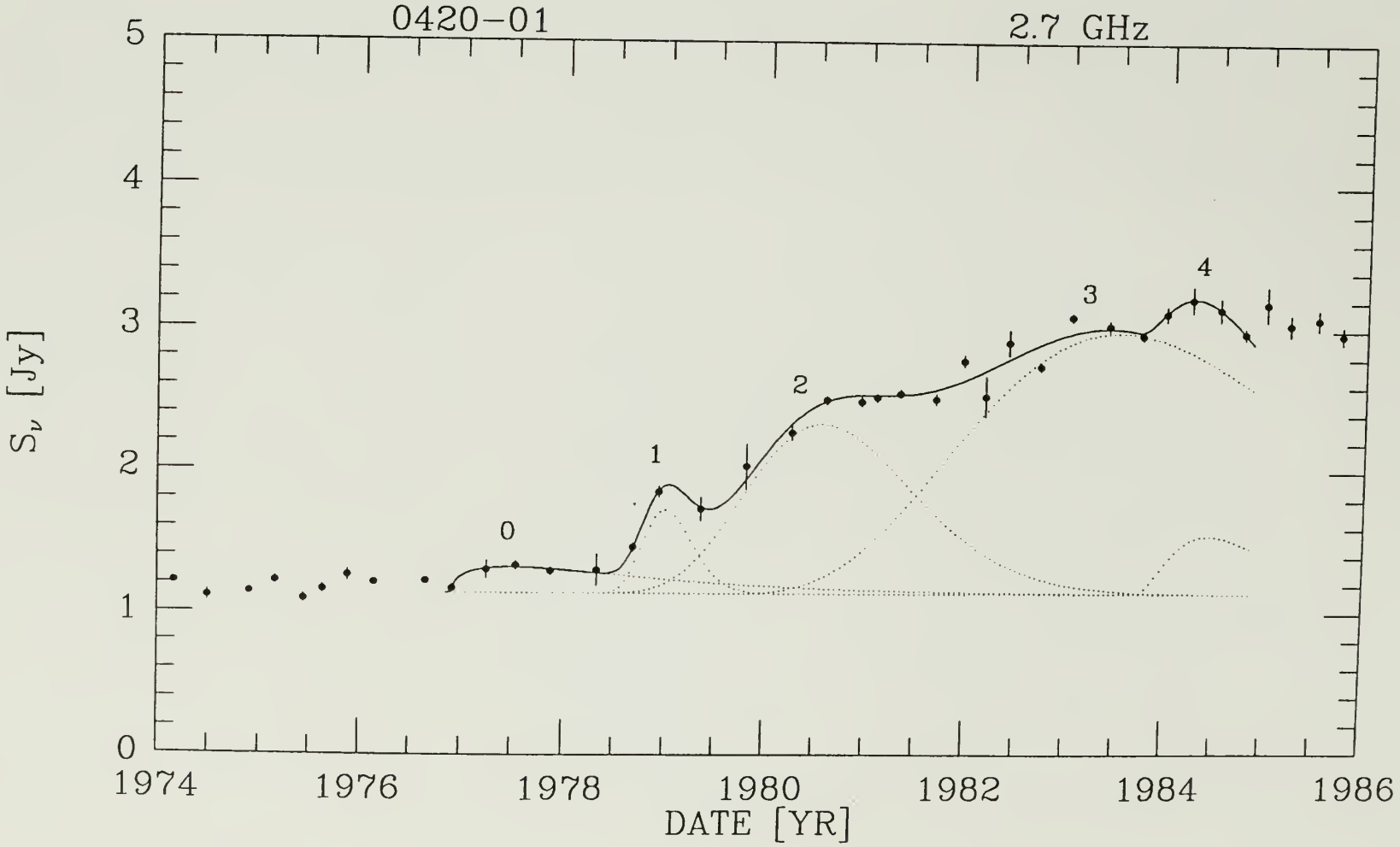
0420−01
2.7 GHz
S_ν [Jy]
DATE [YR]
0
1
2
3
4
5
1974
1976
1978
1980
1982
1984
1986

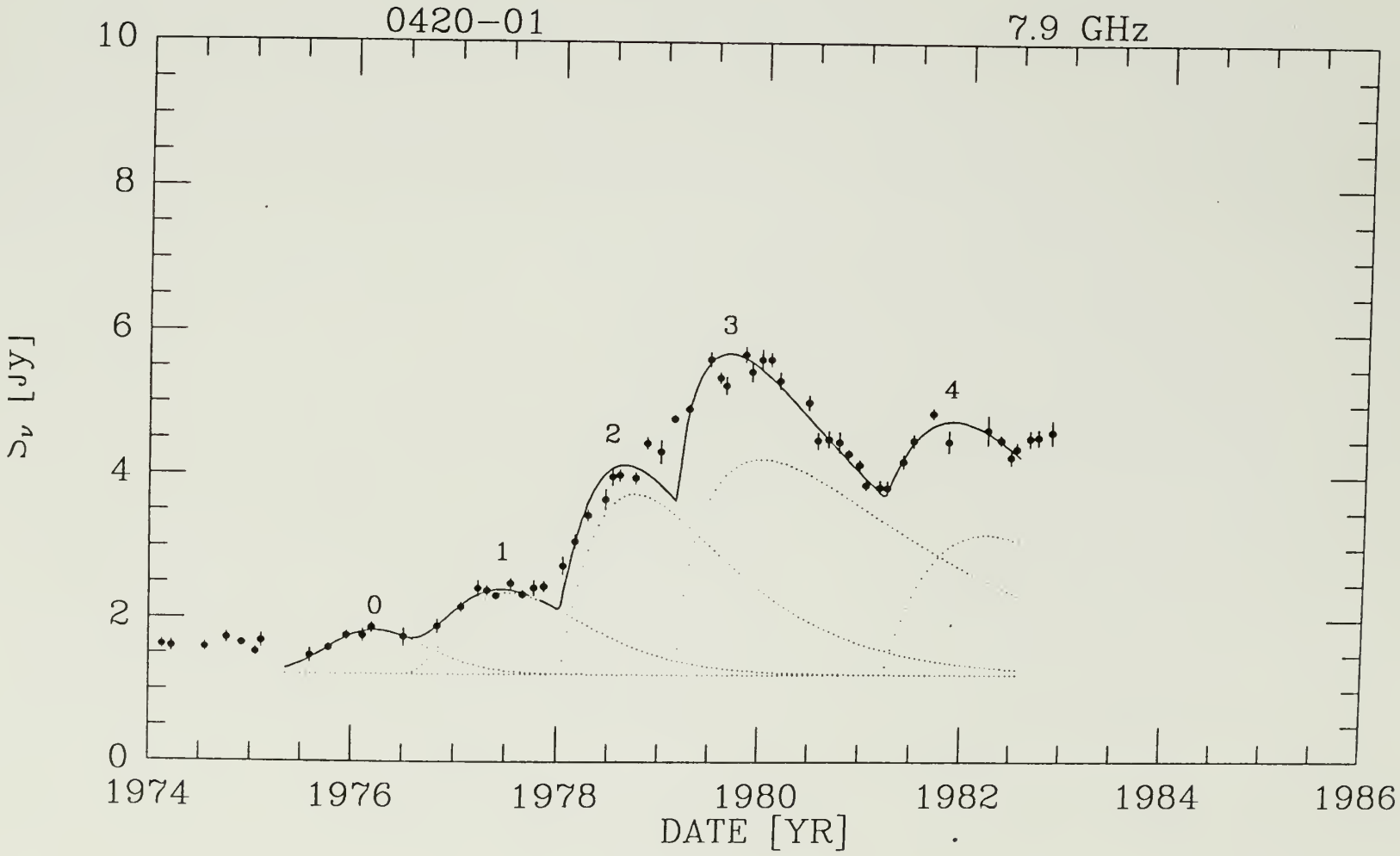
0420−01
7.9 GHz
10
8
6
4
2
0
S_ν [Jy]
0
1
2
3
4
1974
1976
1978
1980
1982
1984
1986
DATE [YR]

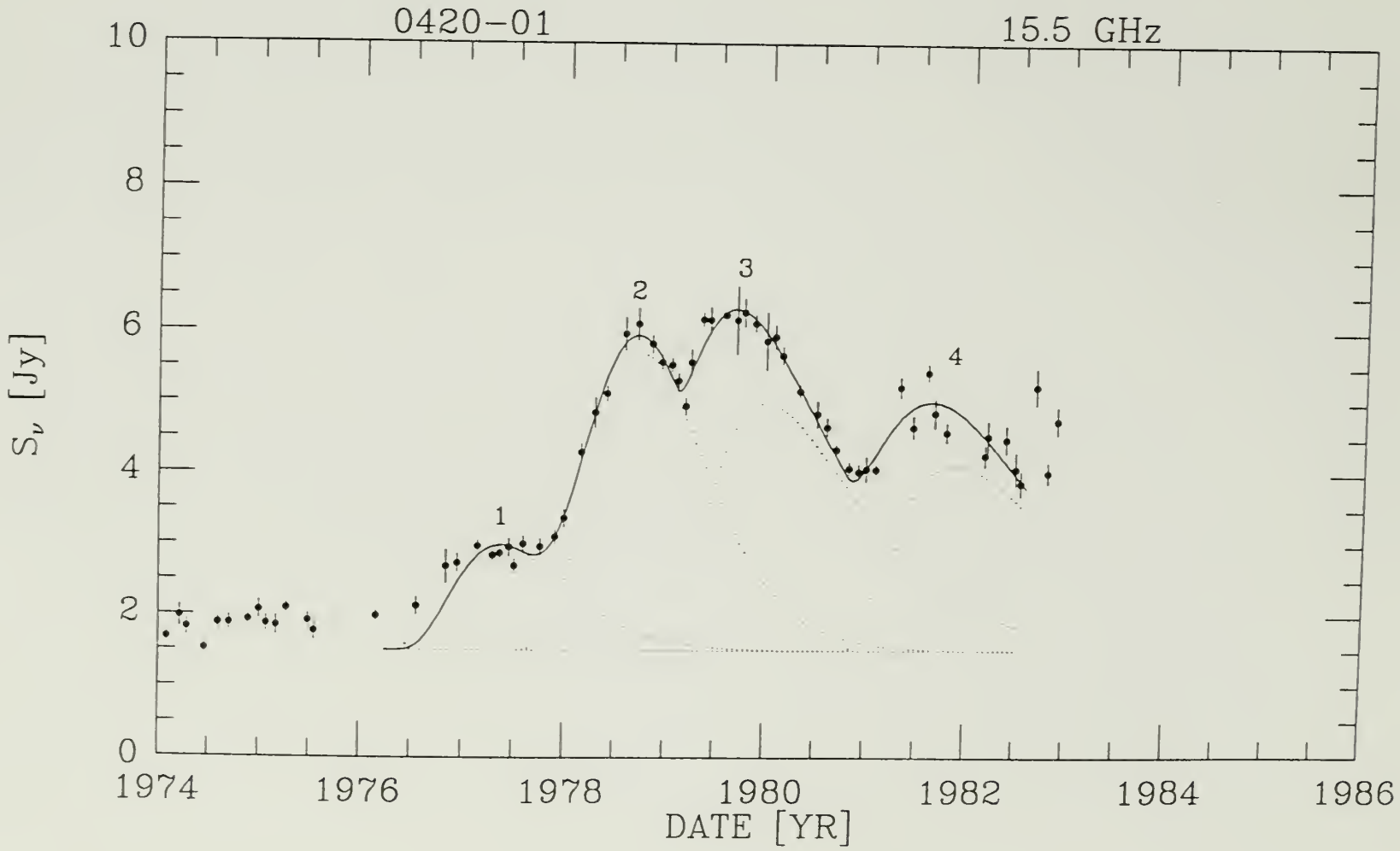
0420−01
15.5 GHz
10
8
6
4
2
0
S_ν [Jy]
1
2
3
4
1974
1976
1978
1980
1982
1984
1986
DATE [YR]

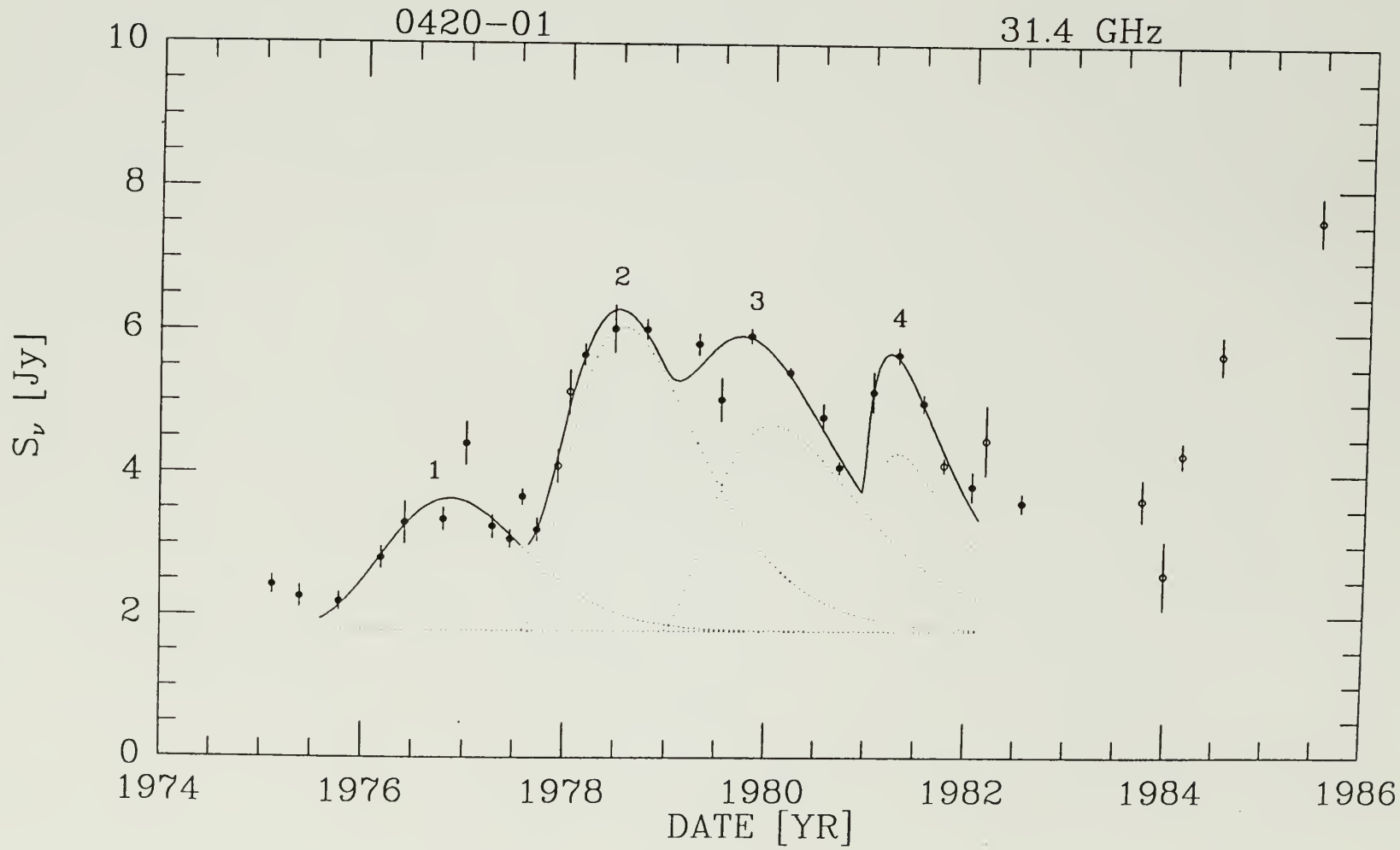
0420−01
31.4 GHz
10
8
6
4
2
0
S_ν [Jy]
1
2
3
4
1974
1976
1978
1980
1982
1984
1986
DATE [YR]

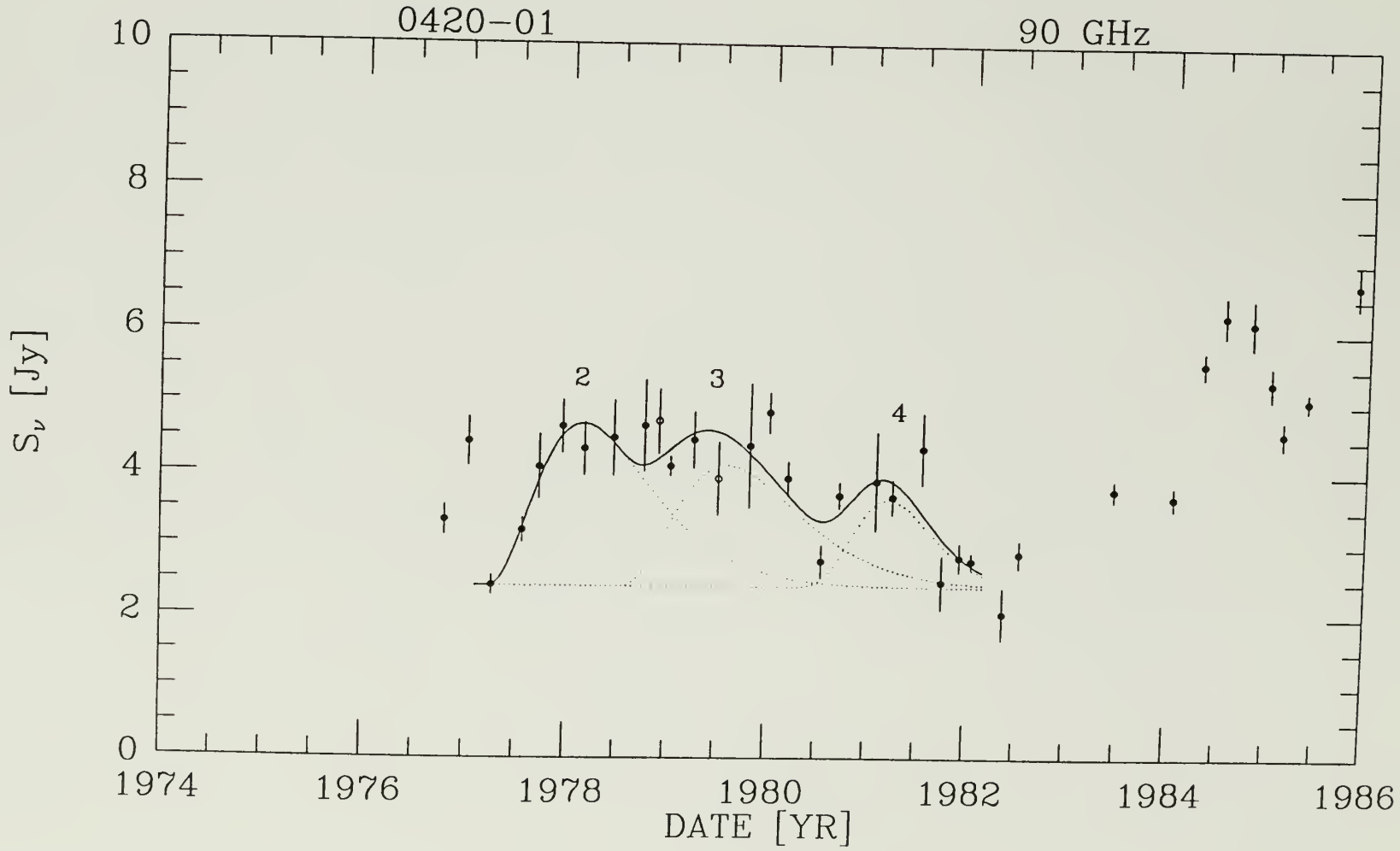
0420−01
90 GHz
10
8
6
4
2
0
S_ν [Jy]
2
3
4
1974
1976
1978
1980
1982
1984
1986
DATE [YR]

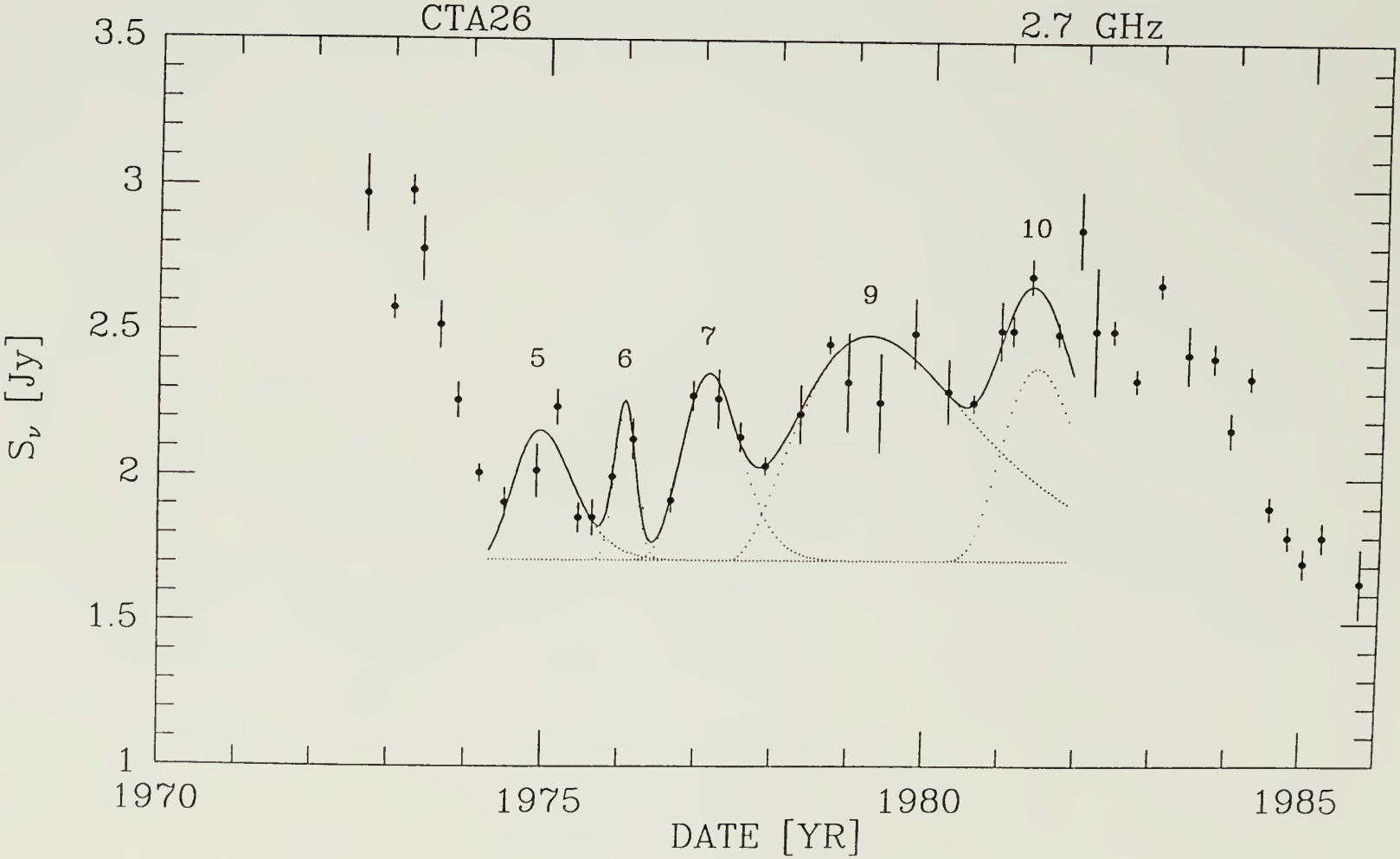
CTA26
2.7 GHz
3.5
3
2.5
2
1.5
1
S_ν [Jy]
5
6
7
9
10
1970
1975
1980
1985
DATE [YR]

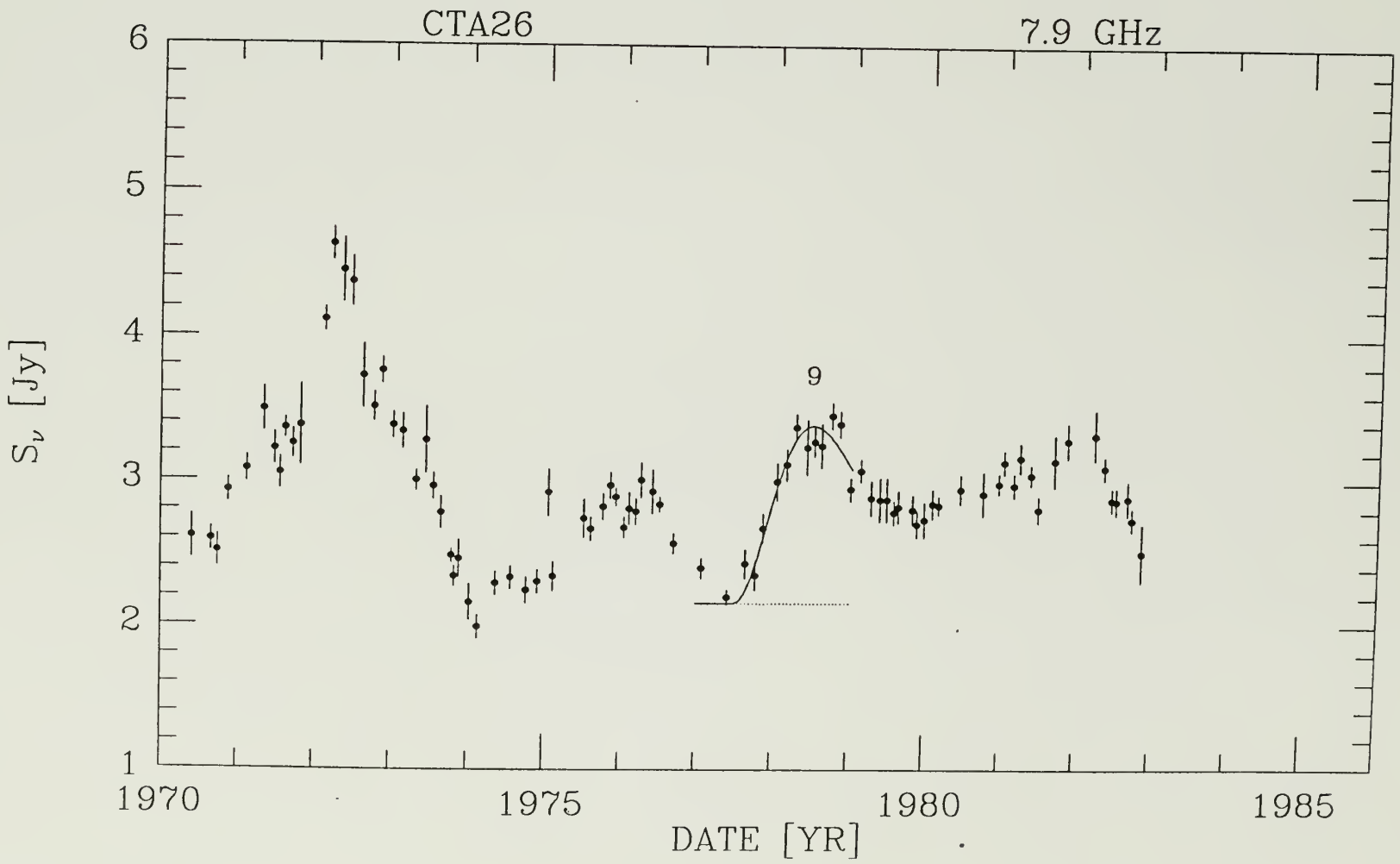
CTA26
7.9 GHz
6
5
4
3
2
1
S_ν [Jy]
9
1970
1975
1980
1985
DATE [YR]

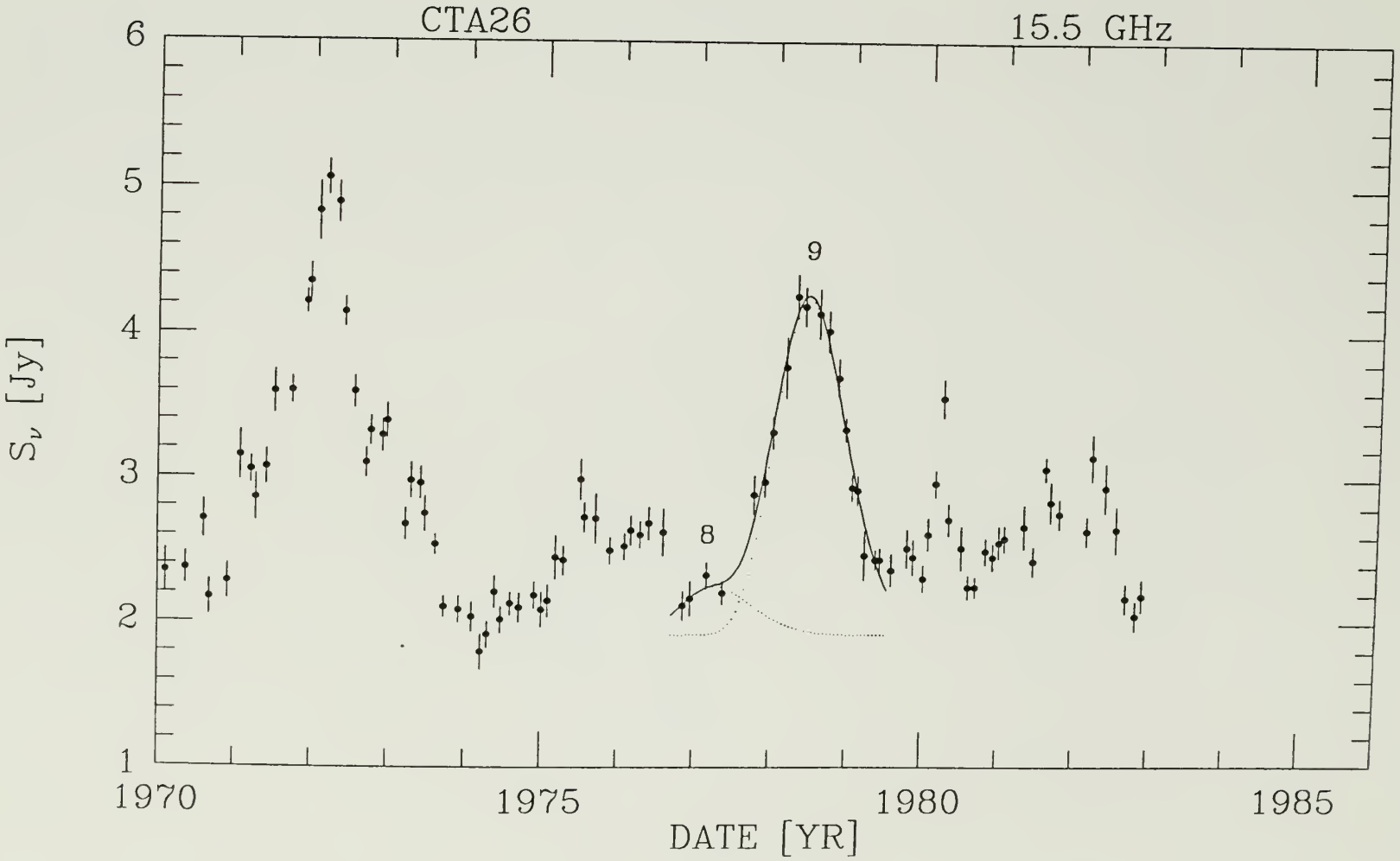
CTA26
15.5 GHz
6
5
4
3
2
1
S_ν [Jy]
9
8
1970
1975
1980
1985
DATE [YR]

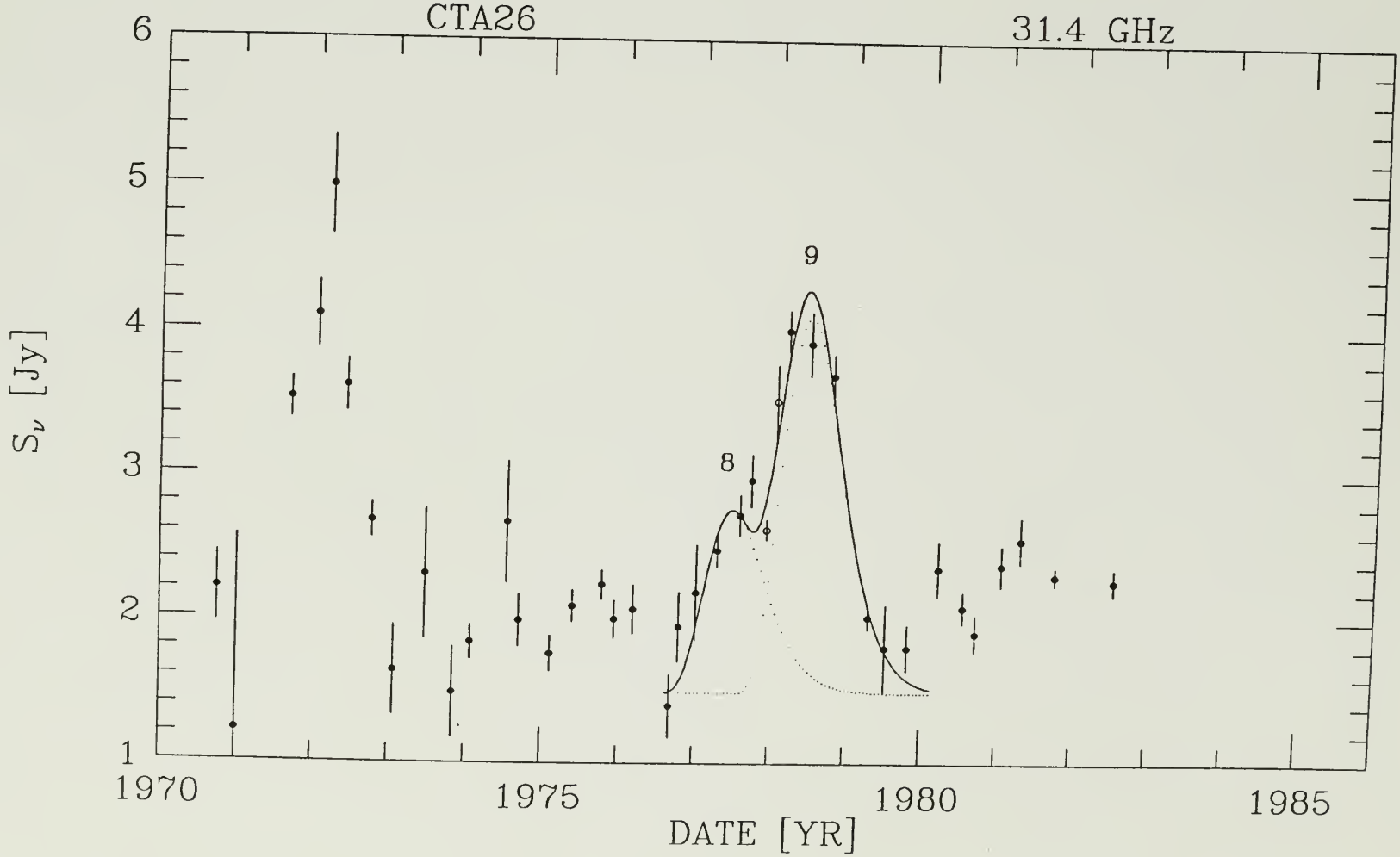
CTA26
31.4 GHz
6
5
4
3
2
1
S_ν [Jy]
8
9
1970
1975
1980
1985
DATE [YR]

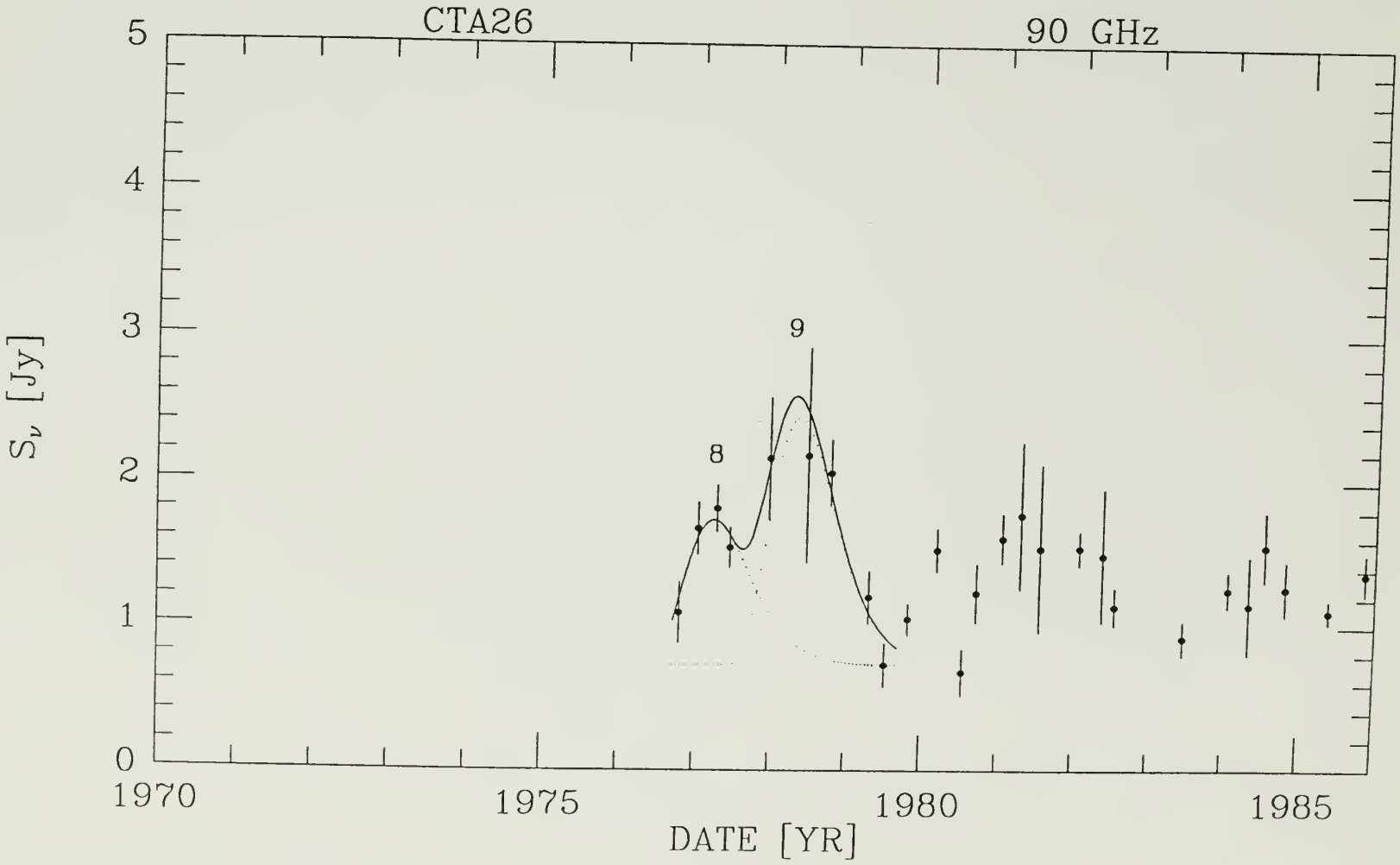
CTA26
90 GHz
5
4
3
2
1
0
S_ν [Jy]
8
9
1970
1975
1980
1985
DATE [YR]

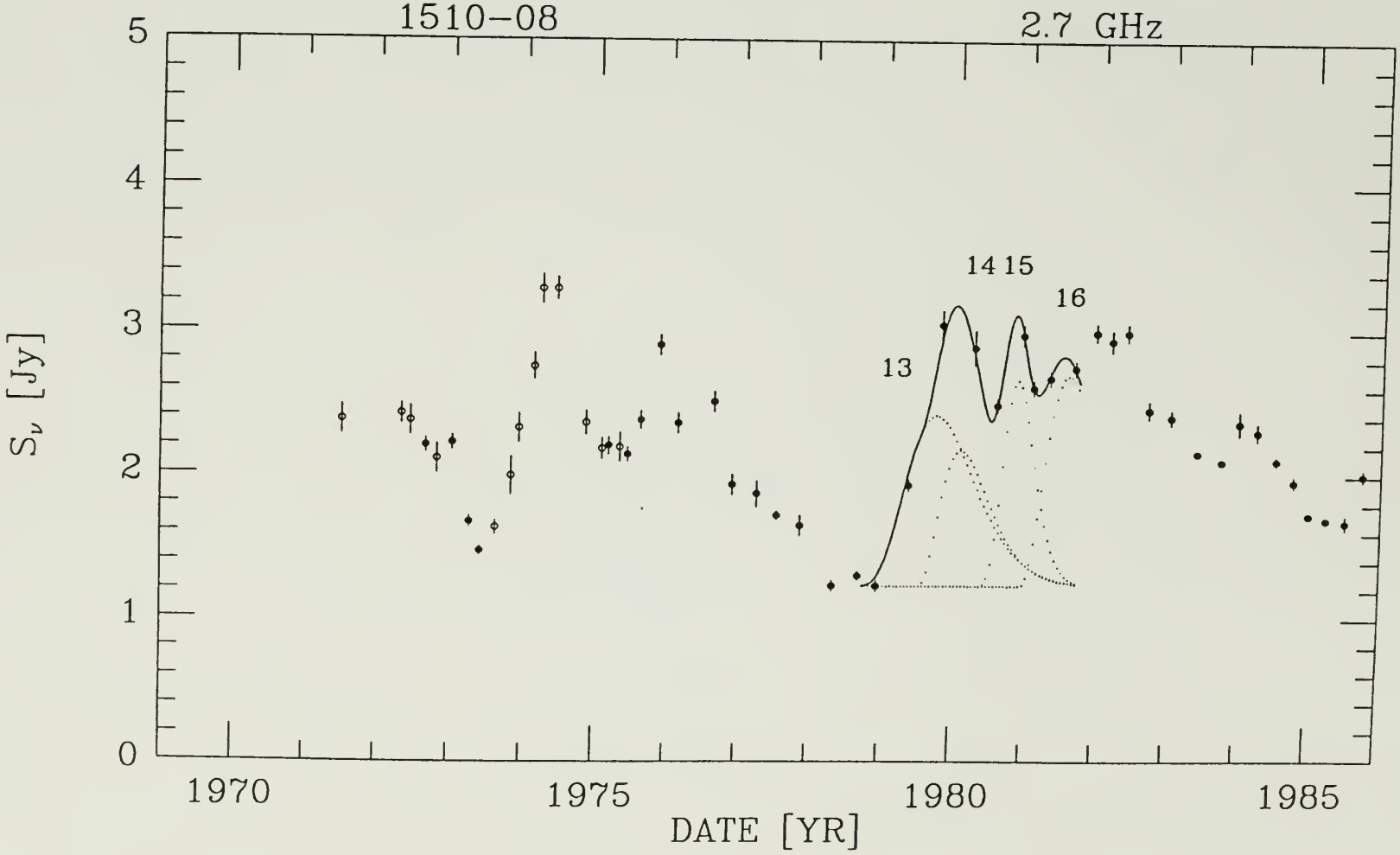
1510−08
2.7 GHz
13
14 15
16
S_ν [Jy]
DATE [YR]
0
1
2
3
4
5
1970
1975
1980
1985

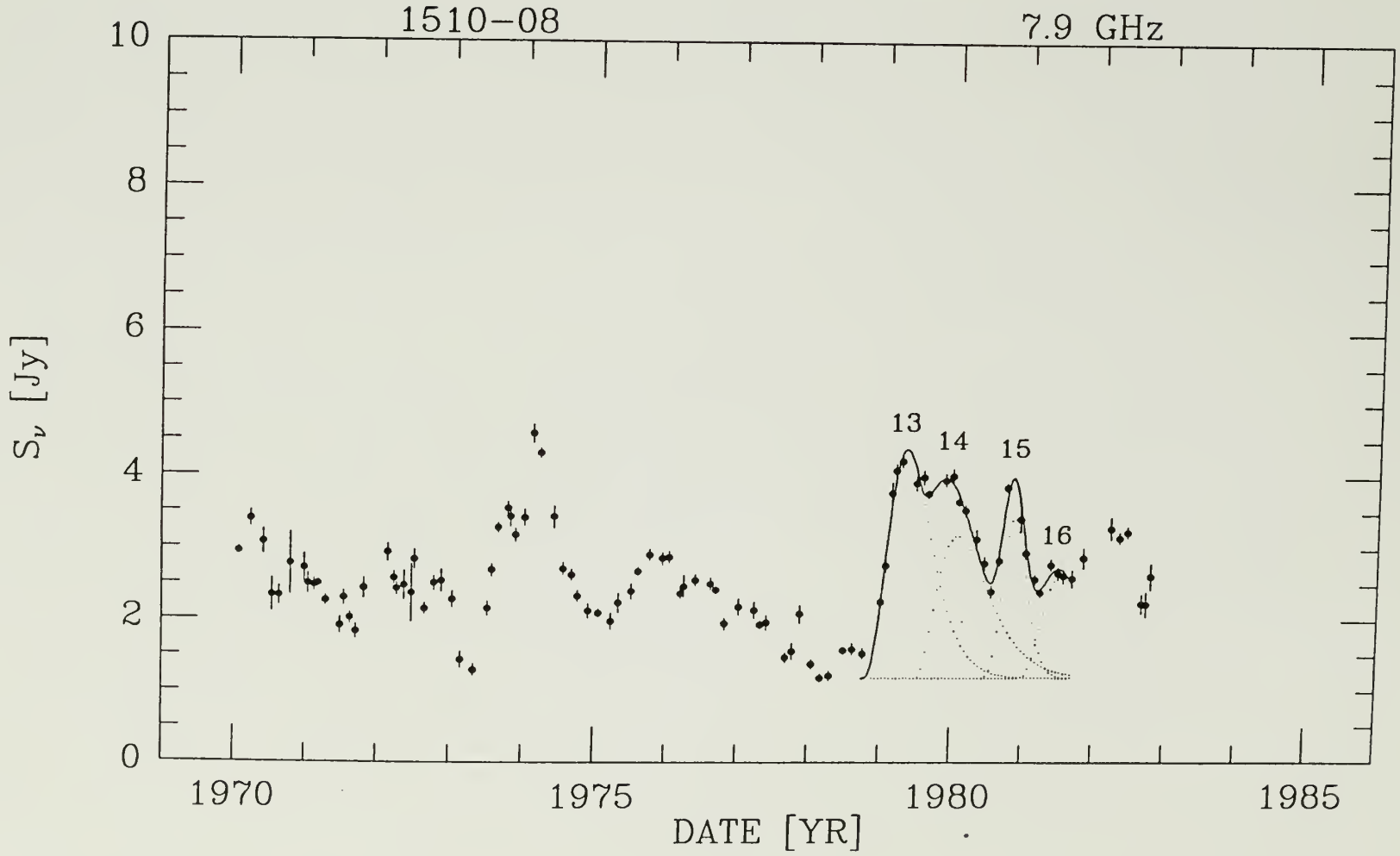
1510−08
7.9 GHz
10
8
6
4
2
0
S_ν [Jy]
13
14
15
16
1970
1975
1980
1985
DATE [YR]

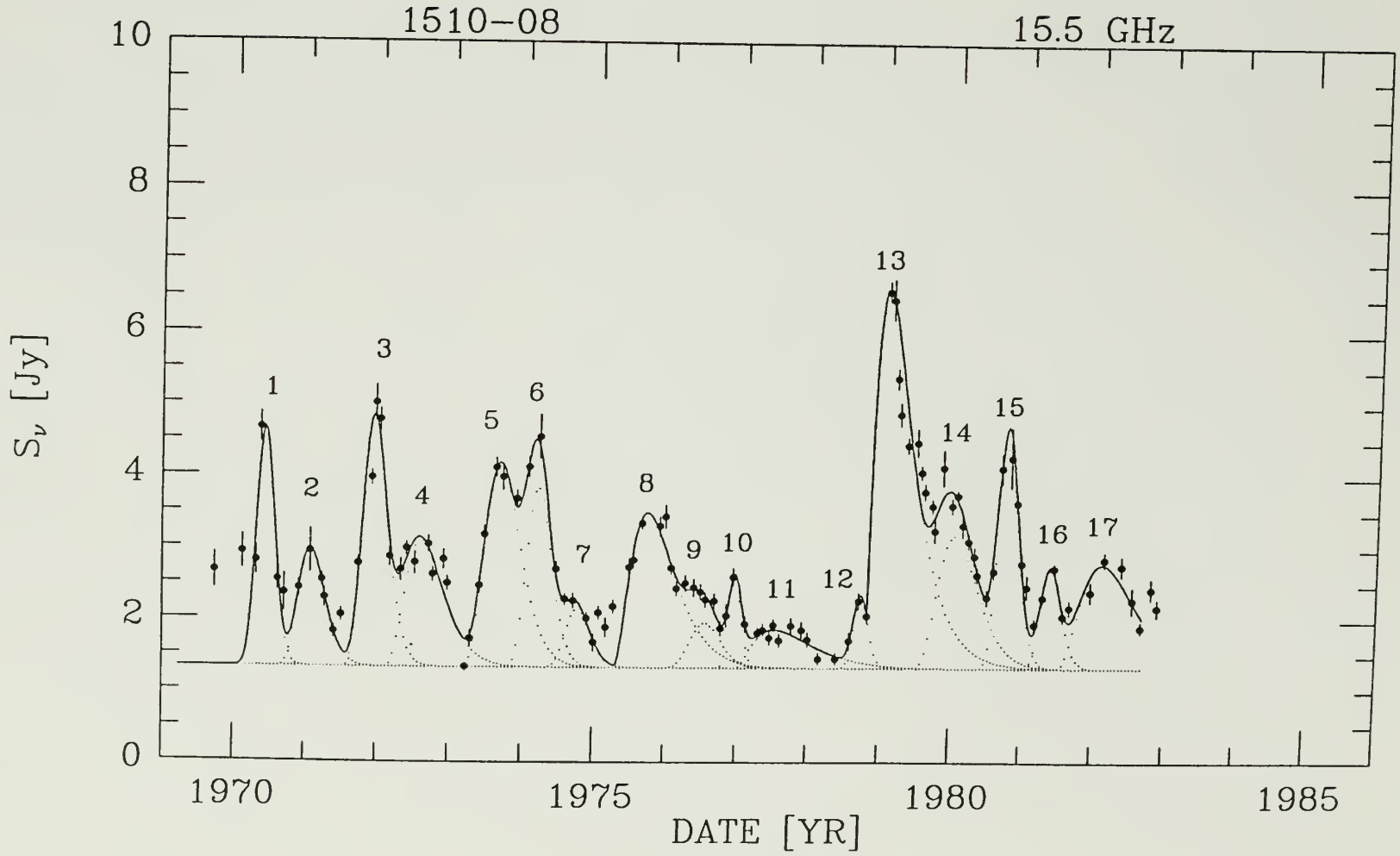
1510−08
15.5 GHz
S_ν [Jy]
DATE [YR]
0
2
4
6
8
10
1970
1975
1980
1985
1
2
3
4
5
6
7
8
9
10
11
12
13
14
15
16
17

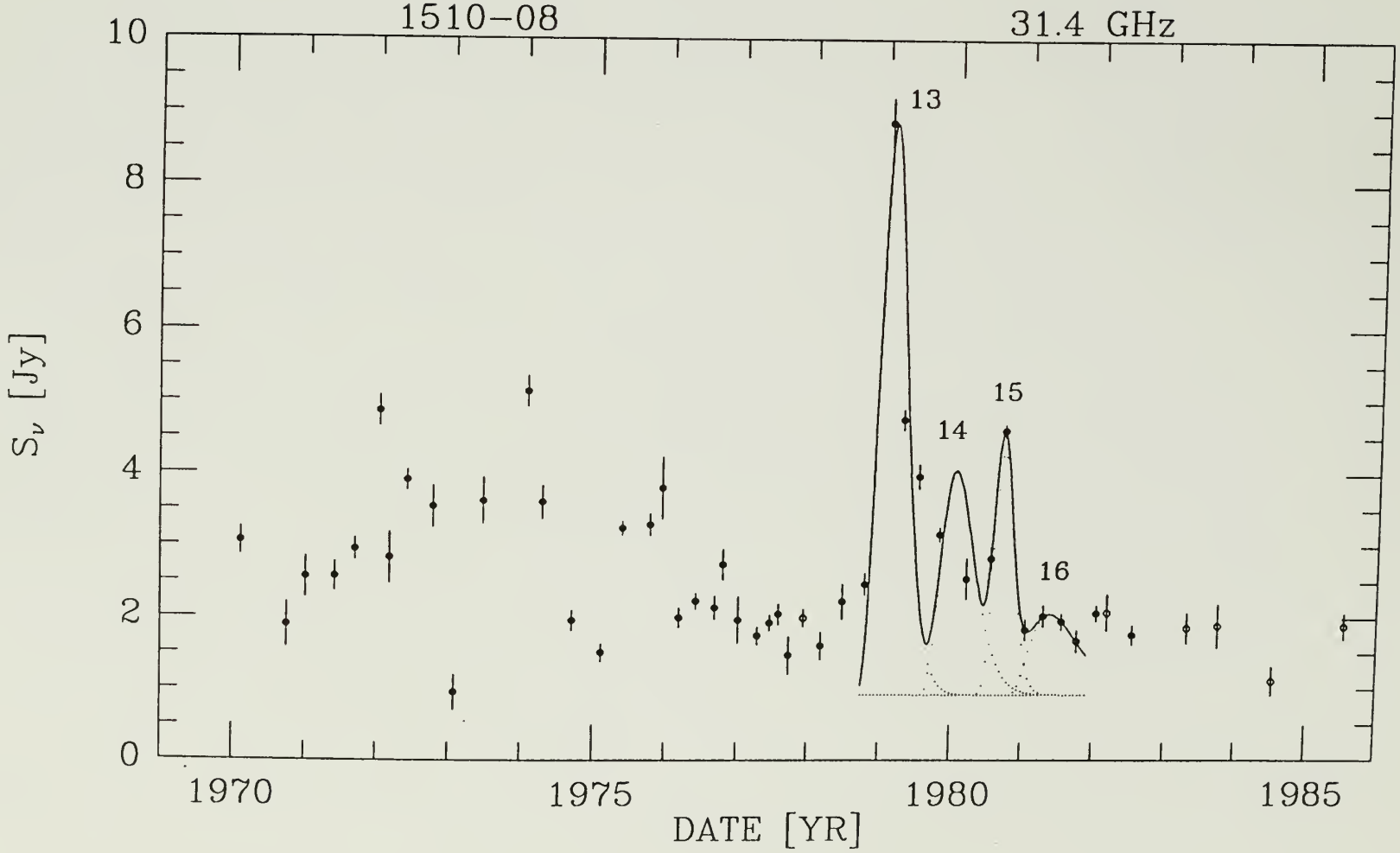
1510−08
31.4 GHz
13
14
15
16
10
8
6
4
2
0
S_ν [Jy]
1970
1975
1980
1985
DATE [YR]

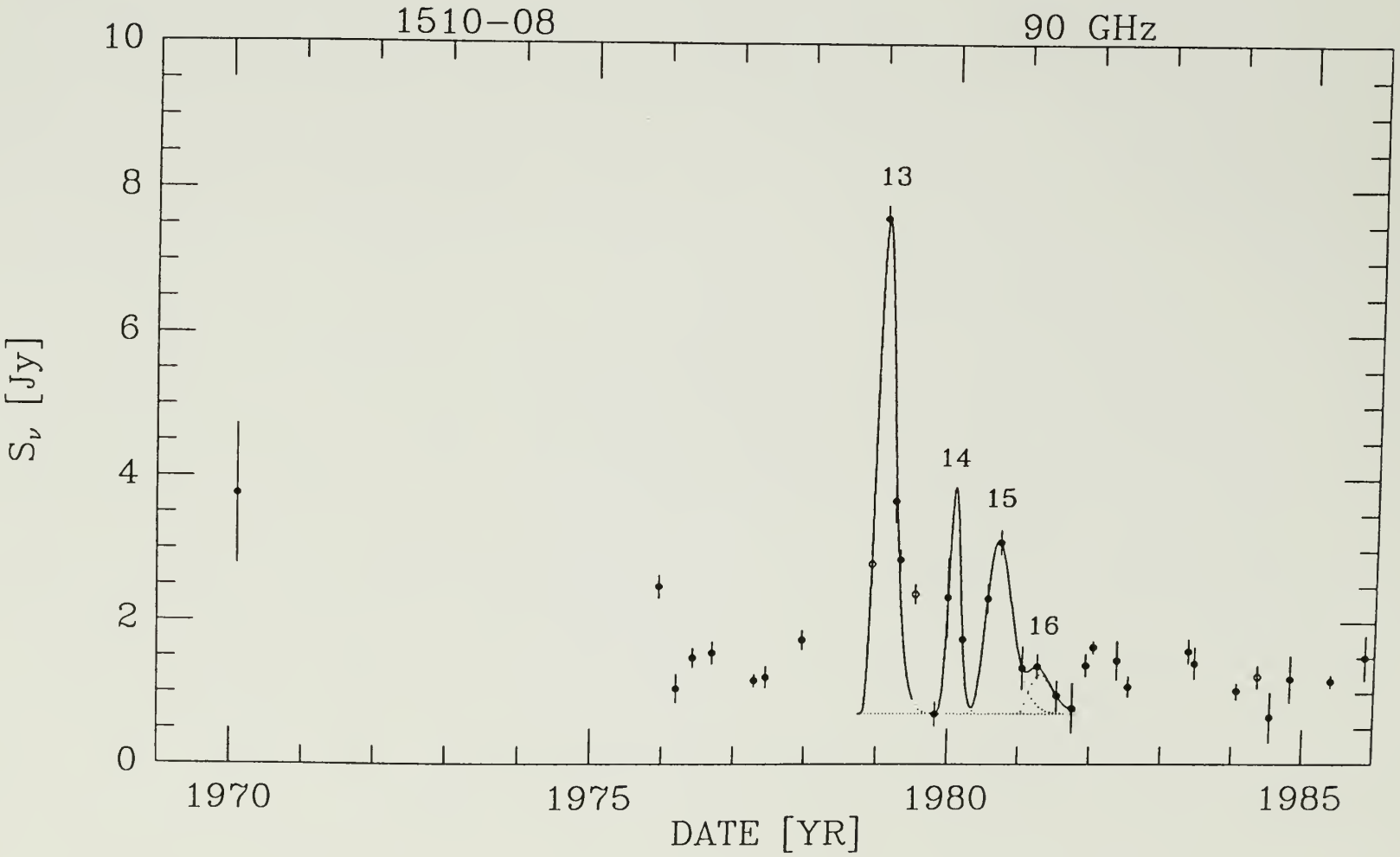
1510−08
90 GHz
13
14
15
16
10
8
6
4
2
0
S_ν [Jy]
1970
1975
1980
1985
DATE [YR]

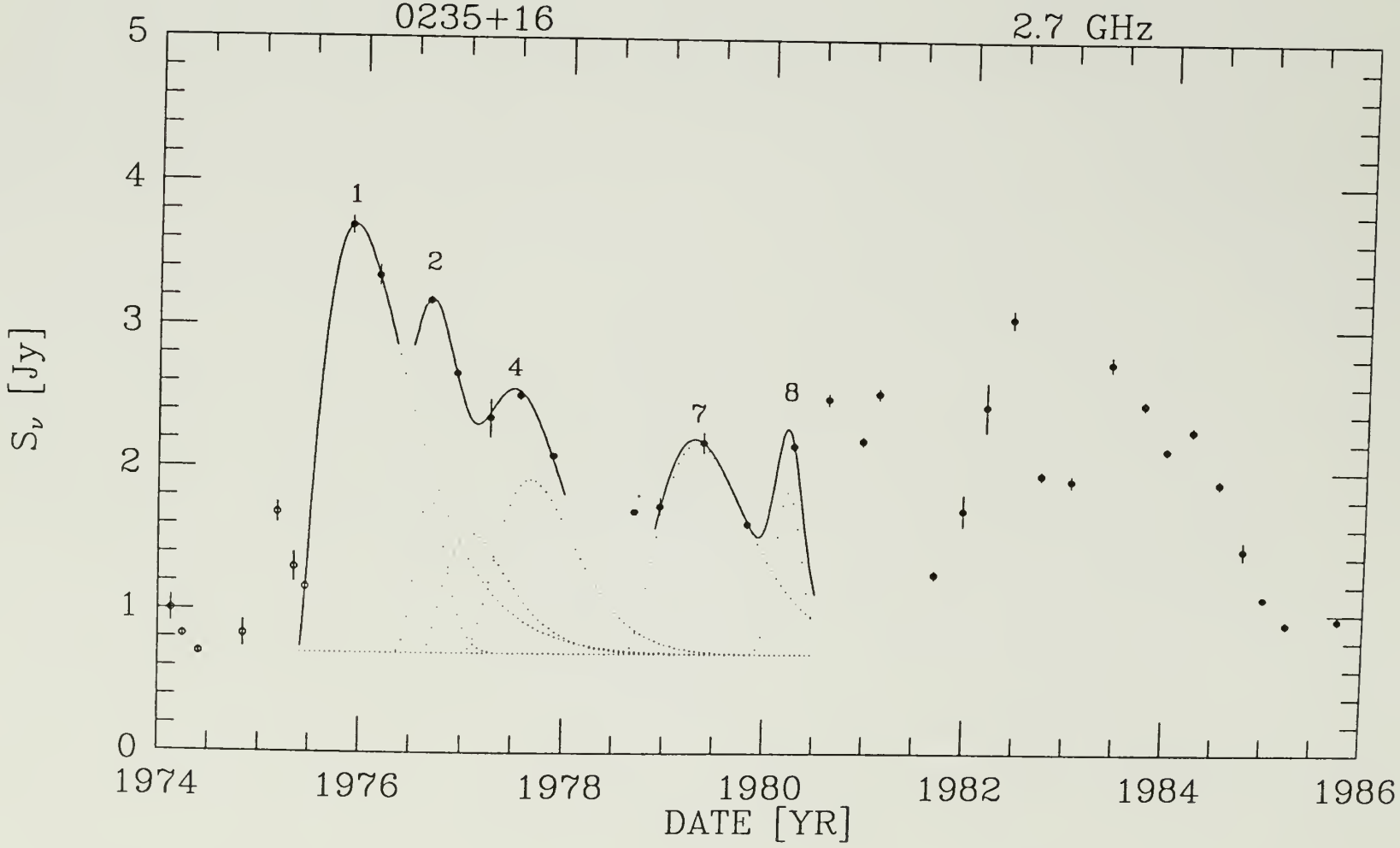
0235+16
2.7 GHz
S_ν [Jy]
DATE [YR]
0
1
2
3
4
5
1974
1976
1978
1980
1982
1984
1986
1
2
4
7
8

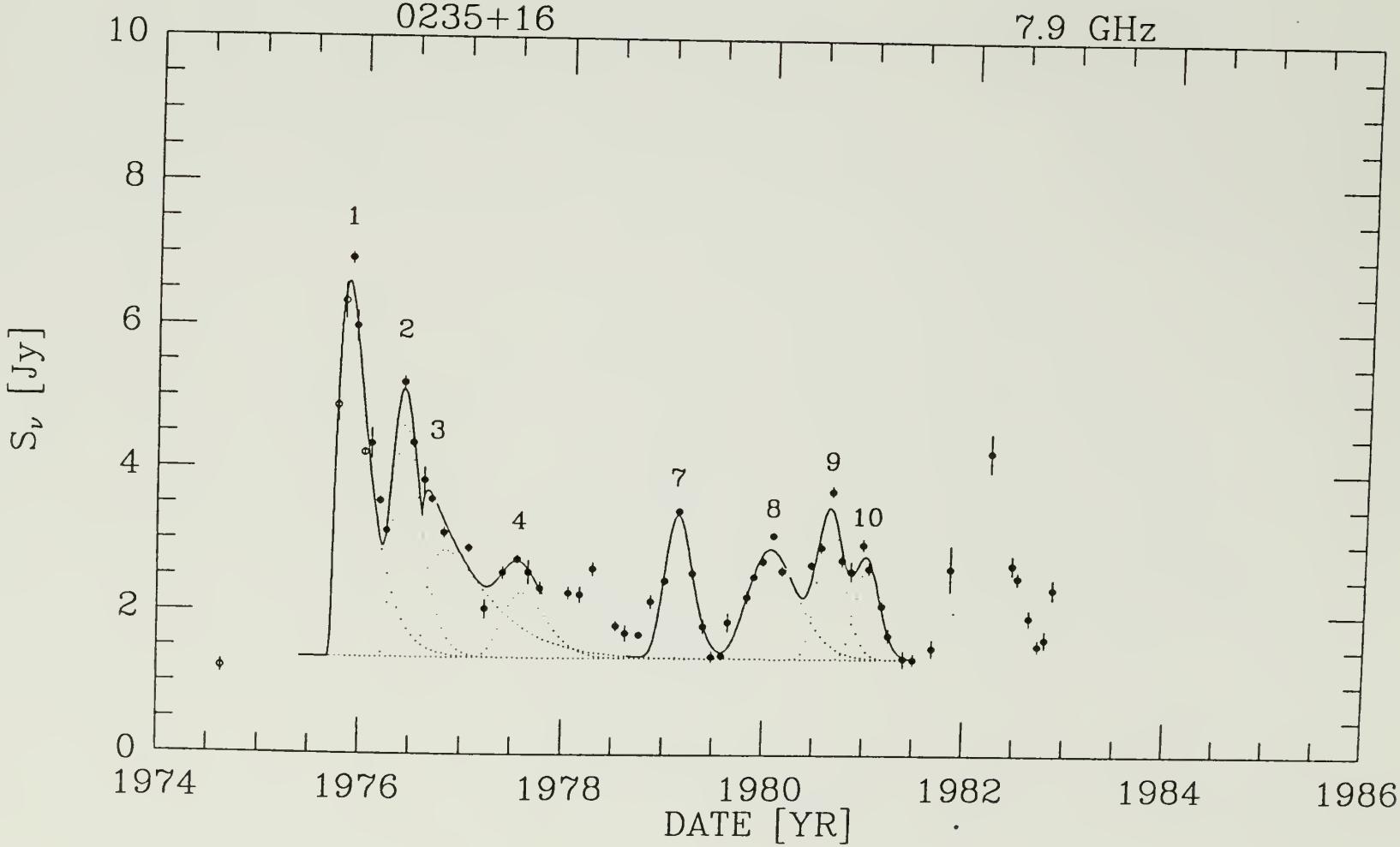
0235+16
7.9 GHz
S_ν [Jy]
DATE [YR]
0
2
4
6
8
10
1974
1976
1978
1980
1982
1984
1986
1
2
3
4
7
8
9
10

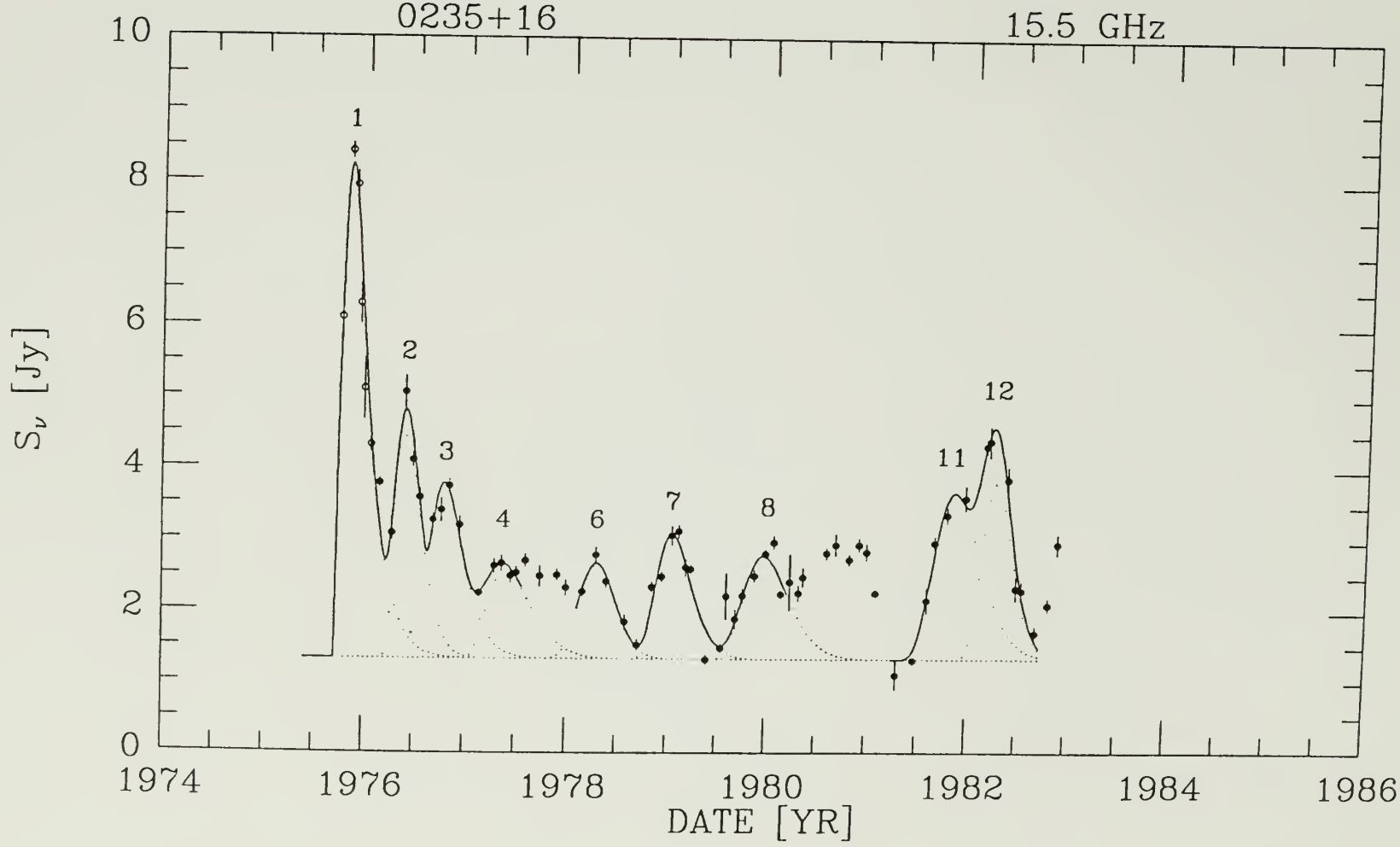
0235+16
15.5 GHz
S_ν [Jy]
DATE [YR]
0
2
4
6
8
10
1974
1976
1978
1980
1982
1984
1986
1
2
3
4
6
7
8
11
12

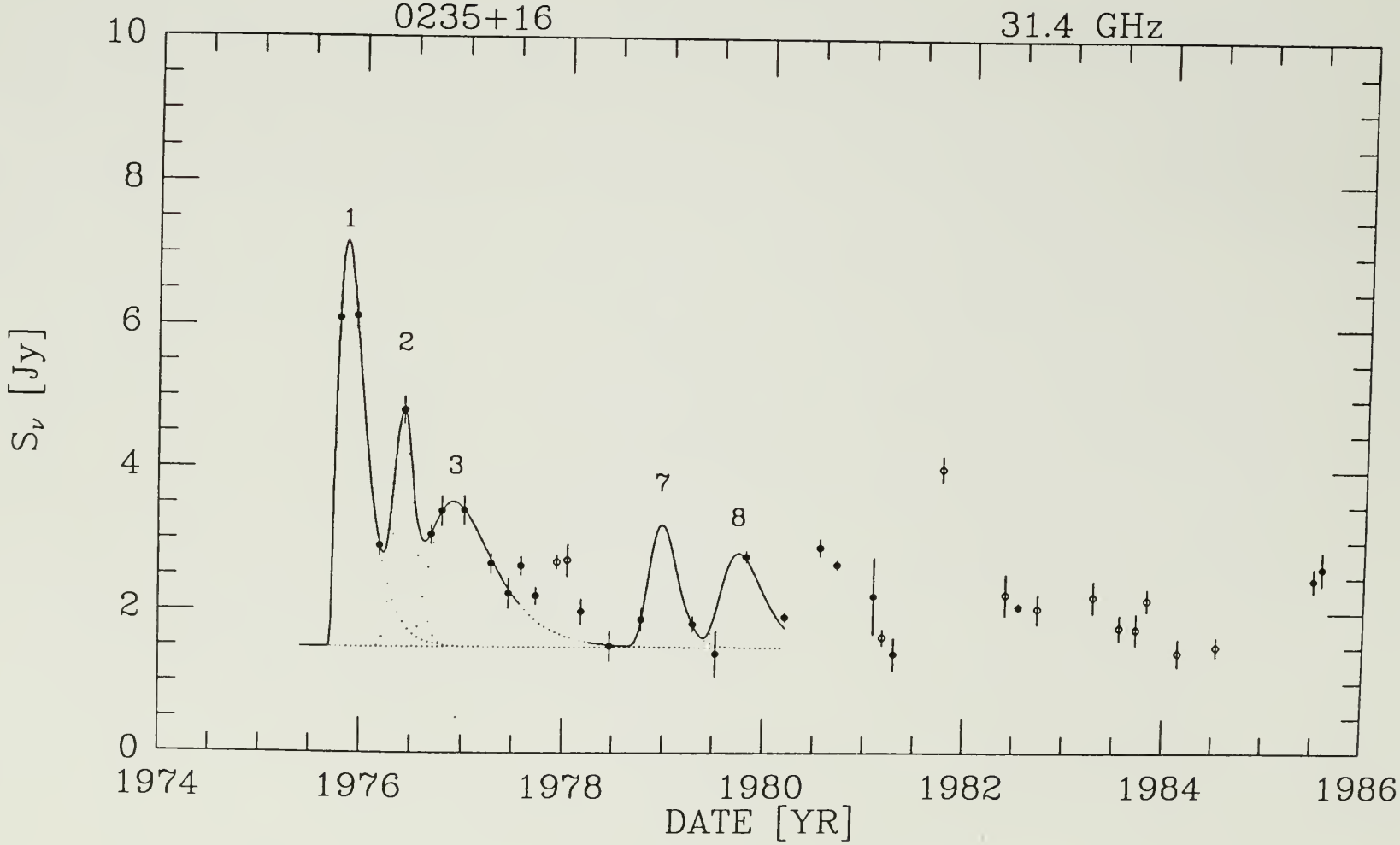
0235+16
31.4 GHz
10
8
6
4
2
0
S_ν [Jy]
1
2
3
7
8
1974
1976
1978
1980
1982
1984
1986
DATE [YR]

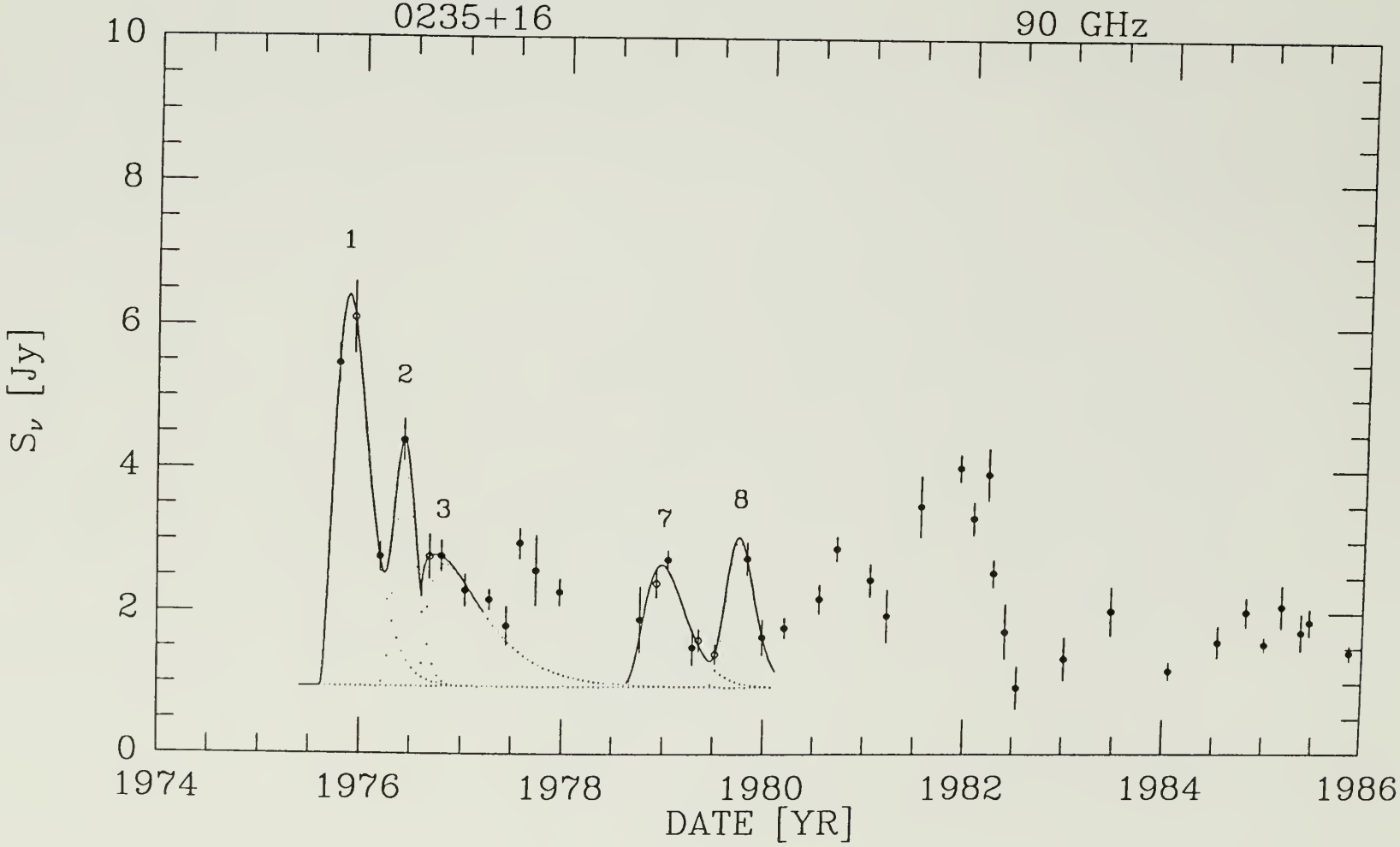
0235+16
90 GHz
10
8
6
4
2
0
S_ν [Jy]
1
2
3
7
8
1974
1976
1978
1980
1982
1984
1986
DATE [YR]

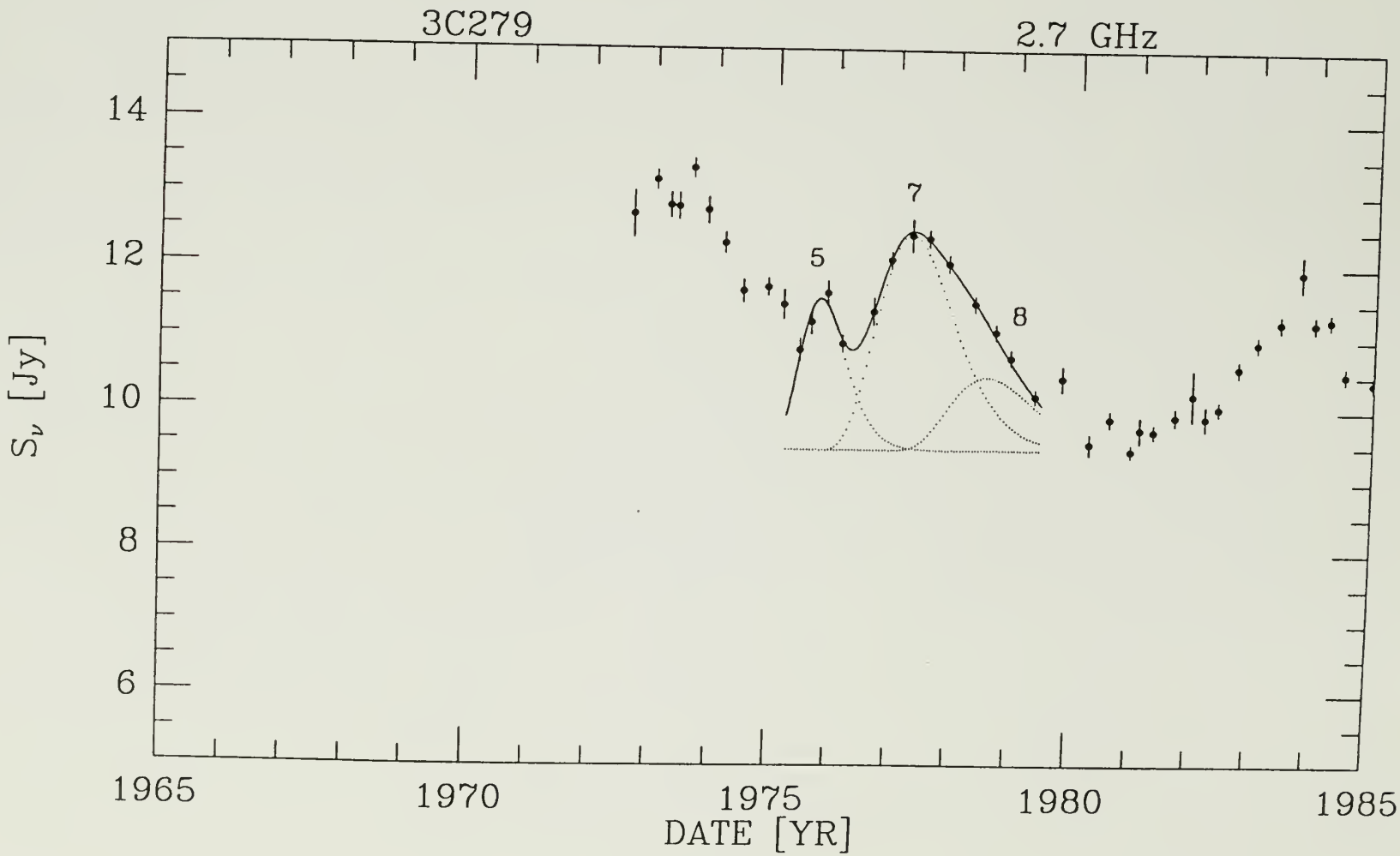
3C279
2.7 GHz
14
12
10
8
6
S_ν [Jy]
5
7
8
1965
1970
1975
1980
1985
DATE [YR]

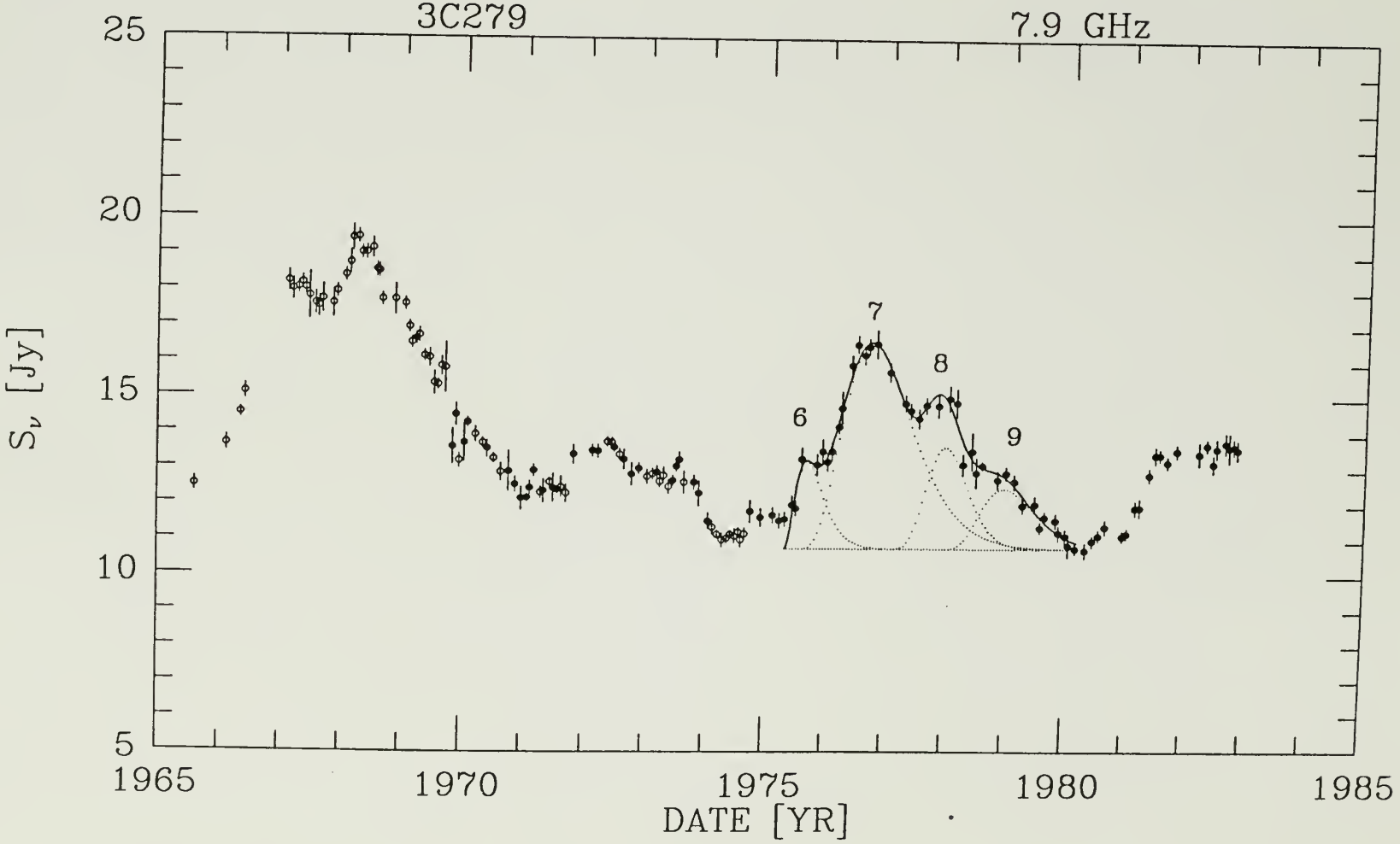
3C279
7.9 GHz
25
20
15
10
5
S_ν [Jy]
1965
1970
1975
1980
1985
DATE [YR]
6
7
8
9

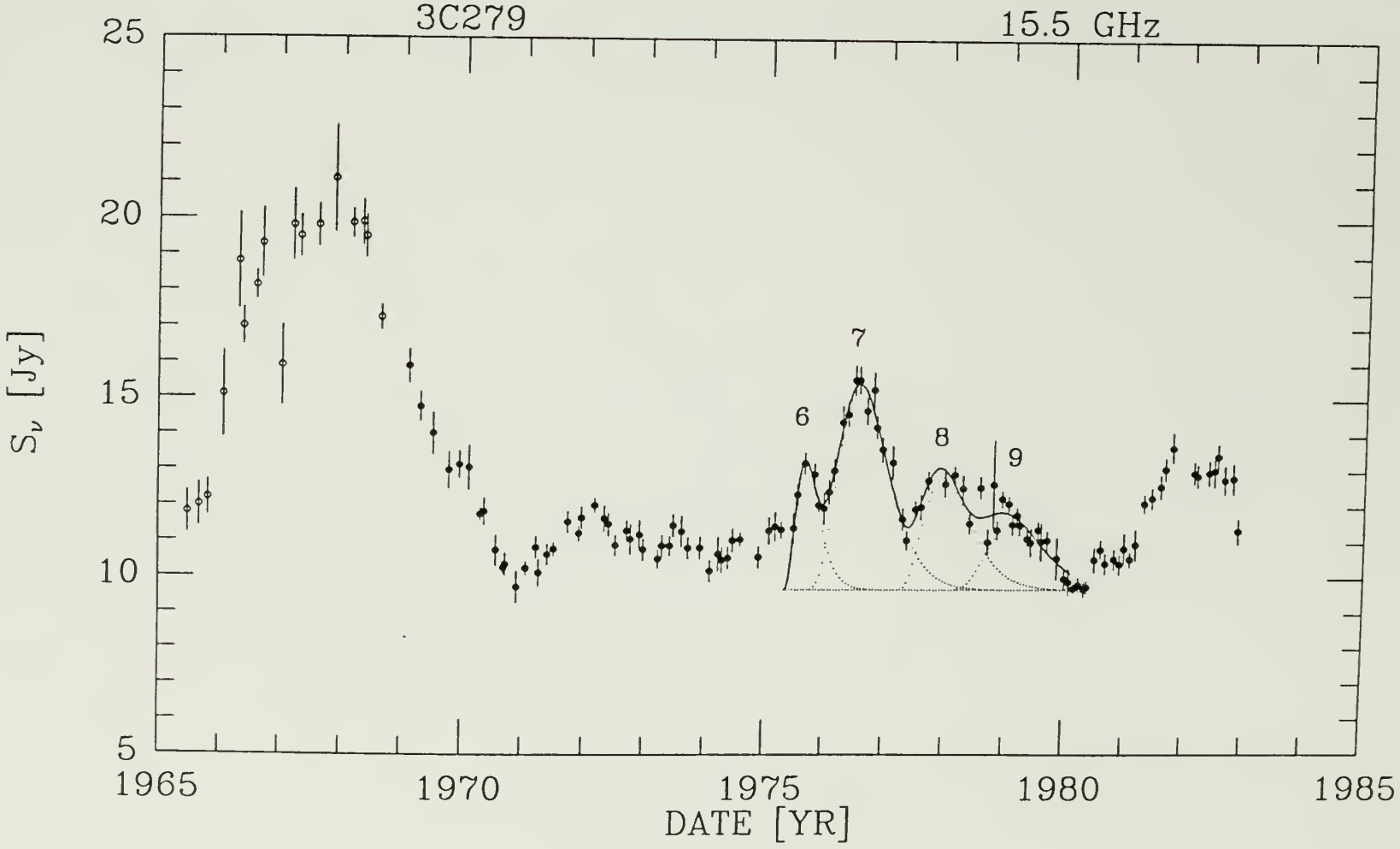
3C279
15.5 GHz
25
20
15
10
5
S_ν [Jy]
1965
1970
1975
1980
1985
DATE [YR]
6
7
8
9

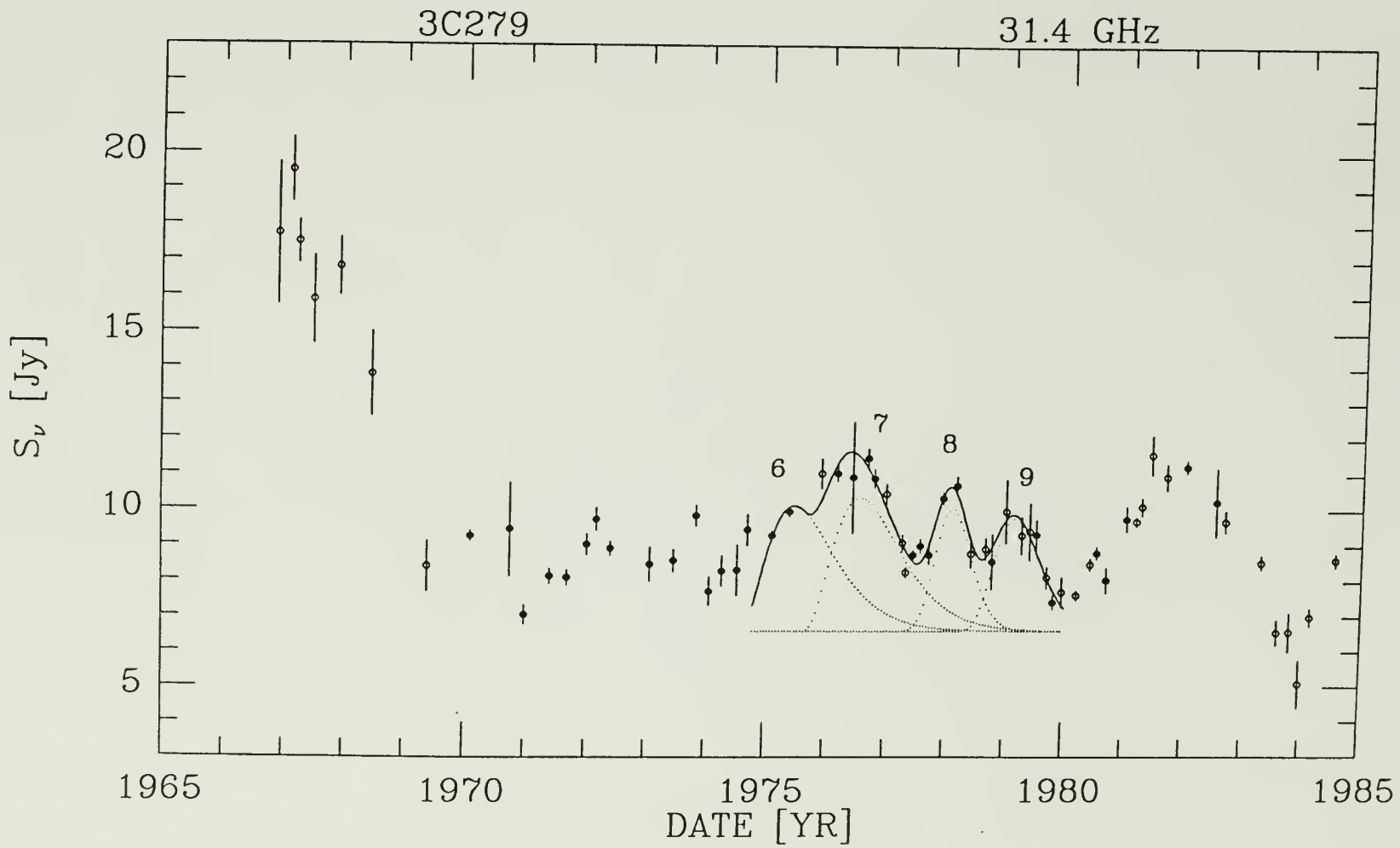
3C279
31.4 GHz
20
15
10
5
S_ν [Jy]
6
7
8
9
1965
1970
1975
1980
1985
DATE [YR]

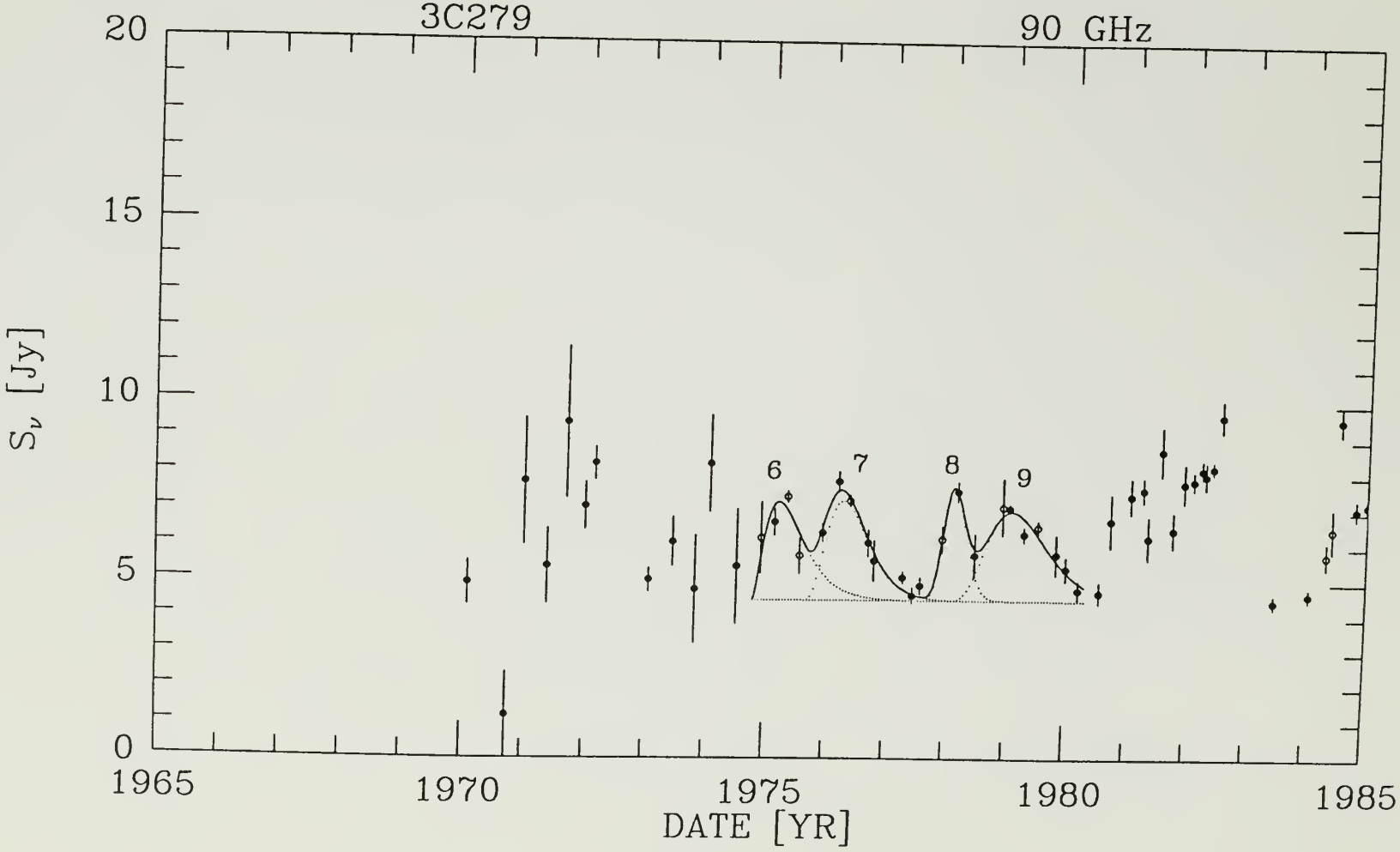
3C279
90 GHz
20
15
10
5
0
S_ν [Jy]
1965
1970
1975
1980
1985
DATE [YR]
6
7
8
9

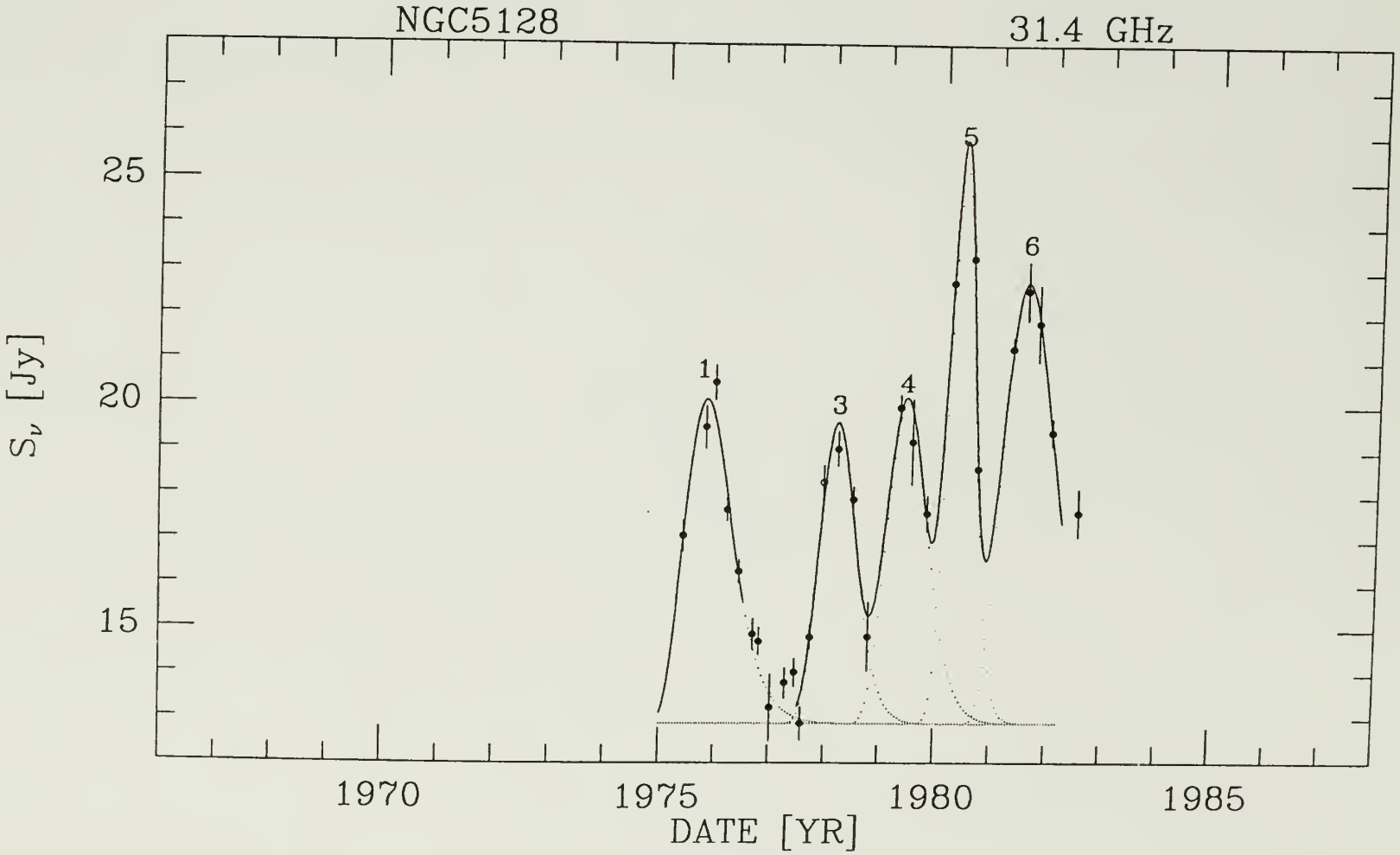
NGC5128
31.4 GHz
25
20
15
S_ν [Jy]
1
3
4
5
6
1970
1975
1980
1985
DATE [YR]

APPENDIX D

OUTBURST SPECTRA COEFFICIENTS

Tables of coefficients obtained from fitting the outburst spectra with equation 3.2. q was fixed at 2.5 for all the fits. Only bursts 5 and 6 in 3C454.3 had 2.7 GHz values available for the spectral fits.

* The epoch of the burst peak at 15 GHz.

† This epoch not used in the outburst analysis because of large errors in the fit.

3C454.3

#	Date	ν_1 [GHz]	A[Jy]	q	p	χ^2_ν
	5 1971.91	4.23± 0.69	3.83±0.74	2.50±0.00	-2.48±0.13	0.77
*	5 1972.31	4.88 0.47	6.87 0.73	2.50 0.00	-2.65 0.09	1.83
	5 1972.71	4.51 0.39	6.62 0.78	2.50 0.00	-2.80 0.11	1.48
	5 1973.11	4.10 0.42	5.53 0.94	2.50 0.00	-3.04 0.19	0.68
	5 1973.51	3.80 0.60	4.48 1.27	2.50 0.00	-3.36 0.40	0.21
†	6 1973.54	32.72±33.69	1.68±1.90	2.50±0.00	-2.96±1.61	0.00
	6 1973.84	20.44 4.33	4.54 1.14	2.50 0.00	-2.64 0.23	0.86
	6 1974.14	15.80 1.97	7.78 0.97	2.50 0.00	-2.79 0.13	2.01
*	6 1974.44	12.13 0.89	9.09 0.74	2.50 0.00	-2.98 0.10	0.47
	6 1974.74	9.38 0.89	8.47 0.82	2.50 0.00	-3.16 0.15	0.31
	6 1975.04	7.06 1.17	7.07 0.66	2.50 0.00	-3.32 0.20	0.43
	6 1975.34	5.54 0.57	6.32 0.86	2.50 0.00	-3.63 0.28	0.48
	6 1975.64	4.76 0.54	5.87 1.52	2.50 0.00	-4.09 0.64	0.28
	12 1981.25	11.70± 1.69	5.07±0.76	2.50±0.00	-2.74±0.14	0.41
	12 1981.55	11.76 0.66	12.49 0.75	2.50 0.00	-2.86 0.06	0.08
*	12 1981.85	10.53 0.49	15.01 0.76	2.50 0.00	-2.93 0.06	1.41
	12 1982.15	9.42 0.52	14.63 0.82	2.50 0.00	-3.14 0.09	0.01
	12 1982.45	9.34 0.63	14.18 0.99	2.50 0.00	-3.63 0.18	1.24

0420-01

#	Date	ν_1 [GHz]	A[Jy]	q	p	χ^2_ν
	2 1978.15	17.80± 4.47	3.94±1.08	2.50±0.00	-2.80±0.30	2.00
	2 1978.45	10.95 1.49	5.23 0.77	2.50 0.00	-2.84 0.16	3.07
*	2 1978.75	11.27 1.18	6.28 0.77	2.50 0.00	-3.04 0.17	2.26
	2 1979.05	11.10 1.25	5.69 0.78	2.50 0.00	-3.13 0.22	1.71
	2 1979.35	10.39 1.66	4.29 0.81	2.50 0.00	-3.14 0.30	1.32

3C279

#	Date	ν_1[GHz]	A[Jy]	q	p	χ^2_ν
7	1976.27	7.37± 1.51	5.19±0.74	2.50±0.00	-2.78±0.13	0.58
* 7	1976.57	5.98 0.64	8.12 0.62	2.50 0.00	-2.94 0.09	3.43
7	1976.87	4.52 0.27	8.66 0.76	2.50 0.00	-3.05 0.09	2.17
7	1977.17	3.95 0.28	7.97 1.00	2.50 0.00	-3.22 0.15	3.09

CTA26

#	Date	ν_1[GHz]	A[Jy]	q	p	χ^2_ν
9	1978.15	10.70± 3.41	2.34±0.76	2.50±0.00	-2.71±0.28	0.02
* 9	1978.45	11.67 2.52	3.31 0.75	2.50 0.00	-2.80 0.23	0.37
9	1978.75	10.90 2.81	2.73 0.75	2.50 0.00	-2.84 0.29	0.31
9	1979.05	8.85 5.06	1.59 0.79	2.50 0.00	-2.83 0.50	0.08

1510-08

#	Date	ν_1[GHz]	A[Jy]	q	p	χ^2_ν
13	1978.95	16.82± 2.23	7.43±1.02	2.50±0.00	-2.85±0.15	2.52
*13	1979.05	16.38 1.84	8.99 1.04	2.50 0.00	-2.65 0.10	0.31
13	1979.15	13.73 1.44	8.14 0.85	2.50 0.00	-2.68 0.09	9.87
13	1979.25	10.51 1.17	6.57 0.76	2.50 0.00	-2.79 0.11	13.43
15	1980.69	13.60± 3.15	3.65±0.84	2.50±0.00	-2.68±0.20	0.99
*15	1980.79	10.00 1.86	4.11 0.76	2.50 0.00	-2.79 0.18	0.06
15	1980.89	7.17 3.23	3.30 0.81	2.50 0.00	-2.85 0.26	0.26

APPENDIX E

OUTBURST SIMULATIONS AND PERIODOGRAM TESTS

This series of plots demonstrates how blending of outbursts and burst amplitude variability affects the periodogram. Ten cases are presented. Test 0 had the amplitudes of all the bursts identical. Tests 1 through 9 had the amplitudes of the bursts distributed as an exponential probability distribution. All the bursts in a particular test had identical decay constants. The plots are in pairs. The first plot presents the 100th simulated time series in the test (except for Test 0, only one simulation was made). The top panel in the second plot presents the Scargle periodogram of the displayed time series. The bottom panel presents a scatter diagram of the amplitude versus the frequency of the largest peak in each periodogram for the test.

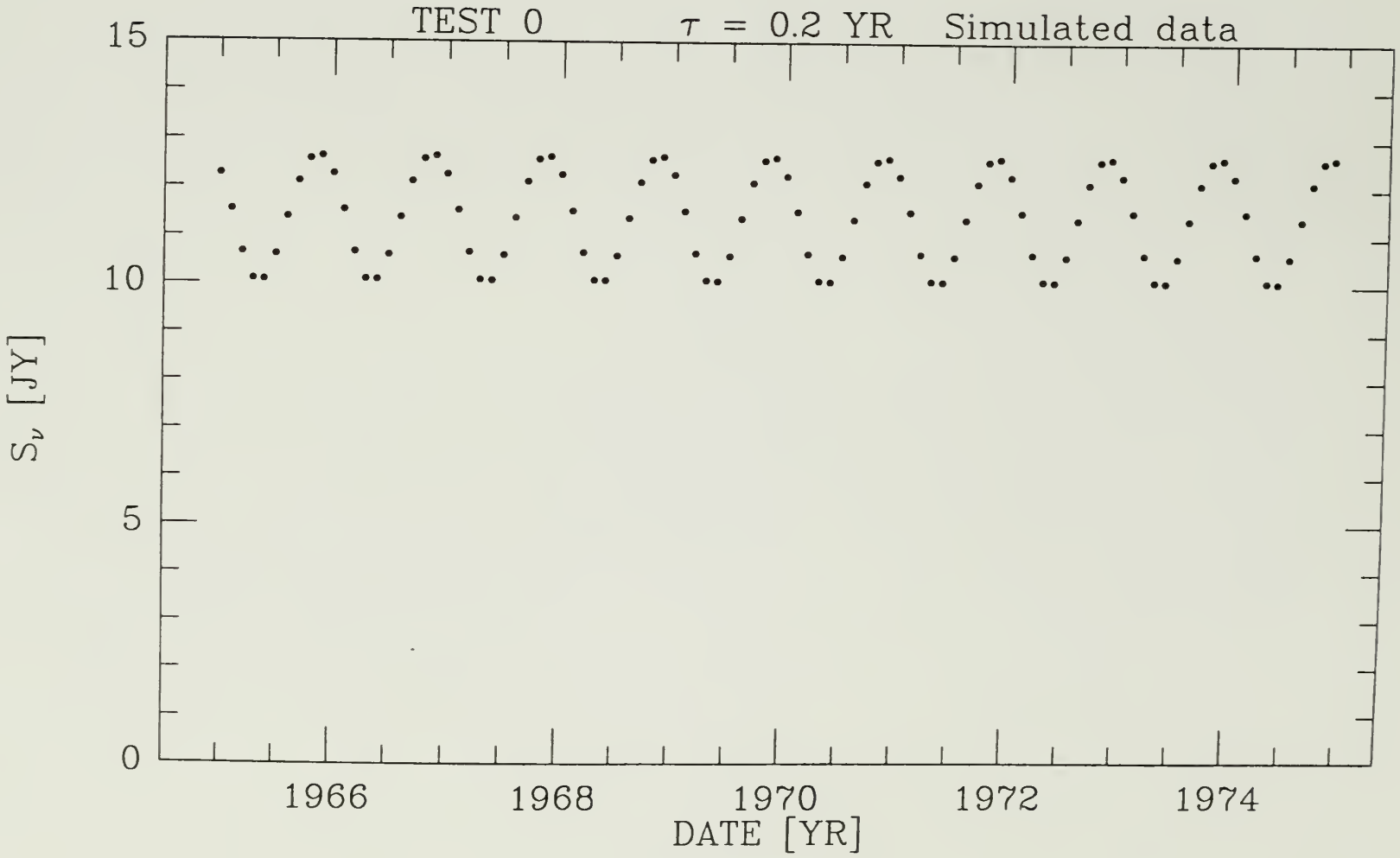
TEST 0
τ = 0.2 YR
Simulated data
15
10
5
0
S_ν [JY]
1966
1968
1970
1972
1974
DATE [YR]

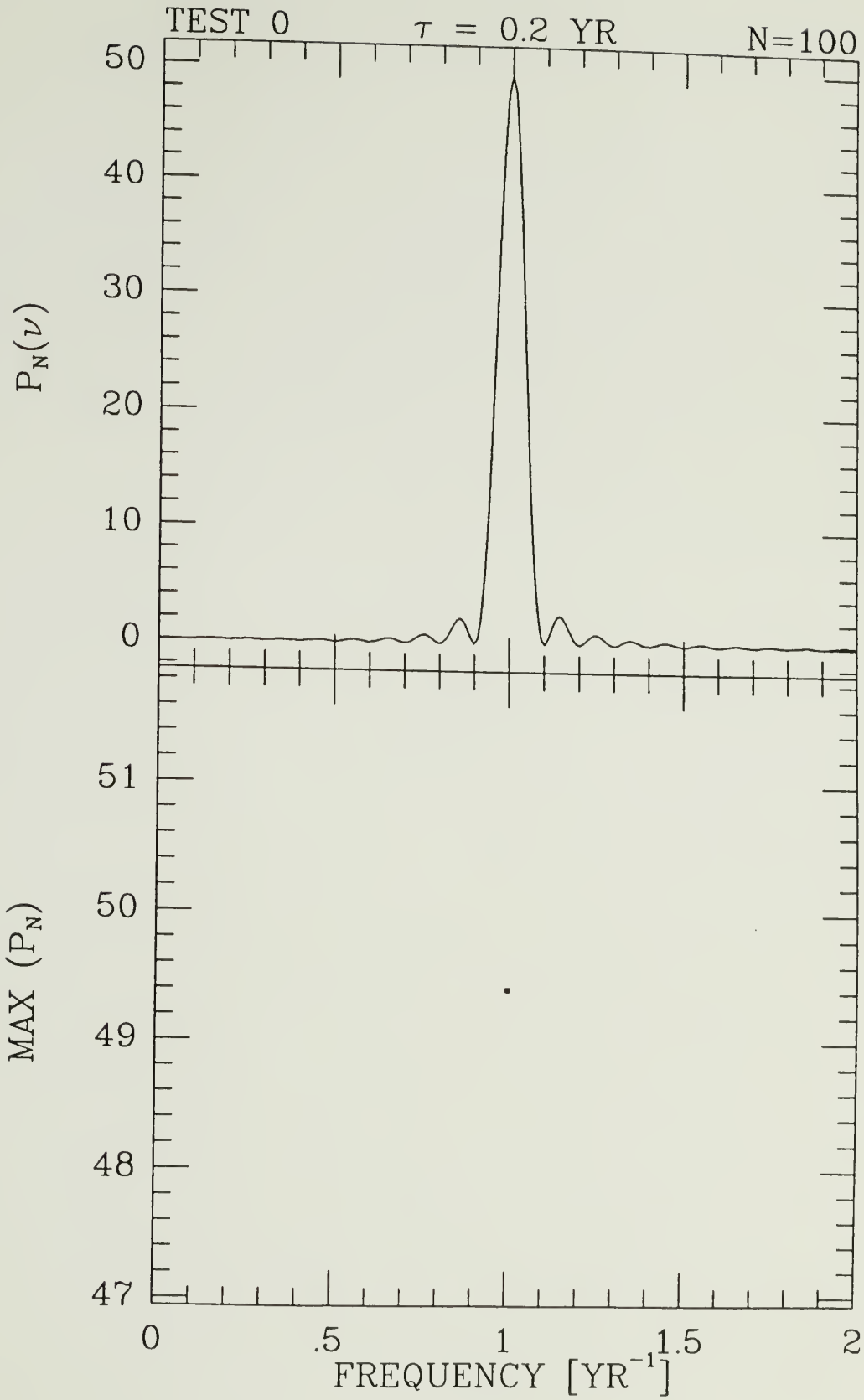
TEST 0
τ = 0.2 YR
N=100
50
40
30
20
10
0
$P_N(\nu)$
51
50
49
48
47
MAX (P_N)
0
.5
1
1.5
2
FREQUENCY [YR^{-1}]

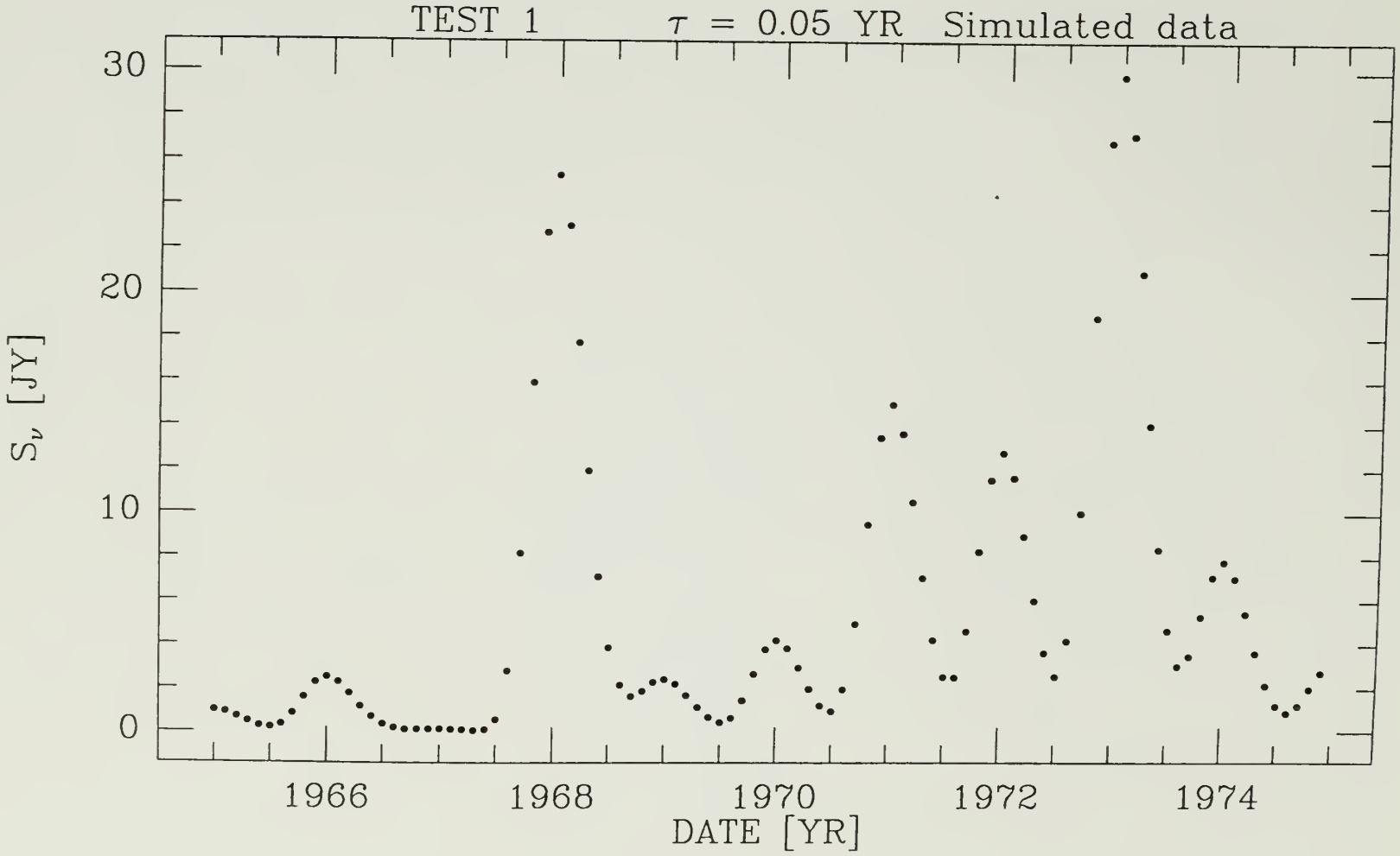
TEST 1
τ = 0.05 YR Simulated data
30
20
10
0
S_ν [JY]
1966
1968
1970
1972
1974
DATE [YR]

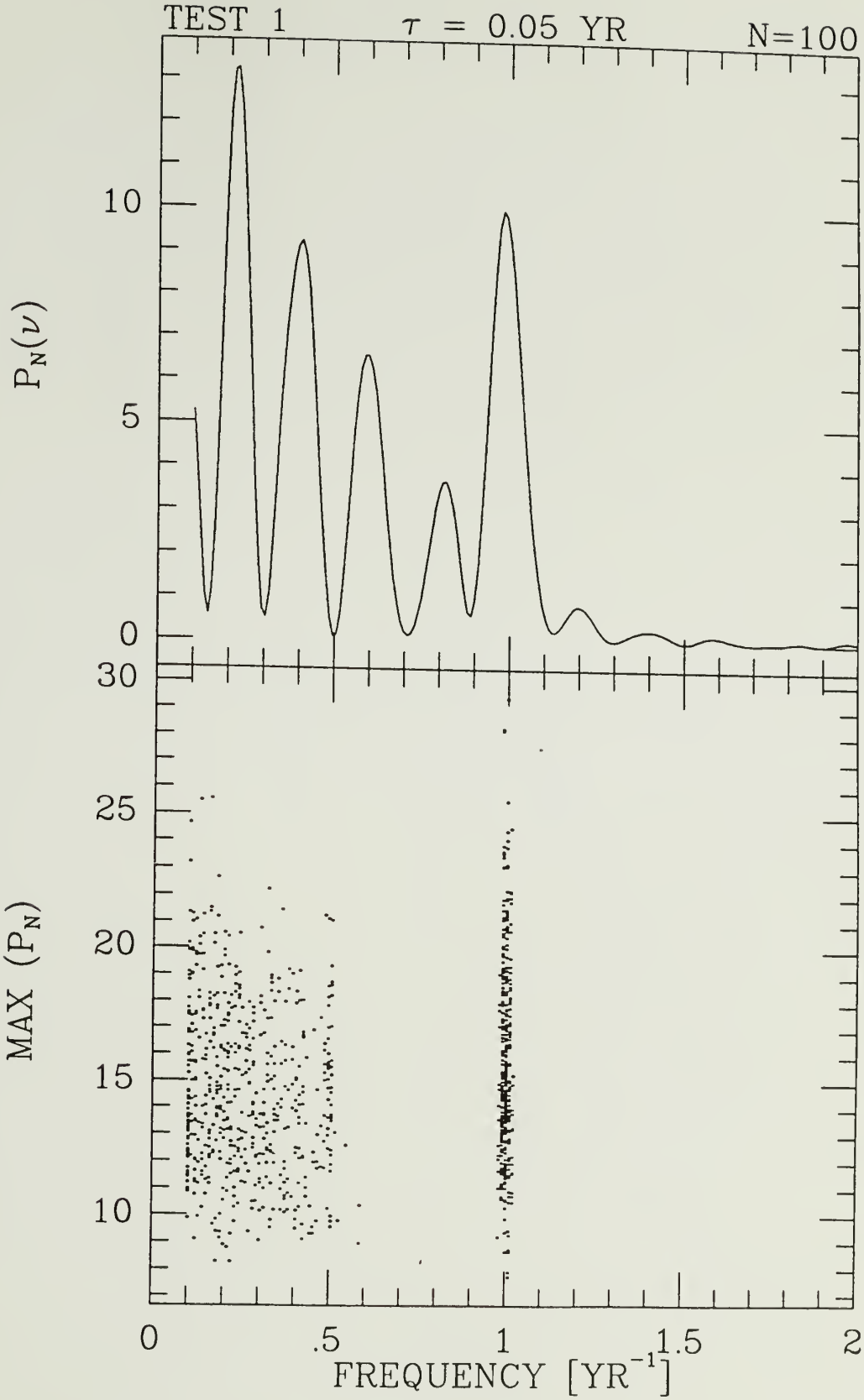
TEST 1
τ = 0.05 YR
N=100
P_N(ν)
10
5
0
30
25
20
15
10
MAX (P_N)
0
.5
1
1.5
2
FREQUENCY [YR^-1]

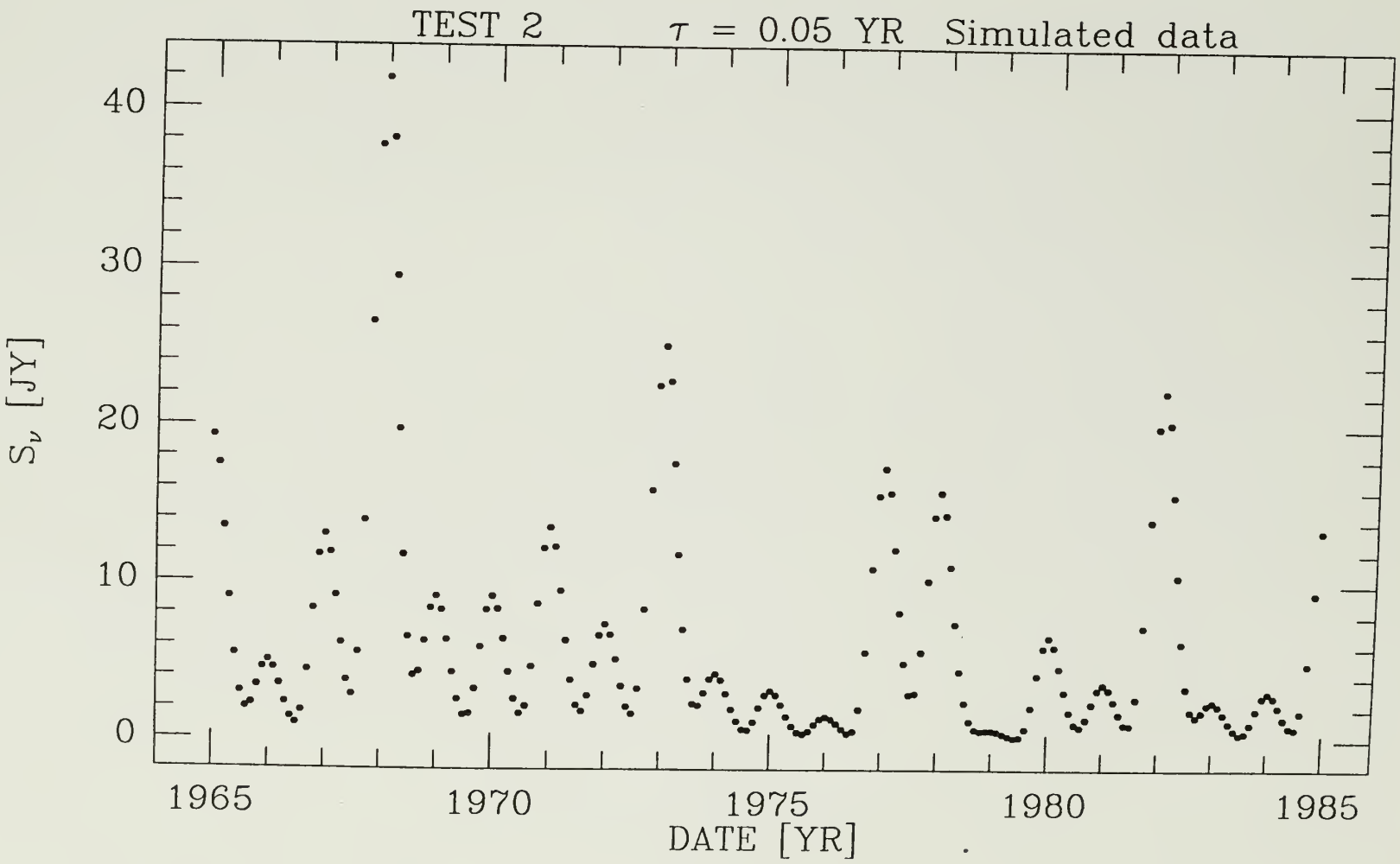
TEST 2
τ = 0.05 YR Simulated data
40
30
20
10
0
S_ν [JY]
1965
1970
1975
1980
1985
DATE [YR]

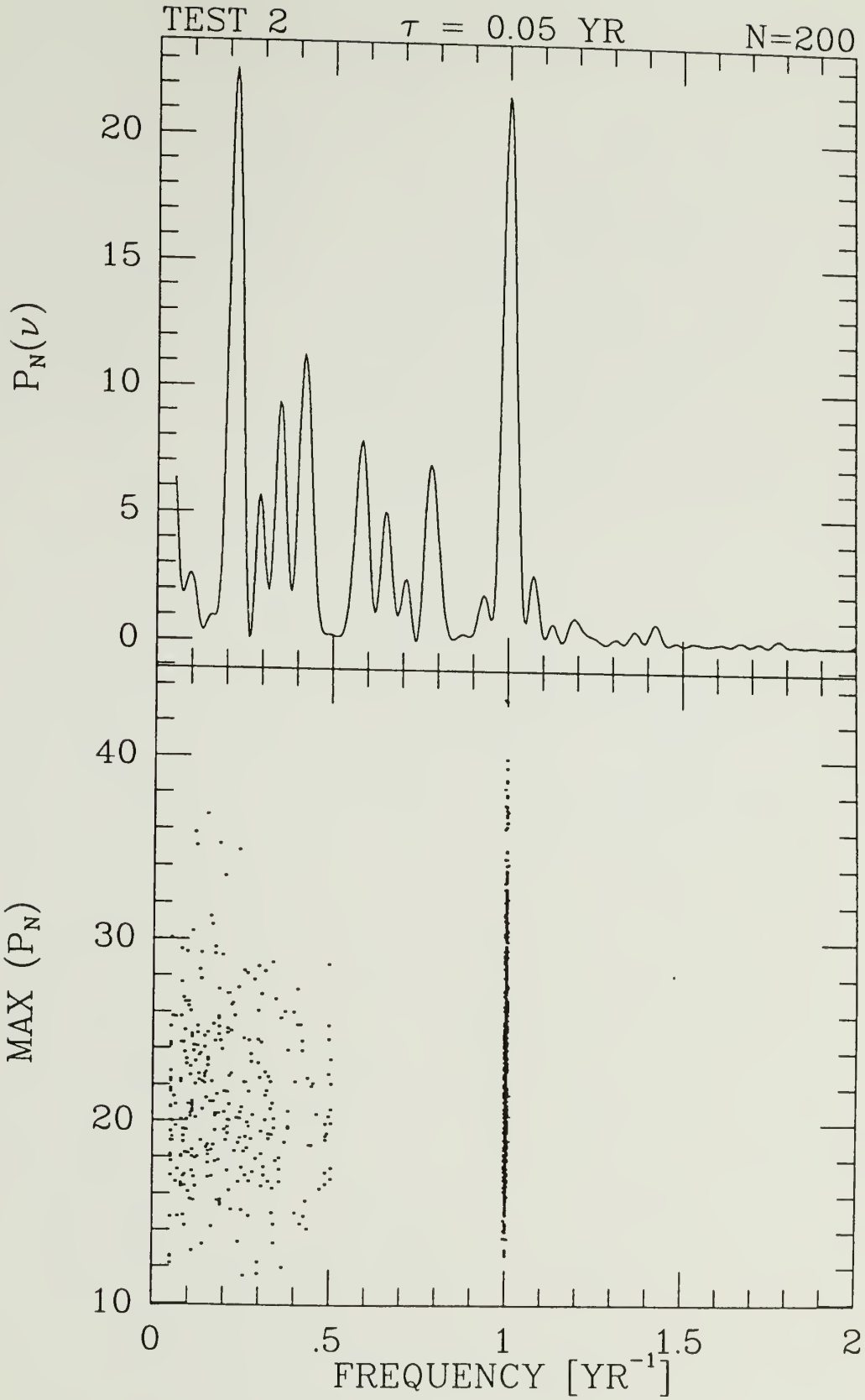
TEST 2
τ = 0.05 YR
N=200
$P_N(\nu)$
20
15
10
5
0
MAX (P_N)
40
30
20
10
0
.5
1
1.5
2
FREQUENCY [YR^{-1}]

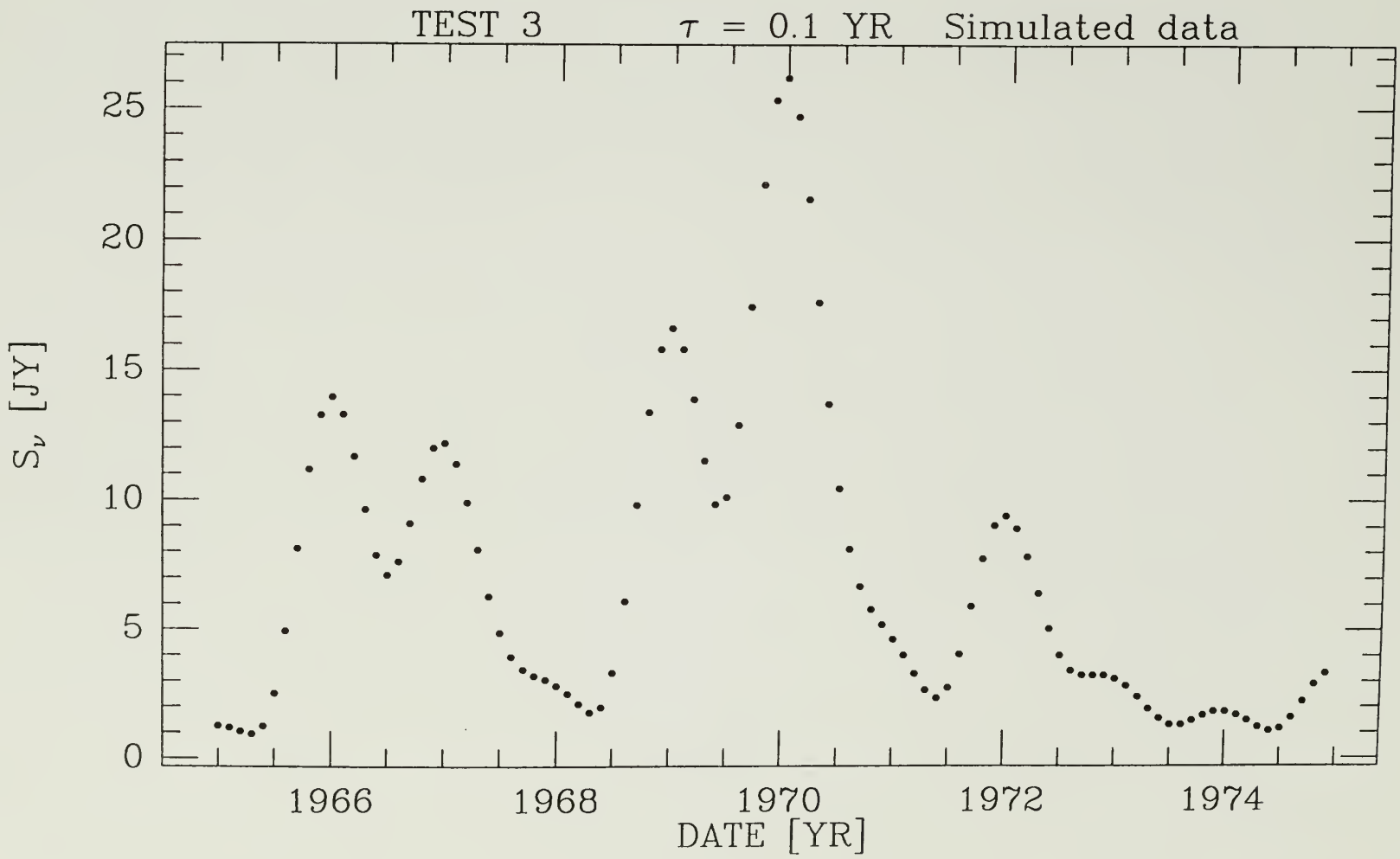
TEST 3
τ = 0.1 YR Simulated data
25
20
15
10
5
0
S_ν [JY]
1966
1968
1970
1972
1974
DATE [YR]

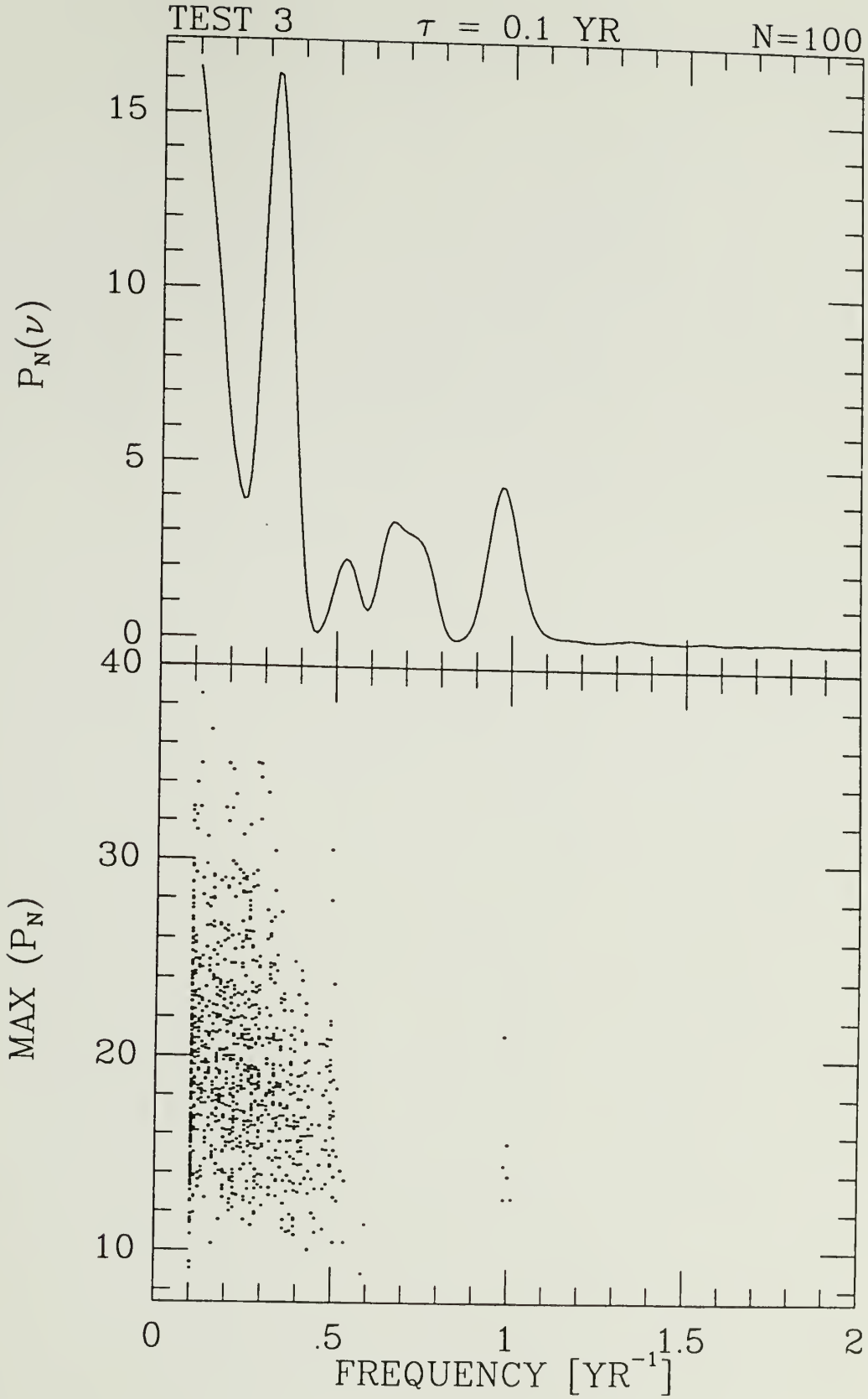
TEST 3
τ = 0.1 YR
N=100
15
10
5
0
P_N(ν)
40
30
20
10
MAX (P_N)
0
.5
1
1.5
2
FREQUENCY [YR^-1]

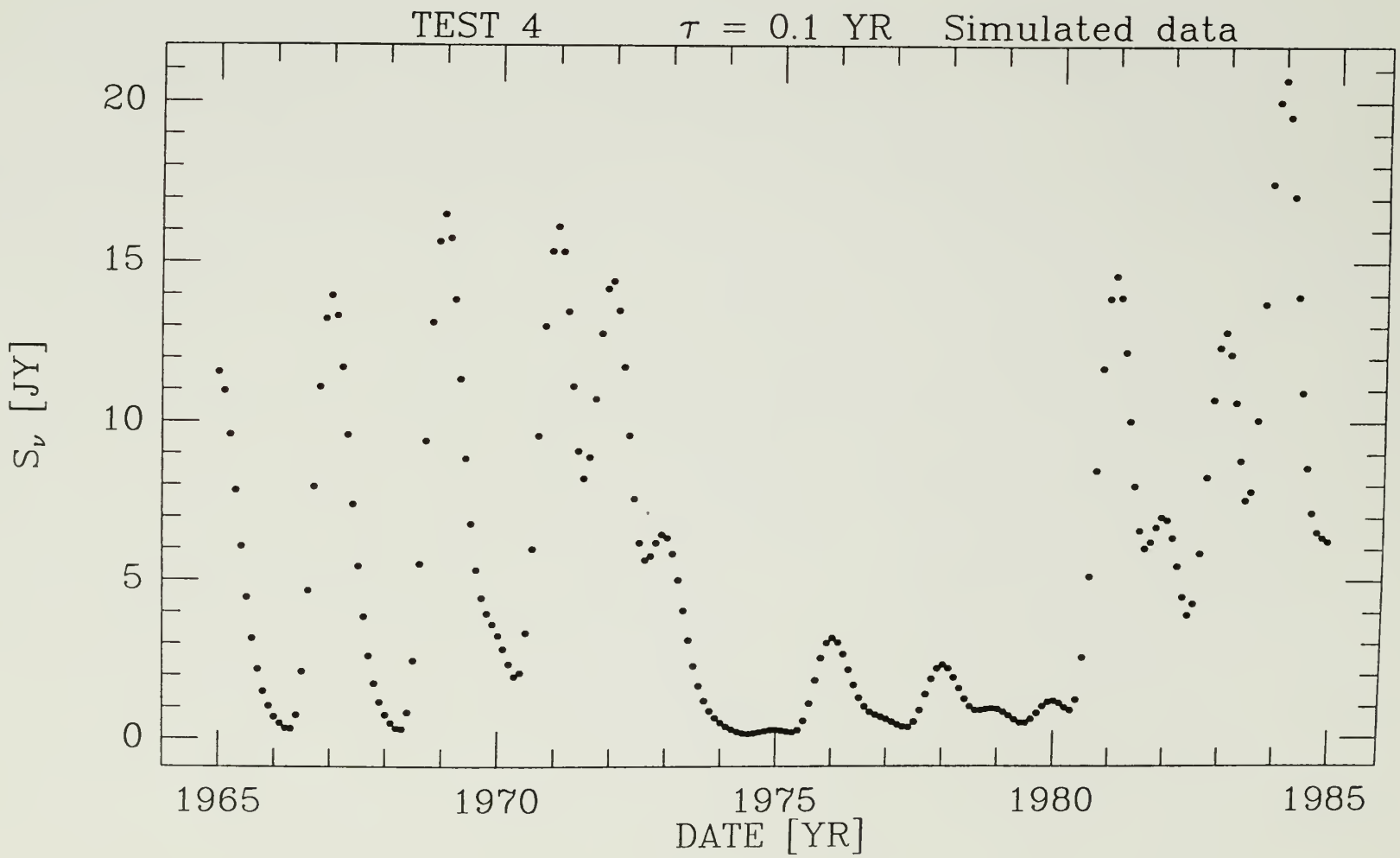
TEST 4
τ = 0.1 YR
Simulated data
20
15
10
5
0
S_ν [JY]
1965
1970
1975
1980
1985
DATE [YR]

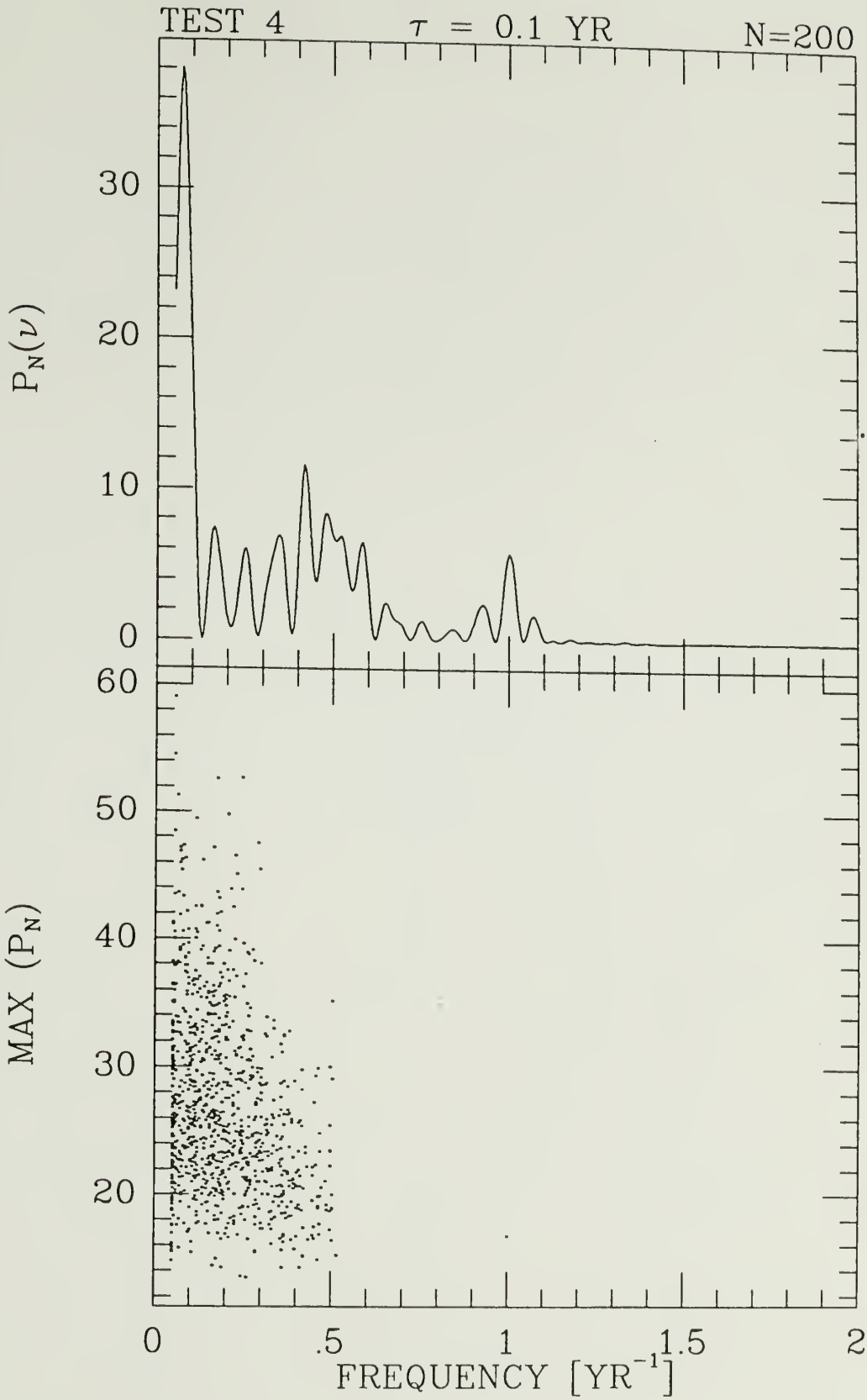
TEST 4
τ = 0.1 YR
N=200
$P_N(\nu)$
30
20
10
0
60
50
40
30
20
MAX (P_N)
0
.5
1
1.5
2
FREQUENCY [YR^{-1}]

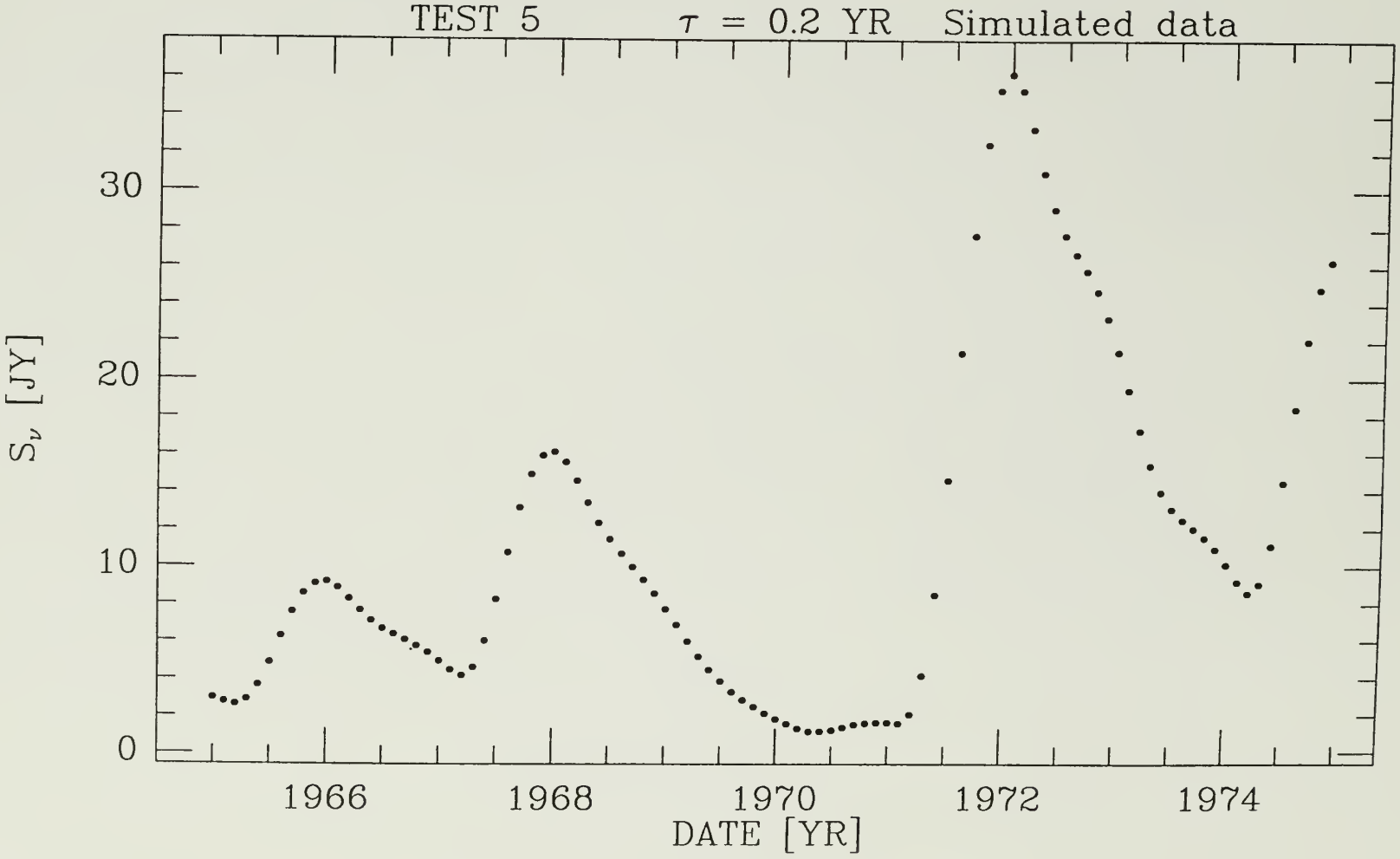
TEST 5
τ = 0.2 YR
Simulated data
30
20
10
0
S_ν [JY]
1966
1968
1970
1972
1974
DATE [YR]

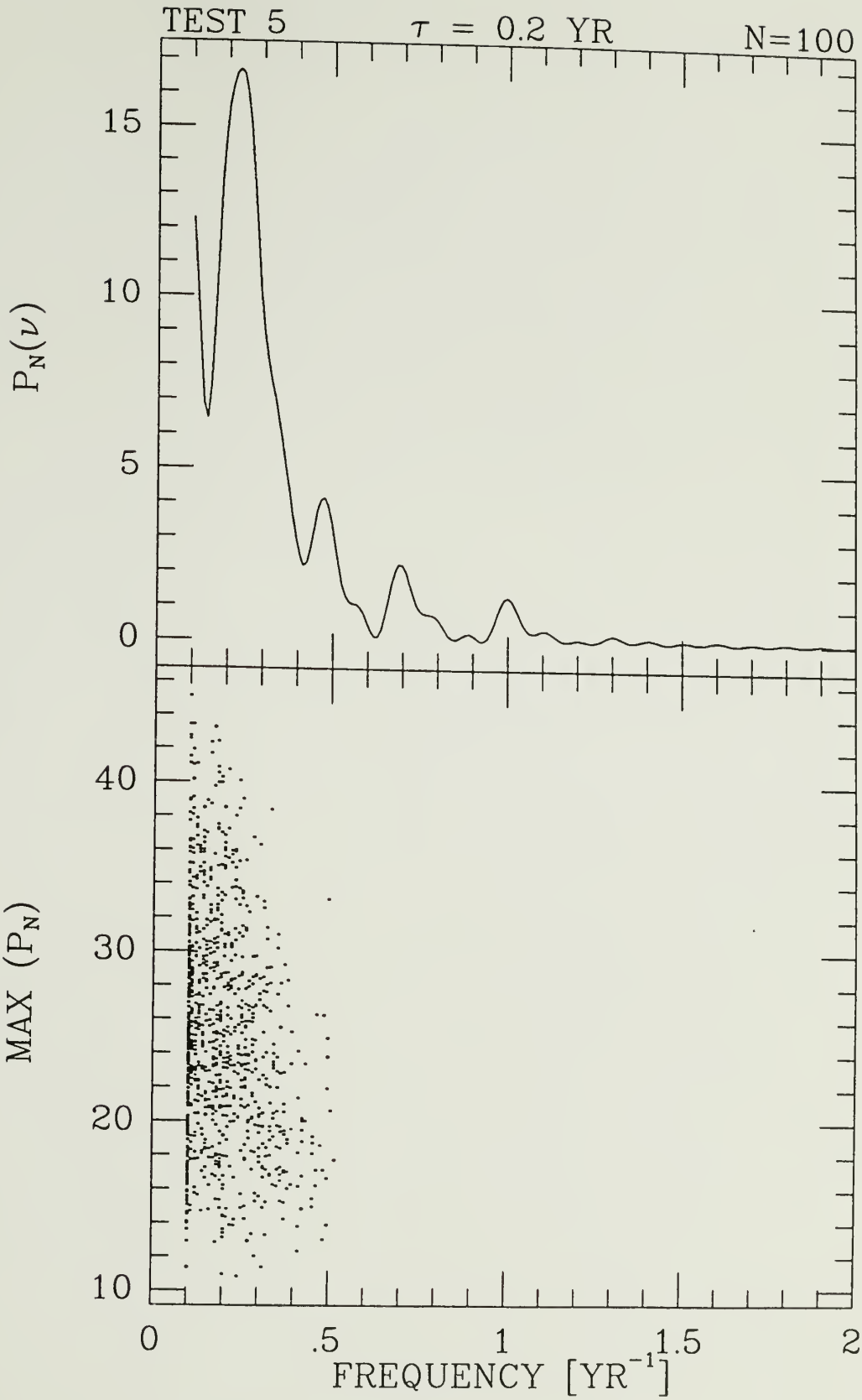
TEST 5
τ = 0.2 YR
N=100
15
10
5
0
P_N(ν)
40
30
20
10
MAX (P_N)
0
.5
1
1.5
2
FREQUENCY [YR^-1]

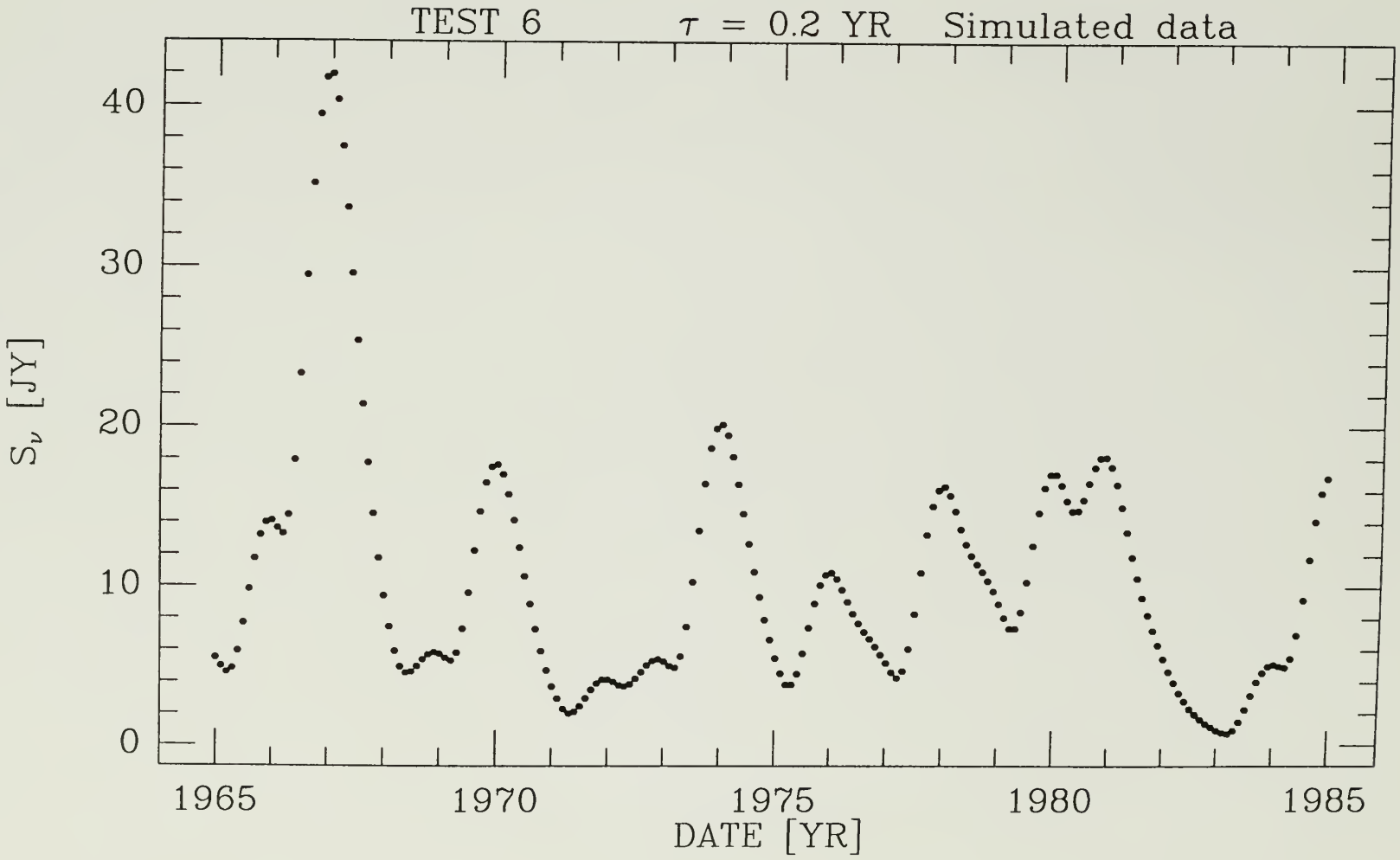
TEST 6
τ = 0.2 YR
Simulated data
40
30
20
10
0
S_ν [JY]
1965
1970
1975
1980
1985
DATE [YR]

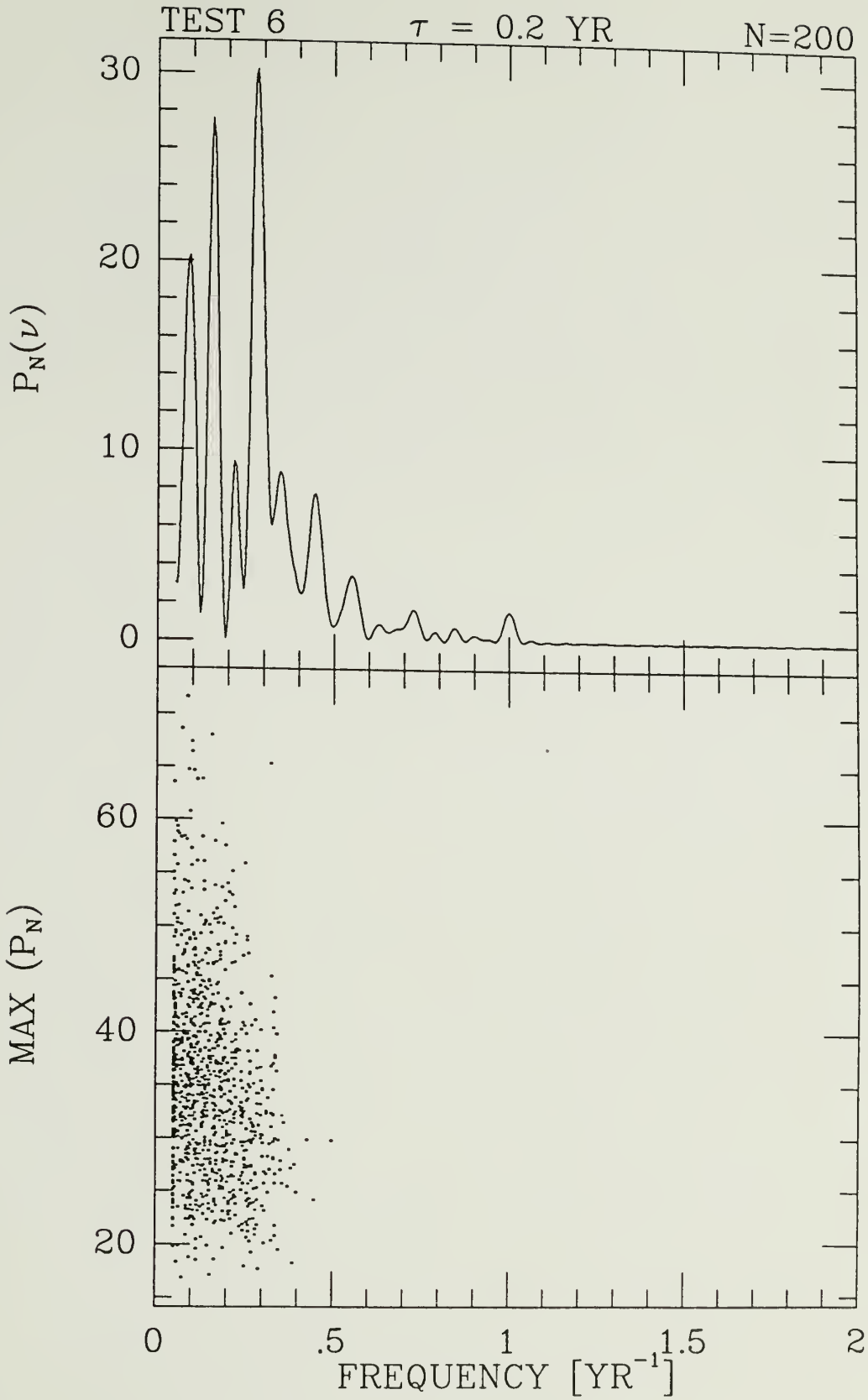
TEST 6
τ = 0.2 YR
N=200
30
20
10
0
$P_N(\nu)$
60
40
20
MAX (P_N)
0
.5
1
1.5
2
FREQUENCY [YR^{-1}]

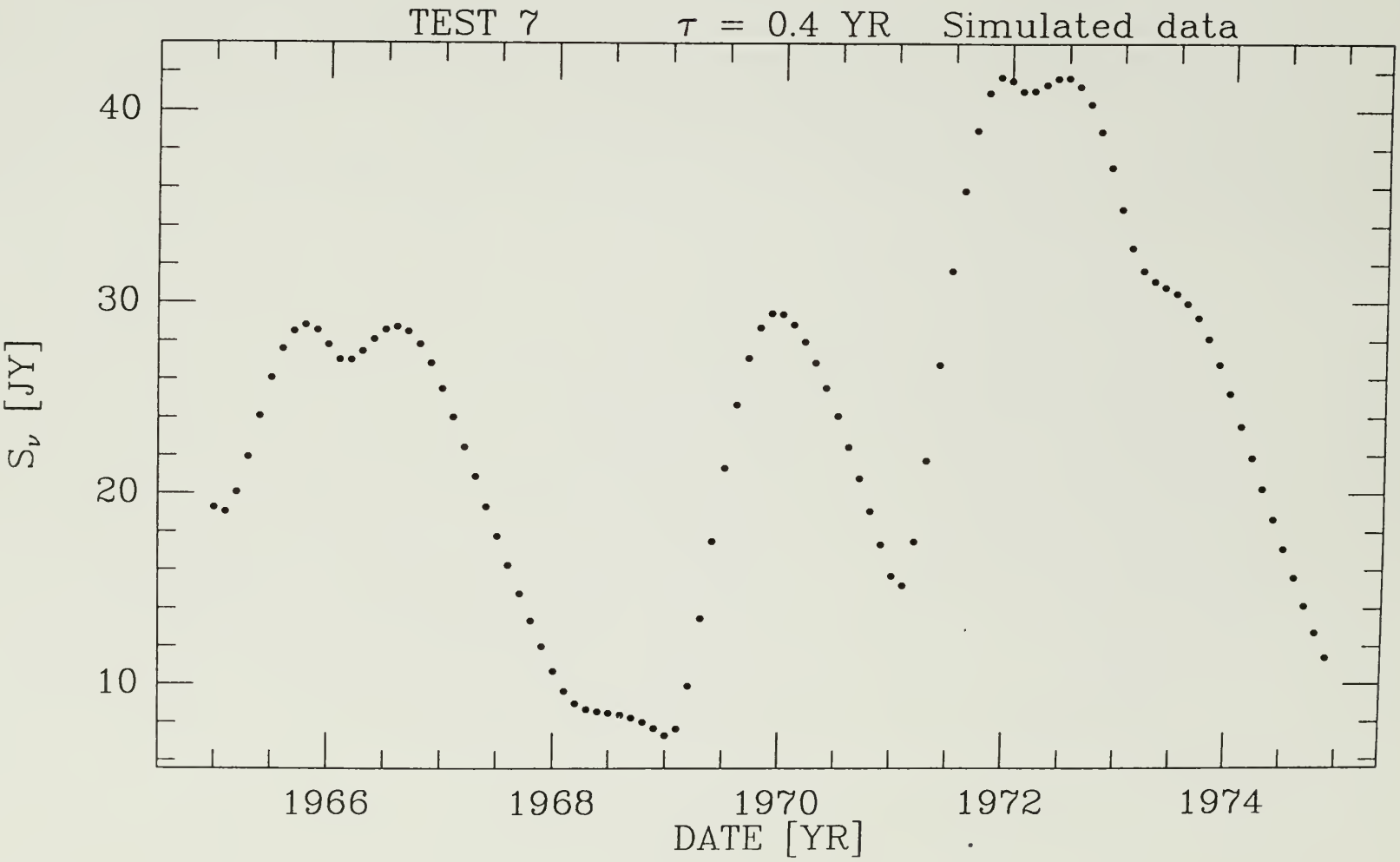
TEST 7
τ = 0.4 YR
Simulated data
40
30
20
10
S_ν [μJY]
1966
1968
1970
1972
1974
DATE [YR]

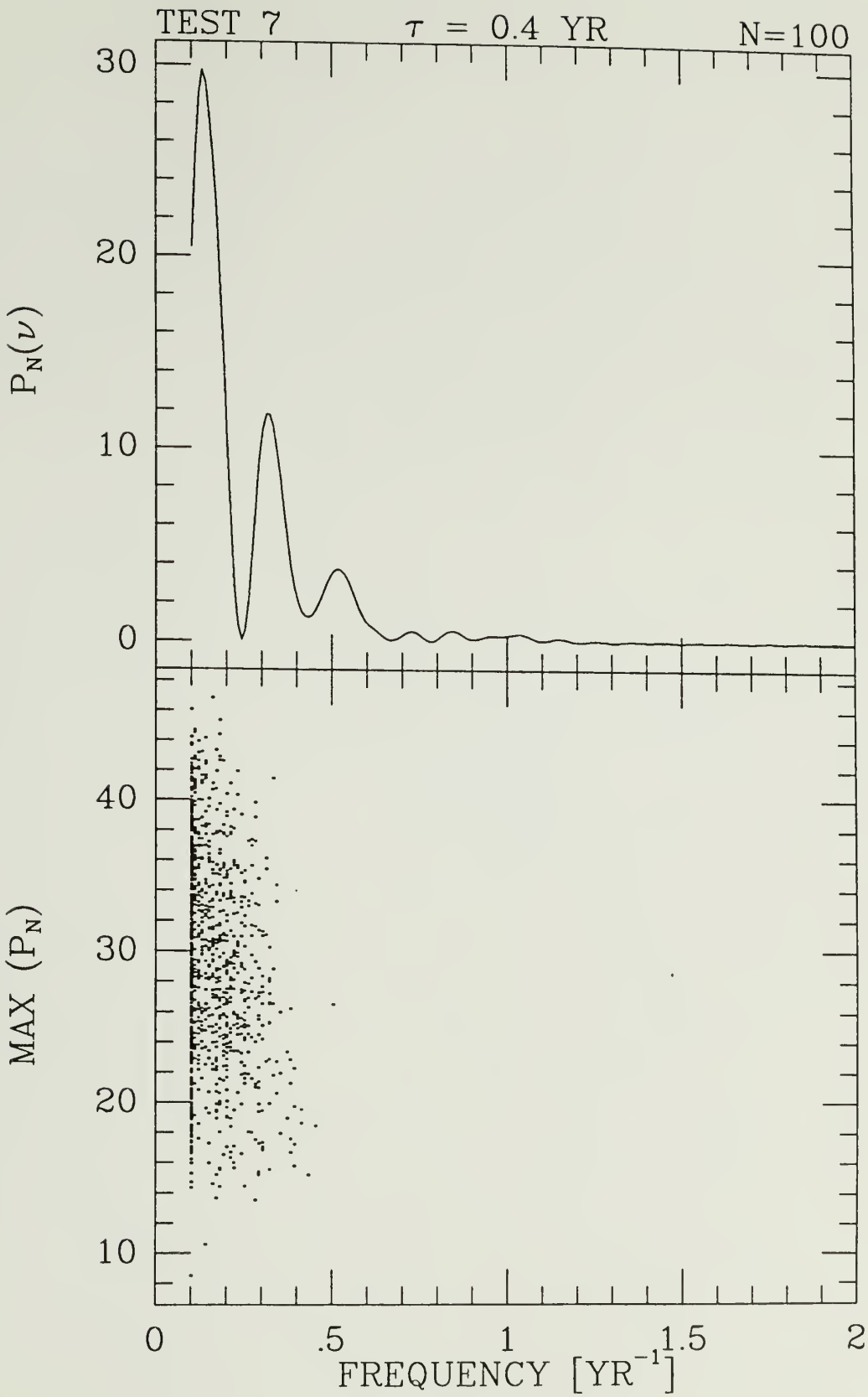
TEST 7
τ = 0.4 YR
N=100
30
20
10
0
P_N(ν)
40
30
20
10
MAX (P_N)
0
.5
1
1.5
2
FREQUENCY [YR^-1]

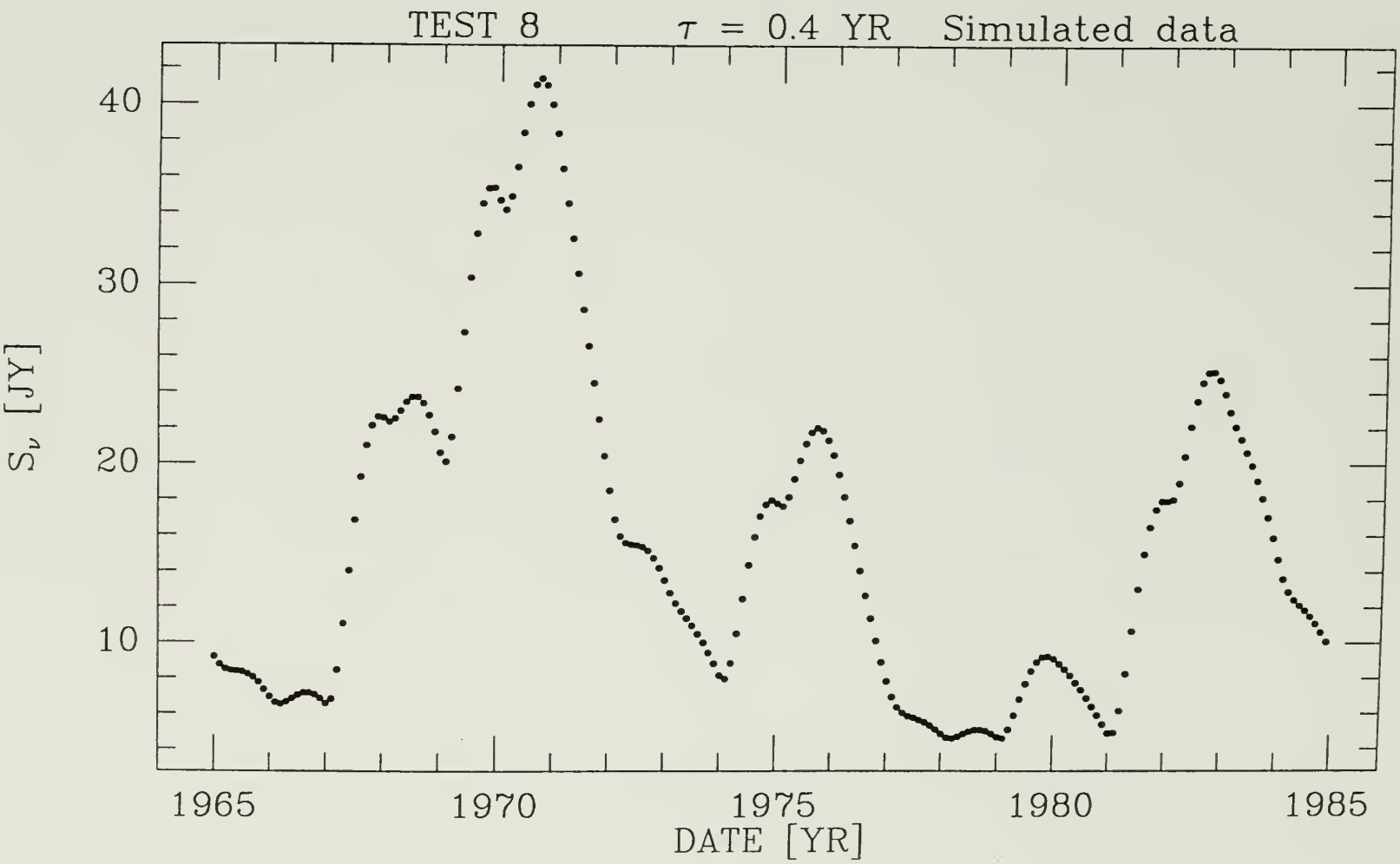
TEST 8
τ = 0.4 YR Simulated data
40
30
20
10
S_ν [JY]
1965
1970
1975
1980
1985
DATE [YR]

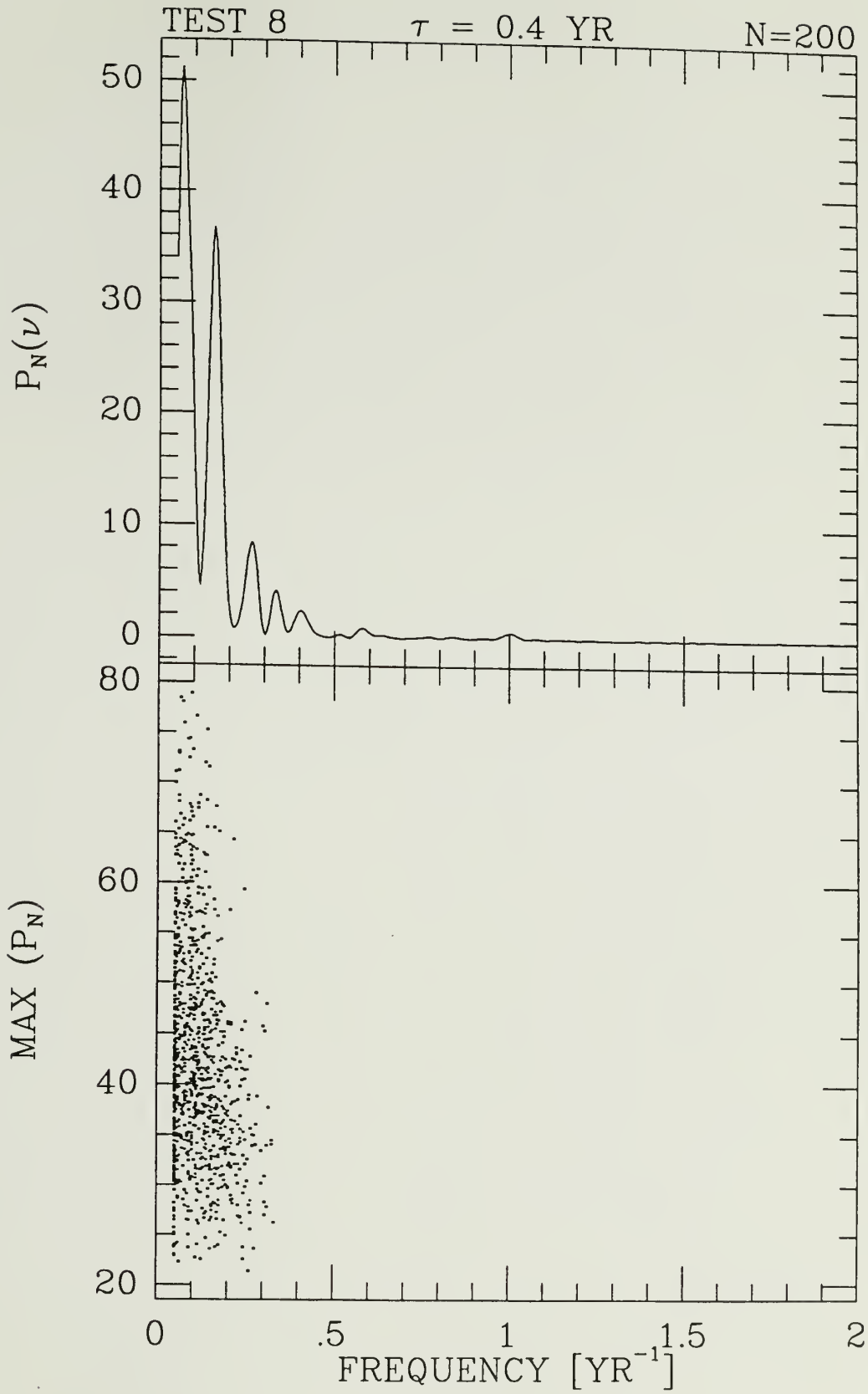
TEST 8
τ = 0.4 YR
N=200
$P_N(\nu)$
50
40
30
20
10
0
MAX (P_N)
80
60
40
20
0
.5
1
1.5
2
FREQUENCY [YR^{-1}]

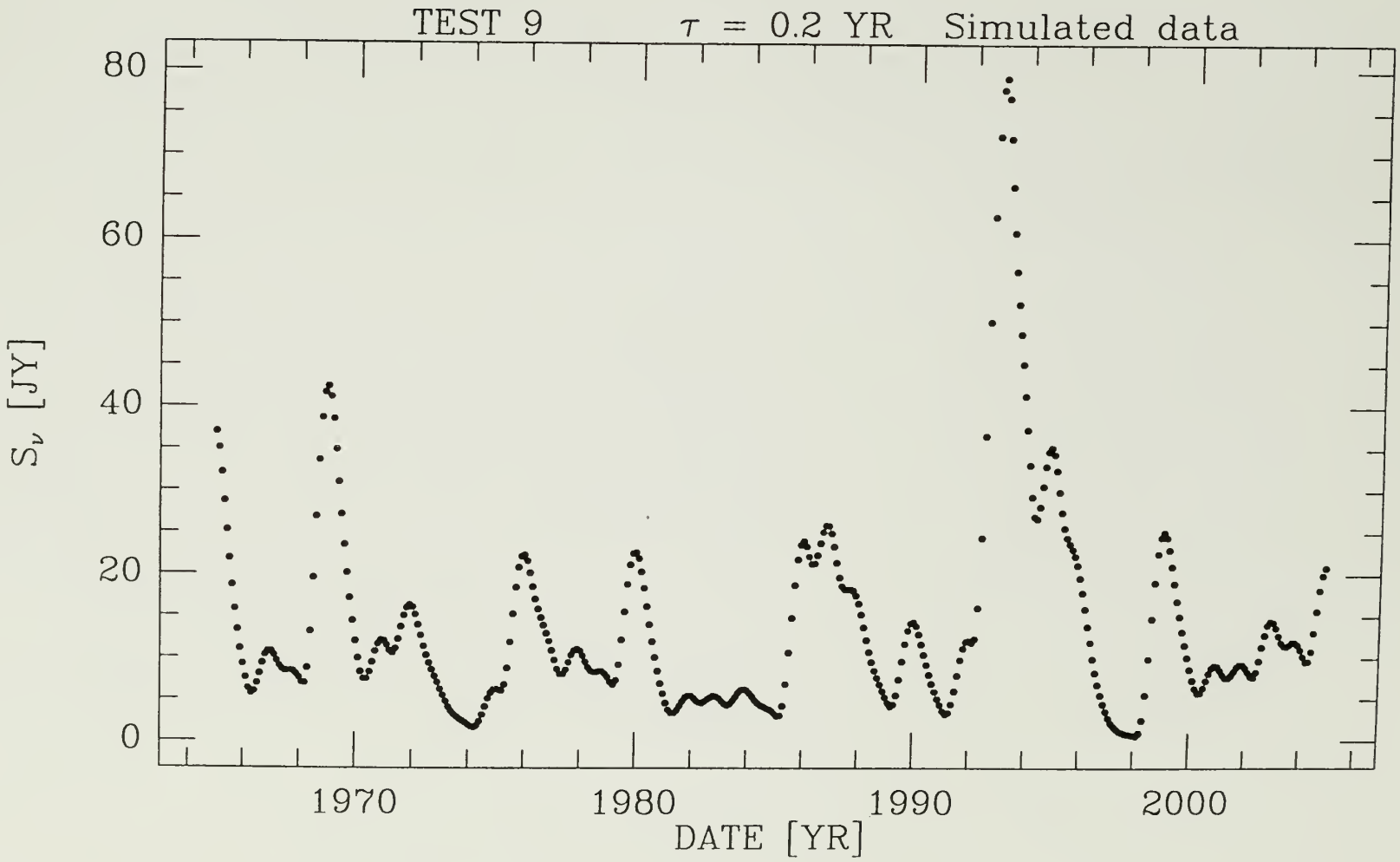
TEST 9
τ = 0.2 YR Simulated data
80
60
40
20
0
S_ν [JY]
1970
1980
1990
2000
DATE [YR]

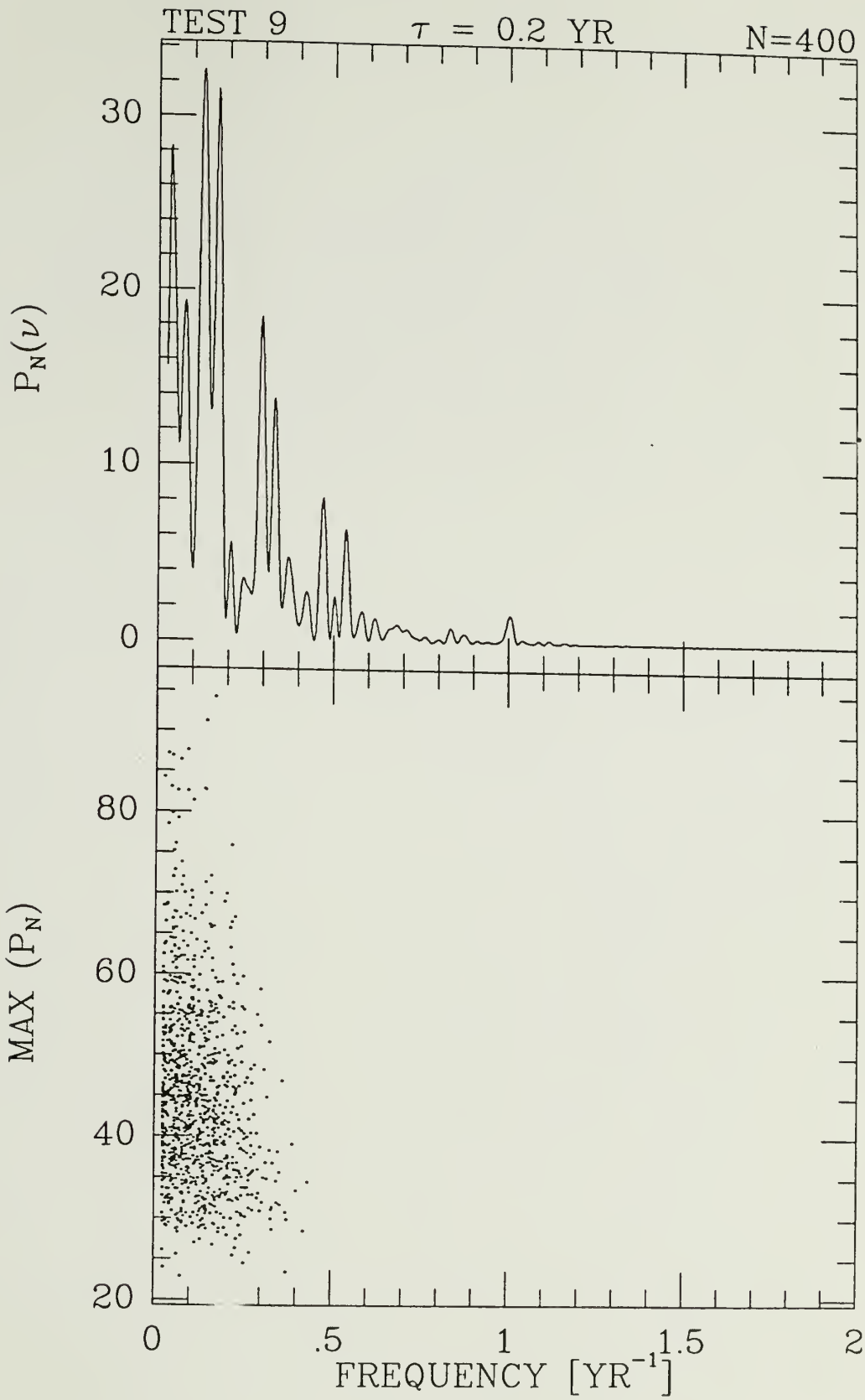
TEST 9
τ = 0.2 YR
N=400
30
20
10
0
$P_N(\nu)$
80
60
40
20
MAX (P_N)
0
.5
1
1.5
2
FREQUENCY [YR^{-1}]

BIBLIOGRAPHY

Abramowicz, M.A., Calvani, M., Nobili, L., 1980, Ap.J. **242**,772.

Abramowicz, M.A., Lasota, J.P., Xu, C., 1986, in *Quasars*, ed. G. Swarup, V.K. Kapahi (Reidel: Dordrecht).

Aller, H.D., Aller, M.F., Latimer, G.E., Hodge, P.E., 1985, Ap.J.Suppl. **59**,513.

Altenhoff, W.J., Baars, J.W.M., Downes, D., Wink, J.E., 1987, Astron.Astrophys. **184**,381.

Altschuler, D.R., Wardle, J.F.C., 1978, Mem.R.A.S. **82**,1.

Altschuler, D.R., Wardle, J.F.C., 1977, M.N.R.A.S. **179**,153.

Andrew, B.H., MacLeod, J.M., Harvey, G.A., Medd, W.J., 1978, A. J. **83**,863.

Balonek, T.J., Ph.D. Thesis, University of Massachusetts 1982.

Barbieri, C. et al., 1977, Astron.Astrophys. **59**,419.

Barbieri, C., Cristiani, S., Omizzdo, S., Romano, G., 1985, Astron.Astrophys. **142**,316.

Barvainis, R., Ph.D. Thesis, University of Massachusetts 1984.

Blandford, R.D., Rees, M.J., 1974, M.N.R.A.S. **169**,395.

Blandford, R.D., Königl, A., 1979, Ap.J. **232**,34.

Cook, D.B., Spangler, S.R., 1980, Ap.J. **240**,7551.

Cotton, W.D., et al., 1980, Ap.J. **238**,L123.

Deeming, T.J., 1975, Astrophy. and Space Science **36**,137.

Dent, W.A., 1965, Science **148**,1458.

Epstein, E.E., Landau, R., Rather, J., 1980, A.J. **85**,1427.

Epstein, E.E., Fogarty, W.G., Mottmann, J., Schneider, E., 1982, A.J. **87**,449.

Fiedler, R.L., Dennison, B., Johnston, K.J., Hewish, A., 1987, Nature **326**,675.

Flett, A.M., Henderson, C., 1981, M.N.R.A.S. **194**,961.

Gaskell, C.M., 1987, in *Astrophysical Jets and Their Engines* ed. W.Kundt (Reidel: Dordrecht).

Geldzahler, B.J., Witzel, A., 1981, A.J. **86**,1306.

Ginzburg V.L., Syrovatskii, S.I., 1965, Ann.Rev.Astron.Astrophy. **5**,297.

Jones, T.W., Hardee, P.E., 1979, Ap.J. **228**,268.

Jones, T.W. et al., 1981, Ap.J. **243**,97.

Kapitzky, J.E., Ph.D. Thesis, University of Massachusetts 1976.

Kaufmann, P., Raffaelli, J.C., 1979, M.N.R.A.S., **187**,23P.

Kinzel, W.M., Dickman, R.L., Predmore, C.R., 1988, Nature **331**,48.

Legg, T.H., 1984, in *VLBI and Compact Radio Sources*, ed. R.Fanti (Reidel: Dordrecht).

Ledden, J.E., Aller, H.D., Dent, W.A., 1976, Nature **260**,752.

Marscher, A.P., 1977, Ap.J. **216**,244.

Marscher, A.P., Gear, W.K., 1985, Ap.J. **298**,114.

Novikov, I.D., Thorne, K.S., 1973, in *Black Holes*, ed. C. DeWitt, B. DeWitt (New York:Gordon and Breach).

O'Dea, C.P., Dent, W.A., Balonek, T.J., 1984, Ap.J. **278**,89.

Owen, F.N. et al., 1978, A.J. **83**,685.

Owen, F.N., Spangler, S., Cotton, W., 1980, A.J. **85**,351.

Pacholczyk, A.G., 1970, *Radio Astrophysics* (San Francisco:Freeman).

Pacholczyk, A.G., 1981, Astrophys. Lett. **21**,87.

Pauliny-Toth, I.I.K., Kellermann, K.I., 1966, Ap.J. **146**,634.

Peterson, F.W., Dent, W.A., 1973, Ap.J. **186**,421.

Penzias, A.A, Burrus, C.A., 1973, Ann.Rev.Astron.Astrophy. **11**,51.

Pineault, S., 1980, Ap.J. **241**,528.

Ponman, T., 1981, M.N.R.A.S. **196**,583.

Press, W.H., Flannery, B.P., Teukolsky, S.A., Vetterling, W.T., 1986, *Numerical Recipes* (Cambridge University Press).

Press, W.H., Teukolsky, S.A., 1988, Computers in Physics NOV/DEC.

Robson, E.I. et al., 1983, Nature **305**, 194.

Salonen, E. et al., 1983, Astron.Astrophys.Suppl. **51**, 47.

Salonen, E. et al., 1987, Astron.Astrophys.Suppl. **70**, 409.

Scargle, J.D., 1982, Ap.J. **263**, 835.

Schloerb, F.P., Snell, R.L., 1980, FCRAO Report #150.

Shklovsky, I.S., 1965, Astron. Zh. **35**, 369.

Sillanpää, A., Haarala, S., Valtonen, M.J., 1986, TURKU-FTL-R107 Informo No. 108.

Sillanpää, A. et al., 1988, Ap.J. **325**, 628.

Sitko, M.L., 1986, in *Continuum Emission in Active Galactic Nucli*, ed. M.L. Sitko (National Optical Astronomy Observatories).

Smith, H.J., 1965, in *Quasi-Stellar Sources and Gravitational Collapse*, ed. I. Robinson, A. Schild, E.L. Schucking (University of Chicago Press).

Teräsranta, H. et al., 1987, Astron.Astrophys.Suppl.Ser. **71**, 125.

Ulich, B.L., 1981, A.J. **86**, 1619.

Valtaoja, E., et al., 1988, Astron.Astrophys. **203**, 1.

van der Laan, H., 1966, Nature **211**, 1131.

Villa, S.C., 1979, Ap.J. **234**, 636.

Vitello, P., Pacini, F., 1978a, Ap.J. **215**, 452.

Vitello, P., Pacini, F., 1978b, Ap.J. **220**, 756.

Webb, J.R. et al., 1988, A.J. **95**, 374.

Witta, P.J., 1985, Physics Report **123**, 117.

Willson, L.A., 1986, in *The Study of Variable Stars Using Small Telescopes*, ed. J. Percy (Cambridge University Press).